DESIGN & COMPUTATIONAL ANALYSIS FOR SATELLITE ATTITUDE CONTROL SYSTEMS AND PERTURBATION CORRECTION ANALYSIS FOR NANOSATELLITES IN LOW EARTH ORBIT WITH UTILIZATION OF KALMAN FILTERS

By

RAJA M
500024818

SCHOOL OF ENGINEERING

(DEPARTMENT OF AEROSPACE ENGINEERING)

SUBMITTED

IN PARTIAL FULFILLMENT OF THE REQUIREMENT OF THE

DEGREE OF

DOCTOR OF PHILOSOPHY

TO

UPES
UNIVERSITY WITH A PURPOSE

UNIVERSITY OF PETROLEUM AND ENERGY STUDIES

DEHRADUN

Month, Year (February 2019)

UNDER THE GUIDANCE OF

GUIDE	**CO-GUIDE**
DR. UGUR GUVEN	**DR. OM PRAKASH**
SENIOR PROFESSOR	**PROFESSOR**
UPES	**UPES**

ACKNOWLEDGEMENTS

It is with a sense of great satisfaction and pride that I am sitting down to pen out my Ph.D research thesis report. First and foremost, we sincerely salute our esteemed Institution **University of Petroleum and Energy Studies, Dehradun, India** for giving this golden opportunity for fulfilling our warm dreams of becoming a Doctorate.

I, first and foremost, would like to express my deepest gratitude to my supervisor, **Dr. Ugur Guven** (Sr. Professor, Department of Aerospace Engineering) who had sown the seed of space/satellite applications in my mind and made me take this as the topic of research. He has been a source of inspiration and a monument of motivation to me throughout this work. Without him, this work would never have been completed. Secondly, my thanks are out to my Co-supervisor **Dr. Om Prakash** (Professor, Department of Aerospace Engineering), who stood with me throughout this tedious journey, for his invaluable contributions and suggestions were ever required. Dr. Om Prakash rightly understood the significance of this work and gave me time space to work amidst the busy academic and co-curricular departmental activities.

I should mention my gratitude to my best friends **Mr. Senthil Kumar** (Assistant Professor, Kumaraguru College of Technology, Coimbatore), **Dr. Sudhir Kumar Chaturvedi, Dr Pravin Jadhav** by word of thanks is not adequate/appropriate. Also, I thank my best students **Mr. Vaibhav Bhatia, Mr. Aman Saluja** for valuable support. I am thankful to my HOD **Dr. Sudhir Joshi** and every faculty colleague of the department of aerospace engineering for their support and cooperation.

What I am today is all because of my parents & family. My father, **K. Munusamy**, Mother **M. Kotiswary,** are thanked whole heartedly for their unwavering extended support throughout my life.

Special thanks to my wife, **Kokila Vasudevan,** who managed and took care of everything to provide me the time, space and peace of mind to finish off this dream task.

Raja M

University of Petroleum and Energy Studies

Aerospace Engineering Department

DECLARATION BY SCHOLAR

I hereby declare that this submission is my own work and that, to the best of my knowledge and belief, it contains no material previously published or written by another person nor material which has been accepted for the award of any other degree or diploma of the university or other institute of higher learning, except where due acknowledgment has been made in the text.

(Signature/name/date)

Date: 14-02-2019
Raja M
500024818
Ph. D Research Scholar
Department of Aerospace Engineering
University of Petroleum and Energy Studies
Dehradun-248007

DEDICATED TO

OM SHAKTHI KALIKAMBAL &

LORD SHRI KRSNA & MY

PARENTS & My WIFE

UPES
UNIVERSITY WITH A PURPOSE

THESIS COMPLETION CERTIFICATE

This is to certify that the thesis on "**DESIGN & COMPUTATIONAL ANALYSIS FOR SATELLITE ATTITUDE CONTROL SYSTEMS AND PERTURBATION CORRECTION ANALYSIS FOR NANOSATELLITES IN LOW EARTH ORBIT WITH UTILIZATION OF KALMAN FILTERS**" by **RAJA M** in Partial completion of the requirements for the award of the Degree of Doctor of Philosophy Engineering is an original work carried out by him under our joint supervision and guidance. It is certified that the work has not been submitted anywhere else for the award of any other diploma or degree of this or any other University.

Prof. Dr. UGUR GUVEN
Senior Professor - Aerospace Engineering
Director - International Affairs
University of Petroleum & Energy Studies
"Energy Acres", P.O. Bidholi, Via Premnagar
Dehradun-248007 (Uttarakhand)

GUIDE

Om Prakash

CO-GUIDE

DR. UGUR GUVEN
AEROSPACE DEPARTMENT
SENIOR PROFESSOR
UPES, DEHRADUN

DR. OM PRAKASH
AEROSPACE DEPARTMENT
PROFESSOR
UPES, DEHRADUN

CORPORATE OFFICE: 210, 2nd Floor, Okhla Industrial Estate, Phase III, New Delhi - 110 020, India.
T: +91 11 41730151-53, 46022691/5
F: +91 11 41730154

ENERGY ACRES: Bidholi Via Prem Nagar, Dehradun - 248 007 (Uttarakhand), India.
T: +91 135 2770137, 2776053/54/91, 2776201
F: +91 135 2776090/95

KNOWLEDGE ACRES: Kandoli Via Prem Nagar, Dehradun - 248 007 (Uttarakhand), India.
T: +91 8171979021/2/3, 7060111775

upes.ac.in

ABSTRACT

An Attitude control system plays the important role to maintain the satellite to desired attitude orientations. The intended application of NANO satellite in low earth orbits (LEO) helps in determining its per-determined orbits from disturbed or perturbed orbit. The LEO orbits typically at an altitude in the range of 160-2000 km. The LEO satellites are widely used for remote sensing, navigation, and military surveillance applications. There is more development in the field of Nano satellite system design and control of a variety of applications. The Numerical ODE integration process helps to find initial position and velocity vectors of the Nano satellite by Runge - Kutta using Cowell's Method. The perturbation simulation is analyzed with MATLAB, General Mission Analysis Tool (GMAT) open source software developed by the National Aeronautics and Space Administration (NASA). The Keplerian results are validated with General mission analysis tool. The design parameters of Nano satellites such as Moment of inertia, North American Aerospace Defense Command (NORAD) two-line element commands, and Geometry parameters are considered. The Nano satellite Attitude control systems (ACS) for SRM Satellite, Pratham (IIT Bombay), NPSAT-1 described in the research work. The high pointing accuracy attitude estimation and feedback control systems are presented. The dynamics attitude controller with feedback is implemented by MATLAB/SIMULINK package. The small satellite is very much essential to collect the information in the space environments. The most of the Keplerian or orbital elements are considered as ideal condition. A satellite is expected to move in the orbit until its life is over. This would have been true if the earth was a true sphere and gravity was the only force acting on the satellite. Under the initial condition the motion of two bodies like Earth –Satellites are considered. Practically, this is not possible. The motion of the body includes the disturbing forces in the orbit. However, a satellite has deviated from its normal path due to several forces. This deviation is termed as orbital perturbation. The changes in the orbital element with respect to secular variations are considered. This work describes the conservative forces like aerodynamic drag and solar pressure. In this thesis, an

overview of orbital perturbation of the six Keplerian elements like semi-major axis, True anomaly, Longitude of ascending node, eccentricity, inclination, Argument of perigee are presented. The numerical simulation to demonstrate the performance of SRM Satellite, Pratham, and International Space Station (ISS) is Performed. The perturbation algorithm is implemented in MATLAB Environment. To maintain the orientation of the satellite it is necessary to design the attitude estimation technique. The Satellite is considered as rigid body representing the attitude parameter. An inertia matrix describes the rigid body dynamics. The attitude orientation of the satellite using Quaternion and Euler angle is derived. Calculation of the Euler angles (Roll angle, Pitch angle, Yaw angle) with Direction cosine matrixes (DCM) have singularity and computational problems compared to the Quaternion method are discussed. In Low earth orbits, satellite will have an enormous amount of aerodynamic drag acting on the satellite body rapidly in low earth orbit due to centripetal force and gravitational attraction because of that satellite dwell time is reduced. An attitude estimation is measured by the orientation of the vectors. An Attitude sensor is used to measure the satellite orientation in the reference frame which will help in accurately predicting the orbit deviation.

In the presents work, LEO orbit satellite attitude control is implemented by Armature control DC Motor acting an actuator. The magnetic torque is having a solenoid coil generating the magnetic flux which interacts with GEO magnetic fields with the help of magnetometers. The GEO magnetic fields modeling is considered in the International Geomagnetic Reference Field IGRF (IGRF-12). The magnetic moments or control torques are generated by the magnetic coil in satellite body or torqrods to determine the attitude angles and angular rates of the body. The attitude (Roll, Pitch, and Yaw) estimations of Nano satellite NPSAT-1 using Kalman filter and fuze the data to on-board attitude sensors like INS/GPS, Magnetometer reference with low earth orbit satellite. A low-cost sensor is used for simulation of Nano satellite with a Kalman filter. This filter predicts the future estimates state from the magnetometer and attitude quaternions. The design specifications are taken to meet the accuracy requirements (desired value ≤ 0.2 seconds) of Nano satellite attitude control. This research work presents the Kalman algorithm with magnetometer and Inertial sensor information. The stabilization of a Nano satellite using magnetic torquer concepts are considered with principle moment of inertia of the model. The feedback signal from on-board sensors compare with reference orbit trajectory and implementation of the Proportional Derivative (PD) controller is constructed. The spacecraft control system used to improve the transient response like overshoot and settling time of the system. Thus, in the design of attitude control rise time, setting time, (desired value ≤ 0.2 seconds), minimum overshoot, and no steady state error were achieved

TABLE OF CONTENTS

LIST OF ABBREVIATIONS AND ACRONYMS

KE = Keplerian elements

EOM: Equation of motion

COE: Classical orbital elements

NORAD: North American Aerospace Defense

HEO: High earth orbit

GEO: Geo-synchronous Earth orbit

CMG: Control momentum gyroscope

SMA: Semi-Major Axis

INS: Inertial Navigation System

GPS: Global Position System

IMU: Inertial Measurement Unit

ISRO: Indian space research organization

NASA: National Aeronautics and Space Administration

CF: Coordinate frame

IF: Inertial frame

ECEF: Earth centered Earth Fixed frame

DCM: Direction cosine matrix

EP: Ecliptic Pole

AN: Ascending node

DN: Descending node

GP: Gyroscopic precision

MT: Magnetic torque

FW: Flywheels

MW: Momentum wheels

AD: Atmospheric drag

as: arcsecond

ISS: International Space Station

MDM: Magnetic dipole moment

VCMGs = Variable-speed CMGs

SGVSCMG: Single gimbal Variable speed control momentum gyroscope

DGV: Double-gimbal VSCMG

LOS: Line of sight

OP: Orbital plane

ADCS: Attitude Determination and Control System

RAAN: Right assertion to ascending node

ODE: Ordinary Differential Equation

PID: Proportional-Integral-Derivative controller

RG's: Rate Gyro's

IGRF: International Geomagnetic Reference Field

IVAB: Inner Van Allen Belt

OVAB: Outer Van Allen Belt

PMS: Permanent Magnet Stabilization

GGS: Gravity Gradient Attitude Stabilization

UT: Unscented transformation

KF: Kalman filter

GNSS: Global Navigation Satellite system

CM: Covariance matrix

UKF: Unscented Kalman Filter

GMAT: General Mission Analysis Tool

TA: True anomaly

SF: Solar Flux $(1353\ W/m^2)$

EO: Earth's Oblateness

EP: Equatorial plane

KF-RE: Kalman Filter Rate Estimator

AP: Argument of perigee

SSE: State Space Equation

EKF: Extended Kalman Filter

GM: Greenwich meridian

VE: Vernal Equinox

LIST OF SYMBOLS

G: Gravitational constant, ($G = 6.674*10^{-11}\ N\ m^2\ kg^{-2}$)

r_{earth}: Radius of the earth, ($6.37 * 10^6$ m)

*m_1: Earth mass, Kg (5.972*10^24 Kg)*

m_2: Satellite mass, Kg

F_i: Forces acting on the i^{th} body

K: Gaussian parameter

ω: Angular velocity

τ: Torque

μ: Gravitational constant Let, $\mu = G * m_1$

a_x, a_y, a_z : Acceleration (x, y, z-directions)

(e_r and e_θ): Unit vectors

h: Angular momentum per unit mass

a: Semi major axis

b: Semi minor axis

e: Eccentricity, ecc

Ω_{RAAN}: Longitude of ascending node

ω: Argument of perigee

i: Orbital inclination

ξ: Real Value

ν: True anomaly, $T_{anomaly}$

v_c: Circular velocity

T: Orbital period

(θ, ψ, φ): Satellite Attitude Rates

q: Quaternion

R_{max}: Rotation matrix, R_B^O(Satellite body to Orbit)

(I, J, K): Inertial reference frame

(x_o, y_o, z_o): Orbital frame

$T_{Satellite}$: Satellite torque

R_{apogee} : Distance between satellite and Earth at apogee point

$R_{perigee:}$ Distance between satellite and Earth at perigee point

r: position vector

v: Velocity vector

c: Velocity of light (3×10^{8} m/s)

Ω: Orbital angular velocity

J_2: Zonal perturbations

$\frac{m_2}{C_d A}$: *Ballistic constant*

C_d: Coefficient of drag

A: Area of the satellite

A_Θ: Area of the SUN

O: orbit

F_{drag}: *Aerodynamic drag force, F_{AD}*

ρ: Air density

H: Atmospheric scale height of density

$R = x_i + y_j + z_k$: Position vectors

$V = u\,i + v\,j + z\,k$: Velocity vectors

Ω_{SUN} & Ω_{MOON}: Longitude of ascending nodes SUN & LUNAR (degrees/day)

ω_{SUN} & ω_{MOON} : Argument of perigee SUN & LUNAR (degrees/day)

a_r: Solar radiation force

a_p: Perturbing acceleration

N: North pole

B: GEO Magnetic field (Earth's Magnets)

ϕ = *Flight path angle*

M: Dipole moments

I: Current in the coil

N: No of turns in the coil

$T_{Required}$: *Required torque*

N: Nadir

Z: Zenith

δ: *Damping ratio*

ω_n: *Undamped natural frequency*

H_s: *Satellite angular momentum*

H_w: *Wheel angular momentum*

l, m, n: Satellite with the principle axis of body

(I_{xx}, I_{yy}, I_{zz}): *Satellite principle Moments of inertia*

J_W : *Moment of inertia of Wheel*

J_G : *Moment of inertia of Gimbal*

c_r: *Reflectivity of SUN*

$T_{gravity}$: *Gravity gradient torque*

K_{Gain}: *Kalman Gain*

x: system state variable

P_{CU}: *Covariance updates*

w_k: *Process Noise*

v_k: *Measurements Noise*

A(nxn): Plant (or) Process Matrix

B: Control matrix

F: Controller Gain

u_d: *Perturbation forces*

H: Measurement matrix

Z_k: *Actual Measurements*

Q_k: *Process covariance*

R_k: *Measurements covariance*

LIST OF FIGURES

LIST OF TABLES

CHAPTER 1

INTRODUCTION

1.1 Overview

The attitude control System (ACS) of satellite is important to maintain the position and orientation of the vehicle into the original orbital plane. There are two methods used for attitude control system, one is active control system and another passive control system. The active control technique requires a signal from feedback sensor signal and applies the signal to vehicle actuator to maintain the orientation of the satellite body. The passive attitude control method uses the gravity gradient technique to stabilize the satellite with respect to its orientation [1]. These methods utilize numerical computation techniques to apply the feedback signal to actuation systems, magnetic torquers, fly wheel, momentum wheels. This work analyzes the various perturbations or disturbances in low earth orbits (LEO) and attitude control of Nano-Satellite with error estimation using Kalman Filters [2]. An especially in a LEO, due to the gravitational attraction, satellites have an enormous amount of aerodynamic drag compared to the high earth orbits (HEO) with little or no aerodynamic drag. The attitude determination (AD) is the integral part of the satellite used to calculate the attitude information for various times with the help of attitude sensors like INS/GPS (Inertial Navigation System/Global Position System), IMU (Inertial Measurement Unit), and Magnetometer, Sun Sensor, Star Sensor, and the Earth sensor [2]. The Satellite attitude governor/control is very important to stabilize the satellite along with its predetermined orientation. Due to the perturbation forces (or) environmental disturbances the satellite may get affected and the original orbit may be changed due to these perturbations. Thus, it is very important to reduce these perturbation forces, as they can cause life term of the satellite to be significantly reduced [3]. It is essential to maintain the satellite pointing accuracy for the proper orientation of the communication, such as GPS antenna pointing towards the ground station on Earth’s surface to transmit and receive the data for telemetry, or the solar panel pointing towards the SUN. This has great importance, since thrusters require energy from sun to re-orient the satellite to the desired path [3]. Mostly, communication system using directional antennas sends/receives signal transmitter to receiver by directional transmission methods or line of sight (LOS) communications. The signals from the satellites are directed towards to the ground station on Earth or inter satellite communications. The solar panels point towards the SUN at an orientation because it consumes more optimal electricity or power. This is especially important, since thrusters require energy from the sun to re-orient the satellite to the desired path [4]. The Remote sensing satellite to capture data from spectrometers/HD cameras focuses terrain surface all the time, and it requires that the camera should be pointing towards Earth's surface for recording accurate data collections. The Telescopic satellite to focus on one location requires the proper orientation schemes. It is also required to use the attitude stabilizing techniques to maintain the required path [5]. The environmental forces also differ at various altitudes. For example, LEO satellites will be affected more by aerodynamic drag and gravitational attraction due to the proximity of earth as compared to the other perturbations. Three body problems can occur at HEO, with Earth-Satellite-Moon attraction problem. The Spacecraft stabilization can be classified into two methods, one as the spin stabilization method and second is gravity gradient method. The spin stabilization methods require energy to control the satellite. The actuators are used to reorient the satellite in the desired path from perturbed path and they act as magnetic torquers at LEO Nanosatellites. An attitude sensor is used to measure the attitude (pitch, roll, and yaw) of satellite and these feedback signals are compared with pre-determined orientations [6]. These signals trigger the dynamics of the vehicles to move the control surface according to the reference trajectory. The magnetic thruster is basically a dipole solenoid coil which interacts with the earth magnetic flux and creates the control torque, which requires maintaining its specific path for low earth orbiting satellites. At the High earth orbit satellite such as GEO Synchronous orbit satellite control momentum gyroscope (CMG) acts as an actuator to generate the necessary control torques [6]. There are various factors affect the lifetime of satellites, such as types of the orbits, perturbation forces, type of satellite parameters, as well as the exposures to the different types of environment. The accurate attitude determination techniques using with attitude sensors (Magnetometer, INS/GPS, and IMU) and control techniques using actuator (Magnetic torquer, Thruster, CMG) are used to increase the life time/mission life and performances of the satellite [7], [8]. The Attitude determination and control system (ADCS) is very important to keep the satellite from disturbed orbit to original orbit. It requires signal from various on-board attitude sensors to compare this signal with the reference trajectory based on how it controls the actuator with suitable (or) required orientation. India has launched 120 satellites at single launcher by "Indian space research organization" (ISRO) which includes the weather monitoring, remote sensing, disaster management, communication & navigation, military operation, and earth observation satellites. The Chandrayan-1 satellite launched into lunar orbit-lunar observation, Mangalyaan-Mars orbiter mission, Chandrayan-II tentatively scheduled launch in 2019 between the months of January to March. The ISS is a major satellite space station that orbits in LEO. However, due to the perturbations, the satellite altitude varies with time. To maintain the accurate planned orbit, it's highly recommended that the attitude determination and control algorithm are used with frequent thruster to re-orient the satellite into mission orbit [9].

1.2. Research Motivation

The improvement of aerospace engineering and space research is becoming highly integrated, complex, knowledge intensive and globally distributed. The aerospace industry needs more accurate results and successful mission to meet the competitive global markets. Therefore, it becomes essential to study, evaluate and analyze the existing systems and identify areas for the improvement of aerospace/space systems. The mathematical modeling and numerical methods are easy to be modelling systems dynamics and behaviors [10]. The simulation tools are widely used to analyze various models of transient responses of actuators and plant dynamics. Its highly recommend, the more pointing accuracy of attitude controls of satellite for getting the optimum results/Mission performances. To design the low cast attitude error estimation using Kalman filters (KF) [11]. The space industry is spending lots of money on the design and development of space mission operations such as launching the satellite, trajectory transfer, formation flying, planetary observations and earth observations to achieve accurate performances and mission effectiveness with qualitative/optimum results, it is requiring satellite high pointing accuracy attitude determination and control systems. The proper ADCS used to increase the lifetime of the vehicle and mission performances [12]. The research focus on to design and analysis of the satellite attitude control with orbital perturbation at low earth orbiting satellite and error estimation using Gaussian filter like Kalman Filters used for updates and measurements of present states and future estimates from satellite attitude sensors. The author Giebelmann J worked on "Development of an active magnetic attitude determination and control system for picosatellites on highly inclined circular low earth orbits" [13]. This work helped to recognize the basic ideas about dynamics of Small/Nano satellite in low earth orbit and attitude control techniques. The research discussed about the magnetic stabilization methods for attitude correction. This impressed me to start the magnetic torquers concepts, how the GEO magnetic field varies with atmosphere inner van Allen radiation belts and outer Van Allen belts used to generate the required torque to adjust the satellite form perturbed orbit to original satellite orbit. Another research work helped me to understand the Kalman Filter, Murty S. Challa has presented [14] "A Simple Attitude Unscented Kalman Filter: Theory and Evaluation in a Magnetometer-Only Spacecraft Scenario" gives me the strong understand about Kalman filter and its operation. The attitude sensor at low earth orbit Nano satellite more rely on Magnetometer and the model is implemented based upon Euler angles. This work mainly focuses on the on-board sensor used to estimate the attitude errors with different condition. The major part of work explains the earth-pointing spacecraft undergoing only small rotation angles. In this section, understand the Kalman algorithm and developed and implemented in MATLAB program. It's very important to specify the work presented by Karatas S "LEO Satellites: Dynamic Modelling, Simulations and Some Nonlinear Attitude Control Techniques" [15]. The research contributed the various dynamics and simulation of LEO satellite attitude control methods widely used for small satellites. The research work discussed about the various perturbations in LEO and these affect the attitude and altitude of the satellite and its orientation. The concepts of various actuation systems at like magnetic torquers, Thruster, CMG, Momentum wheels. The actuator requires the input from the controllers, like P-Proportional, I-Integral, D-Derivatives, PI, PD, PID and make the required control torque to the satellite dynamics [16], [17].

This research work encouraged to focus on research topics to design & analyze of various attitude controls of pitch dynamics, roll dynamics, and yaw dynamics, with a suitable controller incorporated to reduce the oscillation in the system because of the orbital perturbation forces.

1.3. Attitude Modeling Tools

The attitude modeling and simulation for satellite systems are classified into two types; one is attitude determination (AD) and another attitude control system (ACS). To analyze the various orbital perturbation forces at Low Earth Orbiting NANO satellites and motion equations in the form of ordinary differential equation (*ODE*) using Runge – Kutta method was adopted [18]. The International Space Station (ISS), SRM Satellite, Pratham (IITB) Satellite Cowells perturbation algorithm implemented by using **MATLAB/Python** Environments. The perturbation forces change the satellite six orbital elements like Semi-major axis - distance between the perigee to apogee, Angle of inclination, Eccentricity of orbit, Argument of perigee - angle between perigee to line of nodes where satellite crossing of the equator, south to the north pole, Longitude of ascending node (reference with vernal Equinox), True anomaly/Mean anomaly [19]. The attitude determination parts of LEO system are configured by mathematical modeling and simulation using MATLAB (Version 2014) and **Python** (Version 3.7) open source software. The Nano satellites attitudes (Pitch, Yaw, Roll) control parts of SRM Satellite, Pratham (IIT Bombay), NPSAT-1 modeled and developed using **SIMULINK** (Version 2014) control system Toolbox. The analytical model is developed with the help of satellite dynamic equations (refer: https://opensource.gsfc.nasa.gov/projects/GMAT/index.php) and compares the results with General Mission Analysis Tool, **GMAT** (2014 Version 1.1) open source software for validation. The GMAT is developed by the National Aeronautics and Space Administration (NASA) used for Orbit determination, Visualize the various trajectory optimizations, Mission analysis, attitude maneuvers [20], [21]. The Attitude determination and control system (ADCS) of low earth orbiting NANO satellites are analyzed & evaluated with MATLAB/SIMULINK and GMAT and Python (32-bit).

1.4.Organization of Thesis

The construction of the thesis as tracks

Chapter 1 The first chapter contains the overview of attitude control in satellite systems, research motivation and research questions, modeling tools, and Research summary.

Chapter 2 Covers the literature review of LEO Satellites: Dynamic Modelling, Simulations, Attitude control, Error estimation, Analysis perturbation. Discuss the problem statements about research work, how to design the high pointing accuracy attitude determination and control system (ADCS), Research objectives, Scope of the work.

Chapter 3 Briefly describe the satellite attitude reference frames (Inertial frame, Earth frame, satellite body frame, **ECEF** Frame, Orbit frame), Geometry of orbits, Keplerian elements, Rotation matrix, **DCM**, Quaternion, Orbit frame to an inertial frame, Earth frame to an inertial frame, Orbit frame to Satellite body frame.

Chapter 4 Presents the mathematical modeling of satellite dynamics equations and linearization of the equation of motion (**EOM**), Estimation of the disturbance torques subjected into the satellite, various perturbations (Aerodynamic drag and Solar drag) in low earth orbits. Perturbation models by Runge-Kutta using Cowells methods, analysis of the perturbation of Nano-Satellites (International Space Station, Pratham (IIT) Bombay Satellite, and SRM Satellite in LEO.

Chapter 5 Discuss the attitude estimation using Kalman Filter, Priori state estimation, Posteriori state estimation, Estimation of the satellite (NPSAT-1) attitude errors (Pitch, Roll, Yaw) using a Kalman algorithm with the help of INS/GPS and Magnetometers.

Chapter 6 Present the design of an attitude controller of Nano Satellites (Pratham, SRM satellite, ISS, NPSAT-1) Simulink model of rate controllers with perturbation, Comparison of attitude responses/output from Proportional-Derivatives (**PD**) controller.

Chapter 7 (Conclusion and recommendation of future work) presents conclusions derived from the work and significant contributions. A brief scope for further research has been identified to provide direction and possible extensions to the work. The reference presents the details of the technical papers referred in this thesis work.

1.5.SUMMARY

Introductory chapter presents the overview of the dissertation in terms of its research area, motivation and preliminary research questions. The summary of the research work contains introduction, analysis and characteristics of perturbations and attitude control systems in LOW EARTH ORBIT, Aerodynamic drag, solar drag, Kalman Filter Rate Estimator (KF-RE) and state space theory of attitude sensor [23]. This projects briefly discusses perturbation forces, such as aerodynamic drag and solar disturbances and how it affects six orbital elements or classical orbital elements (COE) angle between the orbital plane and equatorial plane, longitude of ascending node, satellite position with respect to perigee, size of the orbit, perigee to apogee distance, argument of perigee, Mean or Eccentric anomaly for circular orbit [24], [25]. The modeling and simulation tools for the analysis of complex system have been introduced. Attitude sensors such as INS/GPS, IMU, Magnetometer, Rate Gyros, SUN sensors, Earth Sensors, Horizon sensors are used for satellite attitude determination [26]. In this thesis low earth orbit attitude sensors like INS/GPS, IMU and magnetometers have been used for NANO satellites attitude determination. The high Earth orbits (HEO) like Geo synchronous earth orbit (GEO) satellites are heavy satellite. The magnetic torquers are used to control the attitude of low earth orbiting NANO satellites. This is also referred as magnetic actuators. The control momentum gyroscope (CMG) is widely used for satellite attitude control at high earth orbits satellite [27]. The magnetometers widely used for attitude control. It consists of solenoid coil or bar magnets, such as permanent magnet or an electromagnet [28]. The coil or conductor wounded in a core material is mounted into the satellite body frame. The current carrying the conductor produces the magnetic flux which can interact with Earth magnets and generate the controlled forces (τ = mB, where τ is torque, m = NIA is dipole and B is GEO-magnetic field) [29]. The torque generated in the device is based upon the number of turns (N) of the conductors and the amount of current (I) passing through the conductor, cross section area (A) of the conductor. The reaction forces generated in the coil creates the magnetic flux which interacts with the earth magnetic fields used to maintain the satellite into the desired orbits [29]. For heavy or large satellites Thruster, Momentum wheels, fly wheels are used to control the actuators of satellite dynamics. The algorithm of LEO attitude determination and control mainly based upon satellite attitude sensors INS/GPS, Magnetometer, Inertial Units. The Attitude control algorithms mainly using magnetometer and Rate Gyro's at low earth orbiting small/Nano satellite. The accuracy and precision of Rate Gyro's are highly reliable at low altitude with time [30]. The magnetometer gives proper attitude data when satellite crosses to near earth's atmosphere and the equator. The earth's atmosphere consists of various magnetic belts like Inner Van Allen Belts (IVAB) and Outer Van Allen Belts (OVAB). The High earth orbit such as GEO synchronous orbit attitude control using control momentum gyroscope consist of small motor attached to the satellite body [30]. The inertia of the satellite (I_{xx}, I_{yy}, I_{zz}) measures with the help of disc attached to the motor. The satellite on-board attitude sensors measure the orientation information of the vehicle compare with pre-determine attitude based on that it produces the error signals to actuate the actuator with the help of suitable controllers. The controllers (Proportional P, Integral I, Derivative D, PI, PD, PID) create required signal to the actuators. The CMG act as an actuator which produces the control signals to satellite model. Mostly, the motor is used to deflect the control surface of the satellite model to re-orient from perturbed path to actual orbit path [30]. The proposed method is used to design, mathematical modeling, Simulation of analyzing the perturbation in LEO, Rate control, Attitude error estimator using Kalman Filter developed by MATLAB/SIMULINK and GMAT package.

The Kalman filter is widely used in Global position system/Inertial Navigation system to estimate errors in the autonomous based navigation system. The main part of this research works to estimate the attitude errors from the sensor. The Kalman filter algorithm is used to find angular rates and minimize the errors in the satellite system. This is recursive in nature. The probabilistic theory white Gaussian or Normal distribution methods are used to minimize the error covariance matrix and standard deviation. The Kalman filter interacts with the satellite control and navigation components such as Rate Gyro's and Magnetometer.

CHAPTER 2

LITERATURE REVIEW

2.1. Outline of Research Problem

A perturbation is a deviation from some typical or expected movement. These irritations, or varieties in the orbital components, can be arranged in view of how they influence the Keplerian components. In orbit, the common varieties speak to a straight variety in the component, brief period varieties are occasional in the component with a period not as much as the orbital period**.** The satellite orbit changes due to the perturbation forces affecting on it. It requires the highest pointing accuracy attitude control and the determination system which is used to keep the satellite into the predicted trajectory. The attitude control design needs a suitable controller to trigger the actuator for the required demands. At LEO, satellite control relies on magnetic torquers, which can interact with GEO (Earth) magnetic field as the resultant torque is used to control the Nano or Small satellites.

Fischel1, R. E, (1963) "Passive Magnetic Attitude Control for Earth Satellites", Advances in the Astronautical Sciences, Volume 11, Western Periodical Company Hollywood, Calif. The research worked on the vertical stabilization scheme which has been incorporated in the low earth orbit [31]. The research discussed about the satellite attitude control using magnetic actuator (or) magnetic torquers in low earth orbiting satellite. The magnetic torquer consists of solenoid coil, the current 'I' in the coil produce the magnetic flux which interacts with GEO magnetic field vectors. The idea was also put through by the research how this magnetic field generates the control torque to controlling the satellite with suitable algorithm/control laws [31]. The control torque from magnetic torquers perpendicular to the Earth field vectors (or) GEO magnetic fields. The attitude control system of small satellite relies on magnetometer signal.

S.K Shrivastava, (1976) "Effects of solar radiation pressure and aerodynamic forces on satellite attitude Dynamics and their utilization for control" [32], The research explains the relative magnitudes of torques due to various forces arising from gravity-gradient, solar radiations, earth and earth-reflected radiations atmospheric and magnetic forces, cosmic dust, etc., depend on the orbital elements and the satellite's shape, size, surface conditions, mass distribution and orientation. The work presents the satellite dynamics and modelling based on the orbital perturbation aerodynamic drag and solar disturbances [33]. The major part of the work discussed upon aerodynamic drag and solar radiation perturbations are the major perturbations, while in low earth orbit satellites the perturbation which has the maximum magnitude is an aerodynamic drag perturbation because the satellite orbit is too close to Earth's atmosphere which is the primary source of perturbation.

M. D. Shuster and S. D. Oh, (1981) "Attitude Determination from Vector Observations", Journal of Guidance and Control, Volume 4: Page No.70-77, the research work explains the different attitude determination techniques, the differences between them and finally contributed towards the selection of most efficient method for attitude determination [34]. Also, the work discussed the mathematical models to collect the inertial frame of reference & the vector component in the satellite body. The work based upon mathematical modeling of satellite dynamics is modelled using Euler's equations for a rigid body motion under the influence of internal and external torques. The author discussed the mathematical modelling of satellite dynamics are modelled by satellite rigid body dynamics with Euler angle equations. The angular motion of satellite changes due to internal disturbances and external disturbances. The attitude these components are used, typically in the form of a quaternion, Euler angles. It takes at least two vectors to estimate the attitude [35]. The main area of the work singular results for certain rotations and the Unit Quaternions are computationally less intense. Therefore, Unit Quaternions are more efficient method to be used for attitude determination.

Toshio Fukushima, (1996) "Generalization of Encke's Method and its Application to The Orbital and Rotational Motions of Celestial Bodies", The Astronomical Journal, National Astronomical Observatory, 2-21-1 Ohsawa Mitaka, Tokyo 181, Japan, Volume 112, Number 3, Received 1995 November 1; revised 1996 May 28. This paper described the several differential equation formulations such as Encke's method and their comparison of a given set of perturbations for a Low Earth Orbit satellite and finally contributed towards the selection of most efficient and accurate method in determining the exact perturbations [36].

WH Steyn, (2001), "Comparison of Low-Earth Orbiting Satellite Attitude Controllers Submitted to Controllability Constraints", the author worked on the Keplerian orbit how the satellite attitudes change with perturbation forces affecting on it [37]. The works present the magnetic torque control the satellite dynamics. The attitude control mainly introduces in the satellite orbital plane only not in the equatorial plane. It was further proposed that if the magnetic field can be taken as periodic changes in the earth's atmosphere. The stabilization platform is achieved by the magnetic moments produced by the satellite body consists of magnetic torque rods. This field interacts with a GEO magnetic field and produces the control signal to the actuator. In the orbit, Dipole is considered as a non-rotating platform with the combined earth magnetic field [38]. By the application of the above-mentioned theory on the stabilization of small/Nano satellite attitude control is achieved by magnetic torques or magnetic moments.

Jonas Elfving, (2002), "Attitude and Orbit Control for Small Satellites", the author presents various Sensors and estimations are used to predict the satellites current position, velocity, attitude and angular velocity [39]. The current work discusses about the designs pointing accuracy of a satellite when using different sensors and actuators so that a craft does not get too expensive. The work based on experimentally analyzed the satellite minimum solar radiation pressure at higher altitude has more effect on satellite, but its radiation influences aerodynamic drag that we have discussed in the atmospheric drag [39]. The orbital elements in the satellite change due to the periodic variations in solar pressure. For calculating the radiation in solar pressure, it's more important the satellite must focus to the SUN. It's clearly understood the author conclude the more orbital decay because of maximum solar radiation pressure.

A.M. Mohammed, A. Boudjemai, S. Chouraqui, (2006) "Magnetorquer Control for Orbital Maneuver of Low Earth Orbit Microsatellite", This work discussed various permanent magnet stabilization (PMS) and Gravity gradient attitude stabilization (GGS). The PMS method introduced the electromagnet into the satellite body frame. The work concentrates the alignment on the magnetic field in the coil with local magnetic moments. The author presents the satellite orbit rapidly decays because of the current in the electromagnet reduces when it is switched off. The satellite alignment controlled by radio signals commend to the electromagnets [40]. In Gravity gradient attitude stabilization, the Earth's gravity gradient is used to achieve vertical stabilization of a satellite. The GGS method the satellite vertical axis is perpendicular to the local magnetic fields. The author explains the attitude dynamics of the satellite along its axis. The attitude representation using Euler methods is widely discussed. The Euler method is used to measure the axis of rotation in the two axes of the satellite body with respect to the inertial reference frame. The satellite Z axis (or) Symmetry axis along with the direction of electromagnets used to stabilize the satellite frame [40]. The differences in Earth's gravitational pull across the satellite mass due to the minor changes in the distance from earth become a significant source of torques in orbits.

Karataş S, (2006) "LEO Satellites: Dynamic Modelling, Simulations and Some Nonlinear Attitude Control Techniques", A Thesis Submitted to the Graduate School of Natural and Applied Sciences of Middle East Technical University [15]. The author worked on the various types of perturbations and the variation of their magnitude of different orbits, which finally contributed towards the selection of most dominant perturbations for Low Earth Orbit satellites. There are two types of magnitude and density variation in solar maxima time and solar minima time. The variation in the solar cycle range is 200 to 250 kilometers and temperature vary from 600K to 1150K. The literature only included the Aerodynamic drag perturbations in the formulation of differential equations.

Diaz, Orlando X, (2010) "Analysis and comparison of extended and unscented Kalman filtering methods for spacecraft attitude determination", the author discussed the Extended Kalman filter (EKF) is used widely for nonlinear error estimation [41].

The objectives of the work minimize probability distribution function and standard deviation. The spacecraft attitude measurements were done using different on-board attitude sensors. The linear variation of sensor measurement KF predicts the future estimates [41]. For nonlinear variations of data from attitude sensors modeled by EKF, UKF and predict the state future estimate.

Wang, P (2010) "Attitude Control of Low-orbit Micro-satellite with Active Magnetic Torque and Aerodynamic Torque", The author presents the satellites use this principle for passive attitude stabilization by deploying gravity gradient booms and somehow dumping initial post-launch angular momentum those spacecraft's can maintain Earth-oriented position through their orbit [42]. There are gaseous and liquid particles present in the atmosphere of every planet and it provides resistance or a force of resistance which is termed as drag to the satellite body when passes through it. As the spacecraft comes to this type of the planet's atmosphere, it experiences the drag forces and it's greater during launch and reentry of a spacecraft into the space. The author worked on LEO satellite is in the altitude of 90 to 800km so the effect of this drag is more, and it will bring down from its nominal orbit [43]. There is some limit satellite enter the atmosphere. It has the effect on the atmospheric density and resulting in an increase in the density increase the atmospheric drag. In altitude 90 Kilometers rapid changes in temperature affect the orientation of the satellite. The author explains the disturbance torque like aerodynamic, solar pressure, magnetic flux, homogeneous of earth [43]. Also discussed the how this disturbance affects in the low earth orbiting satellite and its effects.

Murty S. Challa, (2016) "A Simple Attitude Unscented Kalman Filter: Theory and Evaluation in a Magnetometer-Only Spacecraft Scenario" The author worked on an Unscented Kalman filter to estimate the errors in the satellite from different on-board attitude sensor measurements [14]. The research work presents the various attitude orientation using Euler angle and Quaternion methods. The state space satellite model is developed with plant matrix and measurement matrix with Unscented Kalman Filter. The magnetometer used for attitude measurement with different angles. This work mainly minimizes the error covariance matrix and standard deviation [14].

2.2. Problem Statement

From literature reviews, the satellite attitude control system uncertainties are associated with the performance due to dynamic variations in orbital elements, with this background, the current work planned with the objective to study the performance comparison and enhancement of satellite attitude error modeling and control system design. The attitude of the satellite changes due to several parameters such as orbit types, perturbation forces, satellite parameters, space environments, etc. Because of the attitude variation the pointing accuracy of the spacecraft decreases gradually. The lifetime of the satellite depends upon the proper attitude control mechanism drawn from literatures. The control system is not designed properly; it will affect the mission performances and qualitative results. At low altitude is will have an enormous amount of drag due to the area and mass of the satellite and drag coefficient referred as ballistic $(\frac{m2}{C_d\ A})$ components. There are more gravitational attractions because of the earth's surface at LEO; whereas for GEO satellites having less/or no aerodynamic drag. These perturbation forces change the attitude/orientation of the Nano satellite Semi-Major axis, Inclination of the orbit, Eccentricity, Satellite position with Perigee location, Longitude of Ascending Node, Ascending node to perigee location, and circular orbit Mean anomaly or Eccentric anomaly. The satellite needs accurate orientation while Transmit/Receive the data and telemetry. For Example, The Solar panel should be deflecting line of sight with SUN. Communication unidirectional antennas transmit the signal to ground station require an accurate attitude. Remote sensing satellite needs capturing the terrain information through HD camera need accurate pointing accuracy. It's understood to design the accurate attitude control system of satellite very much important to save the mission life and proper data collection between satellites to control station. The satellite is launched from rocket booster. After firing all the fuels, the satellite moves under the influence of the gravitational field. Because of the initial momentum de-dumpling the satellite in 3D space. The satellite separated from rockets; requires the proper attitude control system. Until that can't serve the purpose solar panel not produces the power because of improper orientation towards SUN. The life span of the satellite based upon how much power in the satellite. For design the accurate attitude control system increases, the satellite mission life and performances. To avoid the space debris or space junks. To find the rate information star tracker fail to measure the rate information during high slew rates 0.5deg/Sec. The rate gyros measure the accurate rate information at all the times.

2.3. Research Objectives and Description

The following are the performance measures considered in the system

a) To analyze the perturbation in Low earth orbit satellite
b) To design and develop the attitude control system for Nano Satellite using suitable controllers.
c) To estimate the attitude errors from on-board sensors and implement the algorithm with Kalman Filter

In the real-world behavior compare with mathematical modeling and simulation are highly recommendable. Matching the results with environmental condition mostly requires in the space industry. The prime objectives for this research to design the high pointing accuracy attitude control for small satellite in low earth orbit. To minimize the errors, deviation and required control torque to command the actuator.

<u>Orbital Perturbation:</u> Low earth orbit perturbations like, Aerodynamic drag, solar drag, etc.

<u>Controller:</u> PD compensator designed for attitude control of Nano Satellite.

<u>Kalman Filter:</u> An attitude error modeling and predicts the position of states and angular rates of the Model.

2.4. Scope of the work

The Scope of the thesis is improvement of algorithm (Attitude control/ Attitude Error Estimation) in future applications and complex problems. The attitude control system (ACS) increases the lifetime of vehicle by incorporating the accurate control techniques in the satellite. The Attitude sensor like Rate Gyro’s highly reliable for attitude control. The reliability of the sensor reduces with time. The satellite losses mission effectiveness and performances because of the less pointing accuracy attitude mechanism and control methods. This problem is overcome with suitable controllers and attitude sensors added to the system. This is economically big challenge in the Aerospace Industry. It is important to maintain the accurate pointing accuracy and orientation of the satellite in the orbit. This will save the money and revenue in the space industry.

The proposed future work in the relevant area may be as follows:

1) Perturbation analysis at LEO
2) Developing the attitude control algorithm
3) Attitude error estimation from attitude sensors

The scope of this work analyzes the perturbation in the low earth orbit and how this affects the satellite parameters and orientation. To design the suitable controller for reducing the oscillation in the orbit and keep the satellite more time in the orbit. This project estimates the deviation of satellite from the nominal orbit to disturb or perturbed orbit. That variation measured by attitude sensors in the mission. To generate the counter moments in the actuators to deflect the control in the satellite like magnetic torques. The International Space Station (ISS) changes the altitude and attitude because of perturbation forces which required frequent thruster to keep the satellite into same altitude also in the same orbit. The ADCS is very much important to keep the satellite into the same orbit orientation. The accurate orientation schemes to achieve the most presided data collection of communications antennas, HD cameras, deploy the solar panels. At 1000KM altitudes there are more changes in the atmospheric environment due to gravitational attractions. It is necessary to generate more control actuation in LEO compare with high earth orbit GEO Synchronous Orbit (above 1000KM). The velocity of the low earth orbit is greater than the GEO orbits. The accurate navigation and control techniques mainly increase the mission life and income in the space industry. Attitude control is used to receive the proper data collection form the sensors and defects the solar panel with the same line of sight focus to SUN especially for back of power during eclipse time.

CHAPTER 3
VEHICLE ORIENTATION IN MICROGRAVITY CONDITION AT LEO

Vehicle orientations is described by coordinate system, two basic methods of coordination system used to represent the vehicle position with respect to inertial axes and vehicle body axes such as Quaternion method and Euler angles methods [44].

3.1 Representing Attitude Information

To represent the attitude (Pitch, Roll, and Yaw) of satellite, Euler angles transformation is accurate enough but sometimes singularity occurs in coordinate transformation. Quaternion representations are used as to avoid singularities [45]. To find the angular components (velocity) in satellite body frame with respect to the inertial reference frame, we assume the earth is an inertial reference frame originated with the center of Earth [46].

3.1.1 Euler Angles Methods

Euler angle method for describing the alignment of the vehicle body axes to inertial coordinate system [47]. To converts one frame into another frame direct cosine matrix (DCM), it is mostly used. Euler angles are Roll angle $\boldsymbol{\varphi}$ – Satellite Rotates about x-axis, Pitch angle $\boldsymbol{\theta}$-Satellite Rotates about y-axis, and Yaw angle $\boldsymbol{\psi}$ - Satellite Rotates about z-axis. The satellite rotations of body axis of the inertial reference axes shown in Figure (3.1). Euler angle has singularity problems as it won't measure the two rotations on the same axes. Overcome this, it is replaced by quaternion orientation to avoid singularity problems [47].

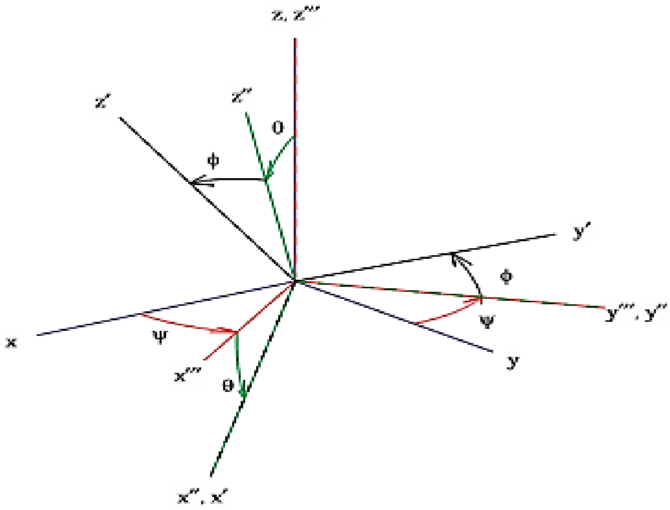

Figure (3.1) Satellite body axis to the inertial axis [47]

The rotation matrix equations are used to finding the position of vehicle frame to reference frame [48]. The satellite frames are b_1 & b_2 & b_3. The most conjoint method of rotation is 313 types. First rotations about the body from place to place b3 axes, Second, rotates the body from place to place b1, third rotates the body from place to place b3. Euler angles (See Figure 3.2) requires the latest transformation about satellite body frame to inertial frame. The roll angles ϕ deflects satellite about the x-axis, the pitch angles θ deflects satellite about the y-axis & the yaw angles ψ deflects satellite about the z axis. Euler angles (3.1) given below [48]

$$\Theta = \begin{pmatrix} \phi \\ \theta \\ \psi \end{pmatrix} \tag{3.1}$$

The rotation matrices (3.2), (3.3), (3.4) are given as follows:

$$R_{x,\phi} = \begin{pmatrix} 1 & 0 & 0 \\ 0 & cos\phi & -sin\phi \\ 0 & sin\phi & cos\phi \end{pmatrix} \tag{3.2}$$

$$R_{y,\theta} = \begin{pmatrix} cos\theta & 0 & sin\theta \\ 0 & 1 & 0 \\ -sin\theta & 0 & cos\theta \end{pmatrix} \tag{3.3}$$

$$R_{z,\psi} = \begin{pmatrix} cos\psi & -sin\psi & 0 \\ sin\psi & cos\psi & 0 \\ 0 & 0 & 1 \end{pmatrix} \tag{3.4}$$

As a result, the rotation matrix (3.5) R_B^o converts the body to orbit frame

$$R_B^o = R_z(\psi)R_y(\theta)R_x(\phi)\begin{pmatrix} c\psi c\theta & -s\psi c\phi + c\psi s\theta s\phi & s\psi s\phi + c\psi c\phi s\theta \\ s\psi c\theta & c\psi c\phi + s\psi s\theta s\phi & -c\psi\, s\phi + s\psi c\phi s\theta \\ -s\theta & c\theta s\phi & c\theta c\phi \end{pmatrix} \quad (3.5)$$

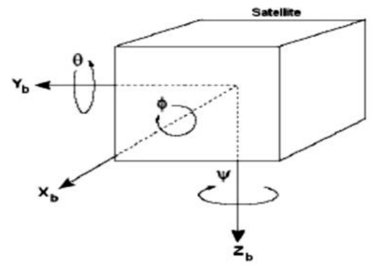

Figure (3.2) Euler Angles representation [48]

$$\boldsymbol{R}^{(inertial\ to\ Body)} = \boldsymbol{Rmat_i^T}\ (\boldsymbol{\psi})\ \boldsymbol{Rmat_j^T}\ (\boldsymbol{\theta})\ \boldsymbol{Rmat_k^T}\ (\boldsymbol{\phi}) \quad (3.6)$$

In real time applications, Euler angle attitude representation methods is well suited techniques to implement Nano satellite attitude control with on- board attitude sensors such as Inertial navigation system (INS) / Global position system (GPS) and Inertial measurement unit (IMU).

3.1.2. Quaternions Method

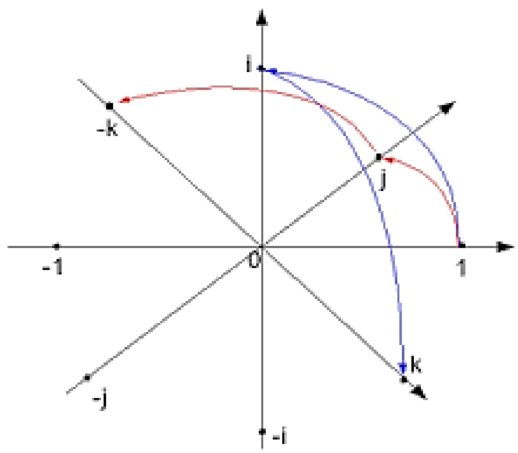

Figure (3.3) Quaternion diagram of transformation from satellite frame [49]

Quaternions method finds the orientation of the body with the help of Euler axis defined by unit vectors $e_i = (e_1\ \&\ e_2\ \&\ e_3)$ and the vehicle can be rotated by angle θ. Both parameters (e_i, θ) used to find the orientation with respect to the inertial frame in space. The dual quaternions have both magnitude and angle. Quaternion doesn't have any singularity problems [49]. It is used to measure the two rotations in same axes.

Table 3.1: Pros and cons of various orientation methods

Attitudes Transformation Methods	DCM	Euler Angles	Quaternions
Advantages	Satellite orientation define by direct cosine matrix	Satellite attitudes (Roll, Pitch, Yaw) If given, the inimitable orientation is defined	No Singularity Problems
Dis-Advantages	Six limitation must be met, non-instinctive	Singularity Problems Exist	Requires Transform Techniques

The proposed research work implements the Quaternion which converts the rotation matrix and transforms it to another frame. In Table 3.1 gives the advantage and disadvantages of various orientation techniques. It has four elements compared to the Euler transformation which has nine elements. The propagation of satellite orientation is calculated by a quaternion. Quaternion method is a more useful transformation from the body frame (satellite) to the inertial frame as compared to the Euler method [50].

Quaternion (q) defines as $q = \xi + i\epsilon_1 + j\epsilon_2 + k\epsilon_3$

It consists of 4 elements, ξ is real value, $i\epsilon_1$, $j\epsilon_2$, and $k\epsilon_3$ is imaginary values.

$$\eta = \cos\frac{\varphi}{2}\ ,\ \varepsilon = \begin{bmatrix} \varepsilon_1 \\ \varepsilon_2 \\ \varepsilon_3 \end{bmatrix} = \begin{bmatrix} k_x \sin(\varphi/2) \\ k_y \sin(\varphi/2) \\ k_z \sin(\varphi/2) \end{bmatrix} \quad , \quad q = \begin{bmatrix} \eta \\ \varepsilon_1 \\ \varepsilon_2 \\ \varepsilon_3 \end{bmatrix} \tag{3.7}$$

The quaternions expressed in the satellite body to orbit (rotation matrix) as: [50]

$$R_B^0\,(q) = R_{\eta,\varepsilon} = I_{3X3} + 2\eta S\,(\varepsilon) + 2S^2\,(\varepsilon) \qquad (3.8)$$

Quaternion rotation matrix is shown in equation (3.9) R_B^o can be written as: [50]

$$R_B^o = \begin{pmatrix} 1-2(\varepsilon_2^2+\varepsilon_3^2) & 2(\varepsilon_1\varepsilon_2-\varepsilon_3\eta) & 2(\varepsilon_1\varepsilon_3+\varepsilon_2\eta) \\ 2(\varepsilon_1\varepsilon_2+\varepsilon_3\eta) & 1-2(\varepsilon_1^2+\varepsilon_3^2) & 2(\varepsilon_2\varepsilon_3-\varepsilon_1\eta) \\ 2(\varepsilon_1\varepsilon_3-\varepsilon_2\eta) & 2(\varepsilon_2\varepsilon_3+\varepsilon_1\eta) & 1-2(\varepsilon_1^2+\varepsilon_2^2) \end{pmatrix} \qquad (3.9)$$

When compared to both attitude determination techniques (Euler & Quaternion), Unit Quaternion method is more commonly used, because this method is not singular for any rotations, while Euler Angles can give singular results for certain rotations. The Unit Quaternions are computationally less intense [50]. Therefore, unit quaternions are more efficient method used for attitude determination.

It has both real and complex numbers coveting the vector from quaternion operation having 30 floating value and 45 processes to transform from a quaternion to a matrix. It was first defined by William Rowan Hamilton. It avoids the singularity difficult in Euler angle transformation from one frame to another frame. The above diagram (Figure 3.3) discuss the two reference frames (x_A, y_A, z_A) and (x_B, y_B, z_B), satellite rotates about z-axis. In case both vectors in both the frames are same, but different value in x component and the y component [51]. The vector 'u' can be described in any frame. For example, vector u has same length and it is significant to describe the quaternion. Quaternion frame 1 to frame 2 converts a vector. Frame 'A' vector denoted to Frame 'B' vector. Quaternion defines the magnitude and direction.

This same quaternion might be notated instead as qBA, where the order of the subscripts now indicates that the quaternion converts the position and velocity in the frame 'A' vector quantity into frame 'B' vector quantity. This form can be helpful when combining quaternions in order as discussed below. Both are used in practice and it is important to always verify the rotation represented.

3.1.3. Geometrical Definitions

The transformation (See Figure: 3.4) from an inertial reference (I, J, K) frame to local orbital frame ($\boldsymbol{x}_o$, $\boldsymbol{y}_o$, $\boldsymbol{z}_o$) is performed by means of the Euler rotation sequence via the rotation angles (**Ω**, *i*, *u*) [53]. The latitude angles denote, *u* = argument of perigee ($\dot{\omega}$)+ true anomaly (ν). The angle of inclination is given by *i (rad/sec),* and vernal equinox with respect to the perigee is given by **Ω** [53].

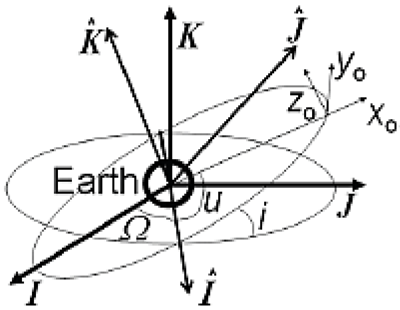

Figure (3.4) Inertial Coordinate (*I*, *J*, *K*) and Orbital Coordinate [53]

The local orbital coordinates (See Figure 3.5) reference ($\boldsymbol{x}_o$, $\boldsymbol{y}_o$, $\boldsymbol{z}_o$) system and Earth Frame is satellite frame is attached to the center of the body called as reference Frame ($\boldsymbol{x}_b$, $\boldsymbol{y}_b$, $\boldsymbol{z}_b$). The nominal attitudes RF is along the orbital reference axes; $\boldsymbol{x}_b$=$\boldsymbol{x}_o$, $\boldsymbol{y}_b$=$\boldsymbol{y}_o$, $\boldsymbol{z}_b$=$\boldsymbol{z}_o$. In this case, the y_b axis is nominally along the velocity direction $\boldsymbol{V}$ [54].

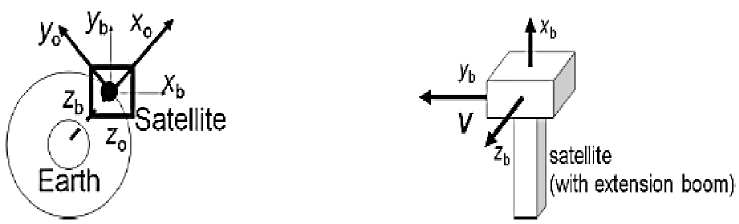

Figure (3.5) (a) Orbital Frame and (b) Body centered Reference frame [54]

The proposed methods study the series of transformations from the orbital coordinate system to the reference frame is 3-2-1 via the (Yaw, Pitch, Roll) angles. [54]

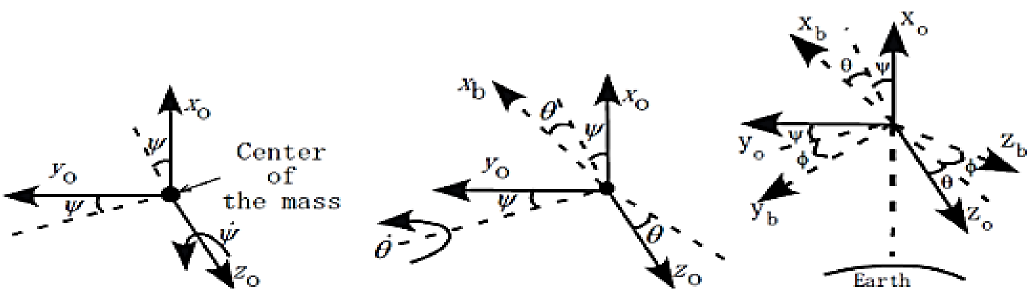

Figure (3.6) Satellite reference frame to orbital reference frame [55]

For, Satellite rotates about the

Satellite rotation about the x_o axis called as ϕ (Roll angle)

Satellite rotation about the y_o axis called as θ (Pitch angle)

Satellite rotation about the z_o axis called as ψ (Yaw angle)

Consider the sketch of Figure 3.6, where *z*-axis indicates yaw rotations and the y axis indicates pitch rotations, and *x*-axis indicates roll rotations [55].

3.1.4. Orientation of the Satellite

Coordinate frame (CF) is used to find the location of the vehicle with respect to the orientation of reference frame as shown in Figure. 3.7. Here, satellite frame is called as a rotating body frame [56]. The following assumption are considered for the simulations, Earth is an inertial reference frame which is fixed. It denotes as a non-rotating frame [56].

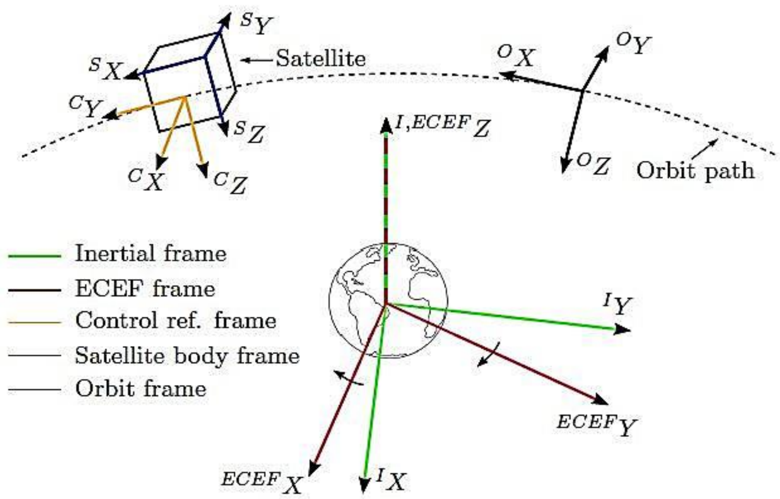

Figure (3.7) Different types of coordinate frame [56]

Earth-Centered Earth Fixed Frame (ECEF): The ECEF is located at the center of earth. The X-axis & Y-axis rotates in the Earth center inertial (ECI) frame or non-rotating frame [57]. We consider earth is an inertial reference frame. The Z-axis located in North Pole. The X-axis crosses among the Greenwich Meridian (GM) and the Equator. This point both longitude and latitude are considered as 0^o degree. The Y-axis considers as right-hand coordinate system [58].

Satellite Body Frame: The body frame is located at the satellite body mass in the center. The body frame attached to the vehicle frame. The Sz-axis located in the Nadir direction of the satellite [57]. The Sx-axis and Sy-axis crosses the orbit frame when the attitude of satellite referred as 0^o degree [57]. In this case all the attitude of satellite pitch, yaw, and roll angles become zero.

Earth center Inertial (ECI) Frame: ECI frame is fixed in space. The Ix-axis located from vernal equinox at satellite concentration on the Earth's surface. This Iz-axis represent the angular velocity direction of the orbit. The axis Iy is orthogonal to Ix and Iz [58].

Orbital Frame: The orbit frame originates with satellite (vehicle) center of the mass. The Nadir position is represented by the axis O_z [57]. This point, the satellite concentration of the earth's surface. The axis Ox represents Satellite motion in the body. Also, axis ox $\perp$ oz. The axis Oy represents the complete right-hand coordinates [58].

3.2. The Earth-Satellite System (Satellite Equation of Motion)

We consider the mass m_1 referred as the earth mass and m_2 as the satellite mass; Newton law of gravitation states that the force of attraction increases when Earth mass and satellite mass increase. Forces of attraction reduce when the distance between the two masses increase [24].

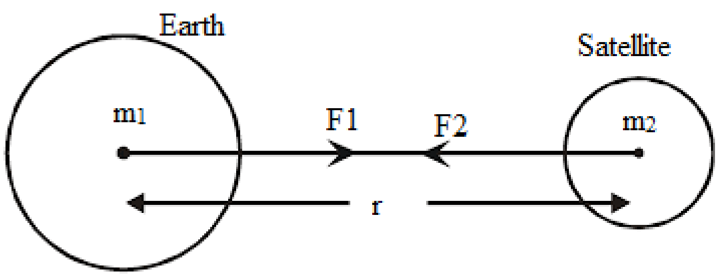

Figure (3.8) Gravitational force between two masses [24]

Where: F1=F2= Attraction forces between two bodies (Large body =Earth; Small body = Satellite), N

G =Gravitational element (constant), ($G = 6.674*10^{-11}$ N m^2 kg^{-2})

m_1 = Consider earth mass, large mass, Kg

m_2 = Consider flying object or satellite, small mass, Kg

r = Line connecting from the earth center to satellite center, m

Two bodies problem considers the Earth and satellite body. This is the easy methods of N-Body problems. Large mass (Earth) considers m_1 & Small mass (satellite) consider m_2. The n-body equation becomes [24]

$$F_1 = m_1\ddot{r}_1 = Gm_1m_2 \frac{r_2 - r_1}{|r_2 - r_1|^3} \quad (3.10) \qquad F_2 = m_2\ddot{r}_2 = Gm_1m_2 \frac{r_1 - r_2}{|r_1 - r_2|^3} \quad (3.11)$$

Combining the equations (3.10) & (3.11) gives: $F_1 = m_1\ddot{r}_1 =$

$$Gm_1m_2 \frac{r_2 - r_1}{|r_2 - r_1|^3} \quad (3.12)$$

And with $r = r_2 - r_1$; $\quad \ddot{r}_2 - \ddot{r}_1 = -G(m_1 + m_2)\frac{r_1 - r_2}{r^3}$ (3.13)

Hence the equation (3.13) is the satellite motion equations of two body.(Primary body, Earth – Secondary body, Satellite) problems [24].

3.2.1. Geometry of Satellite Orbits

The orbit of the satellite follows the geometry conic section. The conic sections consist different joint of plan and cone. Sections are circle, ellipse, parabola, Hyperbola. Circle connects horizontal line, ellipse joins incline slope in the cone, see Figure 3.9. Both curves intersect and make a closed path. The consequential path joins/connect the Hyperbola [57].

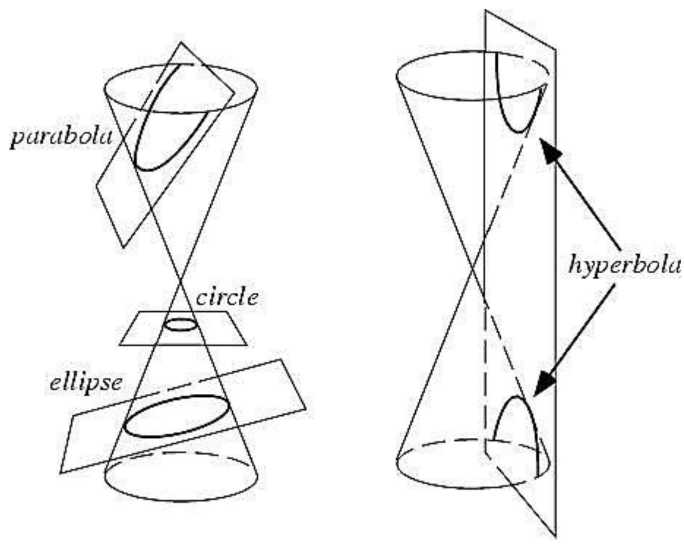

Figure (3.9) Conic Section (Circle, Ellipse, Parabola, Hyperbola) [57]

The parabolic curve is single margin as it creates the elliptical path from the hyperbolic path with parallels to the conic section. The peri-center & apo-center, two points connect the orbit, peri-center is a point where satellite is closest to the object orbiting the Earth's surface.

In Figure 3.10 (a) shows the distance from apogee to perigee point, (SMA) **a**, Size of the orbit (Ecc) **e,** apo-center it's a point where satellite furthest away from the object orbiting the earth's surface. In Figure 3.10 (b) shows the true anomaly, angle between vernal equinoxes to ascending node (**Ω**), angle between perigee to line of nodes from south to north pole, (ω) **ae** is the distance between the centers of earth with respect to center of the focal point. It is determined by the eccentricity of the orbit with respect to the conic section. The eccentricity determines the type of orbit obtained [24]. In Table 3.2 shows the Keplerian parameters.

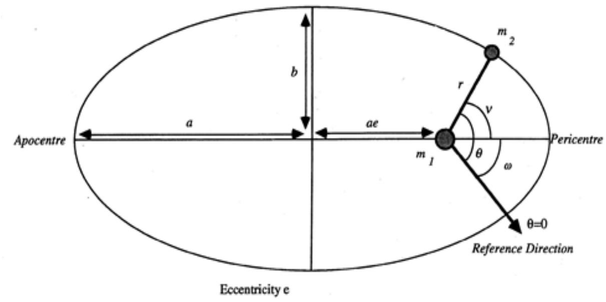

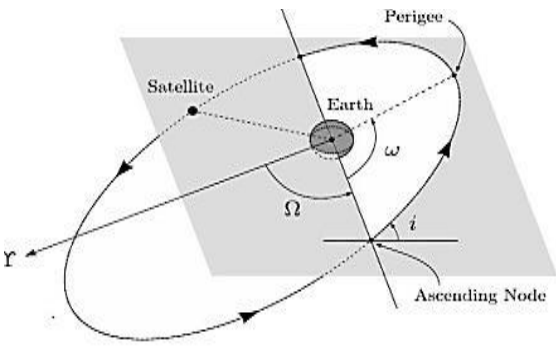

Figure (3.10) (a) Satellite (major/Minor) axis [57]

(b) Satellite position [26]

The orbital eccentricity to determine the shape of the orbit, also other Keplerian element is mentioned in the Figure (3.10). To find the position of the satellite by the knowledge of the angular shift from perigee point to satellite velocity vector direction.

Table 3.2: Description of Keplerian Elements

Elements	Name	Description
A	Semi-major axis	See Figure 3.10 (a)
E	Eccentricity	When multiplied with a, it gives the distance from the epicenter of the orbit to the principal point
I	Inclination	The angle between the equator plane and the orbit plane
Ω	Vernal Equinox (VE) w.r.t (RAAN) Ascending node	Satellite moving from south to north path crosses to the Equator with VE.
Ω	Argument of perigee	Describes the orientation of the orbit
N	True anomaly	The angle between the satellite position to the perigee position

The size of the orbit determines by semi-major axis (SMA) [24]. The size and shape of the orbits represent by Keplerian orbital elements. These elements are mostly used to design the specific characteristics of the orbits (Circular or Elliptical). Also, it describes the orbital motion include mean orbital rates of the satellite

Table 3.3 Orbits with corresponding eccentricities [24]

Eccentricity	Orbit
e = zero	Circular path
The value 'e' between 0 to 1	Elliptical path
e = one	Parabolic path
e greater than 1	Hyperbolic path

In Table 3.3 describe the path of an orbit accurately. The six orbital elements used to fully define an orbital motion of the satellite. The proposed methods discuss the Runge - Kutta Numerical integration to solve ordinary differential equations (ODE) of the orbital motion.

3.2.2. Satellite coordinates and Keplerian equations

In this section (3.2.2) discusses the, classical orbital parameter that is often used is mean anomaly M. In this thesis 'M' used instead of true anomaly ν (Low Earth Circular Orbits). M is defined by equation [59]

$$M = \epsilon - e * \sin\epsilon\,, (3.14) \qquad \cos\epsilon = \frac{e + \cos * \nu}{1 + e * \cos * \nu} \qquad (3.15)$$

The velocity vectors $$\overrightarrow{velocity} = \dot{r}\overrightarrow{e_r} + r\theta\overrightarrow{e_\theta} \qquad (3.16)$$

Acceleration vector $$\overrightarrow{acceleration} = \left(\ddot{r} - r\dot{\theta}^2\right)\overrightarrow{e_r} + (r\ddot{\theta} + 2\dot{r}\dot{\theta})\overrightarrow{e_\theta} \qquad (3.17)$$

Hence, the motion equation (3.16) & (3.17) into circular and diagonal direction

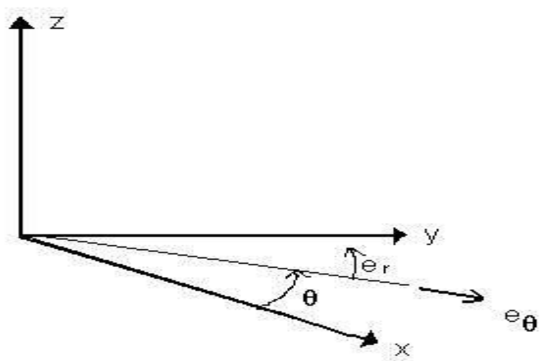

Figure (3.11) Polar coordinates (r, θ) vehicle equation [59]

There are many coordinate systems which explain the satellite motion in the body frame w. r .t inertial frame of reference. Polar coordinate system is easy to describe the orbital mechanics [37]. It has two quantities (r, θ) unit vectors are e_r and e_θ.

In the circular direction the motion equation is

$$\boldsymbol{\ddot{r} - r\dot{\theta}^2 = -\frac{\mu}{r^2}} \tag{3.18}$$

Considered for the simulation's Gravitational parameter, **G** and Mass of the satellite **m** then constant μ is a product of the gravitational constant and the mass of the vehicle Let, μ = G * m this equation expresses mainly acceleration in circular direction [25]. In motion equation diagonal direction

$$r\ddot{\theta} - 2\dot{r}\dot{\theta} = 0$$

This can be restated as

$$\frac{1}{r}\frac{d}{dt}\left(r^2\dot{\theta}\right) = 0$$

$r^2\dot{\theta}$ is constant. $r^2\dot{\theta}$ is equal to the angular momentum per unit mass; h

$$\ddot{r} - \frac{h^2}{r^3} = -\frac{\mu}{r^2} \qquad r(\theta) = \frac{\frac{h^2}{\mu}}{1+\frac{Ah^2}{\mu}\cos(\theta-\theta_0)} \tag{3.19}$$

Where, A and θ_0 are constants. Hence, the equation (3.19) has denoted the polar coordinates of satellite motion [25].

Vectors & Matrices

Notation: Vectors are used to represent the magnitude and direction in 3D space. Vector is connected to the coordinate frame of reference to the Matrix. Vector is the value and its quantity which is used to describe the frame. Matrixes represent the axis (x, y, z)

The Matrix Riccati equations

$$C = P\dot{C} + CP^T - CM^TR^{-1}\,MC + Pn$$

Which relates to the state covariance C; to the plant model P; plant spectral density matrix Pn; the measurement matrix M;

The equation (3.20) of an ellipse is $r(v) = \frac{a*(1-e^2)}{1+e*\cos*v}$ (3.20)

The satellite position with respect to center of object is orbited to Earth considers as **r**, semi-major axis **a**, See Figure 3.12, orbital eccentricity **e** & true anomaly is **ν**. It is simplified at the peri-center and apocentre. [24]

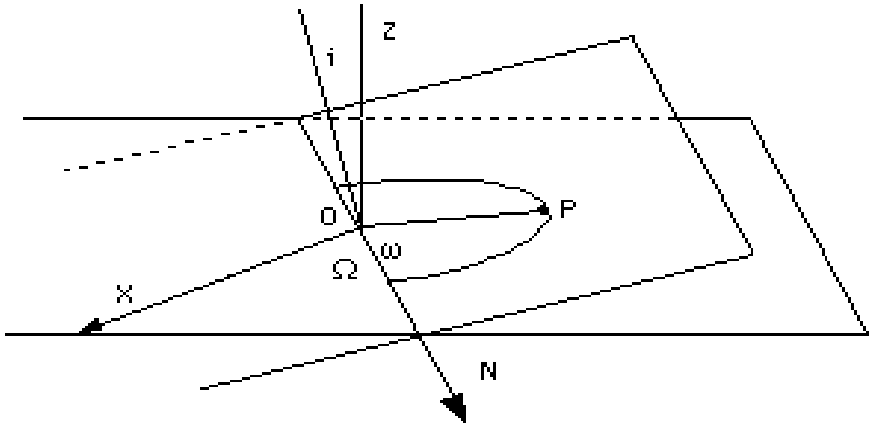

Figure (3.12) Keplerian elements with satellite position in the orbit [24]

At the peri-center ν = 0 & $r_p = a(1-e)$

At the apo-center ν = π & $r_a = a(1+e)$

The orbit is found by identifying

$$h^2 = \mu(1-e^2) \quad (3.21)$$

At the pericentre, angular momentum per unit mass, h, is $r_p v_p$. As h is conserved,

$$a^2 (1-e)^2 v_p^2 = \mu\, a\, (1-e^2) \quad (3.22)$$

This results in the equation (3.22) for peri-center velocity (3.23)

$$v_p = \sqrt{\frac{\mu\, 1+e}{a\, 1-e}} \quad (3.23)$$

Similarly, speed in the apocentre is found to be total energies (See equation 3.24)) is expressed as combining potential energy (P) and kinetic energy (K); **E = P + K,** the total energy E per unit mass is [24]

$$E = \frac{1}{2}v^2 - \frac{\mu}{r_{earth}} \quad (3.24)$$

At the peri-center

$$E = \frac{1}{2}\left(\frac{\mu}{a}\frac{1+e}{1-e}\right) - \frac{\mu}{a(1-e)}$$

The energy equation (3.25) can be restated as

$$E = -\frac{\mu}{2a} \tag{3.25}$$

Substitute equation (3.25) to (3.24)

$$\frac{1}{2}v^2 - \frac{\mu}{r_{earth}} = -\frac{\mu}{2a}$$

Hence, the equation (3.26) of velocity on an elliptical orbit

$$v^2 = \mu\left(\frac{2}{r_{earth}} - \frac{1}{a}\right) \tag{3.26}$$

The time periods of the orbit (3.27) calculated from the cube of the semi-major axis and gravitational parameter and its results

$$\text{Time periods } = 2\pi\sqrt{\frac{a^3}{\mu}} \tag{3.27}$$

Circular Orbits, Parabolic Orbits & Hyperbolic Orbits:

For a circular orbit, Radius r_{earth} is constant for all; the point in the orbit, Eccentricity of the orbit is remaining zero, the circular velocity (3.28) and time periods (3.29) equations of the circular orbit given by [25]

$$\text{Circular velocity} = \sqrt{\frac{\mu}{r_{earth}}}, \tag{3.28}$$

$$\text{Time Period} = 2\pi\sqrt{\frac{{r_{earth}}^3}{\mu}} \tag{3.29}$$

For parabolic orbit eccentricity is one, Velocity equation (3.30) is given by

$$\text{velocity} = \sqrt{\frac{2\mu}{r_{earth}}} \tag{3.30}$$

The time taken to complete one orbit, T → infinity since the semi major axis are → infinity [39].

For, eccentricity in the orbit is (hyperbolic path) e > 1. The velocity equation (3.31) is given by

$$v^2 = 2\frac{\mu}{r_{earth}} + {V^2}_{\infty} \tag{3.31}$$

Where, free stream velocity (3.32) expressed as

$$V_\infty = \sqrt{\frac{GM}{a}} \tag{3.32}$$

Locating/Position of the Satellite Orbit:

To find the position vectors (3.33) of object (satellite) with respect to perigee [24].

$$\mathbf{r}_{\mathbf{initial}} = \frac{\mathbf{a(1-ecc^2\ )}}{\mathbf{1+ecc * cosT_{anomaly}}} \tag{3.33}$$

Where:

- ecc: eccentricity of the orbit
- a: line connecting from apogee and perigee (Semi-major axis)
- $r_{initial}$: radius from the foci of the planet
- $T_{anomaly}$: True anomaly (measure of the angle from the perigee to the position of the satellite

To Calculates the flight path angle (3.34) and velocity (3.35) of spacecraft by following relations [24]:

$$\text{Flight path angle} = \mathbf{arctan}\left(\frac{\mathbf{ecc*sinT_{anomaly}}}{\mathbf{1+ecc*cos\ T_{anomaly}}}\right) \tag{3.34}$$

$$\text{Velocity} = \sqrt{\mathbf{G} * \mathbf{m_1}\ \left(\frac{\mathbf{2}}{\mathbf{r_{earth}}} - \frac{\mathbf{1}}{\mathbf{a}}\right)} \tag{3.35}$$

Energy equation for satellite:

The Energy equation (3.36) of the satellite is calculated by the difference between P and K. From the equation mass of the vehicle/satellite $\mathbf{m_2}$, and satellite velocity as **V,** and Semi-major axis as, **a** [25]

$$E = \frac{\mathbf{m_2 V^2}}{\mathbf{2}} - \frac{\mathbf{Gm_2}}{\mathbf{a}} \tag{3.36}$$

The circular velocity (3.37) of an orbit around an object is defined as [25]:

$$\mathbf{V_{circular}}\ (\mathbf{Vc}) = \sqrt{\frac{\mathbf{K^2}}{\mathbf{r_{earth}}}} = \sqrt{\frac{\mathbf{G*m_1}}{\mathbf{r_{earth}}}} \tag{3.37}$$

Where, for Earth

K^2 = Gravitation constant * Mass of the earth = 3.98* 10^{14} m^3 / s^2, Earth radius ($\mathbf{r_{earth}}$) = 6.37 * 10^6 m, Hence, for escape from earth into circular orbit need velocity of **7.9 km / Sec**

Time Periods Calculation of a Satellite given in equation (3.38)

$$T = (2\pi \mathbf{r_{earth}}^{\frac{3}{2}}) / (K) \tag{3.38}$$

3.2.3. The Three-Body Problem

The controlled 3-body problem is a very good way to describe the forces between Earth, the Moon and a satellite. It consists of a system that includes three masses moving in a plane. Let us assume that Earth has mass m_1, the Moon mass m_2 and the satellite mass m_3. Mass m_3 is a lot smaller than m_1 and m_2, so it can be neglected [24]. The law of gravitation gives gravity force F $^{\sim 1}$ on Earth from the Moon and gravity force F $^{\sim 2}$ the opposite way. They are given in (equation 3.39)

$$F_1 = -F_2 = k^2 \frac{m_1 m_2}{L^2} b_1 \tag{3.39}$$

Let k = Gaussian parameter of gravitation & L is the distance between body 1 and 2. The vector from Earth' center to the Moon center of rotates with an angular velocity $\omega_{earth/moon} = \omega_{b3}$ Earth has position $R_1 = -x_1 b_1$ And $R_2 = -x_2 b_2$ The Moon has Position L Vector is given by L=x1+x2. [24]

The acceleration becomes in equations (3.40) and (3.41)

$$\ddot{a}_1 = \omega_{earth/moon} X \left(\overrightarrow{\omega_{earth/moon}} X \vec{R}_1\right) = \omega^2 x_1 \overrightarrow{b_1} \tag{3.40}$$

$$\ddot{a}_2 = \omega_{earth/moon} X \left(\overrightarrow{\omega_{earth/moon}} X \vec{R}_2\right) = \omega^2 x_2 \overrightarrow{b_1} \tag{3.41}$$

The gravitational and centrifugal forces are in balance. This gives

$$k^2 \frac{m_1 m_2}{L^2} = m_1 x_1 \omega^2 = m_2 x_2 \omega^2$$

And from this Kepler's third law is found at

$$\omega^2 = \frac{k^2 M}{L^3}$$

Where M = m1 + m2.

The position (3.42) of satellite is

$$r = x\overrightarrow{b_1} = y\vec{b}_2 \tag{3.42}$$

The velocity (3.43) of satellite is

$$\vec{v} = \frac{d\vec{r}}{dt} + \vec{\omega}_{ib}\, X\, \vec{r} = \dot{x}\overrightarrow{b_1} + \dot{y}b_2 + \omega(x\overrightarrow{b_2} - y\overrightarrow{b_1}) \quad (3.43)$$

And the acceleration becomes (3.44)

$$\vec{a} = \frac{d^2}{d^2t}\vec{r} + 2\overrightarrow{\omega_{\iota b}}\, X\, \frac{d}{dt}\vec{r} + \vec{\alpha}_{ib} X\, \vec{r} + \overrightarrow{\omega_{\iota b}}\, X\, (\overrightarrow{\omega_{\iota b}}\, X\, \overrightarrow{r}) \quad (3.44)$$

The motion (3.45) of the moving vehicle can be described as [24]

$$\overrightarrow{F_3} = -k^2\frac{m_1 m_3}{{r_1}^3}\left\lfloor (x + x_1)\overrightarrow{b_1} + y\overrightarrow{b_2}\right\rfloor - k^2\frac{m_2 m_3}{{r_2}^3}\left\lfloor (x + x_2)\overrightarrow{b_1} + y\overrightarrow{b_2}\right\rfloor, \quad (3.45)$$

Where,

$$\overrightarrow{r_{v1}} = \sqrt{(x + x_1)^{\,2} + y^2}, \qquad \overrightarrow{r_{v2}} = \sqrt{(x + x_2)^{\,2} + y^2}$$

In x and y direction this results in

$$\ddot{x} - 2\omega\dot{y} - \omega^2 x = -k^2\left[\frac{m_{\,1}}{{r_1}^3}((x + x_1) + \frac{m_2}{{r^3}_2}(x - x_2)\right]$$

$$\ddot{y} + 2\omega\dot{x} - \omega^2 y = -k^2\left(\frac{m_1}{{r_1}^3} + \frac{m_2}{{r_2}^3}\right)$$

This model is usually presented in normalized form where the distances are divided by L and τ = ωt. [24]

The General N-Body Problem:

The system involving of many bodies, the summation of all forces acting on the i^{th} body (3.46) [24]

$$F_i \;= G\sum_{j=1}^{j=n}\frac{m_i m_j}{r_{ij}^3}\;(r_{j-}r_i)\,, \quad i\; not\; equal\; to\; j; \quad (3.46)$$

It follows from Newton's 2^{nd} law of motion in equation (3.47)

$$\frac{d^2r}{dx^2} = G\sum_{j=1}^{j=n}\frac{m_i}{r_{ij}^3}\;(r_{j-}r_i\,)\,, \quad i \neq j; \quad (3.47)$$

3.2.4. Equations of satellite Euler rates

The motion equation of the vehicle or satellite obtained from the total angular (3.48) momentum [60]. $H_{total} = R_{max} * H_{satellite}$ (3.48)

$H_{satellite}$ is the angular momentum for the satellite body frame; R_{max} is the transformation from one frame to another frame (Satellite frame to an inertial frame of reference) [60]

The torque (3.49) on the satellite, $T_{Satellite} = \dot{H}_{Satellite} + \omega \times H_{satellite}$ (3.49)

For, Rigid body $H_{satellite} = I * \omega$ (3.50)

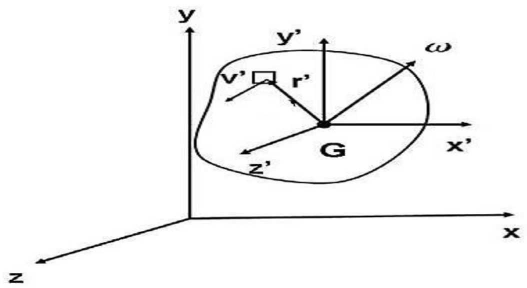

Figure (3.13) Angular velocity and Rates in body frame [60]

In Figure (3.13) illustrate the motion of the satellite under the influence of gravitational force. The variables are defined as the position vector **r**, Velocity vector **v**, angular rate **ω.** The satellite velocity changes due to the angular velocity V_θ (kinetic motion of the vehicle). The angular momentum of the satellite calculates in the satellite body with respect to the inertial reference frame [62]. The orbit frame (Local Vertical Local Horizontal frame-LVLH), satellite body frame, inertial frame one more frame is referred as earth frame. The body frame is fixed with satellite and principle moment of inertia. The proposed analysis considers the orbit frame (3.51) and earth frame (3.52) angular velocity in the inertial frame [63]

$$\omega_{(orbit-Inertial)} = R_{mat(Orbit-Body)} \cdot \Omega_o \text{ (Orbit)} \quad (3.51)$$

$$\omega_{(Earth-Inertial)} = R_{mat(Earth-Body)} \cdot \Omega_e \text{ (Earth)} \quad (3.52)$$

In this thesis considered the attitude sensor is (INS/GPS and IMU) used to measure the angular rates (Pitch **θ**, Yaw **ψ**, and Roll **ϕ**) information in satellite frame. Then, it converts to angular rates of the vehicle body and the orbit frame by using Direct cosine matrix (DCM) the rotation 3-2-1 as equation (3.53) given below [62]

$R_{mat_{(orbit\ to\ body)}} =$

$$\begin{bmatrix} c\theta c\psi & c\theta s\psi & -s\theta \\ -c\phi s\psi + s\phi s\theta c\psi & c\phi c\psi + s\phi s\theta s\psi & s\phi c\theta \\ s\phi s\psi + c\phi s\theta c\psi & -s\phi c\psi + c\phi s\theta s\psi & c\theta c\phi \end{bmatrix} \quad (3.53)$$

C= cos and S = sin terms,

To find the angular velocity (3.54) in the body to orbital frame [62]

$\omega_{\text{(Body-Orbital)}} = (\dot{\phi} - \psi\, S\, \theta)\, \overrightarrow{S_{b_1}} + (\dot{\theta}\, C\, \phi + \dot{\psi}\, S\, \phi \cos\theta)\overrightarrow{S_{b_2}} + (\dot{\psi}\, C\, \theta\, C\, \psi - \dot{\theta}\, C\, \phi)\, \overrightarrow{S_{b_3}}$
(3.54)

Unit vectors are = $\overrightarrow{S_{b_1}}, \overrightarrow{S_{b_2}}, \overrightarrow{S_{b_3}}$, From equation (3.54) find the Euler rates as [63]

$$\begin{aligned} \dot{\phi} &= \omega_1 + \omega_2 \tan\theta \sin\phi + \omega_3 \tan\theta \cos\phi \,, \\ \dot{\theta} &= \omega_2 \cos\phi - \omega_3 \sin\phi \,, \\ \dot{\psi} &= \frac{\omega_2 \sin\phi + \omega_3 \cos\phi}{\cos\theta} \,. \end{aligned} \quad (3.54)$$

In this section (3.2.3) for integrating the rate equation found the Euler angles. This angle represents a satellite reference to orbit reference. The magnetometer is used to detect the attitude of satellite. This signal compare with reference orbit trajectory produces the errors to the PD controllers. The actuator generates the control voltage to trigger the dynamic of satellite at low earth orbit NANO Satellite. The magnetic torques produces the control torque to the satellite [64]. Also correct the attitude errors in the body coordinates. The major role of attitude determination and control system is to bring from satellite perturbed path into an actual orbit path.

CHAPTER 4

MATHEMATICAL MODELING OF SATELLITE DYNAMICS

The proper attitude determination and control (ADCS) system used to stabilize the satellite into pre-determined attitude. The design requirements included this thesis, types of orbit, perturbation forces, types of satellite, and types of space environments. The satellite attitude sensors provide the rate information such as Rate Gyro's, Sun sensor, Star Sensor, Magnetometer [65], [66]. The control is delivered by suitable actuators Momentum Wheels or Magnetic Torquers. The Attitude control algorithm based upon differences between the original attitude signal and feedback signal measured from attitude sensor. The changes in attitude due to the perturbation force it generates the errors in the actuator for maintaining the desired attitude for design the suitable controllers to actuate the actuator to the required attitudes [67], [68].

Angular Momentum = Spacecraft Moment of Inertia * Angular Velocity

$$H = I_{sc}\,\dot{\omega}_{(I/B)} \tag{4.1}$$

$I_{sc} = [I_{xx}\ I_{yy}\ I_{zz}]$ = Spacecraft Moment of Inertia

4.1. Dynamics of the Satellite

The dynamics of satellite derived from angular momentum (4.1) equation. Angular velocity is considered for the simulation, Inertial Reference Frame must be expressed in Body Frame [69].

$$H=\begin{bmatrix} Ixx & 0 & 0 \\ 0 & Iyy & 0 \\ 0 & 0 & Izz \end{bmatrix} \dot{\omega}_{(I/B)} \tag{4.2}$$

$$\dot{\omega}_{(I/B)} = (\dot{\phi}-\Omega_0\psi)\widehat{b_1} + (\dot{\theta}-\Omega_0)\widehat{b_2} + (\dot{\psi}-\Omega_0\phi)\widehat{b_3} \tag{4.3}$$

The angular momentum in the satellite having two parts, one is Angular momentum in the satellite body (H_s), and another angular momentum in the momentum wheel (H_w).

$$H = H_{satellite\ body} + H_{Momentum\ Wheel}$$

It rotates Vehicle/Satellite body with respect to the center of mass. The rate of change of angular momentum is called as external moments [70]

$$M = \left(\frac{dH}{dt}\right)_{Inertial} = \left(\frac{dH}{dt}\right)_{Body} + \dot{\omega}_{(I/B)}\, H \qquad (4.4)$$

To design the attitude determination and control system (ADCS) considered the external moments, including the perturbation forces such as Aerodynamic force, Solar force, Gravitational attraction of the body.

Euler angle and angular rates measured from the torque equation, the attitude dynamics of the satellite equation (4.5), (4.6), (4.7) as given below (pitch, roll, and yaw) [70]

$$\frac{\phi\ (s)}{T_x\ (s)} = \frac{\frac{1}{I_x}}{S^2 + \frac{K_{vx}}{I_x} S + \frac{4\Omega^2 (I_y - I_x) - \Omega h_y + k_x}{I_x}} \qquad (4.5)$$

$$\frac{\theta\ (s)}{T_y\ (s)} = \frac{\frac{1}{I_y}}{S^2 + \frac{K_{vy}}{I_y} S + \frac{3\Omega^2 (I_x - I_z) + k_y}{I_y}} \qquad (4.6)$$

$$\frac{\psi\ (s)}{T_z\ (s)} = \frac{\frac{1}{I_z}}{S^2 + \frac{K_{vz}}{I_z} S + \frac{\Omega^2 (-I_x + I_y) - \Omega h_y + k_z}{I_z}} \qquad (4.7)$$

Orbital angular velocity, **Ω** is constant. The denominator equation of the second order transfer function is denoted as characteristic equation (4.8) is given by

$$S^2 + 2\delta\omega_n + \omega_n^2 \qquad (4.8)$$

$\boldsymbol{\omega_n}$ is Undamped natural frequency, $\boldsymbol{\delta}$ is damping ratio. In the satellite system the type of damping or oscillation desired by natural frequency and damping ratio [71].

Find the pointing accuracy of satellite 0.1 degree from the final value theorem vehicle steady states in each axis [72]

$$f(\infty) = \lim_{t\to\infty} f(t) = \lim_{s\to 0} S\,F(s) \tag{4.9}$$

This is helping to determine the satellite dynamic motion and attitude in satellite frame. Attitude sensor detects the errors in the body coordinates. Euler equation of the satellite is given by [70]

$$T_x = I_x\ddot{\phi} + 4\Omega^2\,(I_y - I_z)\,\phi - \Omega h_y\,\phi - \Omega h_z - \Omega(-I_x + I_y - I_z)\dot{\psi} - h_y\dot{\psi} - h_z\dot{\theta} - I_x\,\dot{\Omega}\psi + \dot{h}_x \tag{4.10}$$

$$T_y = I_y\ddot{\theta} + 3\Omega^2\,(I_x - I_z)\,\theta + h_x\dot{\psi} + \Omega h_z\,\psi + \Omega h_x\phi - h_z\dot{\phi} - I_y\,\dot{\Omega} + \dot{h}_y \tag{4.11}$$

$$T_z = I_z\ddot{\psi} + \Omega^2\,(-I_x + I_y)\,\psi - \Omega h_y\psi + \Omega h_x + \Omega\,(I_x - I_y + I_z)\dot{\phi} - h_x\dot{\theta} + h_y\dot{\phi} - I_z\dot{\Omega}\phi + \dot{h}_z \tag{4.12}$$

From the equation (4.10), (4.11), (4.12) describes the disturbance torque subjected to the satellite. The angular velocity of the satellite is Ω, the angular moment of momentum wheel is $h(x, y, z)$, Moment of inertia of satellite (I_x, I_y, I_z), Angular acceleration of body $(\ddot{\phi}, \ddot{\theta}, \ddot{\psi})$ Angular velocity $(\dot{\phi}\ \ \dot{\theta}, \dot{\psi})$. The torques T (x, y, and z) directions, whenever any perturbation forces acting on a satellite it creates the counter moments because of conservation of angular momentum [70].

4.1. Perturbations in Low Earth Orbit

The perturbations (or) disturbances are orbital variation in the nominal orbit. This variation is periodic nature. These perturbations affect the Keplerian elements such as angular motion of perigee with respect to ascending node, true anomaly, mean anomaly (For Circular Orbits), and right assertion to ascending node (RAAN). The linear changes in the orbit referred as secular variation. It might be small variation or large variation [73]. The variation is less than the orbital period to complete one cycle referred as linear small variation in orbital elements, and large variation the orbital period is greater than the orbital period. For, low earth orbiting (LEO) satellite reflected as two body problems. In this thesis considered the aerodynamic drag, the gravitational attraction of the earth's surface, solar radiation. For, High earth orbits (HEO) is referred as three body problems such as moon attraction, the sun's attraction is mainly affecting the ascending node with respect to the perigee position. This perturbation occurs in the orbit because of ecliptic pole and gyroscopic precision [74]. The planets disturb the earth orbital plane such as Saturn, Jupiter, and Venus. These planets and SUN perturb the lunar orbit around the earth's surfaces. Mostly high earth orbits have little or no aerodynamic drag. HEO satellite travels with less speed compares to the low earth orbiting satellite. The gravitational attractions/pulling near to the atmospheric region having enormous amount of aerodynamic drag acting on the body. At, LEO satellite travels very high speed near to perigee and less speed at apogee [75].

The trajectories analysis Runge- Kutta methods used to compute of orbit multiple body system presented in this thesis. The orbital position calculated by using high performance computing methods in the orbit. The artificial satellite bodies whose orbit enters the atmosphere under the influence of atmospheric drag force and gravitational attractions [76]. Where it is either dis-integrate the satellite in the atmosphere due to the gravitational force acting on a body. To avoid this need to maintain the orbital plane, it requires the frequent firing from the thruster to maintain the satellite as per the required orbital plane from perturbed plane [77]. The shape of the Earth is not perfectly spherical. The homogeneity of earth will cause the perturbation in the orbit. The bulge in near equator and J_2 perturbation forces will make the changes in the orbital elements. When satellite crosses to the equator, it may affect the orbital elements pull towards to the earth's surface [78].

The artificial satellite in the low earth orbit increase day by day. It makes space debris in the near earth's atmosphere. There is the possibility to colloid each satellite changes the orientation and Keplerian elements. To avoid such collation continually monitor the space debris and to keep the satellite in the same orbit requires the attitude stabilization and control mechanism [79]. The satellite position/orientation measured from star sensor, sun sensor, and earth sensor. The feedback signals from attitude sensors compare with references attitude signal based on that dynamic of the actuation system like control momentum gyroscope, fly wheels, magnetic torque generates the control torque to the satellite system [80]. The perturbation equation is very useful to design the Attitude determination and control system (ADCS).

Types of Perturbations

The different types of perturbations

- Atmospheric drag
- Lunar and solar gravity
- Shape of the earth
- Solar radiation

4.2.1 Atmospheric Drag Effects

Atmospheric drag forces vary with altitude at low earth orbit having more aerodynamic drag between 120 KM 160 KM. It reduces the satellite altitude in the earth's atmosphere. When satellite reaches near to Roche limit focal point approximately 80 KM altitudes very rapidly decay the orbital elements. For, above 1000 KM altitudes drag is less changes of satellite orbital elements. This is called as orbital decay [81]. The low earth orbit satellite to decrease the altitude due to large drag affects the satellite body, also decrease the mission lifetime. The drag forces $\mathbf{F_{drag}}$ is increased with velocity **V**; $F_{drag} \perp V^2$. The satellite/vehicle velocity depends upon the different altitudes, also its proportional with Area of the satellite and air density; if the surface area of the satellite increases the drag will also increase. The large amount of aerodynamic drag will strike satellite during launch and Re-Entry period. The Ballistic constant $\frac{m2}{C_d A}$ depends upon the satellite mass, coefficient of drag (For flat plate it is 2), area of the satellite. Mostly low earth orbits the satellite mass is considered as constant [82].

The aerodynamic drag effect is the major force affecting the object or satellite in the low earth orbit (LEO). When the vehicle (satellite) body moving in the atmosphere by GAS particle and liquid particle produces the resistance offered due to drag force. The drag force is more effects during launch the satellite and re-entry the space vehicle [83]. See figure (4.1) when the satellite has entered the upper atmosphere because of the gravitational attraction and aerodynamic drag effect are considered more altitude. Finally, near to earth atmosphere to dis-integrate the satellite parts and further enters because of orbital decay. The satellite attitude reduces because of these perturbation forces. This effect decreases the lifetime of the satellite.

The Cowell's perturbation equations used to design and analysis the perturbations in ideal conditions due to atmospheric drag and solar radiation Pressure in Low Earth Orbit satellite [84]. Their causes and how they affect the spacecraft in the Low Earth Orbit are explained shown in figure (4.2). The perturbation algorithms developed by MATLAB environment.

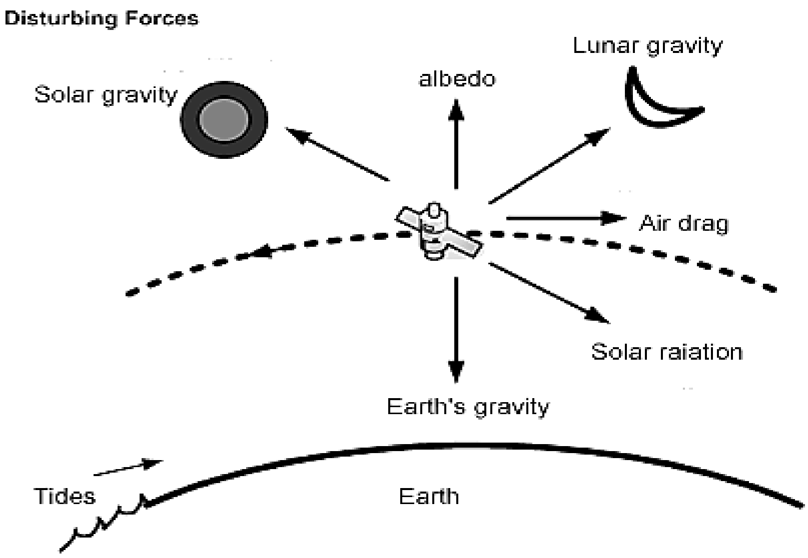

Figure (4.1) Perturbation forces in LEO Satellite [84]

The aerodynamic force of the satellite is given in the equation (4.13)

$$F_{drag} = \frac{1}{2}\rho v^2 A c_d \tag{4.13}$$

Let, F_{drag} aerodynamic parameters of the vehicle body, ρ air density, v is velocity acting on a satellite, A is the Surface Area of the object or Satellite, C_d is the drag coefficient [84].

Typically, for earth's approaching satellites having a more coefficient of drag. It is mainly depending upon the changes in the altitude [85]. The altitude above 90km having extreme ultraviolet radiation and more temperature because of SUN effects with respect to altitude. The altitude between 200km to 260km temperature is reduced from 1150K to 600K because of the solar activity due to high density. Due to SUN effects the solar radiation satellite has maximum decay in day times and minimum solar perturbation decay during eclipse period [85].

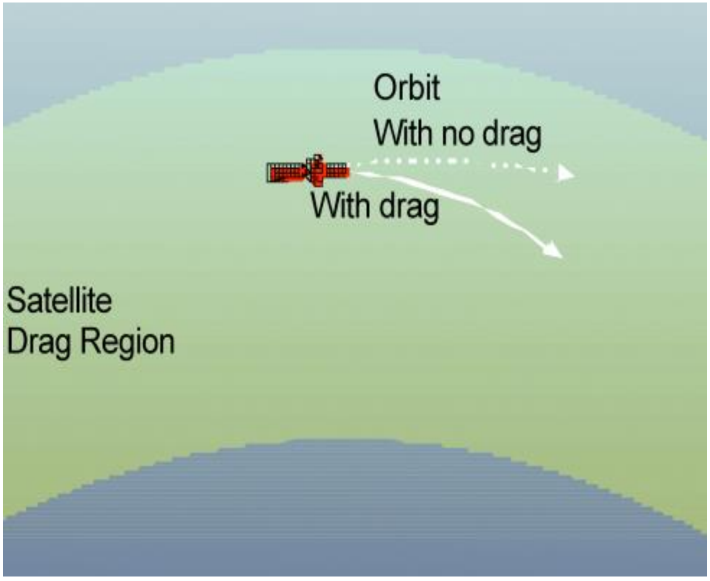

Figure (4.2) Satellite orbit trajectory in drag region [85]

The ADCS of Hubble Space Telescope design specification is 7/1000th point accuracy of arcsecond. The proposed work the accuracy of satellite dependent on disturbance effects accumulating with time. The disturbance/Perturbation arises from internal factors or external factors. The sensor calibration and alignment error create the internal noises and due to the environmental disturbances are external factors. The internal disturbances are closely tied witch spacecraft structure, in particular: internal moving parts and mass or radiation being emitted [86].

For circular orbit the changes in (period, velocity, acceleration) a, T, v per revolution as is given equation (4.14), (4.15), (4.16), (4.17)

$$\Delta_{a_{rev}} = -\frac{2\pi C_d A \rho a^2}{m_2} \tag{4.14}$$

$$\Delta P_{rev} = -\frac{6\pi^2 C_d A\rho a^2}{m_2 V} \tag{4.15}$$

$$\Delta V_{rev} = \frac{\pi C_d A\rho a V}{m_2} \tag{4.16}$$

$$a_r = -\frac{4.5X10^{-8}A}{m_2} \tag{4.17}$$

The Ballistic coefficient (BC) depends upon the mass of the satellite and area of satellite it is described by $m_2/(C_d A)$, BC is constant for most of the satellite. The drag effects are large when the lower valve of ballistic constant and drag is less when high value of ballistic constant [87].

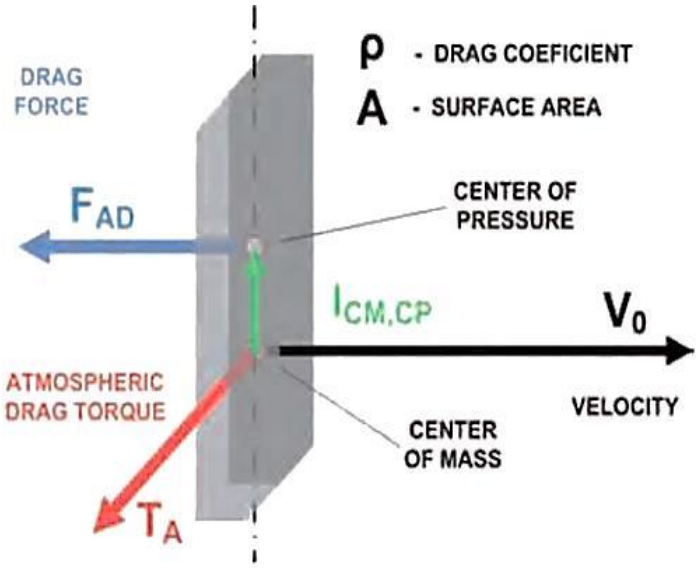

Figure (4.3) Direction of aerodynamic drag force and atmospheric torque [87]

To estimate the lifetime of the satellite life cycle as is given equation

$$L = \frac{-H}{\Delta a_{rev}} \tag{4.18}$$

Hence, the equation (4.18) describes the changes in atmospheric density due to altitude variation and solar changes. H is mean by the atmospheric scale height of density [87].

4.2.2. Solar and Lunar Gravity Perturbation

The three-body problems such as SUN attraction and MOON attraction perturb the satellite into normal orbit to perturbed orbit due to gravitational effects. These types of perturbation due to other body except earth disturb the orbital elements [88]. In High earth orbit satellite attitude is change periodically s due to the ecliptic pole and precision of the gyroscope. The SUN and lunar attractions mainly change the argument of perigee. The vehicle moves in orbit intersecting the equatorial orbit with satellite orbit from South Pole to the North Pole [88]. The equation of perturbation given by the following

$$\Omega moon = -\frac{Cos(inc)}{n} * (0.00338)\ , \quad \Omega sun = -\frac{Cos(inc)}{n} * (0.00154)$$

$$\omega moon = \frac{(4-5*Sin^2(inc))}{n} * (0.00169),\ \omega sun = \frac{(4-5*sin^2(inc))}{n} * (0.00074)$$

Where, the orbit inclination (inc) is i, orbital revolutions per day is n, Both Argument of perigee & longitude of ascending nodes defined as degree/day.

4.2.3. The Flattening or Non-Homogeneity of the Earth

The Earth is not a perfect sphere; it is some extent flattening in the top surface and bottom surface [89]. The Non-homogeneity of earth See. Figure 4.4 causes the harmonics such as J_2 perturbations.

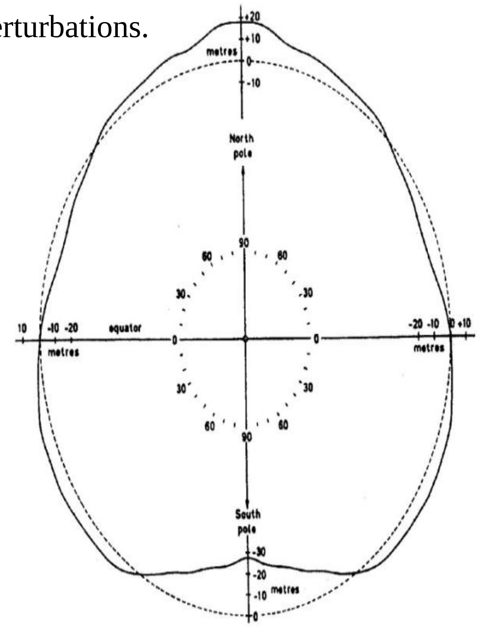

Figure (4.4) Flattening of the Earth's surface with J_2 perturbations [57]

The Earth is slightly bulging on near the equator. Because of the non-homogeneity of the earth's surface at the top and bottom create more change in the high earth orbit especially Geosynchronous Earth Orbits, GEO. The low earth orbit, it is not taking any variation in the orbit after many revolutions [90]. Earth harmonics, $\mathbf{J_2}$ changes the satellite position with respect to the perigee. These variations are periodic nature change the orbital elements.

The equations for this perturbation are [90]

$$\vec{a}E_x = G\,A_{J2}\,(15\,\frac{xz^2}{{r_{earth}}^7} - 3\frac{x}{{r_{earth}}^5})$$

$$\vec{a}E_y = G\,A_{J2}\,(15\,\frac{yz^2}{{r_{earth}}^7} - 3\frac{y}{{r_{earth}}^5})$$

$$\vec{a}E_z = G\,A_{J2}\,(15\,\frac{z^3}{{r_{earth}}^7} - 3\frac{z}{{r_{earth}}^5})$$

Shape of the Earth

When designing the Low Earth Orbits satellite, assuming the earth is purely spherical or symmetrical mass. But most variation in the satellite in the bulge nears the equator. These perturbations are referred as Zonal perturbation depends upon the Geo-potential coefficients and zonal coefficients [91]. The flattening of the earth pole earth potential function, acceleration of the satellite body found from the gradient of potential function depends upon the latitude [91]. The potential function changes the orbital elements because of the non-homogeneity of the Earth's surface from the equation. The variations in Ω_{RAAN} & ω_{J2} due to periodic/secular variation of Earth's Oblateness (**J_2**) equations (4.19), (4.20) as follows

$$\Omega_{J2} = \frac{-1.15n\,J_2\left(\frac{r_{earth}}{a}\right)^2 \cos*(i)}{(1-ecc^2)^2} \qquad (4.19)$$

$$\omega_{J2} = \frac{-1.15n\,J_2\,(\frac{r_{earth}}{a})^2 \cos*i}{(1-ecc^2)^2} \qquad (4.20)$$

Where, n is the number of revolutions/days

J_2 - Zonal Coefficient

r_{earth} - The earth radius

a -Semi Major axis

i -Inclination of orbital Plane

ecc - eccentricity of orbit

4.2.4. Solar Radiation

When design the LEO Nano satellite attitude control system, the major perturbation is solar perturbation periodic variation in the orbital components [92]. The changes in attitudes of LEO satellite due to solar radiation pressure.

The solar radiation pressure force is given in the equation (4.21):

$$p_{sr} = \frac{SF}{c} = \frac{1353}{3 \times 10^8} \ \frac{W/m^2}{m/s} = 4.51 \times \ 10^{-6}\, N/m^2 \qquad (4.21)$$

Where,

Solar Flux (SF) = 1353 W/m^2 (Radiation constant)

Velocity of light (c) = 3×10^8 m/s

The solar force is directly proportional to the SF and inversely proportional to the speed of the light. The disturbances analysis at LEO consider for the simulations torque generated (See Equation 4.22) due to solar radiation is given by: [92]

$$\tau_{\text{Solar-radiation}} = -p_{sr} \times C_r \times A\Theta \times (C_{psr} - C_g) \qquad (4.22)$$

Where,

Visible area of the SUN A_Θ

Reflectivity c_r

Center of pressure c_{psr}

Center of gravity c_g

$$a_r = -\frac{4.5X10^{-8}A}{m2} \qquad (4.23)$$

The cross-section surface area of vehicle/satellite is defined by ‘A’ which observable to the SUN. The total weight (mass) of the satellite is ‘m’ expressed in kg.

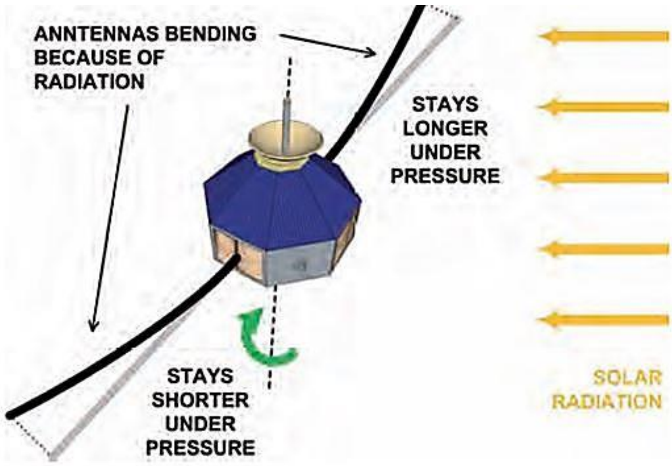

Figure (4.5) Change in satellite cross sectional area due to Solar Radiation [87]

An altitude below 800km having more aerodynamic drag acceleration and less solar radiation force or pressure acting on a satellite [93]. An altitude above 800km having solar radiation pressure (See Figure 4.5) is greater than the aerodynamic drag force. In this region, the predominant effects of perturbation due to the solar activity. The acceleration due to atmosphere drags is a_{ad} and the solar radiation pressure is a_r ; An altitude below 800 KM distance $a_{ad} > a_r$, An altitude above 800KM $a_r > a_{ad}$. It's clearly understood when designing the LEO satellite having more acceleration from the atmosphere drag and less acceleration from solar radiation force. The Keplerian elements change due to solar radiation is the most important factor to perturb the orbit from actual path [92].

4.3. Periodic and Secular Variation

Periodic and secular variation in the Keplerian elements due to atmosphere molecules changes the satellite orientation [73]. These generate the decay function to decrease the orbit life time. In the lower altitudes having dense atmosphere and more aerodynamic drags & more heat disintegrates the satellite, to burn the satellite during the re-entry.

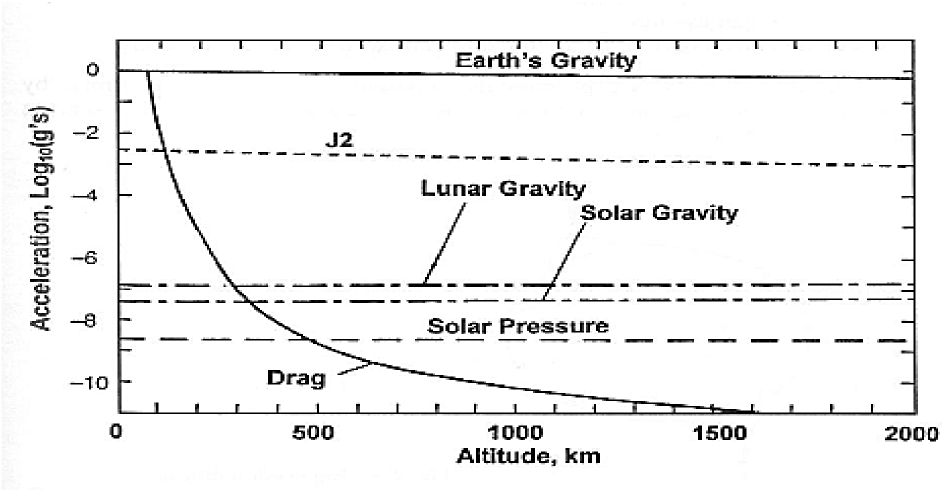

Figure (4.6) various sources of orbital perturbation [73]

The preceding example illustrated the effect of periodic variation. In Figure 4.6 shown the deceleration of vehicles varies with altitude under the influence of various sources of perturbation forces.

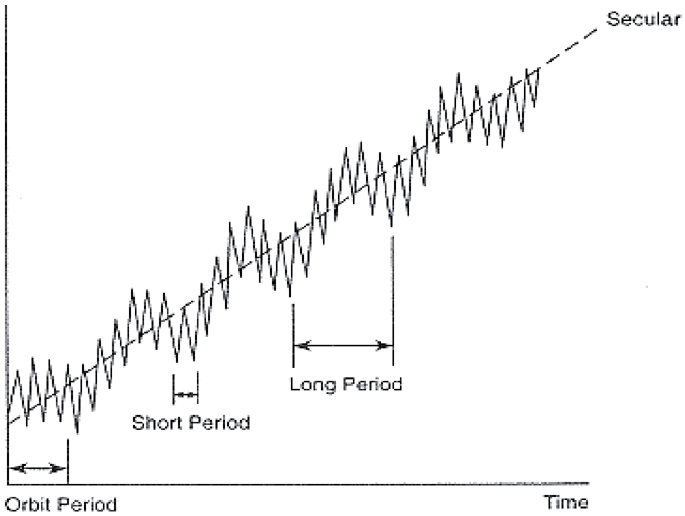

Figure (4.7) Secular variation vs. short & long period variation [73]

There are three types of disturbances from Figure 4.7. [73]

- Short Periodic - Cycles every orbital period.
- Long Periodic - Cycles last longer than one orbital period.
- Secular - Does not cycle. Disturbances mount over time.

Table (4.1) Keplerian Elements vs. Orbital Periods [73]

Orbital Elements	*Perturbations with time*	*Perturbation > Orbital period (Long cycle)*	*Perturbation < Orbital period (Short cycle)*
Semi major axis	*X*	*X*	↑
Eccentricity	*X*	↑	↑
Inclination	*X*	↑	↑
RA of Ascending Node	↑	↑	↑
Argument of perigee	↑	↑	↑
Mean anomaly	↑	↑	↑

↑ Means **YES**, X Means **NO**

In table (4.1) summarizes the perturbation in the orbit short period and long period with Keplerian elements

4.3.1 Decay of Eccentricity

The drag occurs at perigee is more than apogee. See Figure 4.8 shows the decay the orbit eccentricity from apogee and perigee with time in days from Epoch. This indicates the lifetime of the satellite decreases with time [94].

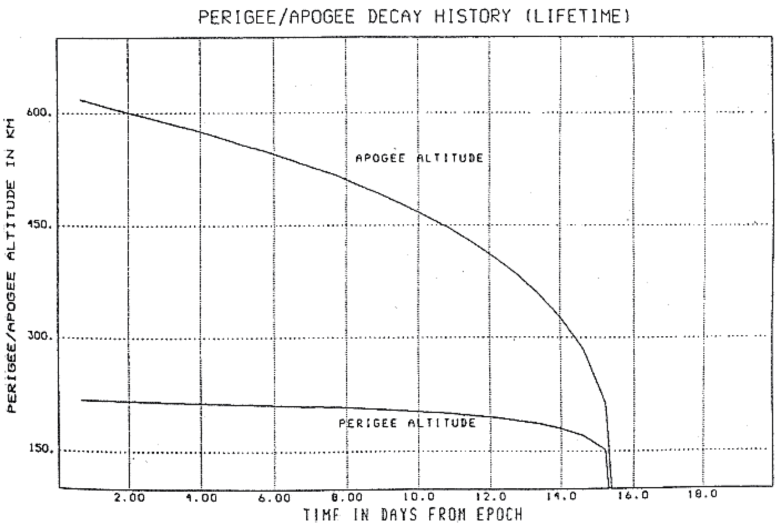

Figure (4.8) Variations in the altitudes between perigee/apogee since epoch [94]

4.3.2. Drag Effects on Eccentric Orbits

When the satellite moves at perigee have constant eccentricity and density with same altitude is illustrate in Figure. 4.9. The altitude of apogee having variation in size of the orbit eccentricity, density with changes in altitude [95].

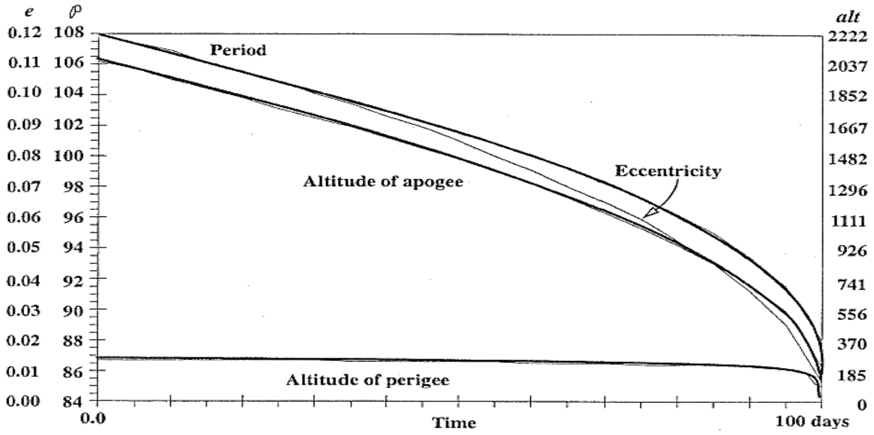

Figure (4.9) Variation in eccentricity, density with different altitudes [95]

ISS Shows the Figure 4.10. Orbital decay with altitude vs years [96].

Figure (4.10) Orbit Decay of the International Space Station (ISS) [96]

4.3.3. Spacecraft Lifetime Solar Activity Effect

In Figure (4.11), (a) and (b) show the mean value of a lifetime (lb/ft^2) and (m^2/kg). Actual values will depend on ballistic constant [97].

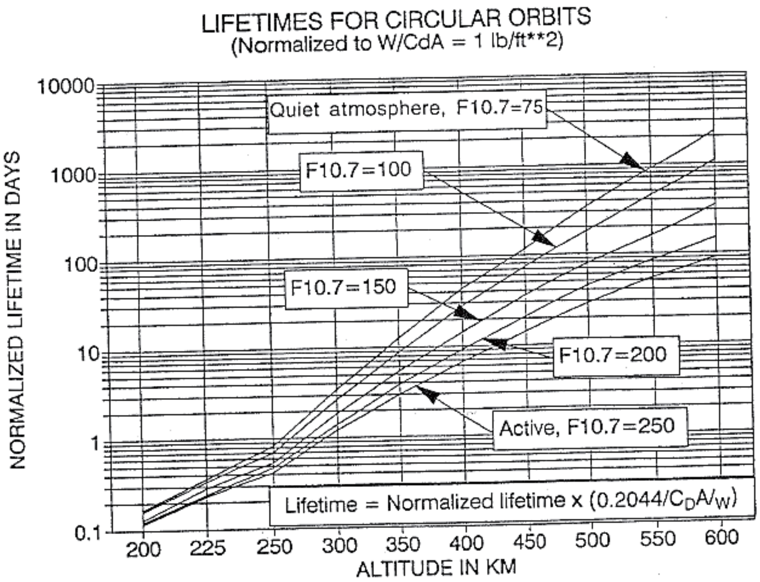

Figure (4.11) Spacecraft Lifetime Solar Activity (a) Altitudes vs. Lifetime (lb/ft^2) [97]

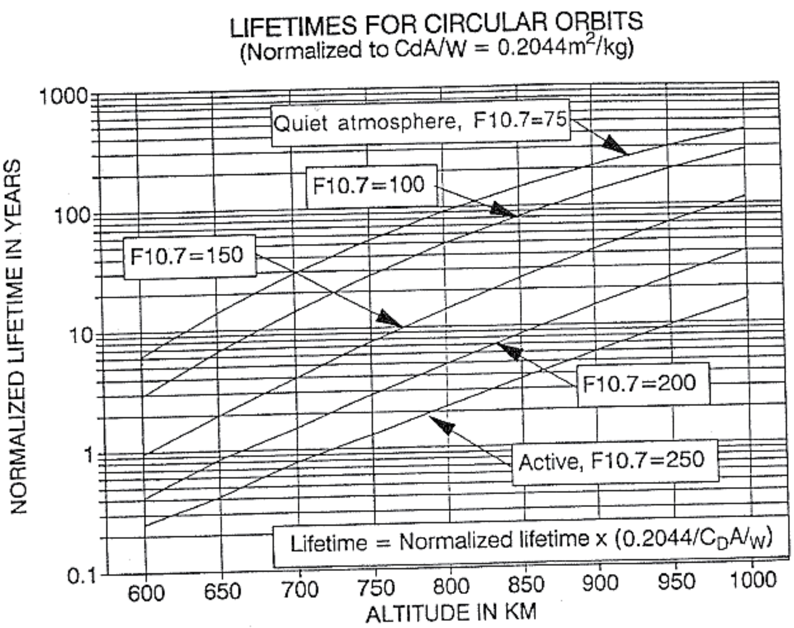

(b) Graph between Altitudes vs. Lifetime (m^2/kg) [97]

4.4. Perturbation Formulations for Numerical Solutions

The perturbations prediction and analyze with the help of numerical equation to determine the orbit position. There are two types of numerical integration used to analyze the perturbation model one is Cowell formation another one Encke's formation. In this thesis consider for Cowells algorithm used to design & simulate the orbit with Keplerian elements. The Cowell methods mainly used to find the changes in acceleration with maintain magnitude of primary acceleration [36]. The Encke's method is very much useful for design high earth orbit (HEO) satellite and interplants operation. These methods are used to predicting the satellite position of in the future (or) next state. The design simulation of orbit is analyzed by a differential equation to identify the disturbed orbit from normal orbit. The differential ordinary integration methods widely used to find the motion of satellite due to perturbations forces [36].

The differential equations used to find the motion equations of the satellite with perturbation in the orbit. At LEO satellite revolves the earth's surface in the form of circular motion [84]. The motion equations are practically 2^{nd} order ordinary differential equations (**ODE**). These formulated equations are used to predict a satellite's upcoming position, velocity, and Keplerian elements. The proposed perturbation design analysis in International space station (ISS), SRM satellite, Pratham satellite implemented with Runge-Kutta numerical methods [98]. This method using ODE Equations to find perturbed trajectory by the knowledge of initial condition and time interval get the actual trajectory. Also, another method Euler method used to predict the oscillating orbit. The Modified Euler methods find the disturbed path from an initial condition of pre-determined path of the orbit. The simulation methods are developed by MATLAB or Global Mission Analysis Tool (GMAT), out of which the results are more accurate, even for larger values of step size (h). These two methods that can be employed in the thesis, formulation of differential equations termed as Cowell's Method at LEO orbits and Encke's Method at HEO orbits [99].

The Cowell's method involves the direct integration of the full equation of motion in rectangular coordinates. Therefore, this method is also known as a direct numerical integration method. This method is mostly used if the values of perturbation are comparable to or greater than the primary body gravity acceleration [84]. The Encke's method involves the changes in the satellite normal orbit and disturbed/Perturbed orbit. The accelerations different between both orbits are integrated and adding in to initial orbit and perturbed orbit. It is, finally results in perturbed satellite state vectors. This method is a more efficient for long interplanetary mission spacecraft, because of the built-in rectification procedure.

The method which can be used for the formulation of a differential equation is a Cowell's method, because it is much more accurate for the Low Earth Orbit (LEO) satellite when compared to Encke's method [36]. Cowell's method is also less complex, i.e., easy to formulate and program. This research work included is aerodynamic drag, solar radiation pressure after the formulation of a differential equation by Cowell's method with orbital perturbation for the simulation

4.4.1. Cowell's construction method

The Cowell's constructions used to find the equations of motion of the satellite and integrating the rectangular coordinate. Illustrate in Figure 4.12, body 'i' moving into the body 1 because of gravitational attraction perturbed orbit to osculate orbit. This method is broadly used to integrate the perturbation acceleration equal to zero [84].

The Cowell's construction equation (4.24) is given below

$$\ddot{r} = -\frac{\mu}{r^3} r + a_{perturbed} \tag{4.24}$$

The Position equation (4.25) and velocity equation (4.26) given by

$$x = \begin{pmatrix} r \\ \frac{dr}{dt} \end{pmatrix} \tag{4.25}$$

And

$$\frac{dx}{dt} = \begin{pmatrix} \frac{dr}{dt} \\ -\frac{\mu}{r^3} r + a_p \end{pmatrix} \tag{4.26}$$

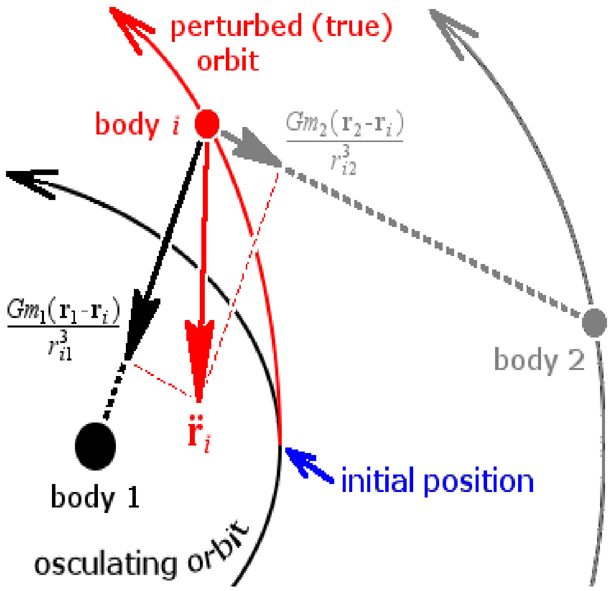

Figure (4.12) Cowell's Method from perturbed orbit to osculate orbit

A Cowell construction is expanded by follows:

1. Set Initial condition, position r = r_0; velocity v = v_0; time t = t_0.

2. Govern changes in time Δt / t_f by n steps

3. Integrate the vector from zero to n steps

    a. To Integrate $\frac{dr}{dt}$ & $\frac{d\dot{r}}{dt}$ To find position vector and velocity vector.

    b. Add time, t = t and Δt.

4. Calculated final position, velocity, time

As we know Aerodynamic Force given as

$$F_{AD} = \frac{1}{2}\rho v^2 C_d A \quad (4.27)$$

Where, ρ = free-stream density

v = free-stream velocity

C_d = Coefficient of Drag = 2.0

A = Area of the satellite body

Aerodynamic acceleration (4.28) or total perturbing acceleration can be calculated as below

$$a_P = a_{AD} = F_{AD}/m_2 \tag{4.28}$$

Where, m_2 = Mass of the satellite body

$$\dot{r} = v \tag{4.29}$$

$$\dot{v} = -\frac{\mu}{r^3} r + a_{AD} \tag{4.30}$$

Hence, the equations (4.29) & (4.30) satellite velocity & satellite acceleration can be solved with the help of the Runge- kutta method [84].

4.2.2. Encke's construction method

The Encke's construction method used to find the perturbed orbit position, velocity from osculating orbit (2-body) by the difference in the acceleration in both the orbit [36].

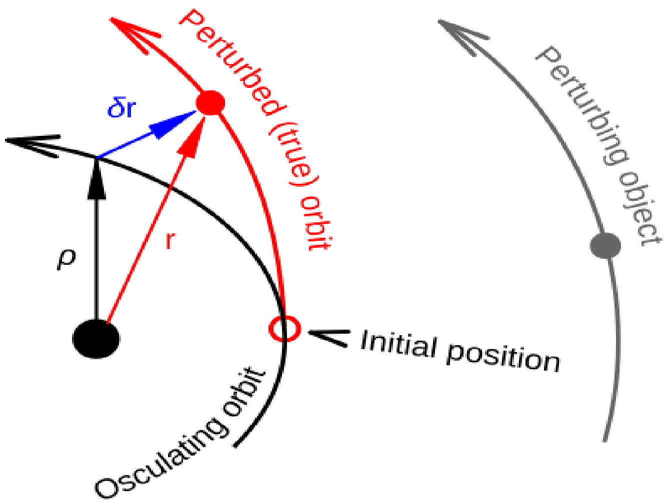

Figure (4.13) Finding the satellite position and velocity of osculating orbit

To integrating this difference and summation of the result gives the position and velocity of osculating orbits (See Figure 4.13) continues till maximum amount of magnitude of position difference some tolerance limit. Osculating orbit position adjusted from the current disturbance state [36].

4.5. Attitude controllers for NANO satellite in low earth orbits

The Magnetic Torquers or Magnetic actuator is used to generate the magnetic flux which interacts with the Earth magnetic flux (GEO Magnetic field). This produces control torque or control forces to satellite. For three axis control, (CMG) Control momentum gyros are used for stabilizing the satellite [100], [101]. The magnetic thruster or armature control DC motor used in in low earth orbits satellite. In this thesis included the dynamics of armature control DC motor with Nano satellite inertia is considered. The Earth's magnetic fields change the satellites attitudes from pre-determined attitude. An actuator used to correct the actual path of satellite orbit even with perturbation. The magnetometer is used to measure the Earth's field (magnetic). The momentum wheel (or) Flywheels used to control the periodic disturbances in satellite [102]. The magnetic control system consists of solenoid coil and Geo-Magnetic field. The NANO satellite weights (mass) considered between 1kg to 10kg. It carries smaller payloads for earth observation or navigation application. The NANO satellite either controlled by active control or passive control techniques. An active control method using Armature controlled DC motor to correct the attitudes of NANO satellites in LEO orbiting satellite [103], [104]. The Control momentum Gyroscope (CMG), Momentum Wheel or Flywheels is used to control the High earth orbiting satellite. The CMG consist of small motor attached with wheels on satellite body [105].

When ADCS design requires the torques on a Di-pole (2-pole magnets) with uniform or constant magnetic field. This field is required for keeping the dipole perpendicular to the constant magnetic field. The Dipole moment is a product of the strength of the pole and it is separated by two plates. It has North Pole (N) and South Pole (S) where both force magnitude is same but different direction. The **M**agnetic **D**ipole **M**oment (MDM) is expressed in NM/T [106], [107]

$$\textbf{Torque (T)} = \mathbf{M * B} \tag{4.31}$$

The Magnetic fields (B) and dipole (M) of the torque (4.31). For air armature (or) conductor, the dipole is

$$\mathbf{M = N * I * A} \tag{4.32}$$

Where (4.32) Coil (or) No of turns in the winding is N, the current in the coil is I, and, the area of the conductor is A, Characteristically, the coil is wounded from place to place of the satellite structure or body [108].

The magnetic fields can be taken as a periodic function for all times, the dynamics of satellite/spacecraft control mechanism and stabilization is achieved by suitable actuator or controllers [109]. By the application of the above-mentioned theory on a satellite actuation system like the magnetic torque control the complete orbit in a fixed dipole and GEO magnetic field. In Figure (4.14) illustrate how to generate the torques or force from magnetic actuator by the help of Dipole and Geo magnetic (earth) fields [110].

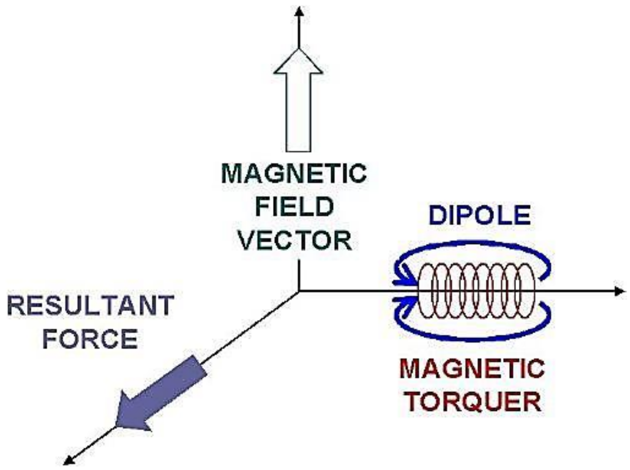

Fig (4.14) Magnetic Actuator [110]

The magnetic torquers are generating the control torque, ***T***control for re-orienting the satellite to prescribed orbits. In the Figure 4.15 shows the magnetic moments, required control torque, T_{Required} and magnetic-flux vector, **B** in the satellite frame from the magnetometer measurements. The control torques requirement should be regular to the magnetic flux, we have ***BT***control = *0* [110]. The most efficient magnetic moment is the one that always points normal to the ***B*** vector, so that ***MT***control = *zero*. The control torques can be calculated from Magnetic field (**B**) and Regulated torque ($\mathbf{T}_{\mathbf{Required}}$). The magnetic torquer generates the control displacement in the satellite, the torquers generates 0.05 N-M at low earth orbit altitude of 1000KM [111], [112].

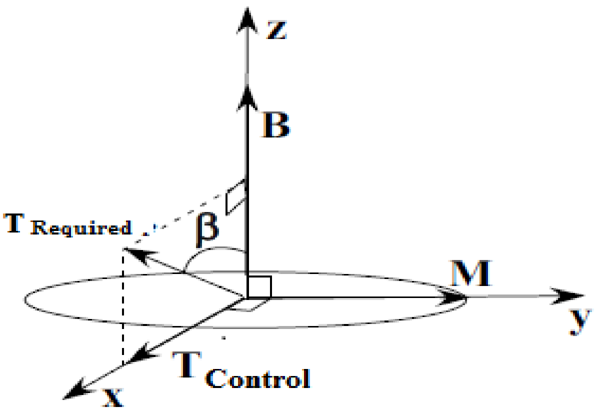

Figure (4.15) Regulator Torque T_R and Magnetic Di-Pole Moment [113]

The respective unit vectors are: (e_x, e_y, e_z) = (**Tcontrol** / $T_{control, M}$/ M, **B**/ B)

Hence, the Control torque (4.33) vector is: (**Tc**) [113]

Tcontrol = ($T_{Required}$ * s * β) e_x = $T_{Required}$ - ($T_{Required}$ * c * β) e_z = $T_{Required}$ - ($T_{Required}$ * c * β) **B**/ B (4.33)

s = sin and c = cos terms

$T_{control}$ = Moment (M) * Magnetic field (B) (4.34)

The **M**agnetic **D**iploe **M**oment (4.34), MDM is the moment of magnetic dipole or solenoid moment; the changes in '**M'** directly affect the control torques and indirectly affect the magnetic field [114], [115]. The pole strength and distance between two magnetic poles are well-defined; M is inversely proportional to the Field vector (Magnetic) **B** and required torque vectors **$T_{Required}$**

$$\mathbf{M} \ \boldsymbol{\alpha} \ \text{Magnetic field} * T_{Required}$$

$$\mathbf{M} = \frac{\text{Magnetic field} \ * \text{TRequired}}{B^2} \qquad (4.35)$$

The Nadir is defining the line of observation from satellite looking at string line to the earth's surface; Satellite and earth have the same line of sight [116]. The Zenith is exactly opposite to the Nadir and the satellite moment around Nadir/Zenith direction is expressed by Yaw angle and velocity direction is expressed by Roll angle, orbit direction (or) movement is expressed by Pitch angle [117].

Solenoid coils

Solenoid is bar magnets and current caring conductor/coil creates the Di-Pole moments. It is an electromagnetic armature used in satellite system. The interaction between the earth magnetic flux vs. Magnetic torquer derives this section [118].

Motion equations (EOM) for twin coil BAR magnet and coil

In free space, a Magnetic field plays the major roles in the permeability. And if we consider closed surface area or nozzle area, permeability of median it is assumed as infinity [118]. Therefore, the magnetic fields are considered zero (=0)

$$\oint_C^1 \boldsymbol{Magnetic\ field} \,.\, \boldsymbol{dl} = \int_s^1 \boldsymbol{J\ nda}$$

Hence, the above equation states, to integrate the magnetic field in the closed path in the surface area **S**. Surface area in the magnetic field is mostly same of the integration of electric current, **I** on the surface path.

4.5.1. IGRF: International Geomagnetic Reference Field

IGRF model is the typical numerical model of GEO magnetic field under changes in the orbit due to perturbation variation [119]. The data are collected from the "International Association of Geomagnetism and Aeronomy" (IAGA). This is an international association to study and observation of magnetism in planetary and terrestrial field. The scalar potential model (4.36) of earth's magnetic field consists of Gauss coefficient and Spherical harmonics as given below [120]

$$V(r,\phi,\theta,t) = a\sum_{\ell=1}^{L}\sum_{m=0}^{\ell}\left(\frac{a}{r}\right)^{\ell+1}\left(g_\ell^m(t)\cos m\phi + h_\ell^m(t)\sin m\phi\right)P_\ell^m(\cos\theta) \tag{4.36}$$

r = Radial distance from the earth center

$\boldsymbol{\phi}$ **=** East longitude

θ = latitude (polar angle)

a = Radius of the earth's surface (*6,371 km* or *3,959 miles)*

g_l^m & h_l^m = Gauss coefficients

p_l^m = Normalized Legendre function (canonical form) of (l is the degree; m is the order)

L = Expansion degree (Max)

The Gauss coefficients may vary linearly with respect to times. IGRF models provide the accurate measurements in the earth magnetic field over a period of times [120].

4.5.2. Attitude control with control momentum gyroscope

The Attitude Control system (ACS) of satellite with control momentum gyroscope attached with a stable platform. It is called as Gimbal (single gimbal or dual gimbals) [121]. The design of the ACS with momentum wheel is shown in Figure (4.16)

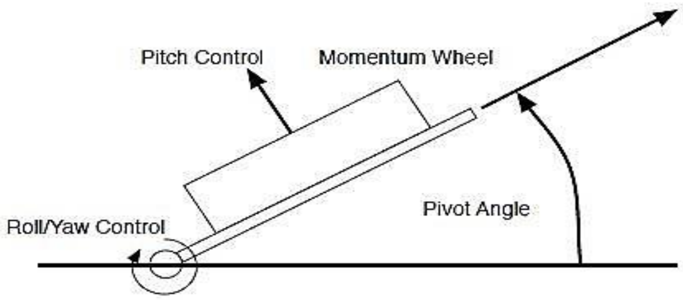

Fig (4.16) Two-axis Attitudes control of satellite with momentum wheels [121]

It is very important to analysis the less weight and low-cost sensors models. The design simulation of ADCS requires the single gimbal variable speed control momentum gyroscopes (SGVSCMG). [122].

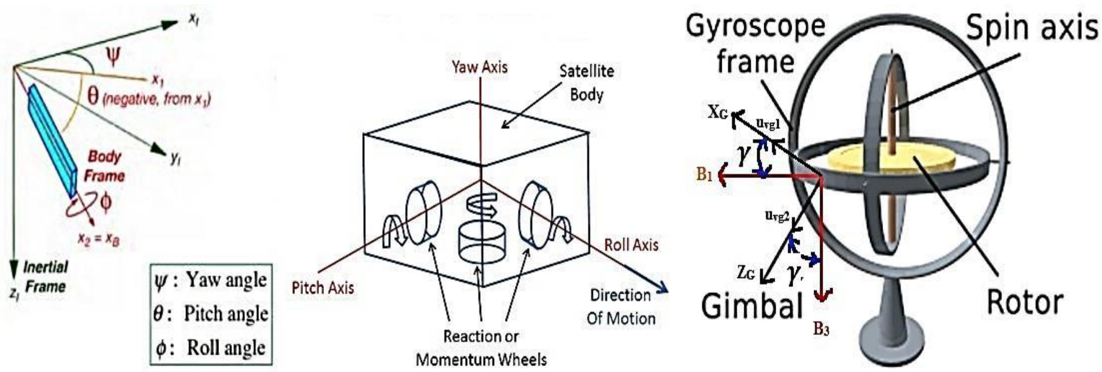

Fig (4.17) Satellite positions and orientations with Gyroscope frame [122]

The Figure (4.17) describes the inertial frame (X_I, Y_I, Z_I) rotations about body frame (X_B/B_1, Y_B/B_2, Z_B/B_3) about the roll axis. The reaction wheels/momentum wheel is attached to satellite body. The Gyroscopes consists of inner gimbals and outer gimbals to calculate angular motions in spin axis. The Gimbal is attached to the rotor or small motor to the gyroscope frame [123]. The Unit vectors are (**u_{vg1}; u_{vg2}; u_{vg3})** respectively. The quaternion parameter represents the attitude orientation of the satellite. These parameters consist of one real quantity and three imaginary quantities used to find the vectors in one frame to another frame vectors. The Quaternion parameters (4.37) relates with the angular frequency defined by [124]

$$quaternion = \left[\!\left[\frac{q0}{\boldsymbol{qv}}\right]\!\right] = \left[\!\left[\begin{matrix}\frac{q0}{qx}\\ \frac{qy}{qz}\end{matrix}\right]\!\right] \tag{4.37}$$

$$\left[\!\left[\begin{matrix}\frac{\dot{q0}}{\dot{q1}}\\ \frac{\dot{q2}}{\dot{q3}}\end{matrix}\right]\!\right] = 0.5 * [\text{quaternion parameters}] * [\text{angular velocity}] \tag{4.38}$$

In the section discuss the quaternion method is described angular momentum of the satellite. Where $q0$, qx, qy, and qz are the parameter quaternion, and angular velocity = $[\omega^1_{satellite}, \omega^2_{satellite}, \omega^3_{satellite}]^T$ are angular vector (4.38) of satellite about the satellite body reference coordinates. [124]

$$Cv^{Inertial}_{Body} = [\![Cv_{jk}]\!] \quad \text{j,k = 1,2,3} \quad C^{Inertial}_{Body} = C^I_B$$

$$Cvjk = \cos * \beta jk$$

$$\dot{Cv}^{Inertial}_{Body} =$$

$$Cv^I_B = [0 \ \ \omega^3_{satellite} \ \ \omega^2_{satellite} \ ; \omega^3_{satellite} \ \ 0 \ -\omega^1_{satellite} \ ; -\omega^2_{satellite} \ \ \omega^1_{satellite} \ \ 0]$$

Direct cosine matrix included in quaternion, because it is an easy way to describe the satellite axis into the inertial reference axis. The DCM is described the control of Z_B axis direction by $Cv^{Inertial}_{Body}$. Hence the equation (4.39) given by

$$\begin{bmatrix}\dot{Cv}13\\ \dot{Cv}23\\ \dot{Cv}33\end{bmatrix} = \begin{bmatrix}Cv11 & Cv12 & Cv13\\ Cv21 & Cv22 & Cv23\\ Cv31 & Cv32 & Cv33\end{bmatrix}\begin{bmatrix}\omega 2\\ -\omega 1\\ 0\end{bmatrix} = \begin{bmatrix}-Cv12 & Cv11\\ -Cv22 & Cv21\\ -Cv32 & Cv31\end{bmatrix}\begin{bmatrix}\omega^1_{satellite}\\ \omega^2_{satellite}\end{bmatrix} \tag{4.39}$$

In the design analysis considered the net angular momentum (4.40) of the vehicle/satellite is not equal to zero. It is constant with respect to a fixed reference frame [125]

$$h_{momentum\,(h)} = \mathbf{J}\,\boldsymbol{\omega} + \boldsymbol{J}_{G(Gimbal)}\ \dot{\boldsymbol{\gamma}}\ \boldsymbol{g_2} + \boldsymbol{J}_{W(Wheel)}\ \Omega\ \ \boldsymbol{g_3} \neq 0 \tag{4.40}$$

Where, J = diag [$J1; J2; J3$] the satellite inertia matrix with gyroscope in the inner gimbal and wheel attached to it. The Wheel moment of inertia, $\mathbf{J_{Wheel}}$ is defecting about Z_G axis and Gimbal moment of inertia, $\mathbf{J_{Gimbal}}$ is rotation about Y_G. The revolution of the Wheel is $\mathbf{\Omega}$

M.O.I is moment of inertia:

The equation (4.41) of satellite as given below [110]

Angular momentum, (h) = $\begin{bmatrix} hmoment1 \\ hmoment2 \\ hmoment3 \end{bmatrix} = \begin{bmatrix} J1\ \boldsymbol{\omega 1} + \boldsymbol{J_{W(Wheel)}}\ \Omega \sin\gamma \\ j2\boldsymbol{\omega 2} \\ J3\ \boldsymbol{\omega 3} + \boldsymbol{J_{W(Wheel)}}\ \Omega \cos\gamma \end{bmatrix}$ (4.41)

$$\dot{h} + \boldsymbol{\omega} \times \mathrm{h} \quad (4.42)$$

The angle of gimbal is $\boldsymbol{\gamma}$ and the acceleration of the wheel is $\dot{\Omega}$ where both are used to produce the feedback torques needed to control the actuator input of the satellite [125].

$$\dot{\gamma} = u1, \qquad \dot{\Omega} = \mathrm{u2}$$

Gradient (Gravity) Torque: (Gt)

Assumptions: Upper-order relations ignored.

The Rigid Satellite body assumed (4.43).

$T_{\text{gravity gradient}} = 3\,[(I_3-I_2)\,m\,n\,i + (I_1-I_3)\,l\,n\,i + (I_2-I_1)\,l\,m\,k]\ _{\theta}2\ /\ (1 + e\cos \nu v)$ (4.43)

Variables: $T_{\text{gravity gradient}}$ = gravity gradient torque [126]

ν = true anomaly

e = orbital eccentricity

I_1, I_2, I_3 = moments of inertia of principle axis of body

l, m, n, = (satellite with principle axis of body) - direction cosines

Gravity gradient stabilization:

Gravity gradient torque disappears:

- An angle between 2 vectors, cosine is zero.
- I1 = I2 = I3
- In the axis one cosine is zero other two moments of inertia equal

The Gravity Gradient Torque ($T_{gravity}$) is referred as a perturbation in the orbit [126]. The maximum moments of inactivity in the orbital plane & minimum moment of inactivity in the local frame this configuration used to re-orient the stabilized satellite. A small mass injected from the satellite body for the de-saturation to stabilize the attitudes of satellite in gravity gradient method (GGM). The GGM method is used for low earth orbit satellite. For, High earth orbit such as geostationary earth orbit (GEO) it has less pointing accuracy to stabilize the satellite [127]. It requires the more effective damping elements/components. The eccentricity decides the size of the orbit. For, Elliptical orbit gravity gradient torques periodically changes the orbital elements.

Motion equation of satellite in the body frame

$$\begin{bmatrix} v1 \\ v2 \end{bmatrix} = \begin{bmatrix} -\Omega * C * \gamma & -S * \gamma \\ \Omega * S * V & -C * \gamma \end{bmatrix} \begin{bmatrix} u1 \\ u2 \end{bmatrix} \qquad C = \cos,\ S = \sin \qquad (4.44)$$

This is dynamic equation (4.44) of the satellite can be used to design the control technique of the satellite model. [127]

4.6. Perturbation Analysis of at Low Earth Orbiting satellite:

The satellite attitude governor/control is very important to stabilize the satellite along with its predetermined orientation. The perturbation forces or environmental disturbances may affect the satellites and the original orbit may get changed due to these perturbations. Thus, it is very important to reduce these perturbation forces as they can cause the life time of the satellite to be significantly reduced [128]. The environmental force differs at various altitudes. The proposed analysis considered for the simulations of LEO satellites affected more by aerodynamic drag and gravitational attraction due to the proximity of earth as compared to other perturbations.

4.6.1. Spacecraft considered: International Space Station (ISS)

The purpose of the International Space Station used for observation in Earth surface at low Earth's orbit satellite. The design for predicting the future missions to the planetary surface such as Mars, Moon, etc. First mission launched to the orbit 1998. It is affected by environmental perturbation, so it requires the frequent thruster to maintain the satellite into the actual orbit. The main aims for the mission are earth observation, trajectory transfer, predicts the future mission, Now ISS is used for commercial purpose and educational & diplomatic conditions [129]. Its perigee is at

403 km and apogee is 406 km and inclination of 51.36 deg. The period of one revolution of this satellite is about 92.5 minutes and it completes about 15.54 orbits per day. It has an orbital velocity of 7.67 km/s. The initial values of ISS (See table 4.2) that are required for the perturbation calculation are given in Appendix B.

Table 4.2: Initial values of International Space Station (ISS) [129]

Epoch Time (GMT)	**2018/092/13:19:31.516**
Initial position [x, y, z] (m)	**[-3754663.80 -5060641.17 -2517733.24]**
Initial velocity [u, v, w] (m/s)	**[5356.846188 -1332.207337 -5317.508141]**
Mass of ISS (kg)	**411326.99584**
Area of ISS (m^2)	**1640.6**

In Figure 4.18; describe the changes in ISS attitude such as position and velocity due to the perturbation forces action on it. This graph shows the change in altitude, earth radius with the altitude of the satellite changes with atmospheric perturbation [130]. The magnitude of position vector (4.45) is:

$$r = \sqrt{x^2 + y^2 + z^2} \qquad (4.45)$$

Let, Position vector = x $_i$ + y $_j$ + z $_k$

x = distance of satellite measured in x-direction (m)

y = distance of satellite measured in y-direction (m)

And, z = distance of satellite measured in z-direction (m)

Similarly, the velocity vector (4.46) of satellite is:

$$V = \sqrt{u^2 + v^2 + w^2} \qquad (4.46)$$

Where, V = u i + v j + z k

u = velocity measured in the direction, x (m/s)

v = velocity measured in the direction, y (m/s)

And,   w = velocity measured in the direction, z (m/s)

The position and velocity vectors are shown in Figures.4.18. & 4.19 respectively and their variations with respect to times use referred from appendix B.

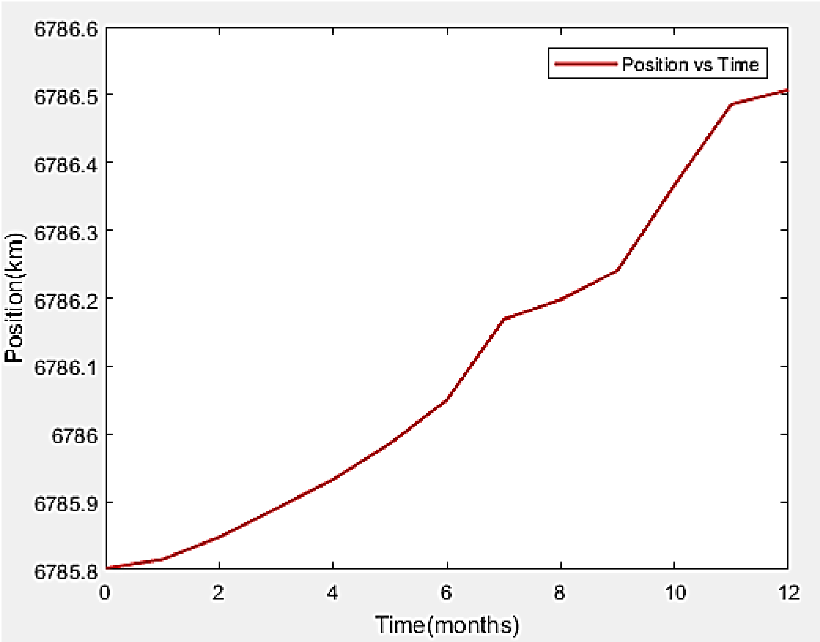

Figure (4.18) Changes in position of the ISS with time

Since, the altitude of ISS satellite is about 350 to 420 km from the Earth's surface. Therefore, the Semi-Major axis will be from satellite altitude and earth center distance.

$$SMA = R_e + (R_{apogee} + R_{perigee}) / 2$$

Where, SMA = Semi-Major Axis distance

Re = Radius of Earth = 6378 km, R_{apogee} = Distance between satellite and Earth at apogee point, $R_{perigee}$ = Distance between satellite and Earth at perigee point

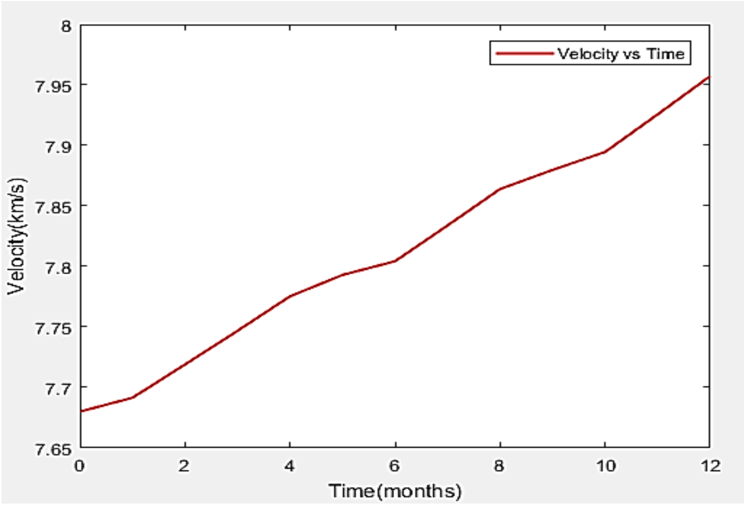

Figure (4.19) Changes in velocity of the ISS time

The orbital components are the parameters required to remarkably recognize a particular orbits. In celestial mechanics these components are for the most part considered in establishing two-body frameworks, where a Kepler orbit is utilized. There is a wide range of approaches to numerically depict a similar orbit, however, certain plans, each comprising of an arrangement of six parameters, are ordinarily utilized as a part of space science and orbital mechanics. A genuine orbit (and its components) changes after some time because of gravitational irritations by different items and the impacts of relativity. A Keplerian orbit is simply a romanticized, scientific estimate at a specific time. The conventional orbital components are the six Keplerian components, after Johannes Kepler and his laws of planetary movement.

Source of Data: The data of the perturbation analysis are based on the sources mentioned below.

NASA 2-Line code- A two-line component set (TLE) is information arranges encoding a rundown of orbital components of an Earth-orbiting object for a given point in time, utilizing appropriate forecast recipe, the state (position and speed) any time before or future can be assessed with some exactness. TLEs can portray the directions just of the Earth-orbiting object [131]. The way to achieve goals is through a well-defined path. The path includes different stages of analysis and observations to be thoroughly kept in mind during the whole process.

4.6.2. Methodology

In flow chart shown in Figure (4.20) describe the Nano satellite perturbations calculation with different atmospheric condition using MATLAB Satellite Control ToolBox (SCT)

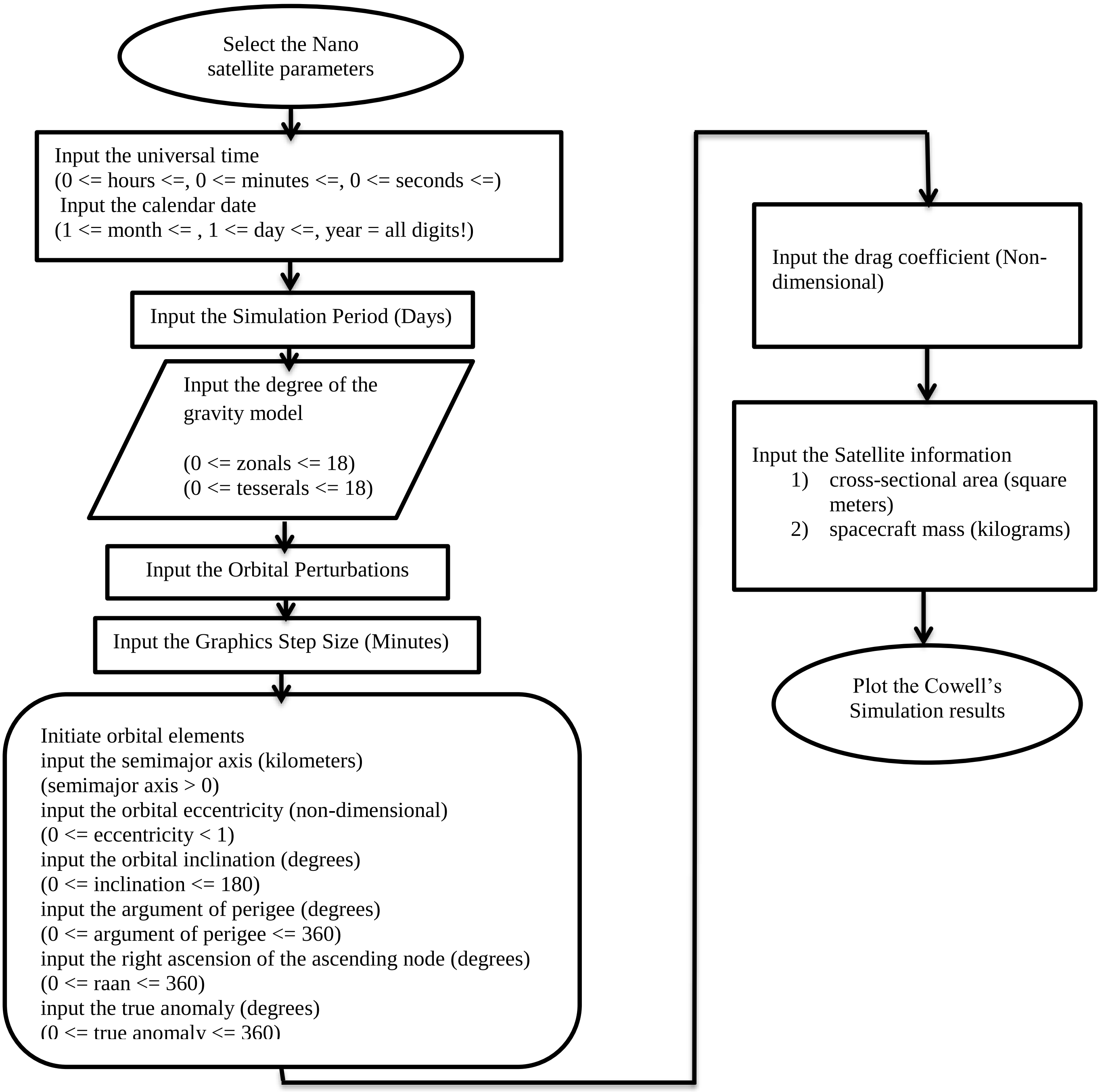

Figure (4.20) Flow chart of Nano Satellite Cowell's orbital perturbation calculations (SCT)

In the Cowell's perturbation algorithms, Nano satellite Keplerian element due to variation in orbital perturbation is estimated. For, simulations considered the suitable design parameters and constants. In the thesis, discusses the perturbation effects in Nano satellites such as SRM satellite, Pratham (IITB) satellite considered. The evaluation of perturbation of satellite is briefly explained. The simulation results illustrate the variation in orbital elements is SMA, orbital inclination, Eccentricity, Argument of perigee, RAAN, True anomaly. For, reference analysis of motion and trajectory equations of satellite considered the International Space station (ISS). The following NORAD data considered for simulation. To implement's the Cowells algorithms using MATLAB environments.

Satellite Selection:

The research focuses around the investigation of a satellite that has been orbiting around the Earth. This can be satellite from the Low Earth Orbit (LEO). A satellite in the LEO orbit is subjected to different drag powers and thus has expanded perturbations and probabilities along its way. The way of the satellite can be exceedingly circular along with little changes in the way and speed. To maintain a strategic distance from such radical conditions in the counts and keeping the examination up to its stamp, engaged towards LEO orbits.

Raw Data Collection

The collection of data for simulations includes the Keplerian elements of the satellites which keep on changing every two weeks. The data used is as follows. (Refers Appendix A)

International Space Station (ISS): Two-Line Elements

1 25544U 98067A 18300.65041667 .00001569 00000-0 31217-4 0 9996

2 25544 51.873 35.151 .000336 135.0151 193.3370 15.53870137139112

Epoch Format	- UTC Gregorian
Epoch	-03 Apr 2018 13:19:31.516

Figure, (4.21) shows the General Mission Analysis Tool describe the orbit with the Epoch formats. The GMAT considers the Universal Time Coordinates (UTC) Gregorian and coordinate frames EarthMJ2000Eq models in Keplerian orbit.

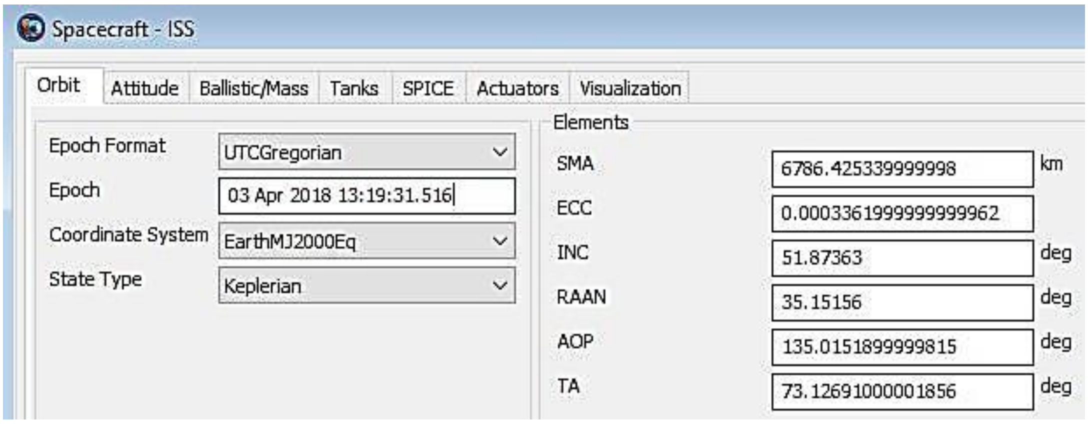

Figure (4.21) Low Earth Orbit analysis of the International Space Station epoch at 03 Apr 2018 13:19:31.516 UTC Gregorian EarthMU2000Eq, General Mission Analysis Tool (GMAT) with Keplerian Elements

In Figure (4.22) the propagator considered for the simulation is Runge-Kutta ODE Integrator with initial step size is 60 seconds, primary body an earth's surface. The Gravity model's EGM-96 has been introduced for both degree and order is 4. The atmospheric model MSISE90 considered for GMAT simulations [132], [133]. The simulation minimum step size 0.001 and maximum step size is 2700 up to 50 attempts.

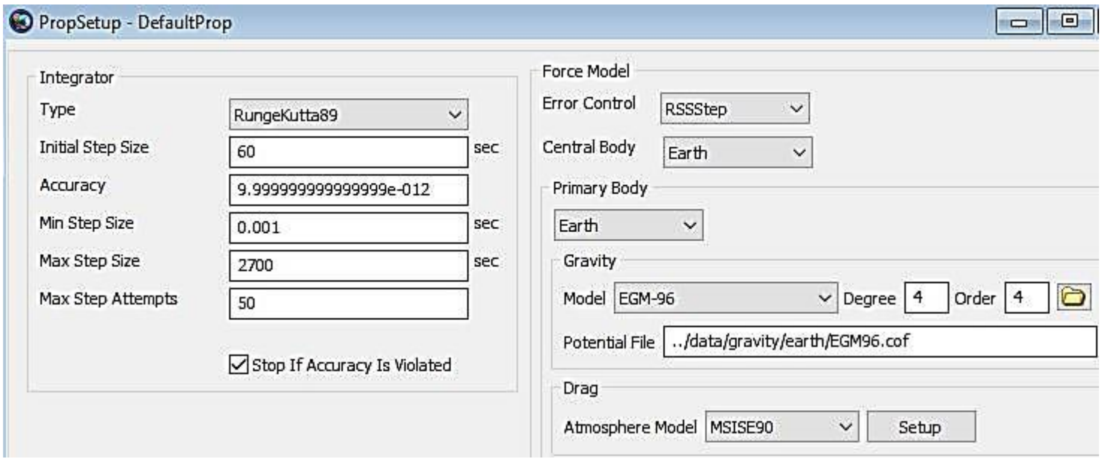

Figure (4.22) Selection of Propagator of ISS Primary bodies are Earth-Satellite given Gravity model EGM-96 and Atmosphere Model MSISE90

Table (4.3) ISS Keplerian, UTC Gregorian 03 Apr 18, 13:19:31.516 [129]

Orbital Parameter's	Simulation values
Semi major axis (SMA)	6786.4253 Km
Eccentricity	0.000336
Inclination	51.873 Degree
RAAN	35.151Degree
Argument of Perigee (AOP)	135.0151
Degree True Anomaly (TA)	73.1269 Degree

The following Keplerian simulations results obtained for International space station (ISS) epoch 03 Apr 2018 13:19:31.516 UTC Gregorian EarthMU2000Eq, the gravitational parameters consider for simulation is 3.98 * 10^{14} (km^3/Sec^2) [133]. In table (4.3) reflect the design parameter of ISS Keplerian element at UTC Gregorian 03 Apr 2018 13:19:31.516**.** The following perturbation forces considered for the International space station includes aerodynamic drag, and solar radiation pressure. The validation of Cowell's simulation results compared with known Keplerian elements. The response of the known orbital elements is modeled by General Mission Analysis Tools. In the GMAT, the Gravity model EGM-96 and Atmosphere Model MSISE90 at Low Earth Orbit satellite has been introduced. The atmospheric model considered the valid assumption used for standard/ accurate results [132].

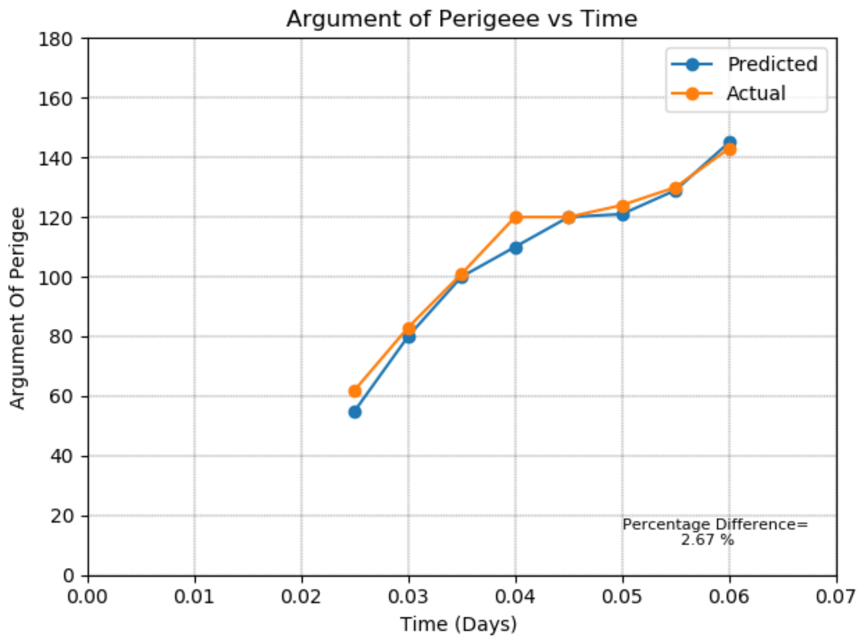

Figure (4.23) Variations of Argument of Perigee with time of International Space Station (ISS) Epoch 03 Apr 2018 13:19:31.516 UTC Gregorian

The argument of perigee usually varies between 0 to 360 degrees in the entire orbit. In perturbation analysis the argument of perigee changes periodically due to orbital perturbations. A large variation can be seen in Figure (4.23) due to proximity of Earth surface. During initial simulation time the value reach up 62 degree and at final time reach 140 degrees. The simulation error tolerance is considered as e^{-8} and step size is 30 Graphics simulations. Figure 4.23 shows increase in argument of perigee from initial to final time values. The result shown in orange color indicates the actual orbital trajectory and BLUE color indicates the predicted trajectory of the International space station modeled by GMAT initial step size 0.001 maximum step size 2700 for 50 attempts has been introduced the coordinate system EarthMU2000Eq. The simulation period of the ISS includes 0.07 times (days). In the simulation, results indicate variations in argument of perigee 80 degrees to 120 degrees between period 0.03 to 0.04 times (days). So, it is desired to model the disturbance equation using Cowell's perturbation ODE solver. The simulation of ODE obtained with minimum errors percentage is 2.67%. The RA of Ascending Node (RAAN) has a secular behavior as well as a periodic variation with low amplitude. The variation is approximately 4.8 to 5.2 degrees between initial and final time.

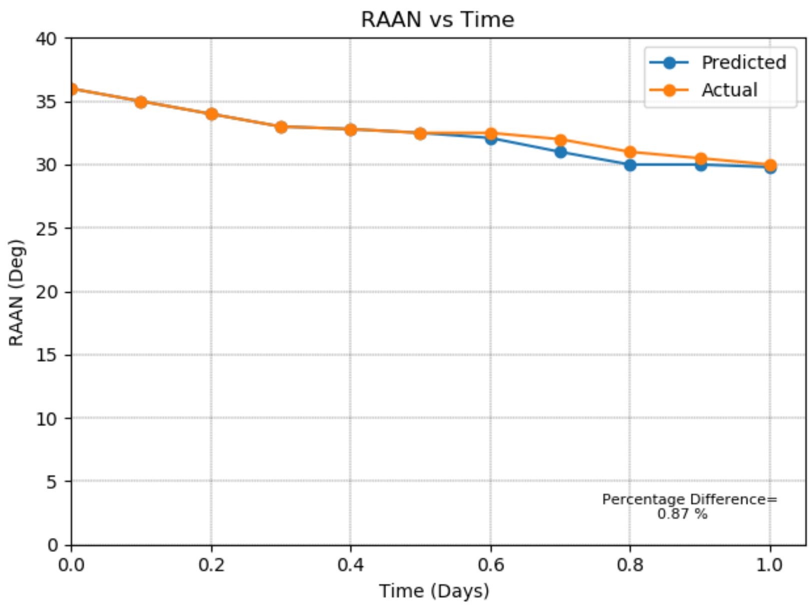

Figure (4.24) Variations of RAAN with respect to time of International Space Station (ISS) Epoch 03 Apr 2018 13:19:31.516 UTC Gregorian

In the simulation, results indicate the variation in an argument of perigee 36 degrees to 30 degrees between the period 0 to 1.2 times (days). So, it is desired to model the disturbance equation using Cowell's perturbation ODE solver. The simulation of ODE obtained with minimum errors percentage is 0.87%. The variations of right assertion ascending node (RAAN) with respect to the vernal equinox (VE) are shown in Figure 4.24. The angular deviation from perigee 403Km to vernal equinox is 30^o of the International Space station. In the simulation the Right Ascension of Ascending Node (RAAN) from intial period 36 deg to 30 deg changes during time 1 (days).

In the simulation, results shows the position of the ISS with respect to perigee. Hence, the variation is very large with respect to initial and final time between 0 to 0.045 times (days). The Figure 4.25 shows an increment in True Anomaly with respect to time period. It is clearly observed the position of satellite in orbit continuously varies with respect to time period. The simulation error tolerance is considered as e^{-8} and step size is 30 Graphics simulations.

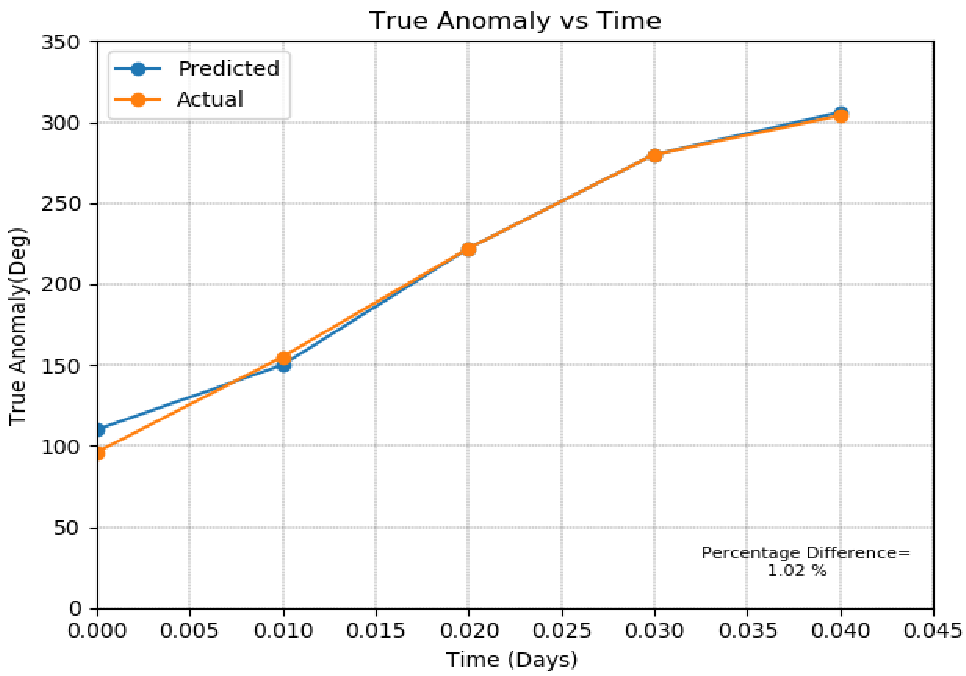

Figure (4.25) Variations of True Anomaly with respect to time of International Space Station (ISS) Epoch 03 Apr 2018 13:19:31.516 UTC Gregorian

The variation is approximately 96 to 300 degrees between initial and final time in orbit. Figure 4.25. shows an increment in True Anomaly (RAAN) with respect to time period. The simulation of ODE obtained with minimum 1.02 percentage (%) of error deviations. Since the apogee and perigee of the ISS satellite are almost equal, therefore, the eccentricity will be small i.e., near to 0, which means that the orbit is almost circular in nature at Low Earth Orbit. In Figure 4.26 shows the actual trajectory (Orange color) and predicted trajectory (Blue color) variation of eccentricity with respect to time periods.

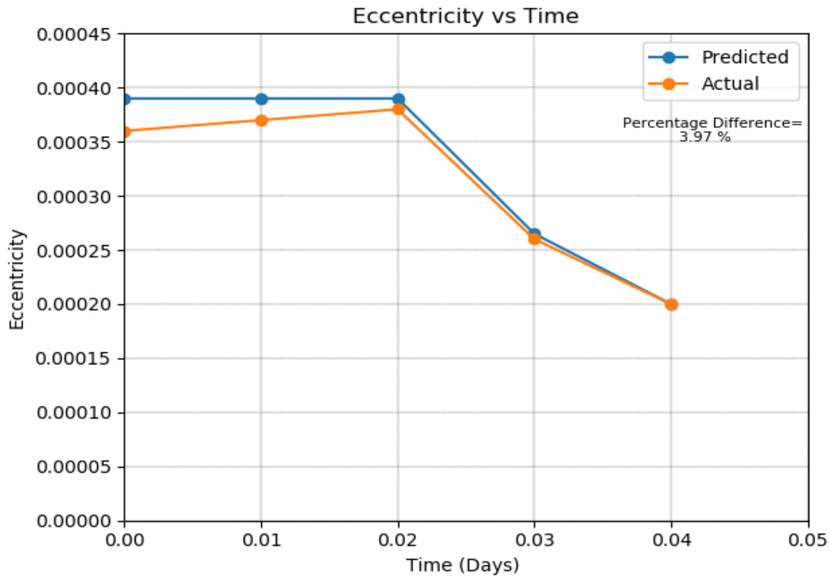

Figure (4.26) Variations of Eccentricity with respect to the time for International Space Station (ISS) Epoch 03 Apr 2018 13:19:31.516 UTC Gregorian

Eccentricity oscillates in orbit due to perturbation forces. The eccentricity decides the shape of the orbit. The simulation periods considered of ISS is 0.05 times (days). The variation of eccentricity from initial simulation time is 0.00036 to final time is 0.00020 in LEO orbit. The orange colour indicates the actual trajectory and BLUE colour indicates predicted trajectory. The Cowell's perturbation algorithm simulation of ODE obtained with minimum errors percentage is 3.97%.

Figure 4.27 shows the variation between orbital inclination and time periods of orbit. The overall change in orbital inclination is 51.875 degrees to 51.845 degrees from initial to final time. The orbital inclination is angle made by satellite orbital plane with respect to Earth's equatorial plane. The change in inclination will change the orientation of the transmitting and receiving antennas on satellite which will make communication of satellite very difficult to receive the information. Therefore, the orbital inclination must be maintained at all time under any perturbation condition.

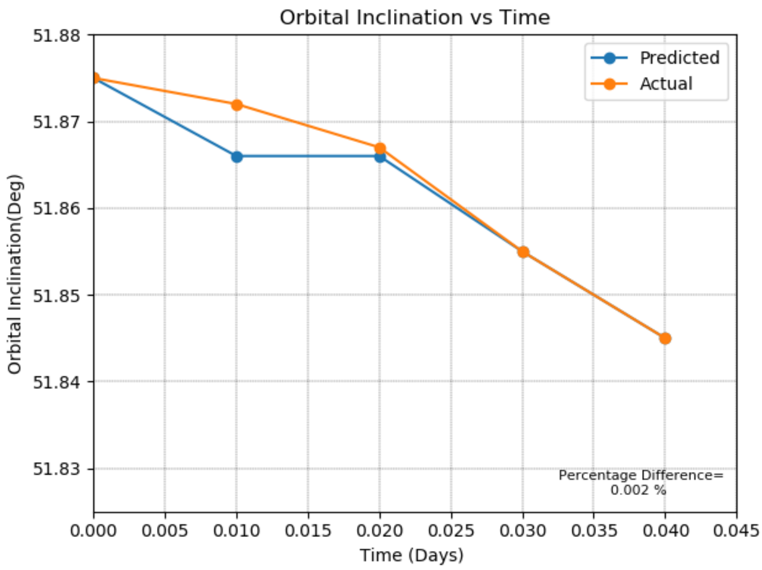

Figure (4.27) Variations of Orbital Inclination with respect to International Space Station (ISS) Epoch 03 Apr 2018 13:19:31.516 UTC Gregorian

The variations of inclination measured from Epoch 03 Apr 2018 13:19:31.516 UTC Gregorian. The Keplerian EarthMJ2000Eq has been introduced 0.045 times (days). The simulation of actual trajectory to the predicted trajectory of orbit obtained with minimum 0.002 errors percentage (%) of the orbit. In Figure 4.28 shows the variations of Semi-major axis with respect to time which varies at an equal interval. As due to aerodynamic drag perturbations, the altitude decreases due to which semi-major axis decreases within a time variation from 0 to 0.040 times (days). This decrease can be prevented by using control mechanisms such as thrusters (DC motor) to reorient the satellite whenever its orientation is disturbed due to any perturbations in the orbit. (discussed in chapter 6 attitude control system) The satellite's Semi-Major axis reduces from 6786 to 6777 km i.e., an altitude changes of almost 9 km within 0.040 times (days). The orange colour indicates the actual trajectory and BLUE colour indicates the Cowell's perturbation algorithm (ODE Solver) predicted trajectory of the orbit. The simulation of ODE obtained with minimum errors percentage is 0.002% from actual trajectory to the predicted trajectory.

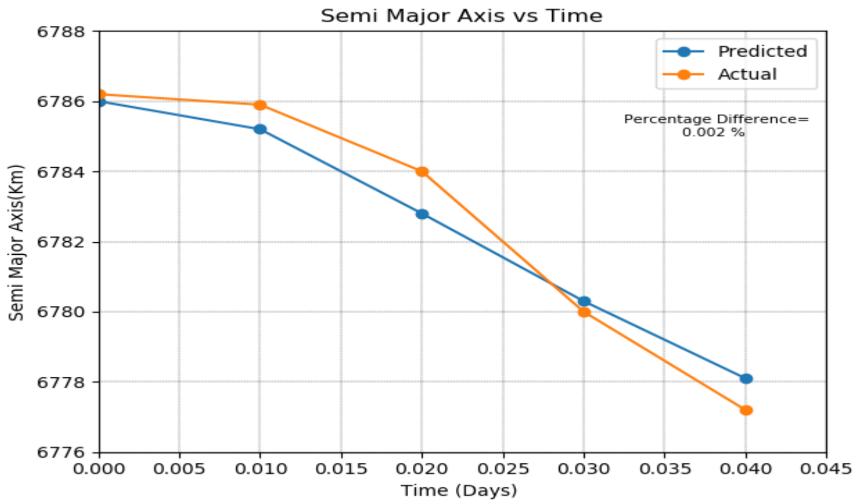

Figure (4.28) Variations of Semi-Major Axis with respect to International Space Station (ISS) Epoch 03 Apr 2018 13:19:31.516 UTC Gregorian

The path travelled by satellite can be visualized by the help of GMAT (General Mission Analysis Tool) software in which the Cartesian state vectors, i.e., position and velocity or Keplerian elements are used as the input at a point of time, known as Epoch and the path of the satellite over the Earth's surface is the output shown in the simulations. The ground track plots (Figure 4.29) shows the orbit view of the satellite corresponding to epoch time 03 April 2018 13:19:31.516 with considered atmospheric drag model in GMAT.

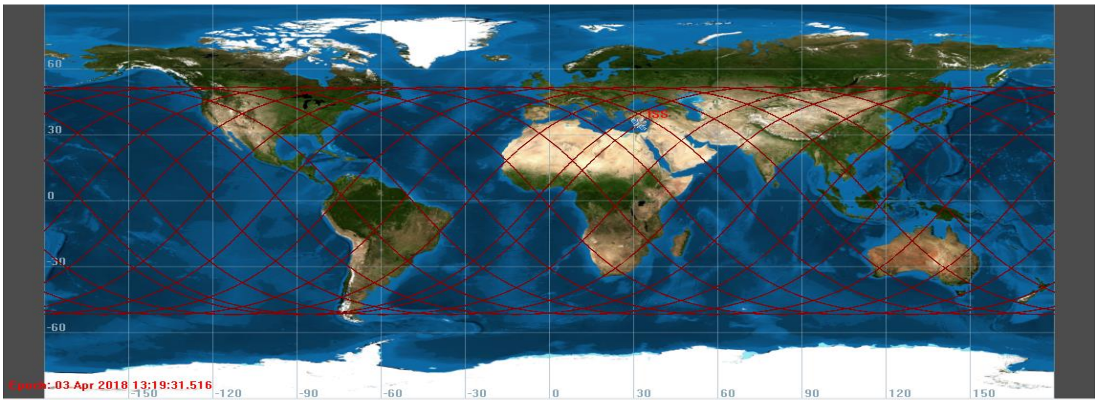

Figure (4.29) Ground Track Plot at Epoch - 03 Apr 2018 13:19:31.516

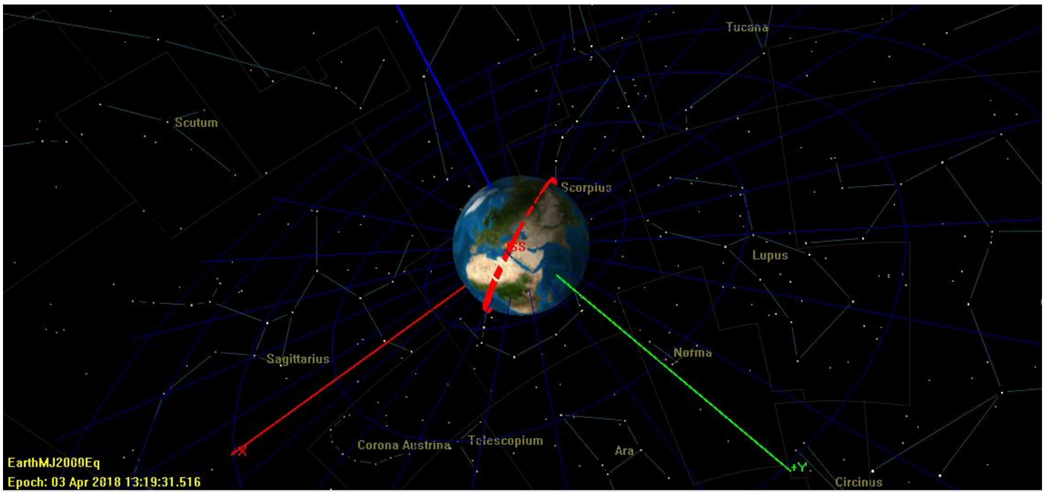

Figure (4.30) Orbit View at Epoch - 03 Apr 2018 13:19:31.516

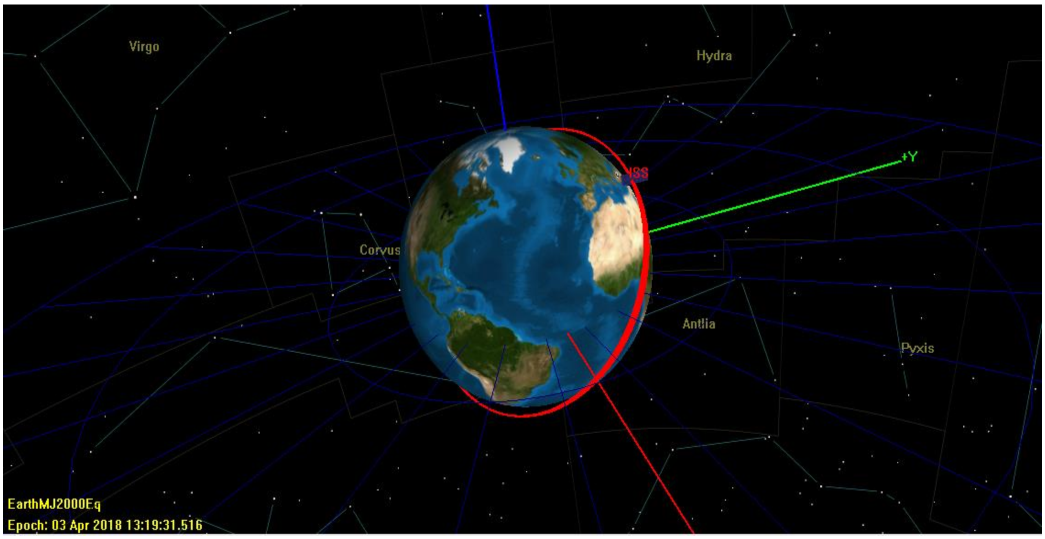

Figure (4.31) Orbit view at EarthMJ2000Eq UTC

The Figure 4.30 & 4.31 show the orbit view at Epoch with corresponding to final values of position and velocity which includes the Atmospheric Drag model in GMAT solved by ordinary differential equation (ODE) with the help of Runge – Kutta method through MATLAB Environment.

Table (4.4) Magnitudes of errors of Keplerian elements of International Space Station (ISS) with actual and predicted trajectory in the orbit with error variation

Semi-Major Axis (Km)			Orbital Inclination (deg)			Argument of Perigeee (deg)		
Magnitudes of Actual (GMAT) Simulations	Magnitudes of Predicted (Cowell's) Simulations	Error Deviations (%)	Magnitudes of Actual (GMAT) Simulations	Magnitudes of Predicted (Cowell's) Simulations	Error Deviations (%)	Magnitudes of Actual (GMAT) Simulations	Magnitudes of Predicted (Cowell's) Simulations	Error Deviations (%)
6786.2	6786	0.2	51.875	51.875	0	62	55	7
6785.9	6785.2	0.7	51.872	51.866	0.006	83	80	3
6,784	6782.8	1.2	51.867	51.864	0.003	101	100	1
6780	6779.9	0.1	51.855	51.855	0	120	110	10
6777.2	6777	0.2	51.845	51.845	0	120	120	0

True Anomaly (deg)			RAAN (deg)			Eccentriciy (deg)		
Magnitudes of Actual (GMAT) Simulations	Magnitudes of Predicted (Cowell's) Simulations	Error Deviations (%)	Magnitudes of Actual (GMAT) Simulations	Magnitudes of Predicted (Cowell's) Simulations	Error Deviations (%)	Magnitudes of Actual (GMAT) Simulations	Magnitudes of Predicted (Cowell's) Simulations	Error Deviations (%)
110	96	14	36	36	0	0.00039	0.00036	0.00003
155	150	5	35	35	0	0.00039	0.00037	0.00002
222	222	0	34	34	0	0.00039	0.00037	0.00002
280	280	0	33	33	0	0.000265	0.000265	0
306	304	2	32.8	32	0.8	0.0002	0.0002	0

The table 4.4 shows the International space station magnitudes of actual simulation (GMAT) and magnitudes of predicted simulations (Cowell's) with minimum error deviation of Keplerian elements in reference low earth's orbit at UTC 03 Apr 2018 13:19:31.516 Gregorian's. The trajectories of GMAT simulation and the Cowell's simulation are close to the nearest integer. The Cowell's predicts the accurate trajectory the satellite deviates from actual orbit. This data is very much useful to estimate the errors in attitudes used to design the proper attitude control techniques. (discussed in chapter 6)

4.6.3. Pratham (IIT- Bombay) Satellite perturbation analysis at LEO.

The Pratham (IIT Bombay) satellite Keplerian elements consider for the simulations is epoch 08 Jul 2018 04:53:04.000 UTC Gregorian EarthMJ2000Eq, the gravitational parameters that has been introduced for simulation is 3.98 * 10^{14} (km^3/Sec^2) [134]

Methodology

Flow chart shown in Figure (4.32) discuss the satellite Keplerian elements of Nano satellite perturbation analysis using Global Mission Analysis tools (GMAT).

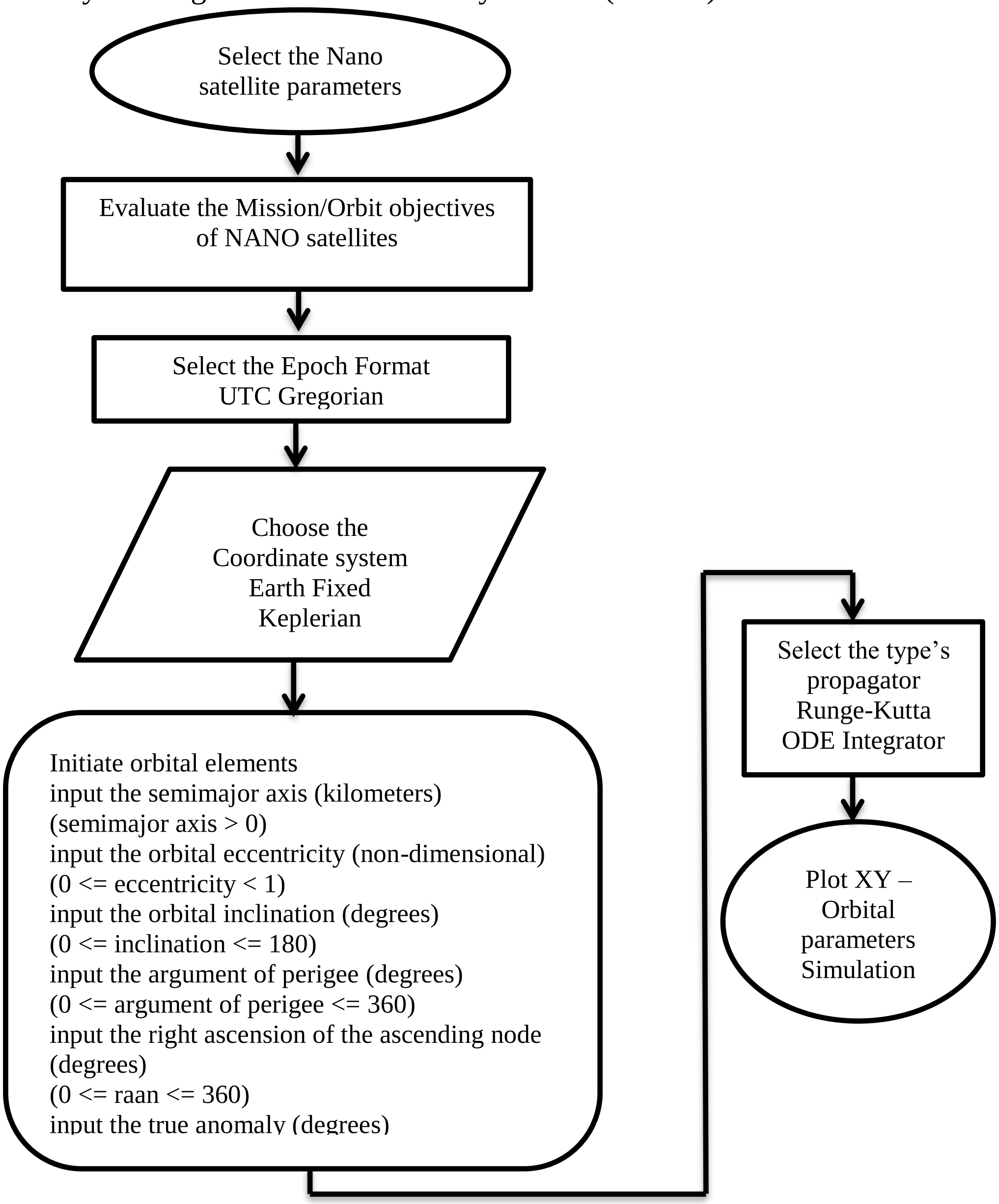

Figure (4.32) Flow chart of Satellite Keplerian GMAT Simulation

The simulation time is minimum step size 0.001 and maximum step size is 2700 up to 50 attempts. The Keplerian elements are referred from NORAD 2-line elements. The perturbation forces aerodynamic drag, solar pressure considered for the simulations. In Table (4.5) considered the Pratham (IITB) satellite simulation parameters using GMAT. In Global Mission Analysis tools (GMAT) perturbation algorithms, Nano satellite Keplerian element due to variation in orbital perturbation is estimated. For, simulations considered the suitable design parameters and constants. In the thesis, discusses the perturbation effects in Nano satellites such as SRM satellite, Pratham (IITB) satellite considered. The simulation results illustrate the variation in orbital elements is SMA, orbital inclination, Eccentricity, Argument of perigee, RAAN, True anomaly. The following NORAD data considered for simulation [135]. To implement's the algorithms using Global Mission Analysis tools (GMAT).

Table (4.5) Pratham satellite simulation data [135]

Epoch Format	UTC Gregorian
Epoch	08 Jul 2018 04:53:04.000
Coordinate System	EarthMJ2000Eq
State Type	Keplerian

NORAD Two-Line Elements of Pratham (Refer Appendix A)

1 41783U 16059A 18295.14940496 .00000065 00000-0 21820-4 0 9994

2 41783 98.116 250.4222 0034299 31.8295 302.1210 14.62950175110526

The data used for perturbation algorithms is given below

Figure (4.33) shows the Universal Time Coordinates as Epoch at 08 Jul 2018 04:53:04.000 UTC Gregorian with Keplerian coordinates EarthMJ2000Eq.

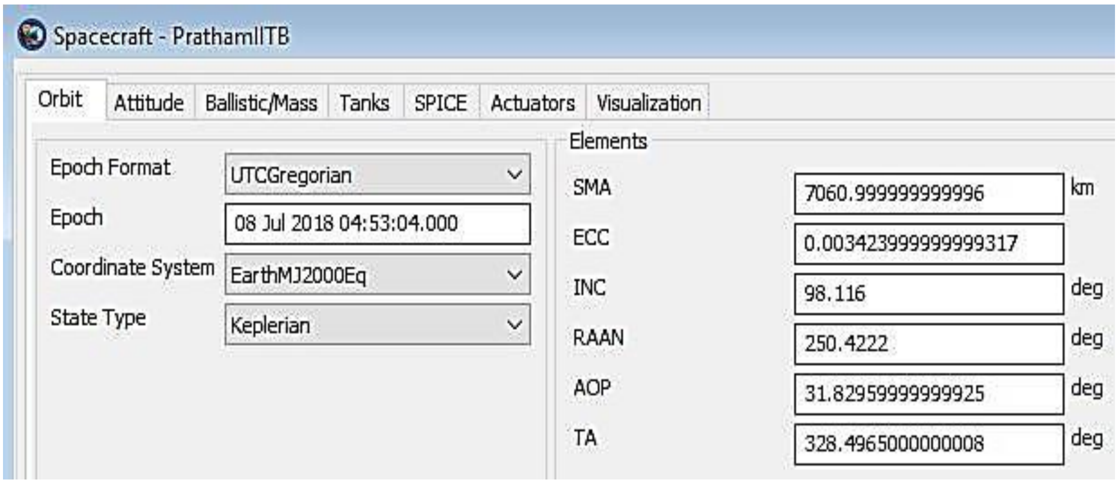

Figure (4.33) LEO analysis of the Pratham, Epoch at 08 Jul 2018 04:53:04.000 UTC Gregorian EarthMJ2000Eq GMAT with Keplerian coordinates

The Keplerian simulations results obtained for Pratham satellite (IIT Bombay), Mass, 10 kg, Size 26×26×26 cm, Orbital angular velocity, Ω = 0.0010346, 817 km altitude, Epoch 08 Jul 2018 04:53:04.000 UTC Gregorian, EarthMJ2000Eq. [134]

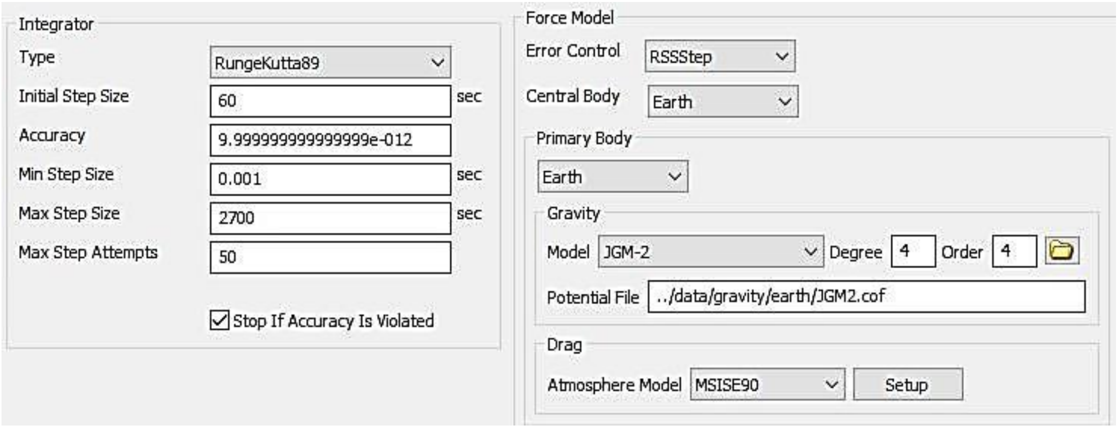

Figure (4.34) Selection of Propagator of Pratham Primary bodies are Earth-Satellite given Gravity model JGM-2 and Atmosphere Model MSISE90

The atmospheric model has been introduced MSISE90 for the GMAT simulations. During simulation, minimum step size 0.001 and maximum step size is 2700 up to 50 attempts. In the perturbation algorithm considered the Runge-Kutta ODE Integrator with initial step size is 60 seconds, primary body an earth's surface. The Gravity models JGM-2 for degree and order is 4.

Table (4.6) Pratham (IITB) satellite NORAD data, Epoch at 08 Jul 2018 04:53:04.000 UTC Gregorian EarthMJ2000Eq [134]

Keplerian Details	NORAD Data
NORAD ID	41783
Int'l Code	2016-059A
Perigee	666.3 km
Apogee	715.3 km
Inclination	98.1 °
Period	98.4 minutes
Semi major axis	7061 km

In table (4.6) shows the NORAD data of Pratham satellite, Epoch at 08 Jul 2018 04:53:04.000 UTC Gregorian EarthMJ2000Eq

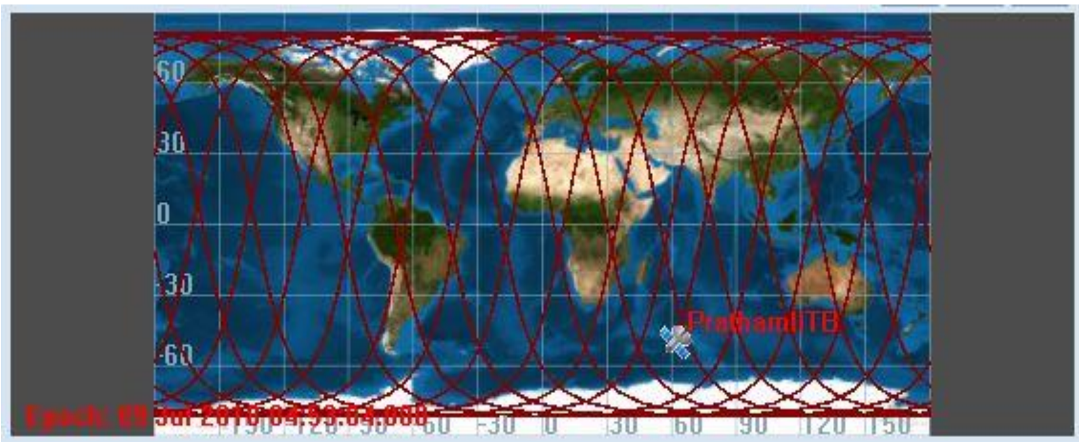

Figure (4.35) Ground Track Plot at Epoch - 08 Jul 2018 04:53:04.000

The path travelled by satellite can be visualized by the help of GMAT (General Mission Analysis Tool) software in which the Cartesian state vectors, i.e., position and velocity or Keplerian elements are used as the input at a point of time, known as Epoch and the path of the satellite over the Earth's surface is the output shown in the simulations. The ground track plots. In Figure 4.35 shows the orbit view of the satellite corresponding to the epoch time 08 Jul 2018 04:53:04.000 with an atmospheric drag model in GMAT.

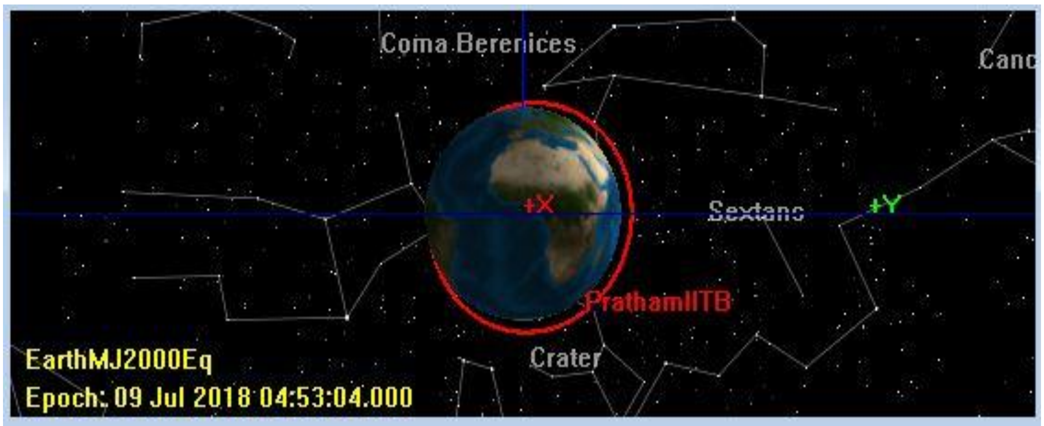

Figure (4.36) Pratham orbit view at EarthMJ2000Eq UTC

The Figure 4.36 shows the orbit view at Epoch with corresponding final values of position and velocity of satellite. In the simulation parameters included the Atmospheric Drag model using GMAT/ MATLAB solved by the ordinary differential equation (ODE) with the help of Runge – Kutta methods. The gravitational parameters considered for simulation is 3.98 * 10^{14} (km^3/Sec^2). The perturbation forces for Pratham includes are, aerodynamic drag, and solar pressure. The validation of Cowell’s simulation results compared with known Keplerian elements. The response of the known orbital elements is modeled by General Mission Analysis Tools. In the GMAT, Gravity model JGM-2 and Atmosphere Model MSISE90 at low Earth orbiting satellite has been introduced. The atmospheric model considered the valid assumption used for standard/ accurate results.

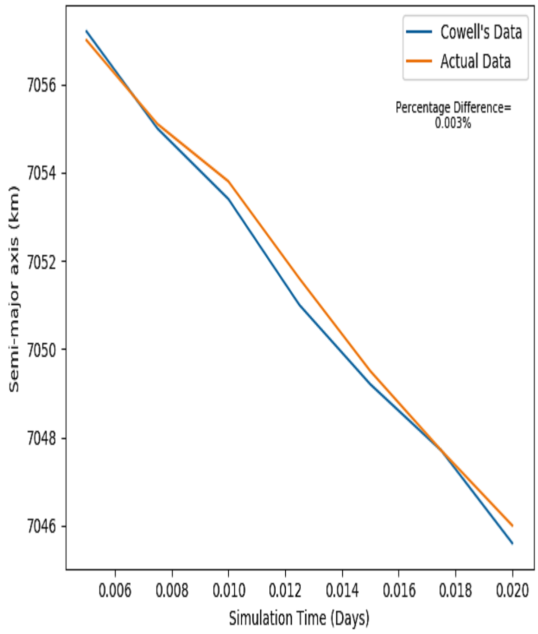

(a)

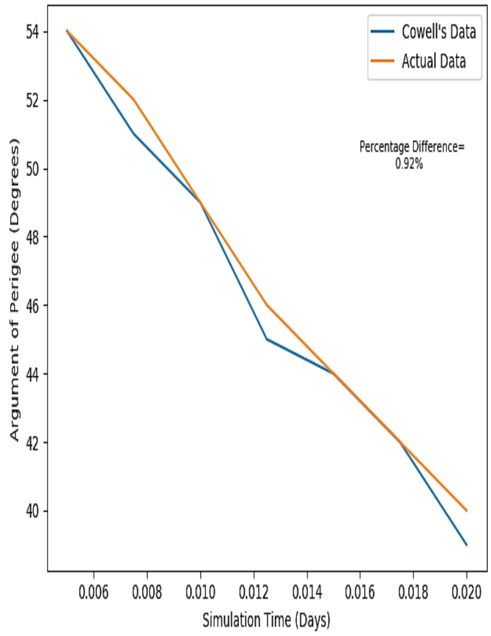

(b)

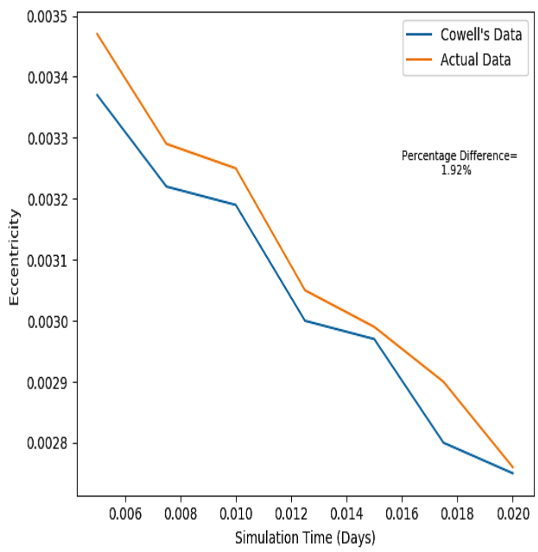

(c)

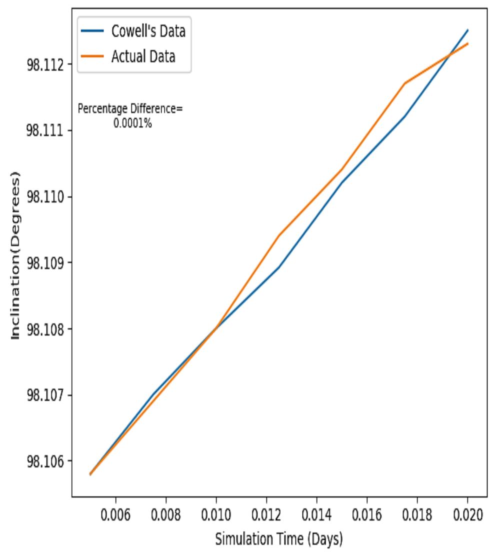

(d)

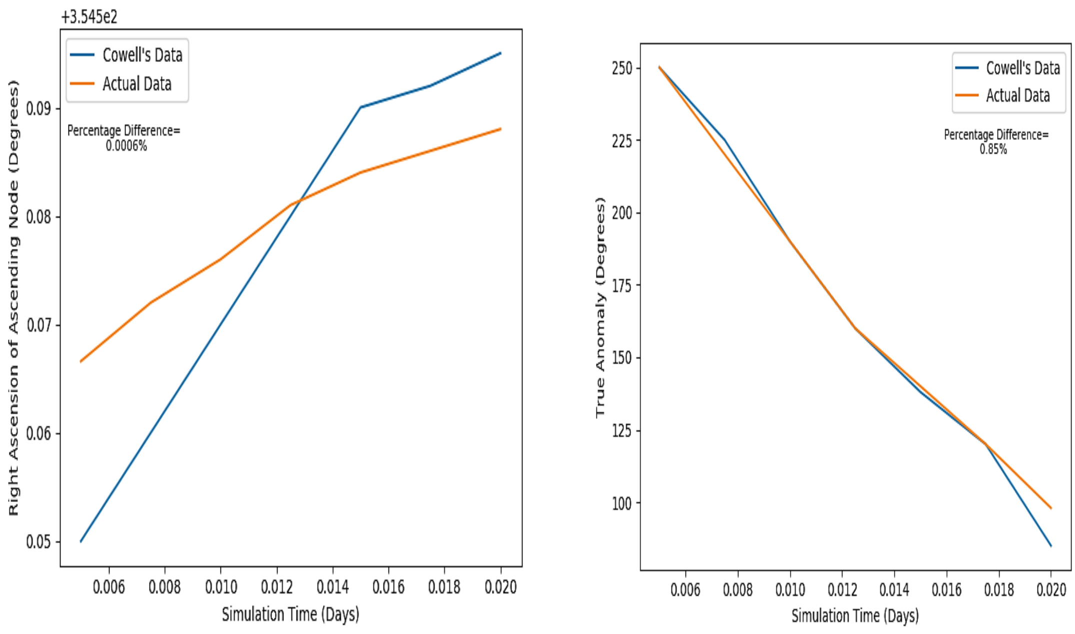

(e) (f)

Figure (4.37) The orbital variations of Pratham satellite Epoch at 08 Jul 2018 04:53:04.000 UTC Gregorian EarthMU2000Eq, Ω = 0.0010346 rad/s in LEO (a) Semi major axis (b) Argument of perigee (c) Eccentricity (d) Orbital Inclination (e) Right Ascension of Ascending Node (f) True Anomaly

The simulation error tolerance is considered as e^{-8} and step size is 30 Graphics simulations. In Figure (4.37) shows the Pratham satellite design of Cowells simulations and GMAT simulations magnitudes of actual orbital trajectory (orange color) and magnitudes of predicted trajectory (blue color) in the orbit.

Table (4.7) (a) Magnitudes of errors of Keplerian elements of Pratham satellite with actual and predicted trajectory in the orbit

Simulation Periods (Days)	Semi-Major Axis (Km)		Errors deviations (%)	Argument of Perigee (Deg)		Errors deviations (%)	Eccentricity		Errors deviations (%)
	Magnitudes of actual data (GMAT) Simulations	Magnitudes of Predicted data (Cowel's) Simulations		Magnitudes of actual data (GMAT) Simulations	Magnitudes of Predicted data (Cowel's) Simulations		Magnitudes of actual data (GMAT) Simulations	Magnitudes of Predicted data (Cowel's) Simulations	
0.005	7057	7057.2	0.003	54	54	0.92	0.00347	0.00337	1.92
0.0075	7055.1	7055		52	51		0.00329	0.00322	
0.01	7053.8	7053.4		49	49		0.00325	0.00319	
0.0125	7051.6	7051		46	45		0.00305	0.003	
0.015	7049.5	7049.2		44	44		0.00299	0.00297	
0.0175	7047.7	7047.7		42	42		0.0029	0.0028	
0.02	7046	7045.6		40	39		0.00276	0.00257	

The Pratham satellite modeled by GMAT initial step size 0.001 maximum step size 2700 for 50 attempts considered the coordinate system EarthMJ2000Eq. The simulation period of the Pratham satellite is taking into 0.020 times (days). In table (4.7) shown the simulation of ODE obtained with minimum error deviations.

Table (4.7) (b) Magnitudes of errors of Keplerian elements of Pratham satellite with actual and predicted trajectory in the orbit (Orbital Inclination, RAAN, True Anomaly)

Orbital inclination		Errors deviations (%)	RAAN		Errors deviations (%)	True Anomaly		Errors deviations (%)
Magnitudes of actual data (GMAT) Simulation	Magnitudes of Predicted data Cowel's Simulation		Magnitudes of actual data (GMAT) Simulation	Magnitudes of Predicted data Cowel's Simulation		Magnitudes of actual data (GMAT) Simulation	Magnitudes of Predicted data Cowel's Simulation	
98.1058	98.1058	0.0001	354.5666	354.55	0.0006	250	250	0.85
98.1069	98.107		354.572	354.56		220	225	
98.108	98.108		354.576	354.57		190	190	
98.1094	98.10892		354.581	354.58		160	160	
98.1104	98.1102		354.584	354.59		140	138	
98.1117	98.1112		354.586	354.592		120	120	
98.1123	98.1125		354.588	354.595		98	85	

In table 4.7 (b) shows the Pratham satellite's minimum error deviation of Keplerian elements with reference low earth's orbit at UTC 08 Jul 2018 04:53:04.000 Gregorian. The magnitudes of actual and predicted trajectories of GMAT simulation and Cowell's simulation are close to the nearest integer. The Cowell's predicts the actual path from perturbed path of satellite in the orbit. This data is very much useful to estimate the errors in the attitudes and to design the proper attitude control techniques discussed in chapter 6.

4.6.4. Perturbation analysis of SRM Satellite

The Keplerian simulations considered for SRM satellite is epoch 08 Jul 2018 04:53:04.000 UTC Gregorian EarthMJ2000Eq, the gravitational parameters consider for simulation is 3.98 * 10^{14} (km^3/Sec^2). The perturbation forces like aerodynamic drag, solar pressure is considered [136].

NORAD Two-Line Elements of SRM Satellite (Refers Appendix A)

1 37841U 11058D   18294.49222615 .00000304 00000-0 21832-4 0 9990
2 37841 19.9730 318.0255 0011948 77.7215   4.576599 14.10617103362738

The following data is used for simulations.

Table (4.8) SRM Satellite design parameters [136]

Epoch Format	UTC Gregorian
Epoch	08 Jul 2018 10:32:46.000
Coordinate System	EarthMU2000Eq
State Type	Keplerian

The simulation minimum step size 0.001 and maximum step size is 2700 up to 50 attempts. The Keplerian elements are referred from NORAD 2-line elements.

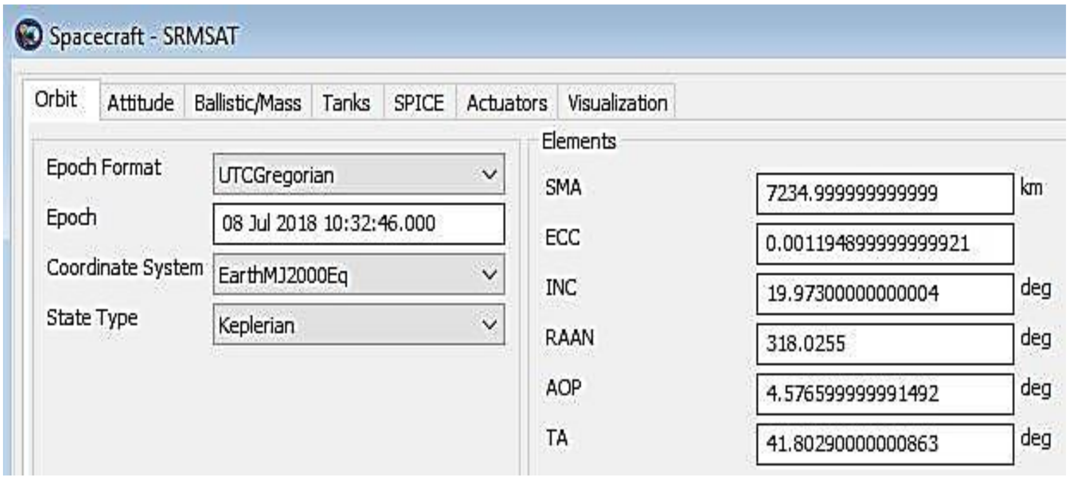

Figure (4.38) LEO analysis of SRM Satellite epoch at 08 Jul 2018 10:32:46.000 UTC Gregorian EarthMU2000Eq GMAT with Keplerian Elements

In table (4.38) shows the SRM satellite design parameters at Universal Time Coordinates as Epoch at 08 Jul 2018 10:32:46.000 UTC Gregorian with Keplerian coordinates EarthMJ2000Eq In Figure (4.38) shows the SRM satellite GMAT simulation considered the UTC 08 Jul 2018 10:32:46.000.

Table (4.9) SRM satellite NORAD data [137]

Keplerian Elements	NORAD Data
NORAD ID	37841
Int'l Code	2011-058D
Perigee	855.7 km
Apogee	873.1 km
Inclination	20.0 °
Period	102.1 minutes
Semi major axis	7235 km

In table (4.9) shows the SRM satellite NORAD data at 08 Jul 2018 10:32:46.000

UTC Gregorian EarthMU2000Eq. The atmospheric model has been introduced MSISE90 for GMAT simulations. The simulation minimum step size 0.001 and maximum step size is 2700 up to 50 attempts.

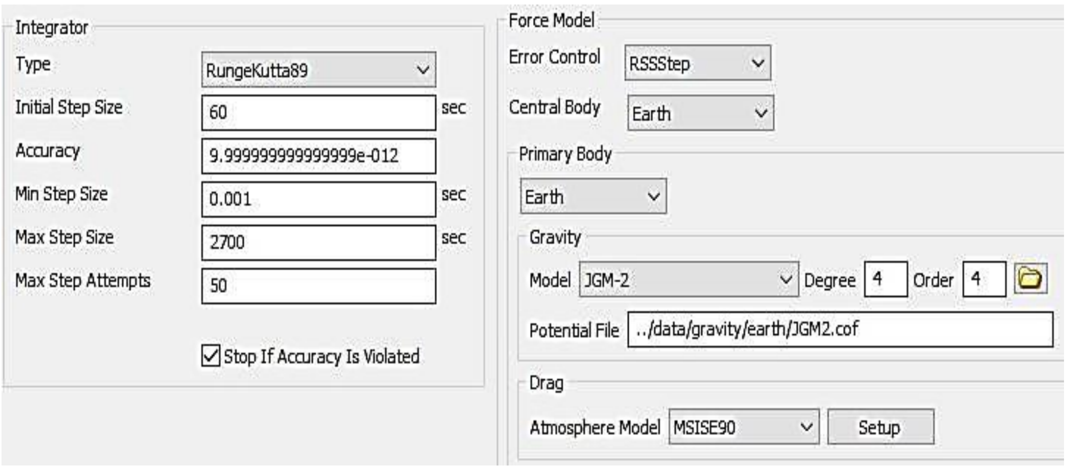

Figure (4.39) Selection of Propagator of SRM satellite Primary bodies are Earth-Satellite given Gravity model JGM-2 and Atmosphere Model MSISE90

In the Figure (4.39) the propagator considered the Runge-Kutta ODE Integrator with initial step size is 60 seconds, primary body an earth's surface. The Gravity models JGM-2 for degree and order is 4.

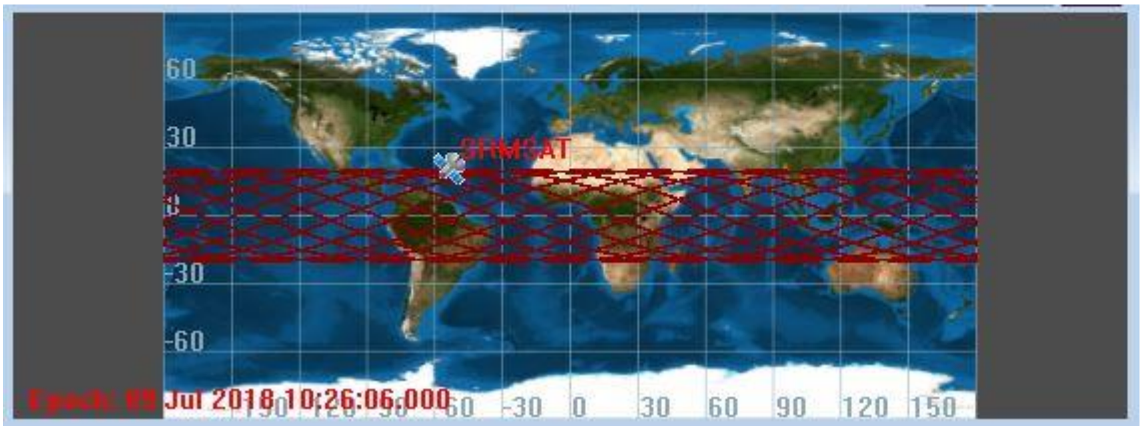

Figure (4.40) Ground Track Plot at Epoch - 08 Jul 2018 10:32:46.000 (UTC)

The path travelled by satellite can be visualized by the help of GMAT (General Mission Analysis Tool) software in which the Cartesian state vectors, i.e., position and velocity or Keplerian elements are used as the input at a point of time, known as Epoch and the path of the satellite over the Earth's surface is the output shown in the simulations. The ground track plots. In Figure 4.41 shows the orbit view of the satellite corresponding to the epoch time 08 Jul 2018 04:53:04.000 with an atmospheric drag model in GMAT.

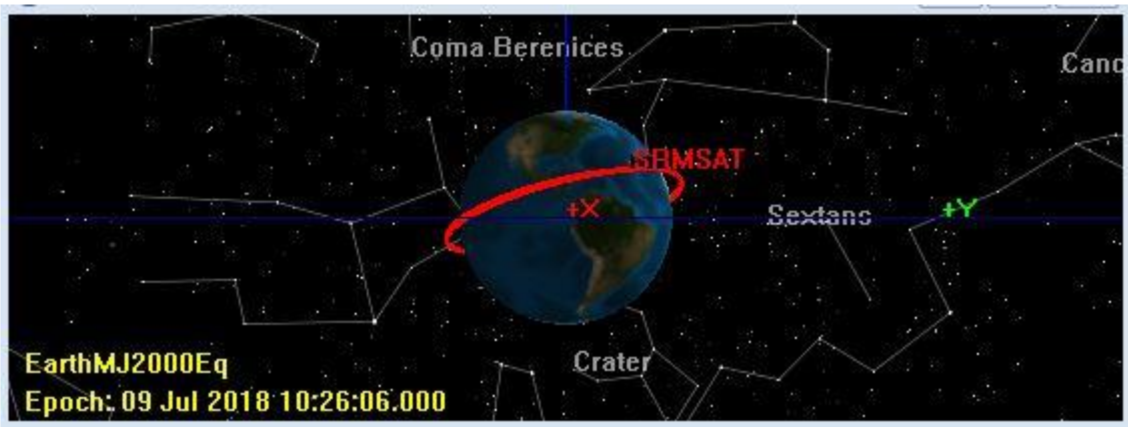

Figure (4.41) Pratham orbit view at EarthMJ2000Eq UTC

The Figure 4.41 shows the orbit view at Epoch with corresponding to the final values of position and velocity. The atmospheric Drag model developed in GMAT/ MATLAB by ordinary differential equation (ODE) with the help of Runge – Kutta methods.

The SRM satellite Keplerian elements considered for simulation is Mass, 10 kilograms (22 lb), Orbital angular velocity, Ω = 0.0010239 (rad/sec), 867 km altitude, Epoch 08 Jul 2018 10:32:46.000 UTC Gregorian EarthMU2000Eq. The gravitational parameters consider for simulation is 3.98 * 10^{14} (km^3/Sec^2) [136]. The SRM Satellite perturbation forces of aerodynamic drag, solar pressure is considered. The magnitude of actual path and predicted path explained in Cowell's/GMAT simulations. The validation of Cowell's simulation results compared with known Keplerian elements. The response of the known orbital elements is modeled by General Mission Analysis Tools. In GMAT has been introduced the Gravity model EGM-96 and Atmosphere Model MSISE90 at Low Earth Orbit satellite [137]. The atmospheric model considered the valid assumption used for standard/ accurate results.

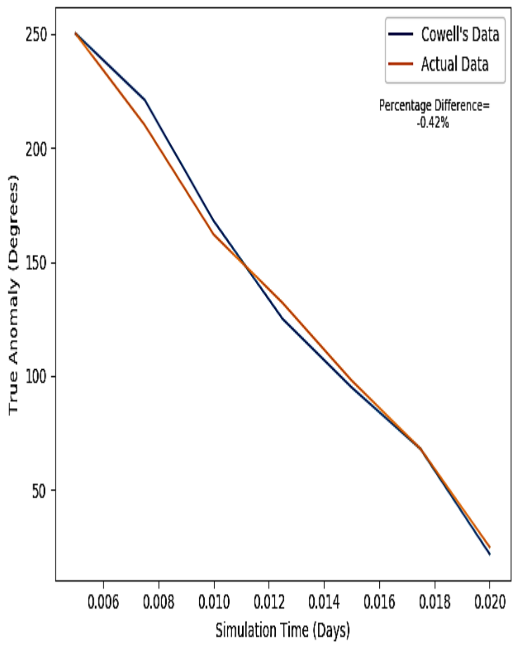
Cowell's Data
Actual Data
Percentage Difference=
-0.42%
True Anomaly (Degrees)
250
200
150
100
50
0.006 0.008 0.010 0.012 0.014 0.016 0.018 0.020
Simulation Time (Days)

(a)

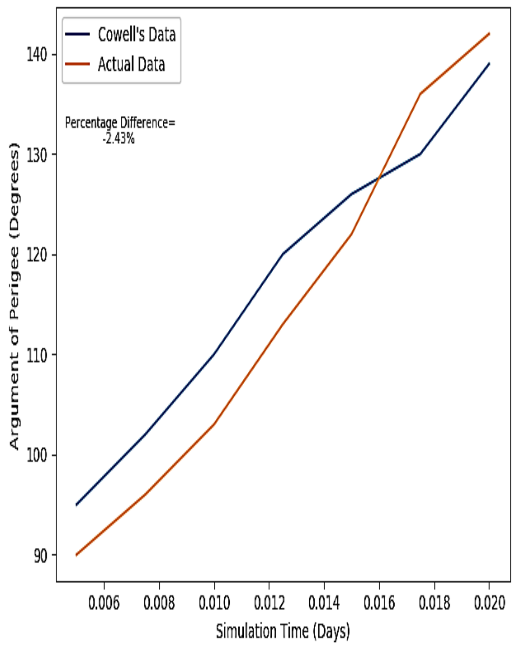
Cowell's Data
Actual Data
Percentage Difference=
-2.43%
Argument of Perigee (Degrees)
140
130
120
110
100
90
0.006 0.008 0.010 0.012 0.014 0.016 0.018 0.020
Simulation Time (Days)

(b)

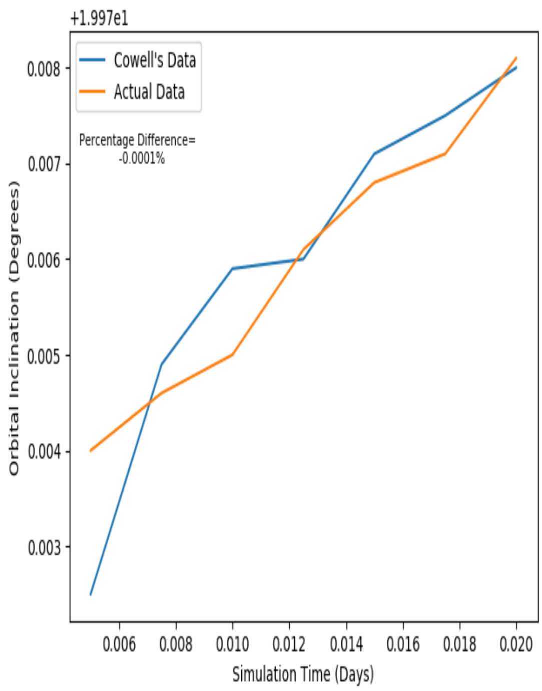
+1.997e1
Cowell's Data
Actual Data
Percentage Difference=
-0.0001%
Orbital Inclination (Degrees)
0.008
0.007
0.006
0.005
0.004
0.003
0.006 0.008 0.010 0.012 0.014 0.016 0.018 0.020
Simulation Time (Days)

(c)

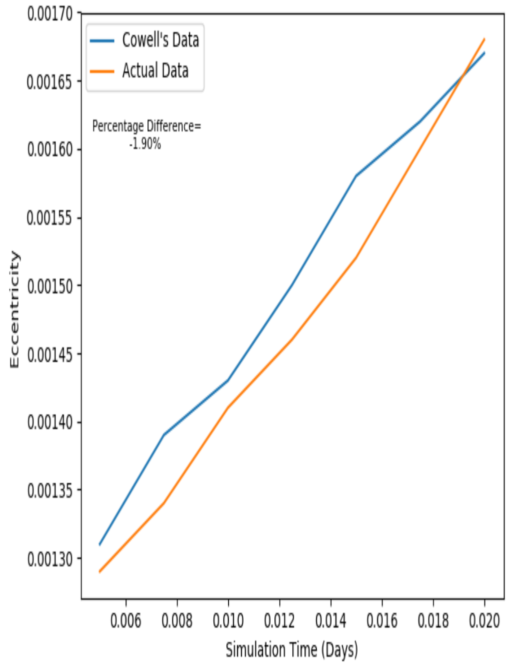
Cowell's Data
Actual Data
Percentage Difference=
-1.90%
Eccentricity
0.00170
0.00165
0.00160
0.00155
0.00150
0.00145
0.00140
0.00135
0.00130
0.006 0.008 0.010 0.012 0.014 0.016 0.018 0.020
Simulation Time (Days)

(d)

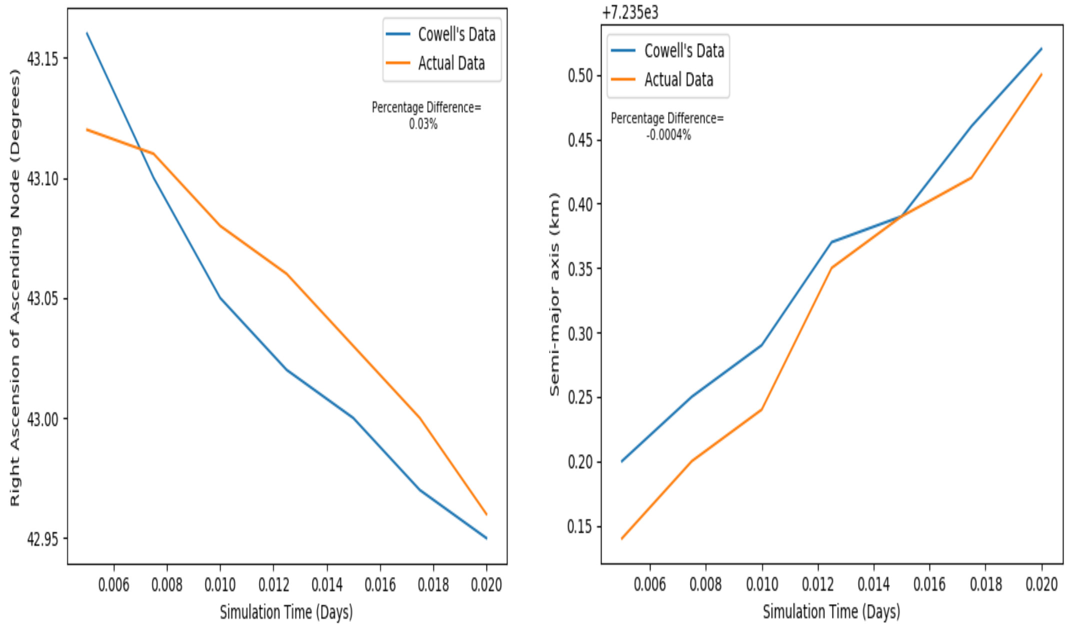

(e) (f)

Figure (4.42) The orbital variations of SRM satellite Epoch at 08 Jul 2018 10:32:46.000 UTC Gregorian EarthMU2000Eq, Ω = 0.0010239 rad/s in LEO (a) True Anomaly (b) Argument of perigee (c) Orbital Inclination (d) Eccentricity (e) Right Ascension of Ascending Node (f) Semi major axis

The errors tolerance is considered as e^{-8} and step size is 30 Graphics simulations. The result shown in figure (4.40) RED color indicates the actual orbital trajectory and BLUE color indicates the Cowell's perturbation trajectory in the orbit. The SRM satellite is modeled by GMAT initial step size 0.001 maximum step size 2700 for 50 attempts considered coordinate system EarthMU2000Eq. The simulation period of the SRM satellite taking into 0.020 times (days). The simulation of ODE obtained with minimum error percentage shown in table (4.4)

Table (4.10) (a) SRM satellite magnitudes of errors with actual and predicted trajectory in the orbit (True Anomaly, Argument of perigee, Orbital Inclination)

Orbital Elements / Simulation Period	True Anomaly		Errors deviations (%)	Argument of Perigee		Errors deviations (%)	Orbital inclination		Errors deviations (%)
	Magnitudes of actual data (GMAT) Simulation	Magnitudes of Predicted data Cowel's Simulation		Magnitudes of actual data (GMAT) Simulation	Magnitudes of Predicted data Cowel's Simulation		Magnitudes of actual data (GMAT) Simulation	Magnitudes of Predicted data Cowel's Simulation	
0.005	250	250	0.42	90	95	2.43	19.974	19.9725	0.0001
0.0075	210	221		96	102		19.9746	19.9749	
0.01	162	168		103	110		19.975	19.9759	
0.0125	132	125		113	120		19.9761	19.976	
0.015	98	95		122	126		19.9768	19.9771	
0.0175	68	68		136	130		19.9771	19.9775	
0.02	25	22		142	139		19.9781	19.978	

Table (4.10) (b) SRM satellite magnitudes of errors with actual and predicted trajectory in the orbit (Eccentricity, RAAN, Semi-major axis)

Eccentricity		Errors deviations (%)	RAAN		Errors deviations (%)	Semi-Major Axis		Errors deviations (%)
Magnitudes of actual data (GMAT) Simulation	Magnitudes of Predicted data Cowel's Simulation		Magnitudes of actual data (GMAT) Simulation	Magnitudes of Predicted data Cowel's Simulation		Magnitudes of actual data (GMAT) Simulation	Magnitudes of Predicted data Cowel's Simulation	
0.00129	0.00131	1.9	43.12	43.16	0.03	7235.14	7235.2	0.0004
0.00134	0.00139		43.11	43.1		7235.2	7235.25	
0.00141	0.00143		43.08	43.05		7235.24	7235.29	
0.00146	0.0015		43.06	43.02		7235.35	7235.37	
0.00152	0.00158		43.03	43		7235.39	7235.39	
0.0016	0.00162		43	42.97		7235.42	7235.46	
0.00168	0.00167		42.96	42.95		7235.5	7235.52	

In the table 4.10 (a) and (b) shows the SRM satellite actual and predicted trajectory minimum error deviation of Keplerian elements with reference low earth's orbit at UTC 08 Jul 2018 10:32:46.000 Gregorian. The orbital path of GMAT/ Cowell's simulation is close to the nearest integer. The Cowell's algorithm predicts the accurate trajectory the satellite from disturbed orbit. This data is very much useful to estimate the errors in the attitudes and to design the proper attitude control techniques discussed in chapter 6. Attitude control design

Simulation Period (Days)	SRM satellite						Pratham satellite						International Space Station (ISS)					
	Semi-Major Axis (Km)	Orbital Inclination (deg)	Argument of Perigeee (deg)	True Anomaly (deg)	RAAN (deg)	Ecc	Semi-Major Axis (Km)	Orbital Inclination (deg)	Argument of Perigeee (deg)	True Anomaly (deg)	RAAN (deg)	Ecc	Semi-Major Axis (Km)	Orbital Inclination (deg)	Argument of Perigeee (deg)	True Anomaly (deg)	RAAN (deg)	Ecc
0.005	7235.1	19.974	90	250	43.12	0.00129	7057	98.1058	54	250	354.567	0.00347	6786.2	51.875	62	110	36	0.00039
0.0075	7235.2	19.9746	96	210	43.1	0.00123	7055.1	98.1069	52	220	354.572	0.00329	6785.9	51.872	83	155	35	0.00039
0.01	7235.2	19.975	103	162	43.05	0.00141	7053.8	98.108	49	190	354.576	0.00325	6,784	51.867	101	222	34	0.00039
0.0125	7235.4	19.9761	113	132	43.02	0.00146	7051.6	98.1094	46	160	354.581	0.00305	6780	51.855	120	280	33	0.00027
0.015	7235.4	19.9768	122	98	43	0.00152	7049.5	98.1104	44	140	354.584	0.00299	6777.2	51.845	120	306	32.8	0.0002

Table (4.11) Keplerian elements GMAT Simulation of SRM satellite, Pratham (IITB) Satellite, International Space station (ISS)

Simulation Period (Days)	SRM satellite						Pratham satellite						International Space Station (ISS)					
	Semi-Major Axis (Km)	Orbital Inclination (deg)	Argument of Perigeee (deg)	True Anomaly (deg)	RAAN (deg)	Ecc	Semi-Major Axis (Km)	Orbital Inclination (deg)	Argument of Perigeee (deg)	True Anomaly (deg)	RAAN (deg)	Ecc	Semi-Major Axis (Km)	Orbital Inclination (deg)	Argument of Perigeee (deg)	True Anomaly (deg)	RAAN (deg)	Ecc
0.005	7235.2	19.9725	95	250	43.16	0.00131	7057.2	98.1058	54	250	354.55	0.00337	6786	51.875	55	96	36	0.00036
0.0075	7235.3	19.9749	102	221	43.1	0.00139	7055	98.107	51	225	354.56	0.00322	6785.2	51.866	80	150	35	0.00037
0.01	7235.3	19.9759	110	168	43.05	0.00143	7053.4	98.108	49	190	354.57	0.00319	6782.8	51.864	100	222	34	0.00037
0.0125	7235.4	19.976	120	125	43.02	0.0015	7051	98.10892	45	160	354.58	0.003	6779.9	51.855	110	280	33	0.00027
0.015	7235.4	19.9771	126	95	43	0.00158	7049.2	98.1102	44	138	354.59	0.00297	6777	51.845	120	304	32	0.0002

Table (4.12) Keplerian elements Cowell's Simulation of SRM satellite, Pratham (IITB) Satellite, International Space station (ISS)

The SRM satellite, Pratham (IITB) Satellite, International Space station (ISS) variations in Keplerian elements using GMAT Simulation shown in table (4.6). The table clearly indicates the changes in ISS position and velocity due to the perturbation forces action on it. This result shows the change in altitude, earth radius with the altitude of the satellite changes with atmospheric perturbation. ISS perigee position is at 403 km and apogee position is 406 km and inclination of 51.36 deg. The period of one revolution of this satellite is about 92.5 minutes and it completes about 15.54 orbits per day an orbital velocity of 7.67 km. Since, the altitude of ISS satellite is about 350 to 420 km from the Earth's surface. Therefore, the Semi-Major axis will be from satellite altitude and earth center distance. Epoch Format: UTC Gregorian, Epoch: 03 Apr 2018 13:19:31.516, the time period consider for the simulation is 0.005 to 0.015 (Days), it is clearly understood the semi-major axis vary from 6786.2Km to 6777.2Km. The altitudes nearly decrease to 9 km. Also, discuss the other Keplerian elements variation in shown in the table (4.6). The Keplerian simulations results obtained for Pratham (IIT Bombay) satellite at Epoch 08 Jul 2018 04:53:04.000UTC Gregorian EarthMJ2000Eq (Refers Appendix C). The Keplerian simulations considered for Pratham satellite (IIT Bombay) Mass, 10 kg, Size 26×26×26 cm, Orbital angular velocity, Ω = 0.0010346, 817 km altitude. The Gravity models, JGM-2 and atmospheric model, MSISE90 has been introduced for degree and order is 4. The SRM satellite considers the Universal Time Coordinates as Epoch at 08 Jul 2018 10:32:46.000 UTC Gregorian. The Runge-Kutta propagator considered ODE Integrator with initial step size is 60 seconds, primary body an earth's surface. In table (4.7) shows the variation in the Keplerian elements Cowell's Simulation of SRM satellite, Pratham (IITB) Satellite, International Space station (ISS). The table (4.6) & (4.7) shows the comparative analysis of Keplerian elements and error deviation in GMAT/Cowell's simulation. The Cowell's simulation used to validate the GMAT simulation measures the minimum error deviations. This is used to generate the controlled input to actuator re-orient satellite in to the desired attitude with atmospheric conditions. Also, it is helping to design the suitable controller of satellite.

CHAPTER 5

ATTITUDE ERROR ESTIMATION ANALYSIS USING KALMAN FILTER

The linear estimates of measurement and prediction of the state (or) information from the attitude sensor using the Kalman Filter (KF) are widely used. The KF is more efficient and accurate method used to predict the performance in the linear system [138]. The Non-linear estimate of measurements and predictions of the state (or) information's from the attitude sensor using Extended Kalman Filter (EKF). The Extended KF is more efficient and accurate method used to predict the performance in non-linear system. The unscented transformation (UT) occurs in the state equations [139]. The nonlinear system estimated by first and second order ordinary differential equations (ODE) in UKF, EKF and UKF are unlike for derivatives or Jacobians in the estimate the performance equation and state equation. It requires the propagating state covariance matrix, filter circulates state, and standard deviations are circulated. This indicates the random changes in the state or uncertainty of the system. In Figure (5.1) illustrate the estimated attitude with angular rates of satellite using Kalman filter [140].

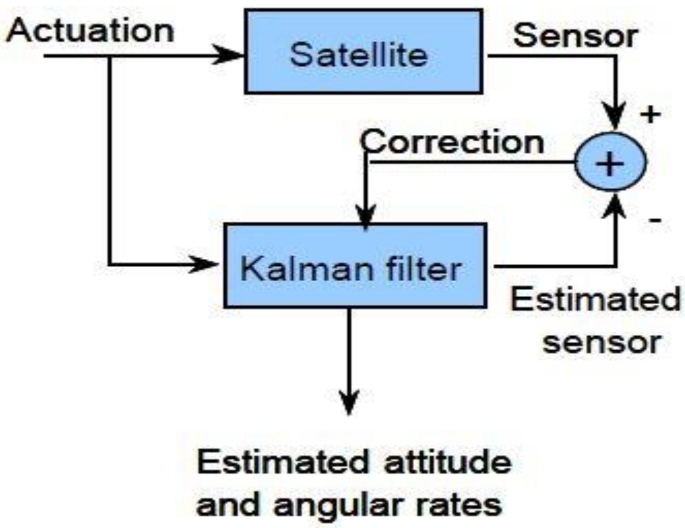

Figure (5.1) Attitude Error corrections with Kalman Filter [140]

5.1. Algorithms of error estimation using Kalman Filter

The state vectors in the system/plant dynamics predict and estimate of errors using Kalman filter. It is based upon the past estimates in process and present measurement with the disturbance signal from attitude sensors [141]. The mean square error is minimized from the filter.

For estimating the state vectors Kalman filter requires two steps

- Prediction
- Update

Estimating the Process: State is controlled by stochastic equation (linear form)

The process (or) plant represents the input of the system and various state space parameters along with process noise (w_k) and measurement equation represents the output of the system along with noises in the sensor measurements (v_k). The Process (5.1) and measurements (5.2) equation as given below [142], [143]

Process: $x_{k+1} = A_k x_k + Bu_k +$ Process Noise (w_k) (5.1)

Measurement: $Z_k = H_k x_k +$ Measurements Noise (v_k) (5.2)

The process noise and measurement noise both or not related to each other's. The w_k and v_k considered at standard probability distribution.

"A(nxn)" Matrix representing the state at time step k

"B" Matrix representing the requires the input signal to x (state)

"H" Measurement matrix representing to the state Z_k

$\overline{x_{prıorı}}$ = Priori state estimate k of the process

$\overline{x_{posterıorı}}$ = Posteriori state estimate k of the measurement

The probability methods predict the future estimate with the help of previous state information and current measurement from the satellite attitude sensor [144]

$$\overline{x_{posterıorı}} = \overline{x_{prıorı}} + K(Z_k - H_k \overline{x_{prıorı}}) \quad (5.3)$$

“K” is the Kalman Gain,

“Z_k” is the Actual Measurements

“$H_k\overline{x_{prıorı}}$” is the Predicted Measurements

The Gain Matrix K is (n X m) is reducing the posteriori error covariance. The system for estimating the process of Kalman filter requires the feedback signal, output feedback into the input of the model. In the model estimating the measurements of feedback signals includes the disturbances (or) errors in the signal [145].

5.1.1. Numerical modeling of Kalman filter

- Time update
- Measurement update

Time update methods mainly focus to estimate error covariance and present state information to find previous estimates from next time step [146].

Measurements update method focus to the measurement from the previous signal from feedback to find the best future estimate. Time update methods used to predict response of the system, it is called as “Predictor”. Measurement update methods used to correct the response of the system; it is called as “corrector”

Mathematical calculation using predictor-Corrector method

Time updates find the current estimate from the system [147]. The measurement updates find the future estimate (Shown in Figure 5.2) from the system by actual measurement at that times.

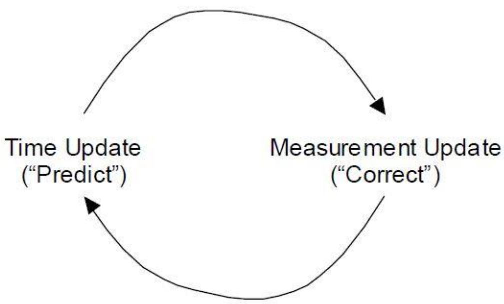

Figure (5.2) Predict/Estimate the Errors in the system [149]

The proposed estimation algorithm considered the state of system and error covariance estimate the step k to step k+1. The measurements update equation to find the Kalman gain, update the measurement with Z_k and update the error covariance of the state [148]. The process $\mathbf{P_k}$ and measurement $\mathbf{R_k}$ is and covariance matrix. The measurements updating the state with the help of priori and posteriori state and the Kalman gain to find the actual measurement, Z_k. The process of time-measurement (See Figure-5.3) update steps is repeated with a previous estimate to predict the new estimate [149], [150]. This is called as “recursive nature” of the Kalman filter.

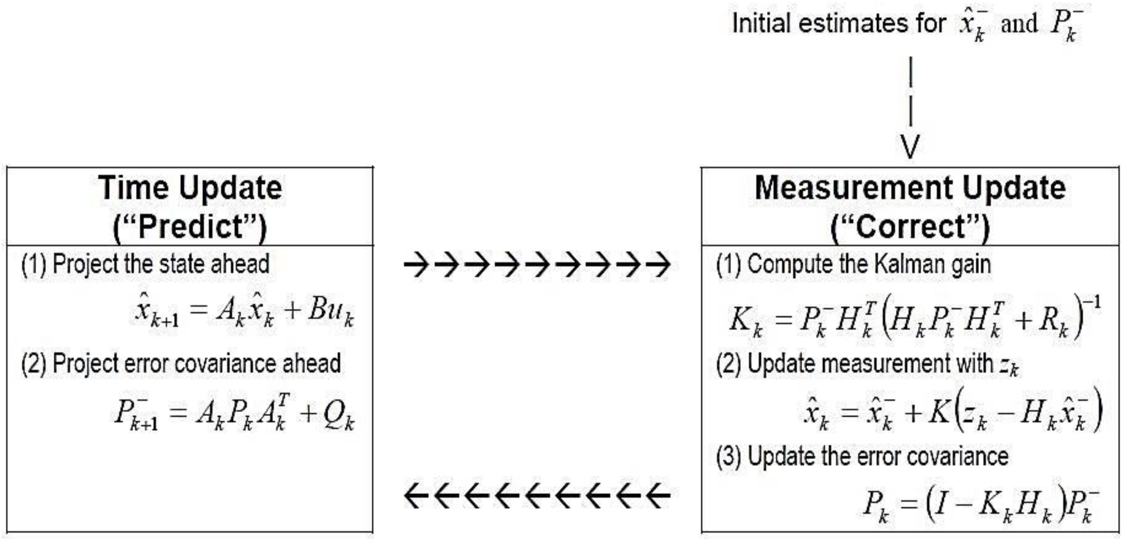

Figure (5.3) Implementation of Kalman filter algorithm [149]

After the covariance matrix implementations of Kalman filter (KF) used to calculate the past estimates before starting operation of the time – measurement updates. The Attitude sensor data gives the measurement information used to determine variance error. The process covariance is less accurate or less deterministic; it indicates the uncertainty of the process model. For tuning the P_k and R_k are more important to get the accurate measurements in the satellite/plant till the Kalman gain K_k stabilize the value [150]. The process covariance Q_k changes dynamically because of the noisy measurements. So, this value should be adjusted to the differential dynamic equation. The magnitude of process covariant changes the dynamics of the system. The KF predicts the position and angular rates of satellite from attitude sensors (INS/GPS & IMU) [151], [152].

The magnetometer used to estimate the attitude rates (yaw angle, pitch angle, and roll angle) for the vehicle/satellite. The variation in earth magnetic flux produces the noisy measurements in the plant or model [153]. The state future estimates (5.4) and actual measurements (5.5) as given below

$$\overrightarrow{x_{k+1}} = \phi_k \overrightarrow{x_k} + \underline{\Delta}_k \overrightarrow{u_k} + \overrightarrow{w_k} \tag{5.4}$$

$$\overrightarrow{Z_k} = H \overrightarrow{x_k} + \overrightarrow{v_k} \tag{5.5}$$

w_k: Process or plant covariance white noise, Q

v_k : Sensor noise covariance , R

The attitude sensor noise (process/measurement) (R_k/Q_k) Signals (5.6) & (5.7) covariance matrix defined by, [153]

$$R_k = \mathrm{E}\left[\overrightarrow{v_k} \quad \overrightarrow{v_k^T}\right] \tag{5.6}$$

$$Q_k = \mathrm{E}\left[\overrightarrow{w_k} \quad \overrightarrow{w_k^T}\right] \tag{5.7}$$

5.1.2. Motion equation of satellite

The satellite accurately measures the attitude rates where it crosses to the line of nodes in the orbit. The motion equations describe the satellite movements of a particular position in the orbits.

The State variable is [41]

$$\vec{x} = \left[\phi \quad \dot{\phi} \quad \theta \quad \dot{\theta} \quad \psi \quad \dot{\psi}\right]^T$$

The satellite dynamic state space equation (SSE)

$$\frac{\overrightarrow{dx}}{dt} = \mathrm{A}\vec{x} + \mathrm{B}\vec{u}$$

The acceleration of satellite body (5.8), (5.9) and (5.10) given as

$$\ddot{\phi} = \left[\frac{-4\Omega^2(I_y-I_z)\phi+\Omega h_y\phi-\Omega(-I_x+I_y-I_z)\dot{\psi}+h_y\dot{\psi}-h_z\dot{\theta}+I_x\dot{\Omega}\psi}{I_x}\right] - \left[\frac{\dot{h_x}}{I_x}\right]+\left[\frac{T_{spx}+\Omega h_z}{I_x}\right] \tag{5.8}$$

$$\ddot{\theta} = \left[\frac{-3\Omega^2(I_x-I_z)\theta-h_x\dot{\psi}-\Omega h_z\psi-\Omega h_x\phi+h_z\dot{\phi}}{I_y}\right] - \left[\frac{\dot{h_y}}{I_y}\right]+\left[\frac{T_{spx}+I_y\dot{\Omega}}{I_y}\right] \tag{5.9}$$

$$\ddot{\psi} = \left[\frac{-\Omega^2(-I_x+I_y)\psi+\Omega h_y\psi-\Omega(I_x-I_y+I_z)\dot{\phi}+h_x\dot{\theta}-h_y\dot{\phi}-I_z\dot{\Omega}\phi}{I_z}\right] - \left[\frac{\dot{h_z}}{I_z}\right]+\left[\frac{T_{spz}-\Omega h_x}{I_z}\right] \tag{5.10}$$

A is process model [41]

Plant matrix, A

$$= [0\ 1\ 0\ 0\ 0\ 0;\ \frac{-4\Omega^2(I_y-I_z)+\Omega h_y}{I_x}\ 0\ 0 - \frac{h_z}{I_x}\ \dot{\Omega}\ \frac{-\Omega(-I_x+I_y-I_z)+h_y}{I_x};\ 0\ 0\ 0\ 1\ 0\ 0;$$

$$-\Omega\frac{h_y}{I_y}\ -\frac{h_z}{I_y}\ -\frac{3\Omega^2(I_x-I_z)}{I_y}\ 0\ -\Omega\frac{h_z}{I_y}\ -\frac{h_x}{I_y};\ 0\ 0\ 0\ 0\ 0\ 1;\ -\dot{\Omega}\ \frac{-\Omega(I_x-I_y+I_z)-h_y}{I_z}\ 0$$

$$\frac{h_x}{I_z}\ \frac{-\Omega^2(-I_x+I_y)+\Omega h_y}{I_z}\ 0]$$

Control matrix, B = [0 0 0; 1 0 0; 0 0 0; 0 1 0; 0 0 0; 0 0 1]

Control to the Actuator of satellite, u = $-Fx+u_d$ (5.11)

"F" is the controller Gain

"u_d" is the sum of perturbations forces

$$\frac{\overrightarrow{dx}}{dt} = (A-BF)x_o + B\overrightarrow{u_d} \tag{5.12}$$

This is a satellite equation of motion (5.12) of body. For implementing the Kalman filter, it requires data from on-board attitude sensors (INS/GPS & IMU) to predict the next state. Refer Annexure B. The satellite attitude control system needs the current attitude data. Using the error estimation KF algorithms used to predicts the future (or) next state [154].

Parameter estimators & classifications of weights: [155], [156]

Weight for state and estimate parameter

$$Weight = W_0^m = \frac{state}{measuement+state}$$

Prepare the filter factor with estimated significance of constraints

$$\text{State value } (t_o) = \text{Expected Value } \{x_0\}$$

$$x_0 = \text{Initial state parameter}$$

Covariance for the parameters

$$px_0 = \text{Expected Value } \{(\text{state } (t_o)\text{-}x_o)\ (\text{state } (t_o)\text{-}x_o)^T\}$$

The standard deviations are calculated. The initial conditions simulation considered $\sqrt{\text{covariance matrix}}$ for the estimator of parameter. Equation for the state:

$$X_{initial} = \text{function of xi, u, w, and t}$$

Covariance form for the state:

$$= \sum_{t=0}^{2L} W_i^C\ (xi - x)\ \ (xi - x)T$$

Measurements (Expected): Output = h (state)

Mean measurement: $= \sum_{t=0}^{2L} W_i^M\ yi$

The covariance's is [156]

$$P_{yy} = y = \sum_{t=0}^{2L} W_i^C\ \ (yi - y)\ (yi - y)T$$

$$P_{xy} = y = \sum_{t=0}^{2L} W_i^C\ \ (xi - x)\ (yi - y)T$$

The Kalman gain (K_{Gain}) = $P_{xy}\ p_{yy}^{-1}$

5.1.3. Methodology

In the flow chart shown in Figure (5.4) describes the state flow steps for estimating the errors in attitude sensors (INS/GPS and IMU) using Kalman algorithm. The Kalman algorithm used to calculates the state variables $[\phi \quad \dot{\phi} \quad \theta \quad \dot{\theta} \quad \psi \quad \dot{\psi}]$. Considered the six-state variables for simulations

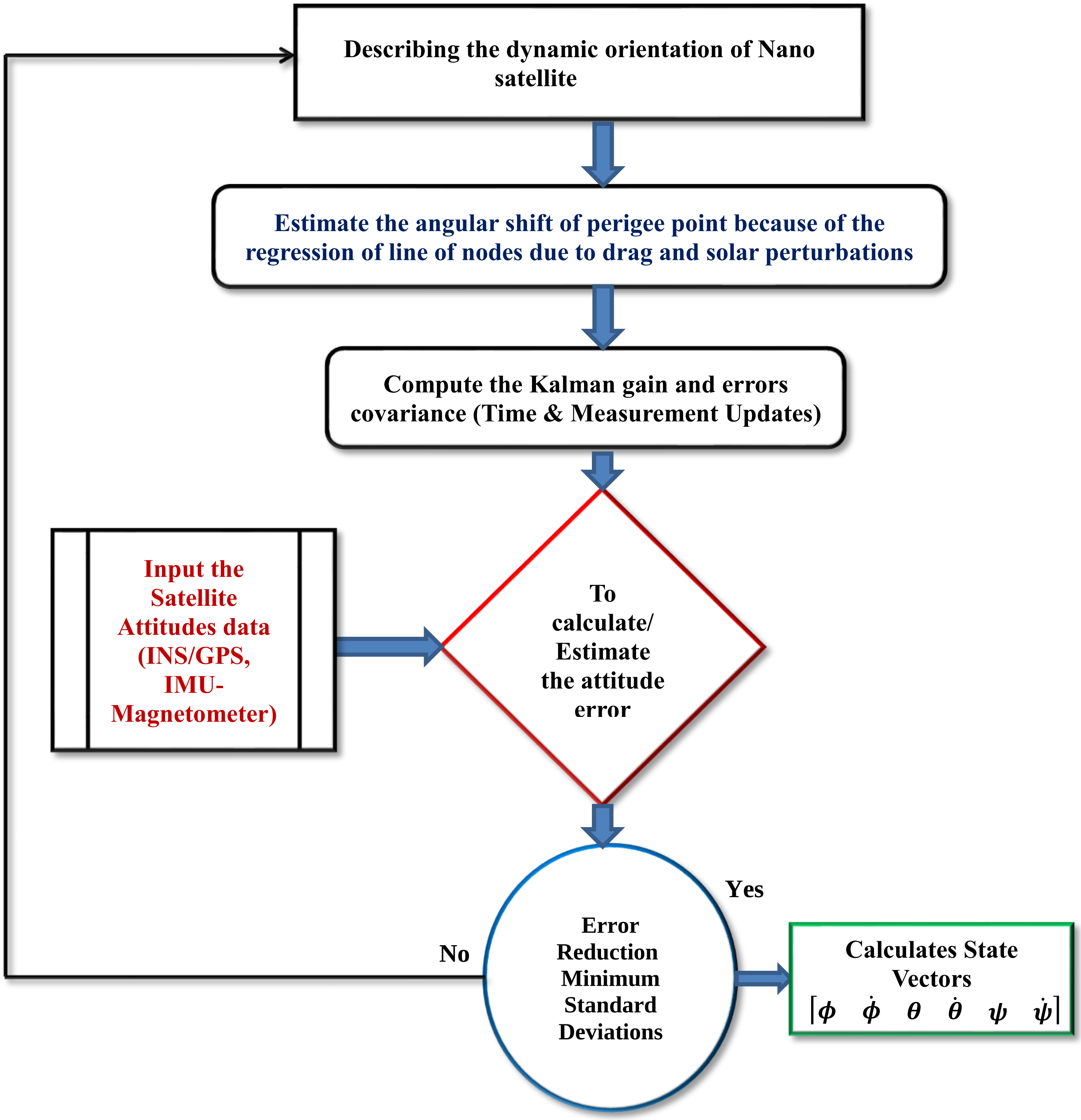

Figure (5.4) Flow chart for attitudes error estimation using Kalman Filter

The state update is X = state +Kalman Gain (K) (Actual measurement(y) -$\dot{y}$)

Covariance updates (P_{CU}): [155] P_{CU} = P-K_{Gain} P_{yy} K^T

'y' is the actual measurement matches the time for updated state.

The update classification starts by including constraint design random sequence of covariance or uncertainty (Quncer) P_{CU} = P + Quncer

The parameter update: w = w + K (y -$\dot{y}$)

Covariance updates (P_{CU}): P_{CU} = P- K_{Gain} P_{yy} KT

'y' is the actual measurement matches the time for updated state.

Hence, nonlinear state equations are $\dot{r}$ = v

$$\dot{v} + \frac{Gravitational\ Parameter*r}{(r^T r)3/2} + \sum_K ak = \frac{f}{m} \quad [156]$$

The satellite mass is 'm' position vector is 'r' solar pressure force on the satellite is 'f'. In Figure (5.5) Shows the attitude error estimation using KF.

u_d (Disturbance (3X1) Matrix)

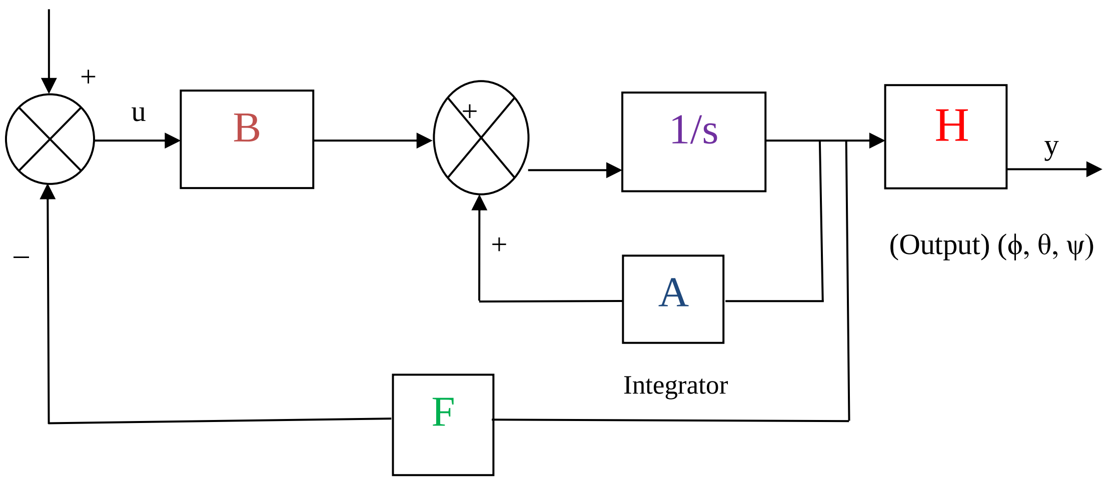

Controller Gain (3X6) Matrix

Figure (5.5) Block diagram of Kalman filter state estimation

Where, A = Process or Plant (6X6) Matrix

B = Control (6X3) Matrix

H = Measurement (3X6) Matrix

x =State (6X1) Matrix, = $\left[\phi \quad \dot{\phi} \quad \theta \quad \dot{\theta} \quad \psi \quad \dot{\psi}\right]^T$ (5.13)

F= PD Controller (3X6) Matrix [136]

State space equation [157]

State, $\dot{x} = Ax + Bu$

Output, $y = Hx$

Control Input, $u = -Fx + u_d$ (5.14)

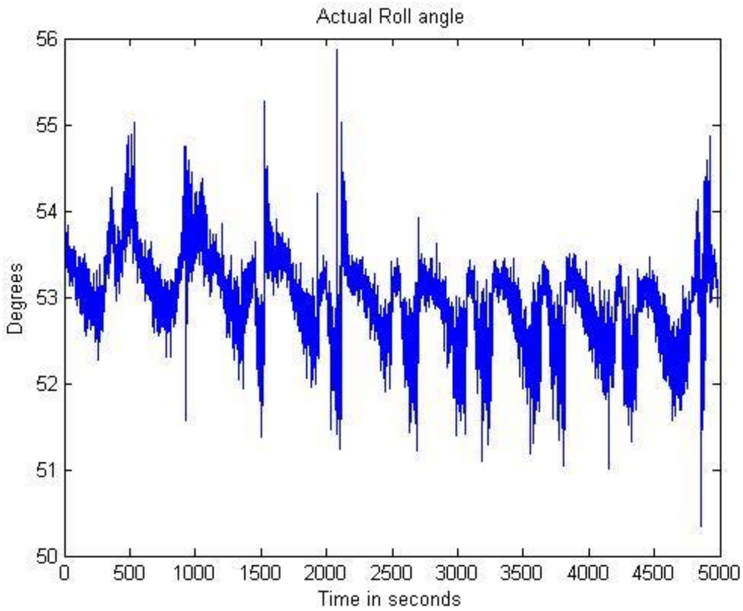

Figure (5.6) Roll attitude dynamics of NPSAT-1 to consider the principle moment of inertia (I_x = 24.67, I_y = 22.63, I_z = 11) kg-m^2 the actual attitude data (0-5000 Seconds) measured from the on-board attitude sensor IMU and Magnetometer with reference to low earth orbit trajectory

The Kalman filter algorithms used to estimate the errors in the real time raw data (Roll angle, Pitch angle, Yaw angle) measured from on-board attitude sensor. The KF simulation considered the step time 0 – 5000 second attitude data from reference low earth orbiting satellite in the entire orbit [158]. Refers Appendix-D, for implementing the Kalman filter algorithm, it is necessary to consider the known constants. In the simulation considered total disturbance torque (T_d) is 1.04×10^{-4} N.m. The disturbance torques due to atmospherics parameters is aerodynamics perturbation, solar radiation pressure [32]. The Kalman filter simulation employed in one entire orbit period, the time taken to complete one cycle. The satellite it's starting from one node with respect to the equator and complete with same node [24]. The one orbit simulation is very useful to estimate the changes in orbit from normal orbit to perturbed/disturbed orbit. In figure (5.6) shows the NPSAT-1 actual roll data.

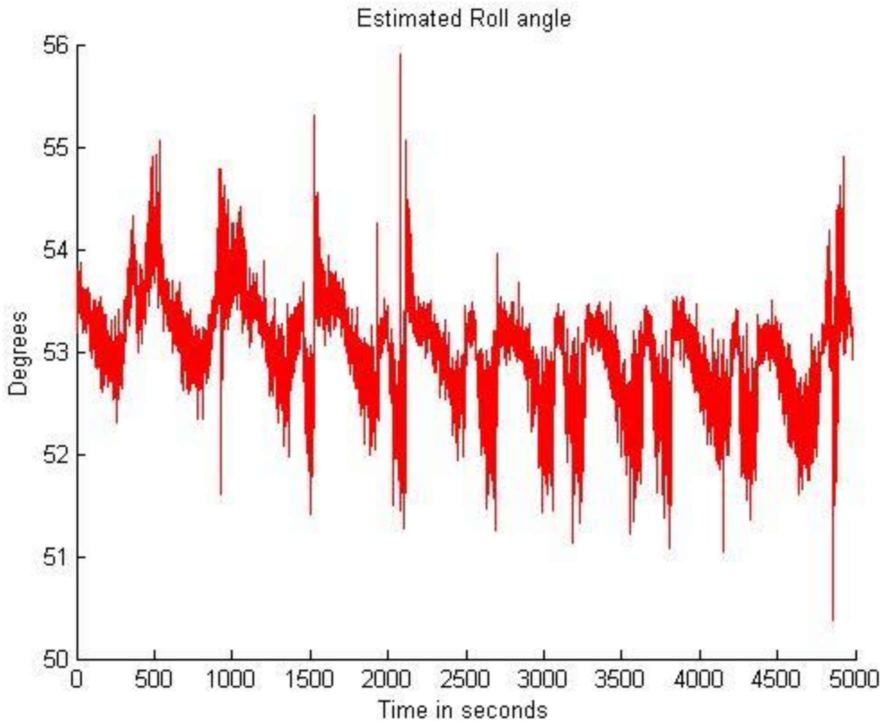

Figure (5.7) Roll attitude dynamics of NPSAT-1 to consider the principle moment of inertia (I_x = 24.67, I_y = 22.63, I_z = 11) kg-m^2 the Predicted/Estimated attitude data (0-5000 Seconds) using a Kalman filter algorithm

The initial simulation parameters considered is angular momentum of momentum wheel, h = 10 (Nms.), angular velocity, ω = 0.0011068 (rad/s), Disturbance torque 1.04 X 10^{-4} (Nm), step time duration, dt = 0.1 (seconds) [158]. The attitude data from on-board sensors in the IMU and Magnetometer size is referred in the code is mag = magneto', [m n] = size (mag); 'm' is No of raw in the data; 'n' is No of column in data attached in the report. The initial state matrix $\boldsymbol{X_0}$ is 6X1, represents six states (roll angles, roll rates, pitch angles, pitch rates, yaw angles, yaw rates). For considered the suitable assumptions for estimate the accurate measurements with less error in the system. In figure (5.7) shows the NPSAT-1 estimated data with K.

$$\textbf{State vector: } \vec{x} = \left[\boldsymbol{\phi} \quad \dot{\boldsymbol{\phi}} \quad \boldsymbol{\theta} \quad \dot{\boldsymbol{\theta}} \quad \boldsymbol{\psi} \quad \dot{\boldsymbol{\psi}}\right]^{T}$$

To initialize the Kalman filter, for Initial error covariance matrix, 6X6 all the diagonal elements considered as 10^{-6}, process noise covariance matrix, Q is e^{-6}, measurement noise covariance matrix, R is e^{-2}. [157]

Table (5.1) Estimation of NPSAT-1 satellite attitude errors between actual and estimated attitudes, principle MOI (I_x = 24.67, I_y = 22.63, I_z = 11) kg-m²

Satellite Attitudes (deg) / Time (Sec)	Roll angle (deg)	Roll_est (deg)	Roll_error (%)	Pitch angle (deg)	Pitch_est (deg)	Pitch_error (%)	Yaw angle (deg)	Yaw_est (deg)	Yaw_error (%)
1	52.25	52.26058	0.0105759	1.49	1.490342	0.0003419	185.21	185.2472	0.0372326
2	53.73	53.74337	0.0133675	1.03	1.037456	0.0074558	186.72	186.7805	0.0605032
3	53.57	53.5912	0.0211958	1.24	1.232838	-0.007162	186.21	186.2891	0.0790596
4	53.63	53.66126	0.031255	1.57	1.554645	-0.015355	186.03	186.0984	0.0683692
5	53.66	53.68892	0.028917	0.85	0.836801	-0.013199	186.46	186.5266	0.0666276
6	53.53	53.55635	0.0263453	0.85	0.839388	-0.010612	185.52	185.5977	0.0777251
7	53.55	53.57896	0.0289636	0.63	0.616321	-0.013679	186.1	186.1913	0.091326
8	53.65	53.68638	0.0363823	1.49	1.468582	-0.021418	186.08	186.1687	0.0886713
9	53.77	53.8068	0.0367995	1.22	1.198406	-0.021594	186.55	186.6286	0.0786264
10	53.46	53.49238	0.0323761	1.63	1.613036	-0.016964	185.94	186.0229	0.0828918

In table (5.1) shows the variations in attitudes with reference of low earth orbit satellite data collected from the initial position to next 10 Seconds. The actual attitude information is measured by IMU and Magnetometers. It clearly understood the roll angle slightly oscillates from 52.25 degrees to 53.46 degrees as shown in the figure (5.5). The pitch angles nearly constant (0 to 5000 Sec) in the entire orbit [157]. The yaw angles oscillate from 185.21 degrees to 185.94 degrees. The NPSAT-1Kalman algorithm estimates the attitude error deviations in the orbit.

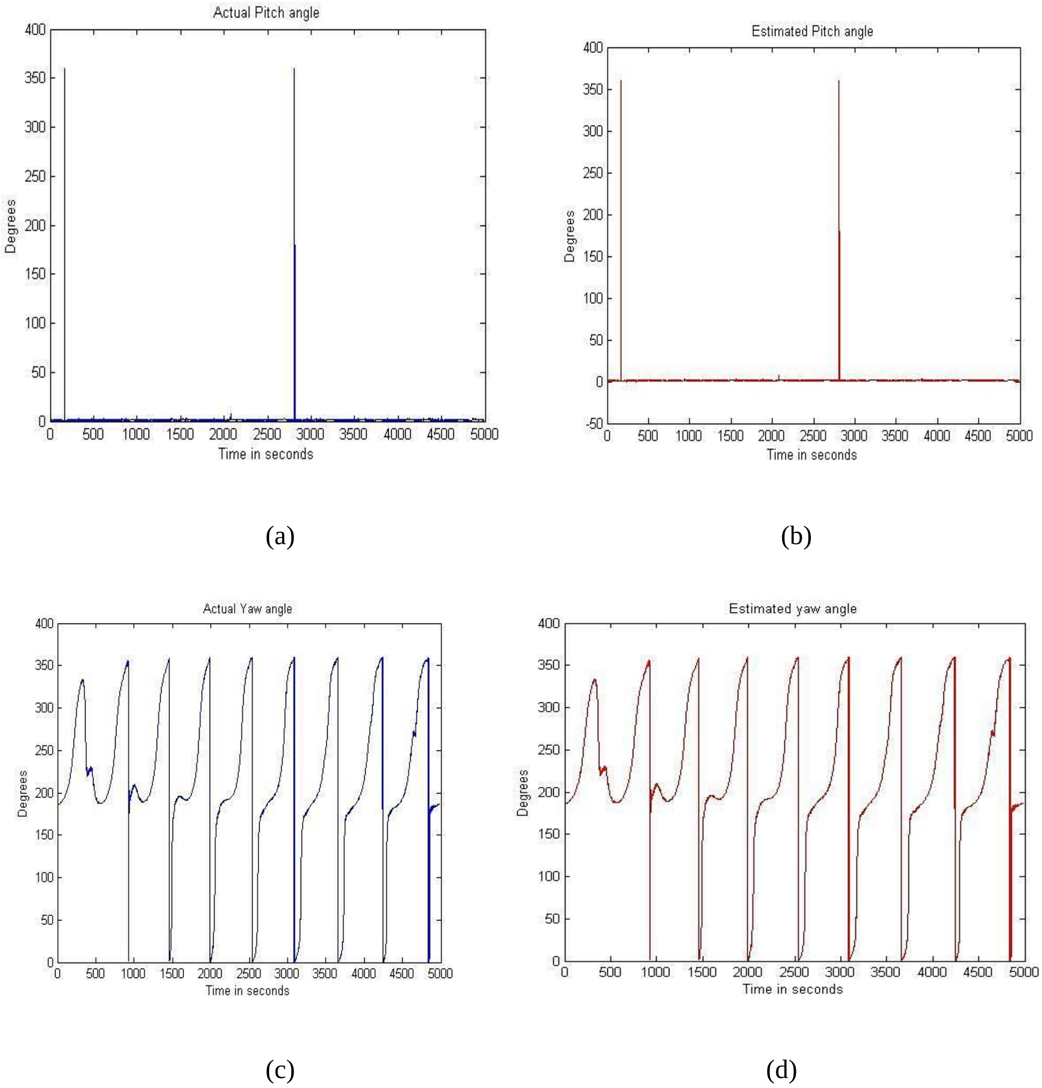

(a) (b) (c) (d)

Figure (5.8) Pitch/Yaw attitude dynamics of NPSAT-1 to consider the principle moment of inertia (I_x = 24.67, I_y = 22.63, I_z = 11) kg-m^2 the (a), (c) is Actual attitudes (pitch/yaw) data (b), (d) is Predicted/Estimated attitude data (0-5000 Seconds) using a Kalman filter algorithms

In the Figure (5.8) shows the numerical simulation of NPSAT-1 pitch/yaw attitude dynamics compare with actual attitudes and predicted/estimated attitudes. The measurement noise covariance matrix R, e^{-2} used to minimize the errors in the system [158]. The Kalman simulation generates the error covariance matrix as shown in below. The Kalman filter simulation used to estimates the State vectors

Table (5.2) NPSAT-1 State vectors measurements from IMU and Magnetometers

Time in Sec	$\boldsymbol{\phi}$ *deg*	$\dot{\boldsymbol{\phi}}$ deg	$\boldsymbol{\theta}$ *deg*	$\dot{\boldsymbol{\theta}}$ *deg*	$\boldsymbol{\psi}$ *deg*	$\dot{\boldsymbol{\psi}}$ *deg*
1	0.010576	0.007941	0.00034	0.00051	0.03723	-0.0057
2	0.013368	0.013435	0.00746	-0.0111	0.0605	-0.0042
3	0.021196	0.026652	-0.0072	-0.0224	0.07906	-0.0265
4	0.031255	0.024125	-0.0154	-0.0198	0.06837	-0.0428
5	0.028917	0.021914	-0.0132	-0.0175	0.06663	-0.0365
6	0.026345	0.02574	-0.0106	-0.0217	0.07773	-0.0322
7	0.028964	0.03255	-0.0137	-0.0287	0.09133	-0.0385
8	0.036382	0.034036	-0.0214	-0.0299	0.08867	-0.0529
9	0.0368	0.02928	-0.0216	-0.0249	0.07863	-0.0521
10	0.032376	0.029406	-0.017	-0.0252	0.08289	-0.0431

Error covariance matrix: (Calculated from Kalman Simulations)

3.35E-06	1.86E-07	-1.21E-06	-6.78E-07	-8.23E-07	-3.24E-06
1.86E-07	2.36E-06	-7.34E-07	-1.21E-06	2.56E-06	-8.23E-07
-1.21E-06	-7.34E-07	3.51E-06	1.94E-07	7.77E-07	3.39E-06
-6.78E-07	-1.21E-06	1.94E-07	2.51E-06	-2.75E-06	7.77E-07
-8.23E-07	2.56E-06	7.77E-07	-2.75E-06	8.04E-06	1.49E-06
-3.24E-06	-8.23E-07	3.39E-06	7.77E-07	1.49E-06	7.04E-06

u_d (Disturbance matrix):

0.000452857721929469

0.0110725956694653

-0.000996727272727273

The results of NPSAT-1 Kalman numerical simulation produce error covariance matrix and disturbances matrix considered the step time 0 – 5000 second attitude data from reference low earth orbiting satellite in the entire orbit [159]. Refers Appendix-D, For Implementing the Kalman filter algorithm, it is necessary to consider the known constants.

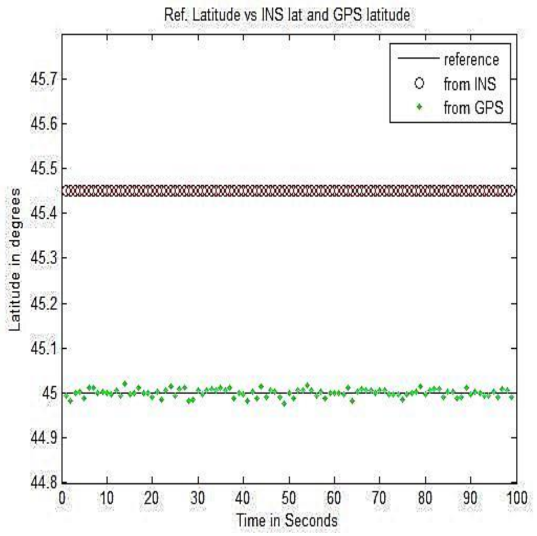
Ref. Latitude vs INS lat and GPS latitude
reference
from INS
from GPS
Latitude in degrees
Time in Seconds

(a)

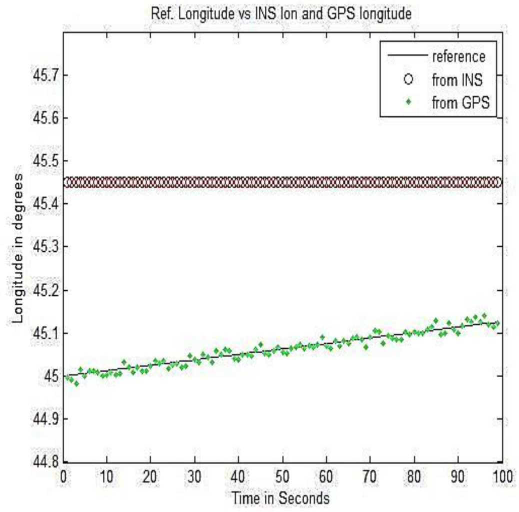
Ref. Longitude vs INS lon and GPS longitude
reference
from INS
from GPS
Longitude in degrees
Time in Seconds

(b)

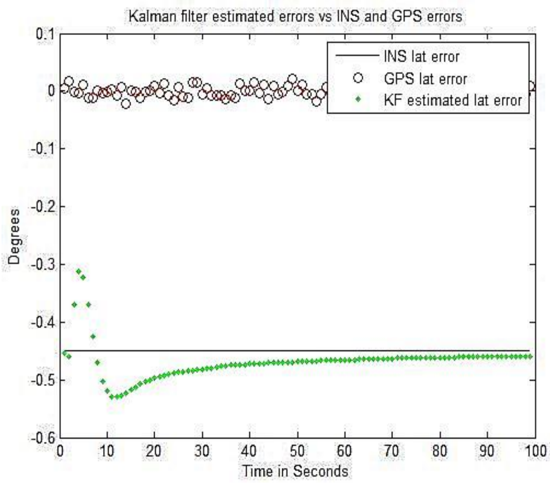
Kalman filter estimated errors vs INS and GPS errors
INS lat error
GPS lat error
KF estimated lat error
Degrees
Time in Seconds

(c)

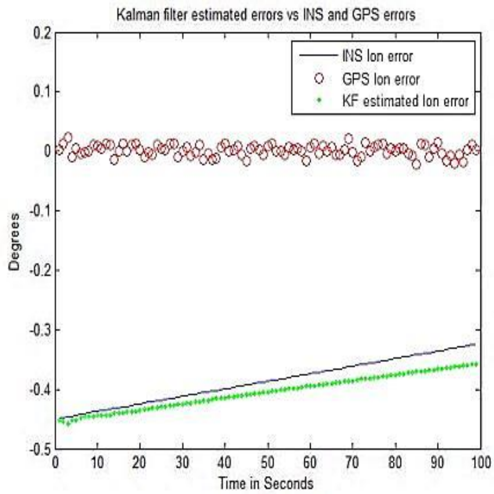
Kalman filter estimated errors vs INS and GPS errors
INS lon error
GPS lon error
KF estimated lon error
Degrees
Time in Seconds

(d)

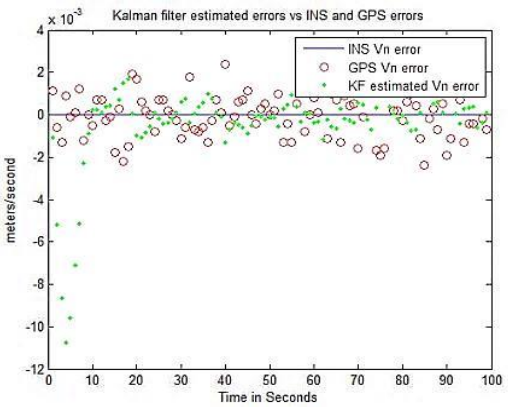
Kalman filter estimated errors vs INS and GPS errors
x 10^-3
INS Vn error
GPS Vn error
KF estimated Vn error
meters/second
Time in Seconds

(e)

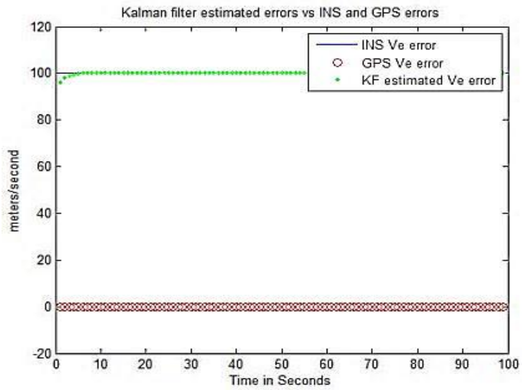
Kalman filter estimated errors vs INS and GPS errors
INS Ve error
GPS Ve error
KF estimated Ve error
meters/second
Time in Seconds

(f)

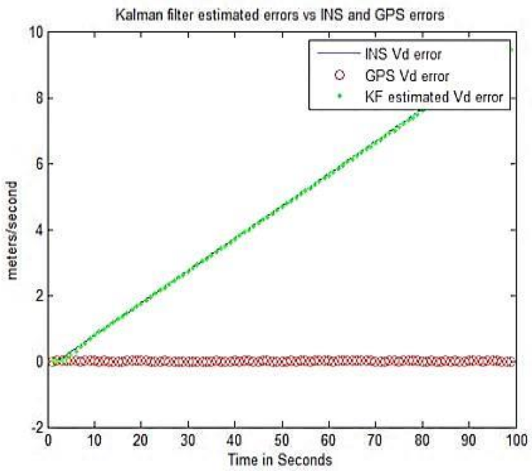

(g)

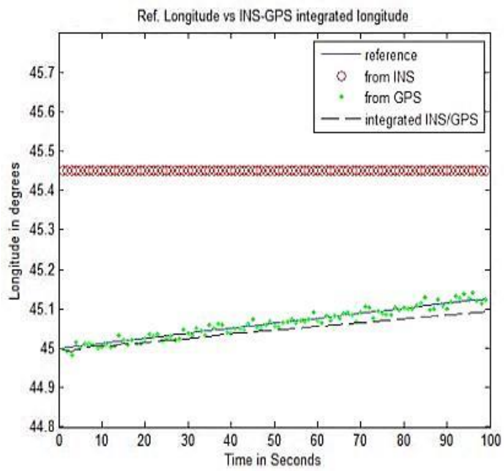

(h)

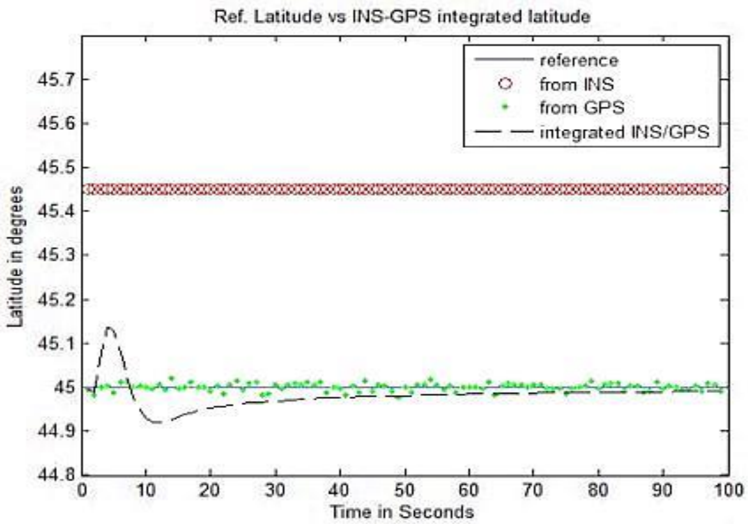

(i)

Figure (5.9) Estimates the attitude errors from on-board sensor INS/GPS (a) Reference latitude of INS and GPS (b) Reference longitude of INS and GPS (c) KF estimated the latitude errors (d) KF estimated the longitude errors (e), (f), (g) KF estimated the errors in INS /GPS in Navigation frame respectively V_n, V_e, V_d (h) Integrated INS/GPS in reference longitude (i) Integrated INS/GPS in reference latitude

Table (5.2) clearly indicates the oscillation in roll angles and yaw angles in the orbit. The pitch angle is constant in the entire orbit. The state vectors $\vec{x} = [\phi \quad \dot{\phi} \quad \theta \quad \dot{\theta} \quad \psi \quad \dot{\psi}]^T$ considered the moment of inertia $I_x = 24.67$, $I_y = 22.63$, $I_z =$

11 [158]. The actual attitude information is measured by IMU and Magnetometers [140]. In Figure (5.9) shows the NPSAT-1 estimates the attitude errors simulation results of integration of INS/ GPS in the satellite model [160], [161].

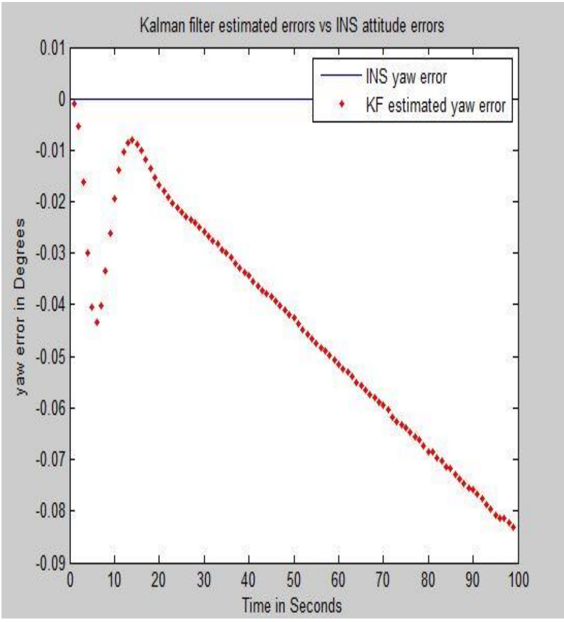

(a)

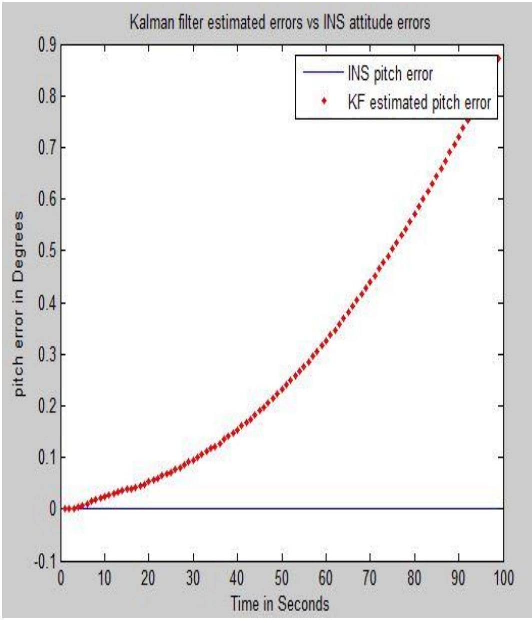

(b)

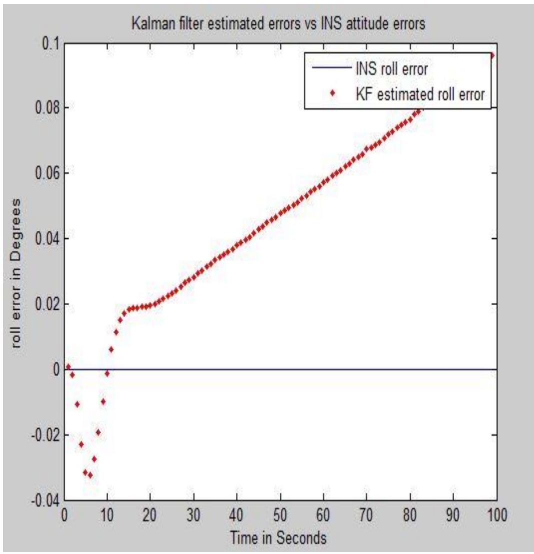

(c)

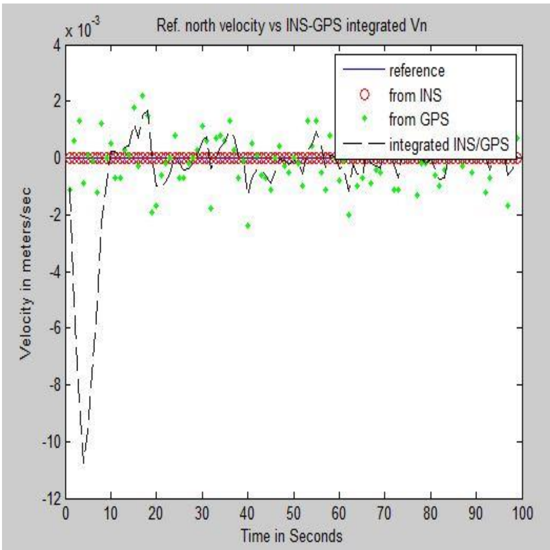

(d)

Figure (5.10) Kalman filter estimated the attitude actual errors from INS and Kalman filter errors (a) Attitude yaw errors (b) Attitude pitch errors (c) Attitude roll errors (d) Integrated INS/GPS with reference North Velocity

In Figure (5.10) shows the Kalman filter simulation of INS/GPS attitude data attitudes (Yaw, Pitch, Roll) data in x, y, z direction in navigation frames measured by an attitude sensor in reference with low earth orbit trajectory. The simulation time consider in the model is 0-100 Seconds [162].

GPS Errors (%)						INS Errors (%)			Simulation of KF Errors (%)		
Height	Latitude	Longitude	Vd	Ve	Vn	Height	Latitude	Longitude	Roll	Pitch	yaw
-0.0119	0.0043	0.002668	-0.0001	0.0006	0.0011	0	-0.45	-0.448732	8.87E-04	-8.03E-08	-0.00085
-0.0064	-0.0013	0.022005	0.0003	0.0002	-0.0013	0	-0.45	-0.446195	-0.01069	0.000589	-0.01605
0.006	-0.0029	-0.009827	0.0007	0.0011	0.0009	0.001	-0.45	-0.444927	-0.02288	0.002602	-0.03004
-0.0055	0.0115	0.005141	0.0001	0.0001	-0.0001	0.0029	-0.45	-0.443659	-0.03143	0.006291	-0.0404
0.011	-0.0119	-0.00329	0.0014	-0.0003	0.0001	0.0059	-0.45	-0.44239	-0.0325	0.010729	-0.04327
-0.0009	-0.0119	-0.002322	-0.0006	-0.0014	0.0012	0.0098	-0.45	-0.441122	-0.02746	0.015088	-0.04004
0.02	0.0004	-0.000254	0.0013	-0.0002	-0.0012	0.0147	-0.45	-0.439854	-0.01914	0.018969	-0.03353
0.0049	-0.0033	0.010015	0.0007	0.0005	0	0.0206	-0.45	-0.438585	-0.00988	0.022289	-0.02608
-0.0046	-0.0017	0.009483	0.0001	-0.0016	-0.0005	0.0275	-0.45	-0.437317	-0.00128	0.025196	-0.0193

Table (5.3) Kalman Filter estimates the errors in on-board attitude sensors GPS/INS

The reference longitude data of GPS are 45^0 and a reference longitude of INS is measured from 45.45^0 in the actual orbit.

The simulation considered the step time 0 – 100 second attitude data from (GPS/INS) reference at low earth orbiting satellite in the entire orbit. Refers Appendix-D, For Implementing the Kalman filter algorithm, it is necessary to consider the known constants [163], [164]. The measurement noise covariance matrix R, e^{-2} used to minimize the errors in the system. The minimum covariance values desired the less error in the measurements due to the perturbations [165]. The table (5.3) indicates the minimum errors in GPS, and INS with implementation of Kalman algorithms [141], [160]. The attitude data of GPS/INS considered the LEO trajectory. This result mainly predicts the future estimate used to control the attitude orientation/control of the satellite.

CHAPTER 6

SATELLITE ATTITUDE CONTROLLER

6.1 Overview

The Attitude Control System (ACS) is important to maintain the satellite into prescribed/determined orbit from perturbed/disturbed orbit. The attitude (Roll angle, Pitch angle, and Yaw angle) of satellite changes due to the orbital perturbation. It is mandatory to control & correct the attitudes of the satellite into the actual orbit [166], [167]. This chapter presents the design of the attitude controller for NANO satellites as given below

- NPSAT-1 Satellite,
- SRM Satellite
- Pratham (IIT Bombay) Satellite

The controller is also used to reduce the oscillation due to the perturbation forces where affects the attitude of the satellite. Also, it is decreasing the errors in the satellite system dynamics [168]. The effects of satellite dynamics without controller and with controllers are compared.

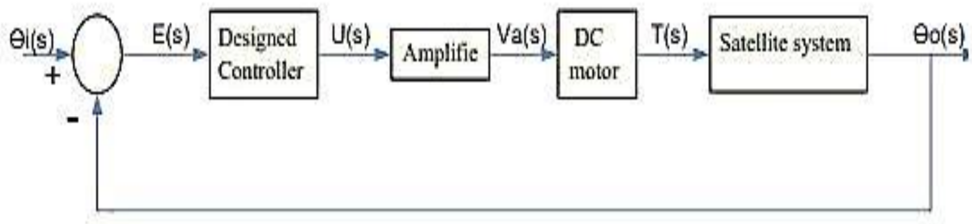

Figure (6.1) Satellite Attitude Control System [169]

The design of Proportional – Derivative (PD) controller has been introduced for various transient responses of the NANO satellite attitude corrections. In Figure (6.1) shows the satellite attitude control system, the actual attitudes measure by Gyros which can be compare with reference attitudes. The comparator produces the error signals E(s) fed to the controllers. The PD controllers introduced in satellite control system. The steady-state is settled exactly at 1 (zero steady-state error). Hence there is no need for integral control. The PD controller generates the Armature voltage (**V_a**) supply the DC motor to control armature current (**I_a**) in the input circuit. The DC motor act as an actuator, DC motor output is Torque (**T**). The armature coil consists of shaft used to derive the load. The Attitudes determination and control system (ADCS) the satellite inertia considered as load [168]. In the input circuit, due to variation in the armature voltage, the output circuit satellite inertia (Load) induces the angular velocity (**ω**). This angular velocity generates because of the mutual inductance in the secondary circuit. In secondary coil induces the back-e. m. f (***b***) due to the changes in the current in the primary coil. The torque is inversely proportional to armature current shown in equation (6.1)

$$\mathbf{T = K\, I_a} \tag{6.1}$$

K = Torque constant;

$$\mathbf{T} \propto \mathbf{I_a}$$

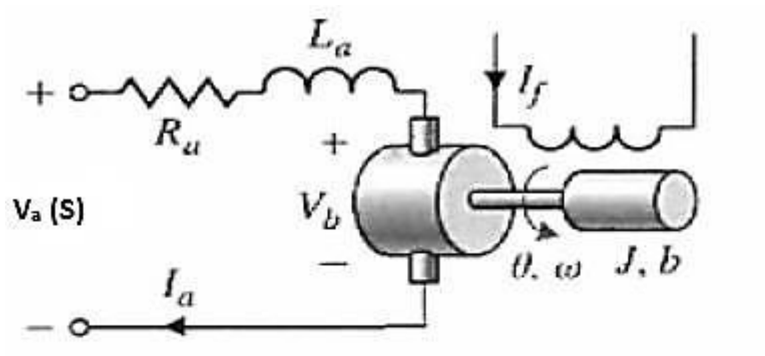

Figure (6.2) Armature controller DC motor [168]

In figure (6.2) shows the armature-controlled DC motor, **R_a** is armature resistance, **L_a** is armature inductance, **V_b** is back e. m. f voltage, **J** is the moment of inertia, **b** is the back e. m. f constant, **I_f** is field current [168]. The magnitude of back e. m. f voltage is opposite to the input voltage.

$$\mathbf{V_b = k\, \omega} \tag{6.2}$$

Hence, the equation (6.2) back e. m. f voltage is inversely proportional to the angular velocity derive the satellite inertia. The back e. m. f is expressed as V/(Radian/Sec). In the proposed design considered back e. m. f. constant is 0.85. In ACS, V_b = 0.85 V generate the angular velocity ω (1 Radian/Seconds). The one Ampere current (I) produce the torque 0.85 (Nm). Since, the torque is proportional to the armature current. This is highly used to control the attitudes of Nano satellite [169]

The transfer function of armature-controlled DC motor is given in equation (6.3)

$$\frac{T(s)}{V_a(s)} = \frac{K}{L_a\ s + R_a} \qquad (6.3)$$

Table (6.1) ACS DC Motor design Parameters [168]

Torque constant, K	0.85
Armature Inductance, L_a	0.003H
Armature Resistance, R_a	1 Ohms (Ω)
Back e. m. f. constant, b	0.85

In table (6.1) shows the ACS design parameters, the sensitive of Gyro is (V/ (deg/Sec). For, measure the actual attitude from satellite the Gyro gain chosen as one. (Gyro Gain = 1). The second order charactertics equations consider for satellite attitude dynamics. The various transient response of the NANO satellite time domain signal reached the maximum value Rise time (t_r), the time at maximum amplitude occurs peak time (t_p), the ratio of oscillation of critical damping to actual damping Maximum overshoot (%MP), at the time the signal reached the final value Settling time (t_s), the value of percentage of errors in the system Steady state errors (e_{ss}) [168]. This control torques used to stabilize the orientation of a satellite into actual path in orbit [169].

Discussed Control System Design Response Specifications:

- Settling time ≤ 0.2 seconds
- Improve the Peak time, Rise time
- Reduces the overshoot (Damping)
- Zero steady state error

6.2. Methodology

The proposed method used to design the Nano satellite attitude control transient response of using PD controllers.

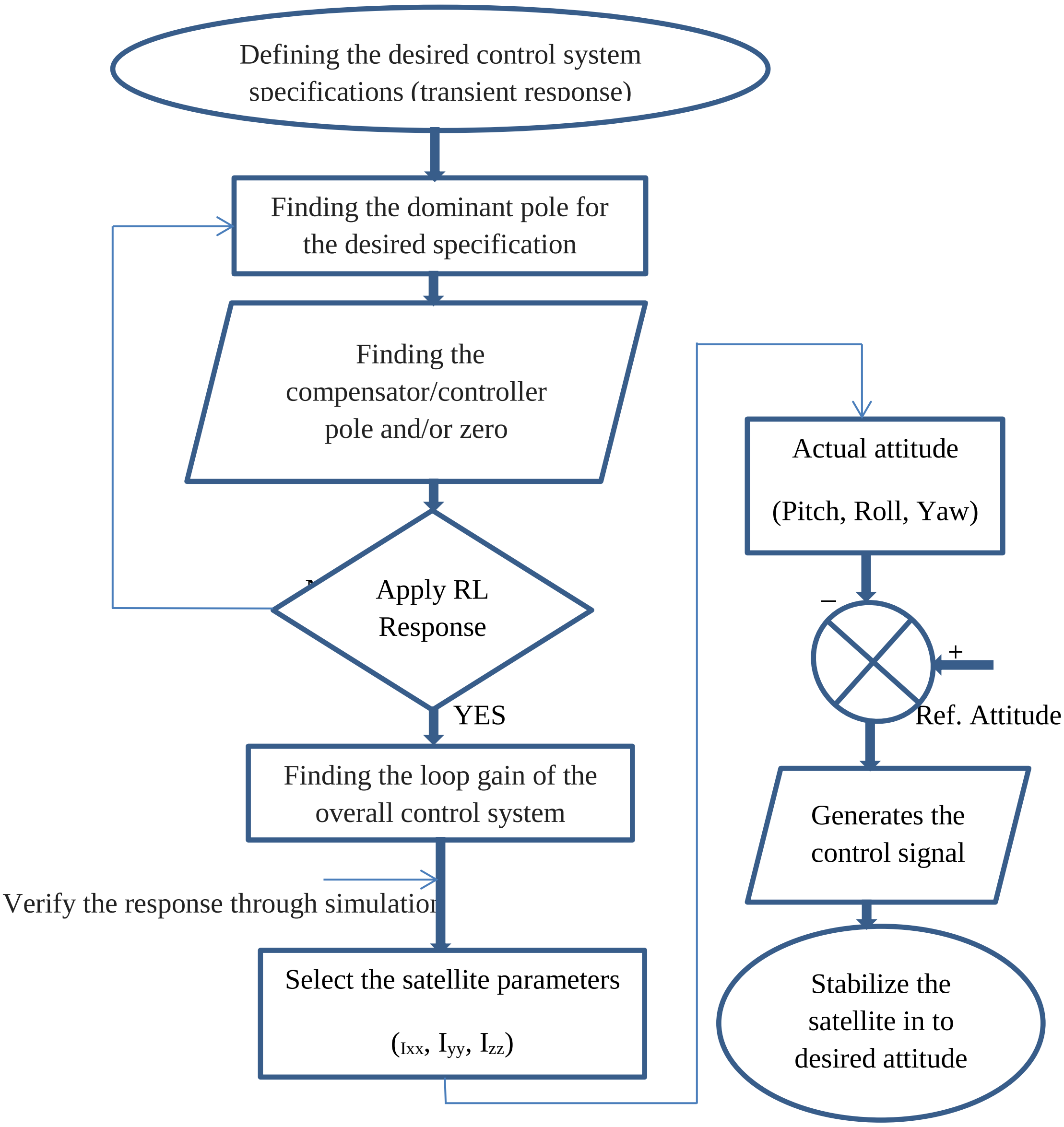

Figure (6.3) Flow chart for satellite attitude controller design

The Proportional-Derivative (PD) controllers have been introduced in Nano satellite/plant attitude control. In flow chart shows (See Figure 6.3), when design a PD controller to improve the transient response (Rise time, Overshoot, Peak time and Settling time). Theoretically, the damped frequency of oscillation is $\omega_d = \omega_n \sqrt{1-\xi^2}$, ω_n is the natural frequency of oscillation (rad/seconds) [166]. The plant is referred as satellite dynamics. The PD controller, proportional Gain $\mathbf{K_p}$-Errors proportional to the system, Derivative Gain **K_d-** Derivative of errors in the system [168]. The design of satellite control systems consists of two parts one is Attitude determination (AD) another Attitude control (AC). The satellite subsystem used to determine the attitude, predict the future attitude, and control the attitude of satellite [167]. This chapter includes the attitude control part of the NANO spacecraft/satellite attitude corrections [170]. The main part of ADCS is actuator and spacecraft dynamics, controllers and attitude sensors. The satellite attitude sensor such as Gyro's used to determine the actual attitudes. The satellite reference input signal compares with feedback signal from attitude sensor. If there is any variation in the feedback signal with respect to reference/pre-determined attitude, then initiate the actuator to generate the control torque/forces. The damping ratio desired the types of oscillation. The equations $-\xi\omega_n \pm j\omega_d$ first part indicates the real value; second part indicates the imaginary value. As per the design specification the settling time less than 0.2 seconds is calculated by $\xi\omega_n = \frac{4}{0.2}$ = **20** [166].

$$\tan(34.3) = \frac{\omega_d}{20} \quad \Rightarrow \quad \omega_d = \mathbf{13.64}$$

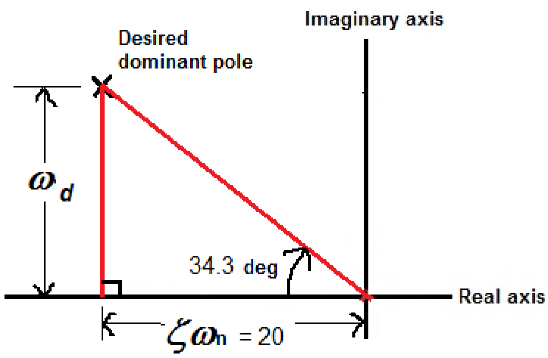

Figure (6.4) Location of closed dominant pole in the S-Plane

To determine the imaginary part value it require to find the angles from closed dominant pole, draw the line from closed dominant pole to origin of the s-plane (or) frequency plane, $\theta = \cos^{-1}(\xi) = \cos^{-1}(0.826) =$ **34.3°** as shown in Figure 6.4 (Here, for design point of view, the **overshoot percent is taken as 1%** (equal to a damping ratio of **0.826**) [166]. As per the design specification of Nano satellites (NPSAT-1, SRM Satellite, Pratham Satellite) is settling time of 0.2 seconds.

6.3 Algorithms –Various steps to follows design of Attitude controller

STEP 1. Defining the desired control system specification (transient response and steady-state error).

STEP 2. Finding the dominant pole for the desired specifications.

STEP 3. Design the compensator/controller pole and/or zero.

STEP 4. Calculates the loop gain of the overall control system.

STEP 5. Verify the response through simulation.

An algorithm of Nano satellite (NPSAT-1, Pratham Satellite, and SRM Satellite) attitude control implemented using MATLAB Tools. Also, the closed loop poles help to find the gain of the system using **Root Locus** (RL) methods. In design simulation considered the satellite attitude control, Satellite Attitude determination (SAD), Satellite Attitude Prediction (SAP), Satellite Attitude Control (SAC). The SAD is the process of computing the orientation of satellite with pre-determined point accuracy from on board sensors [171]. The SAP is the process of estimating the future attitude of the satellite model. The SAC is the process of controlling the orientation of the satellite. In table (6.2) shows the Nano satellites design parameter considered for simulations [134], [136], and [172]

Table (6.2) Nano satellite attitude control design parameters

	Satellite Details		
	NPSAT-1	**Pratham Satellite**	**SRM Satellite**
Altitude	550 km altitude, Low Earth circular orbit (LEO)	817 km altitude, Polar Sun Synchronous Orbit (PSSO)	867 km altitude, Low Earth circular orbit (LEO)
Orbital angular velocity, Ω	0.0011068 rad/s	0.0010346 rad/s	0.0010239 rad/s
I_{xx}	24.67 kg-m^2	0.116 kg-m^2	6.2911 kg-m^2
I_{yy}	22.63 kg-m^2	0.109 kg-m^2	5.9162 kg-m^2
I_{zz}	11 kg-m^2	0.114 kg-m^2	4.6085 kg-m^2
Three attitude axes (Roll, Pitch, Yaw) are decoupled			

6.4. Attitude Control: NPS Aurora Satellite (NPSAT-1) [172]

The principle moment of inertia of NPSAT-1 satellite is [24.67, 22.63, 11] kg-m^2. The angular velocity of the satellite 0.0011068 rad/s at 550 km Altitude [172]. The closed loop response of roll attitude dynamics is $\frac{\phi\,(s)}{T_x\,(s)}$. The input of the model is torque and output is actual attitudes (Roll angle, Pitch angle, and Yaw angle) of satellite [173]. The Gyro gain is taken as one. The sensitive of Gyro is (V/(deg/Sec). For getting the actual attitudes from model, this feedback signal compares with predetermined attitudes. The errors signal is generated from comparators fed to Armature control DC motor. The DC motor act as an actuator.

6.4.1. NPSAT-1 Roll attitude control system

The comparison of reference roll and feedback signals measured from Rate Gyro's (RG) produces (Ref. from figure 6.1) the errors in the system. These errors are minimized from controllers and generate the control torque to the satellite dynamics. Principal moments of inertia of NPSAT-1 [172]

$$=\begin{bmatrix} 24.67 & 0 & 0 \\ 0 & 22.63 & 0 \\ 0 & 0 & 11 \end{bmatrix} \text{kg-m}^2$$

As per the design specification of NPSAT-1 is settling time is ≤ 0.2 seconds considered the closed dominant pole is **–20±13.64*j***. The error signal expressed in e (t), Satellite input/reference roll signal (ϕ_{ref}) expressed in degree. The output of the satellite system is ϕ (t).

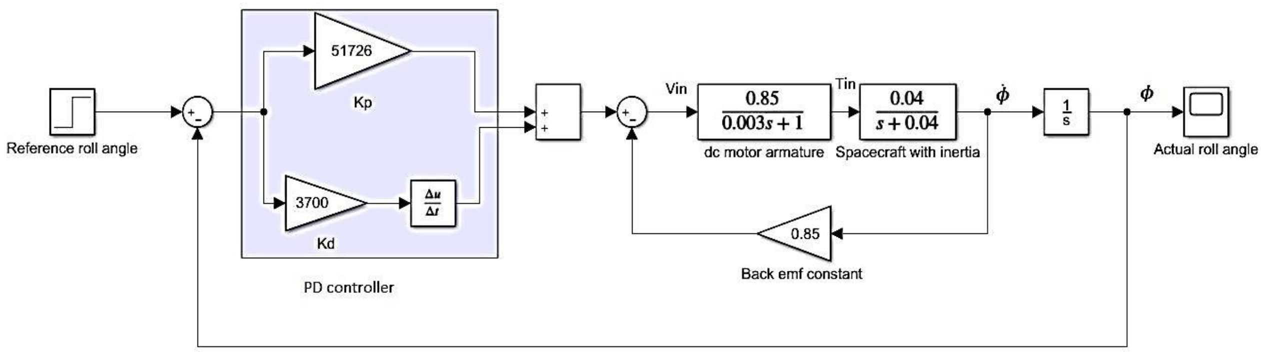

Figure (6.5) NPSAT-1 Roll attitude control system

The step response Figure (6.5) of the roll attitude transfer function without controller given below.

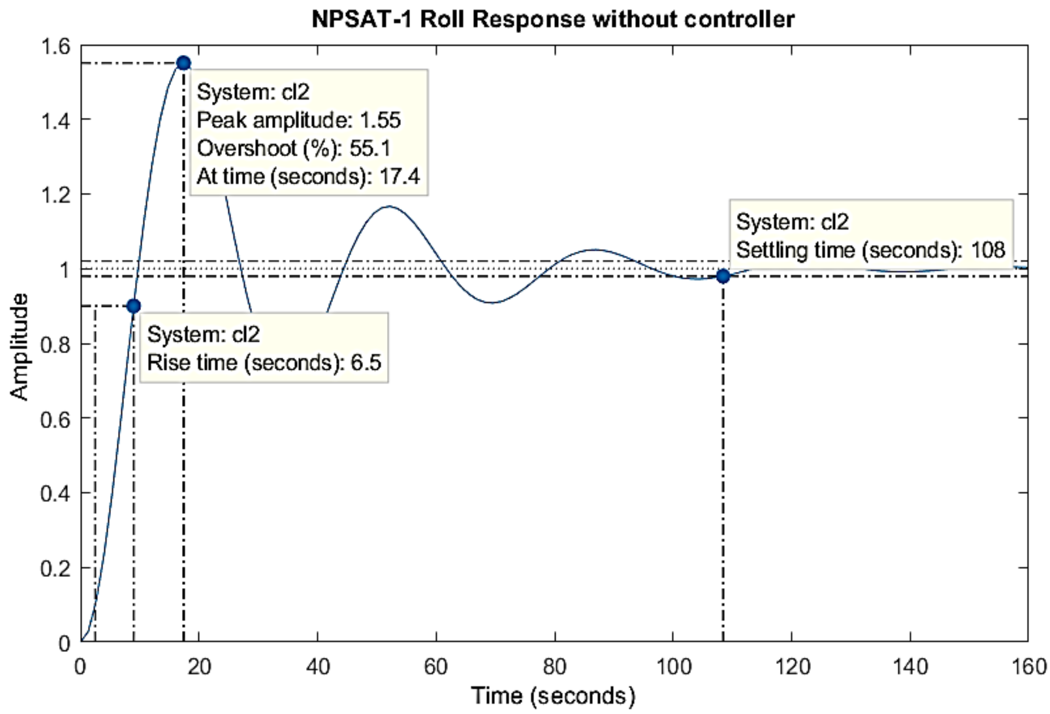

Figure (6.6) NPSAT-1 Roll attitude response with step command

From Figure 6.6, it is clear the damping of the roll attitude system overshoot is 55.1%. The oscillation gradually reduces with settling down at time 108 seconds (we need to reduce it to ≤ 0.2 seconds). The system doesn't have steady state transient response errors so, not requires the Integral (I) controller [166]. The NPSAT-1 roll attitude dynamics clearly indicates, there are three poles in the dynamics one on the origin of the s-plane another is -0.0639 and -333.264 illustrate in Figure (6.7) finding the angles θ_1, θ_2 and θ_3 from closed dominant pole to other poles and zeros [167]. There are no zeros in the pole-zero plots. This method used to design the PD compensated controller by using root locus analysis find the zero location. For, finding the PD controller zero (z_c), The line connecting from complex pole to pole at the origin and pole at -0.0639 and -333.264 (Refers Appendix E). Let us assume complex pole considered as '**A**' [166]. The angles from complex pole (Equation 6.4) A = 180^0 – (summation of angle measure from complex pole to other poles) + (summation of angle measure from complex pole to other zeros)

$$= 180 - (\theta_1 + \theta_2 + \theta_3) \quad (6.4)$$

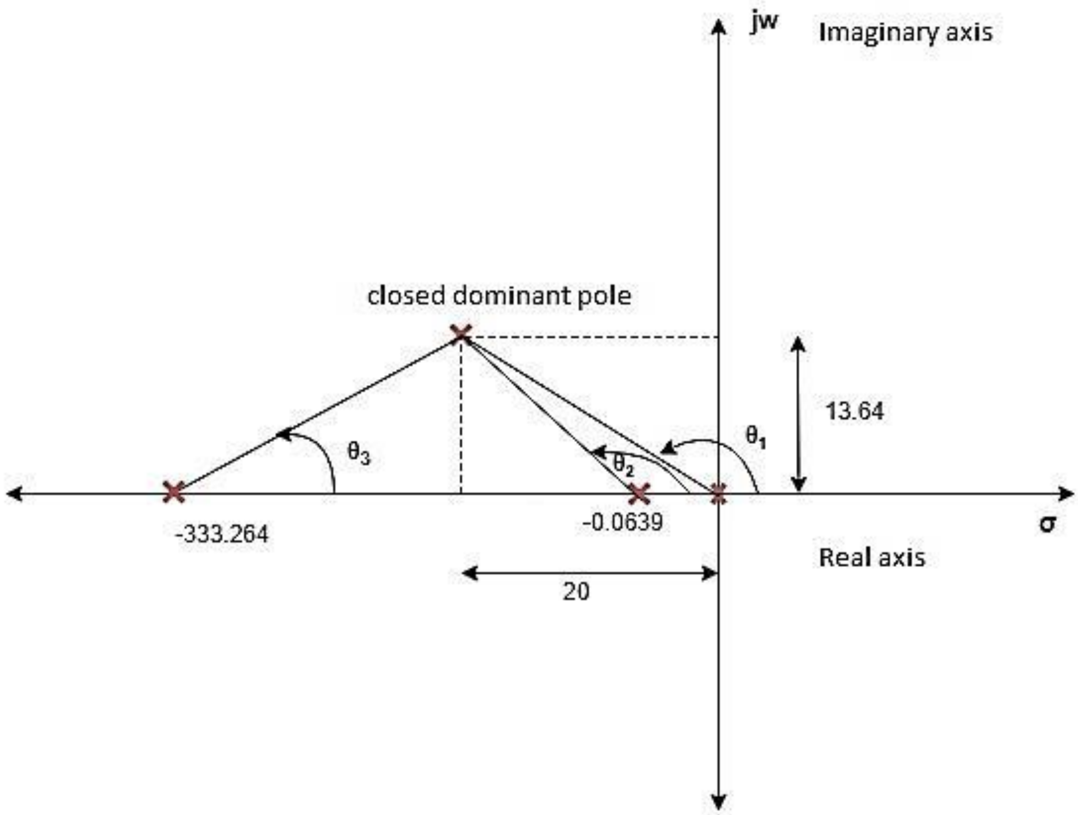

Figure (6.7) PD compensated design (Complex pole to others pole)

The angles from closed dominant pole to others pole are

θ_1 = 180^0 – $\left[tan^{-1}\ \left[\frac{13.64}{20}\right]\right]$= 145.7°

θ_2 = 180^0 - $\left[tan^{-1}\ \left[\frac{13.64}{20-0.0639}\right]\right]$ = 145.614°

θ_3 = $\left[tan^{-1}\ \left[\frac{13.64}{-333.264-20}\right]\right]$ = 2.493^o

Substitute the angles from closed dominant pole to others poles θ_1, θ_2, and θ_3 in equation (6.4) [167]

= 180 – (145.7 + 145.614 + 2.493) = **–113.807°**

Now, find the PD compensated zero from Figure (6.8) from angle measured from complex pole A (**-113.807^0**)

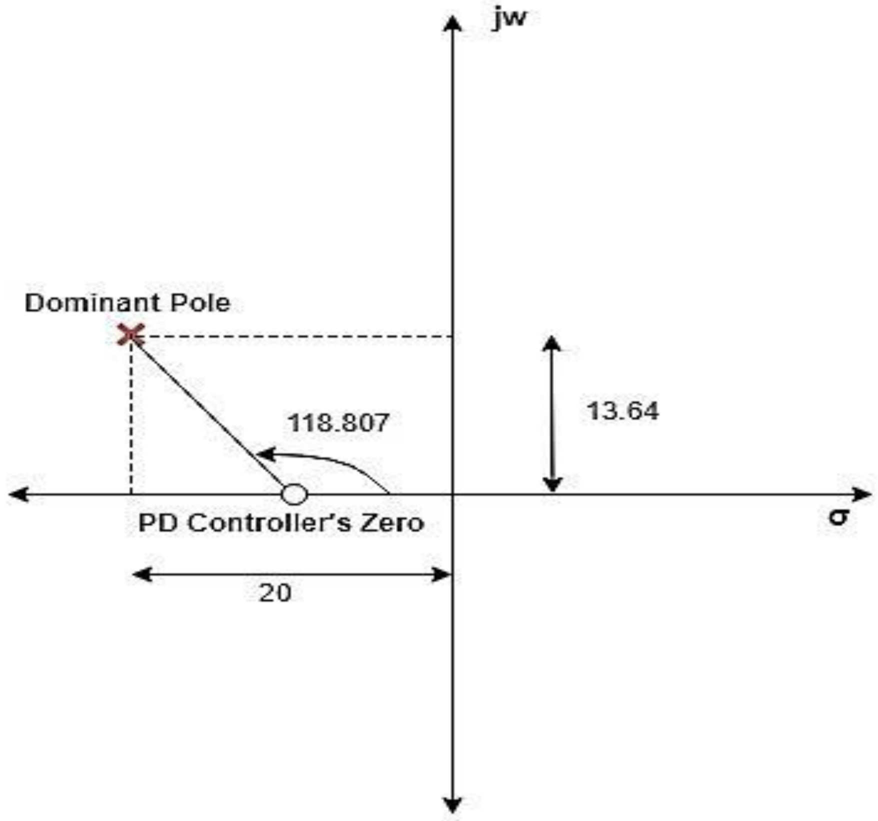

Figure (6.8) Finding the location of the attitude PD controller

Using the geometry shown in Figure 6.8, tan (180^0 - 113.807^0) = $\frac{13.64}{20-z_c}$

To design the PD compensator zero (z_c) from above geometry calculates the value **–13.98.** Now, the PD controller dynamics is ***K* (s + 13.98).** The K is the loop gain [166]. Since the system have three poles, so there are three root locus, one travel from origin travel to negative real axis, another two-root locus start at -159 ± 108i (Break in point) then, travel perpendicular to real axis. In figure (6.9) shows the NPSAT-1 Roll Root Locus response indicates gain is 3700 at overshoot (1%), the damping ratio, $\boldsymbol{\xi}$ is 0.826, undamped natural frequency, $\boldsymbol{\omega_n}$ is 192 (rad/Sec). Here, for design point of view considered one percent overshoot (1%) a damping ratio equal to **0.826**. To Calculates the angle from given equation (6.5)

$$\theta = \cos^{-1}(\xi) = \cos^{-1}(0.826) = \mathbf{34.3}^\circ \qquad (6.5)$$

Draw the straight line at angle 34.3^0 from origin left of the s-plane, when this line crossing to RL at pole -159 ± 108i, Record the loop Gain as per damping ration 0.826.

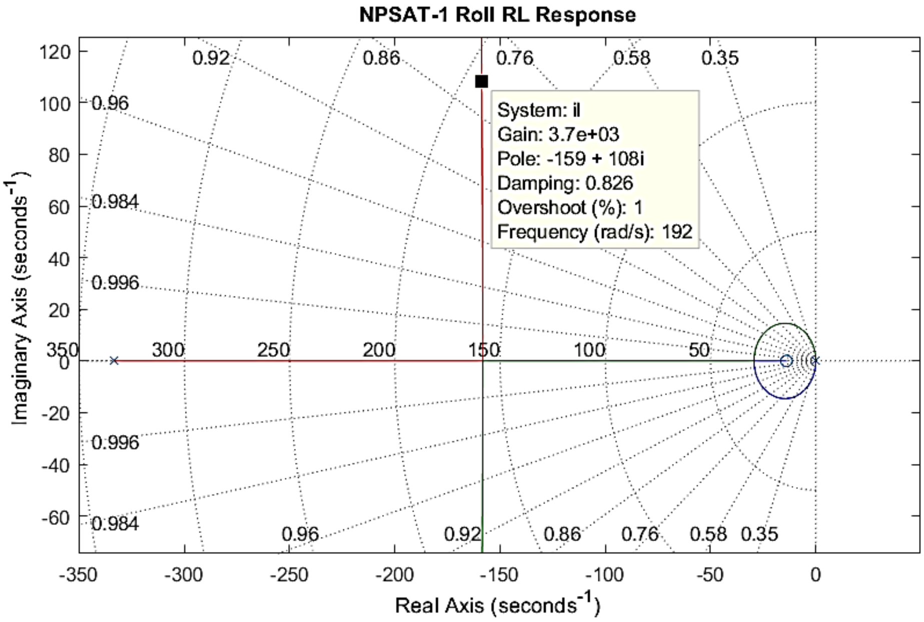

Figure (6.9) NPSAT-1 Roll attitude Root locus response

The MATLAB Simulation for closed loop system includes the DC motor dynamics, satellite roll attitude dynamics, and PD compensator. (Refers Appendix E)

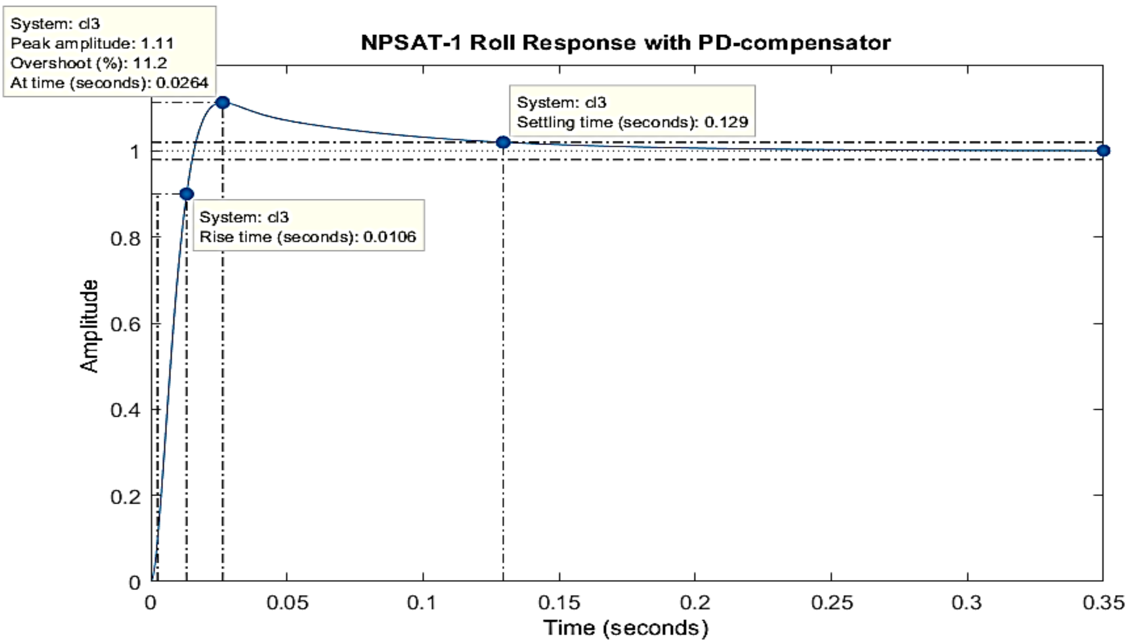

Figure (6.10) NPSAT-1 Roll Attitude Response with PD controller

In Figure 6.10 shows, as per the design specification considered system settling time is (≤ 0.2), the system responses after implemented the PD compensated controller is

0.129 Sec, rise time is 0.0106, overshoot is improved 11.2 %, and peak time is 0.025 with 1.11 peak amplitude were achieved. The NPSAT-1 SIMULINK responses of roll attitude control diagram shown in Figure 6.11. This model includes the dynamics of armature-controlled DC motor cascade with spacecraft inertia considered the back e. m. f. constant 0.85. To introduce the PD controllers ***K* (s + 13.98),** K is 3700 loop gain calculating from Root locus analysis. The input step signal considered for satellite attitude control model, the variation in transient response output is measured from scope block. In figure (6.11) shows the NPSAT-1 Roll response without controller, it is noticed peak amplitude occurs at 18 seconds peak time [174], [175]. Also, the response settles down at settling time 108 seconds with zero steady state errors

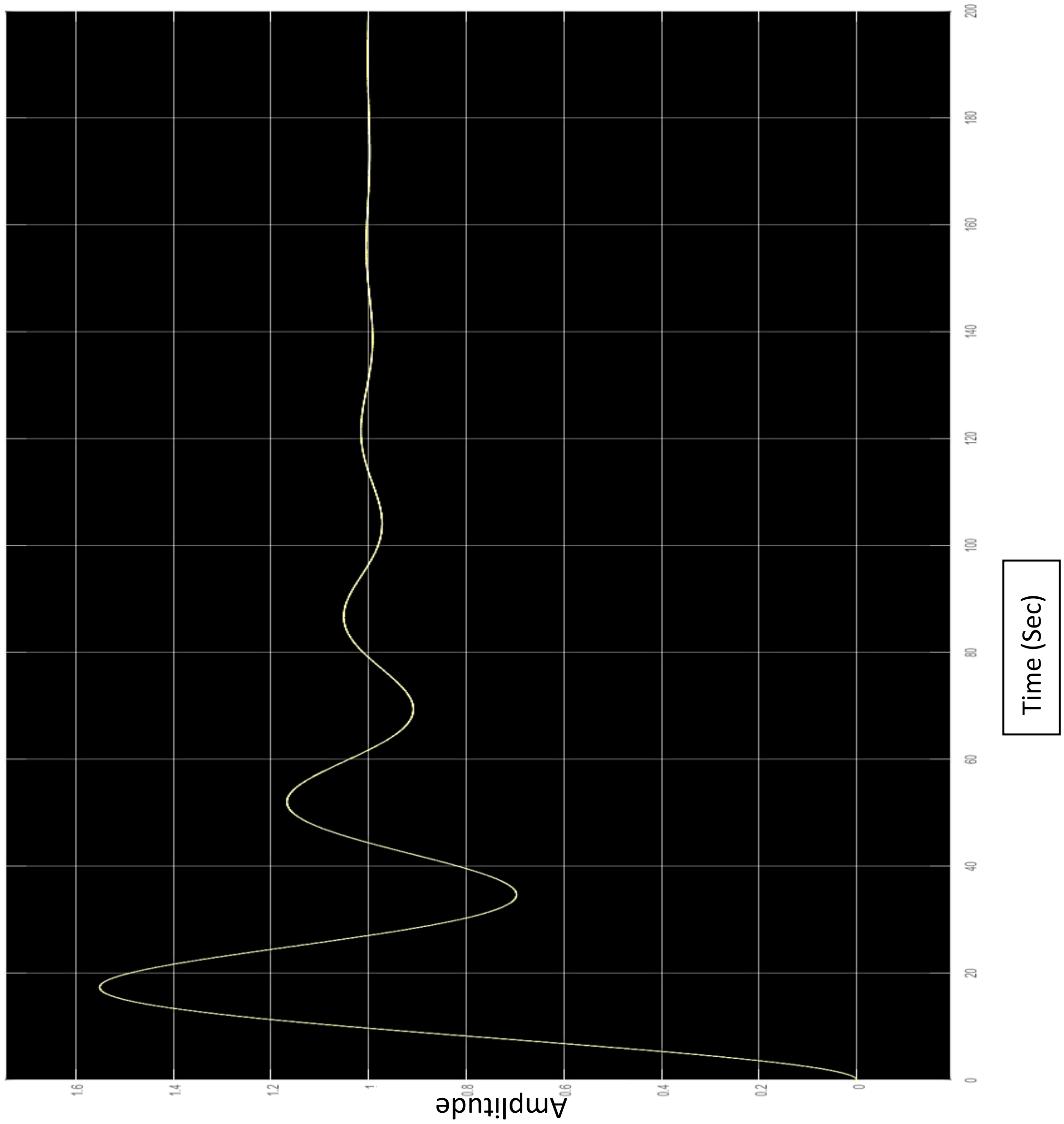

Figure (6.11) NPSAT-1 Response from Roll attitude control without controller

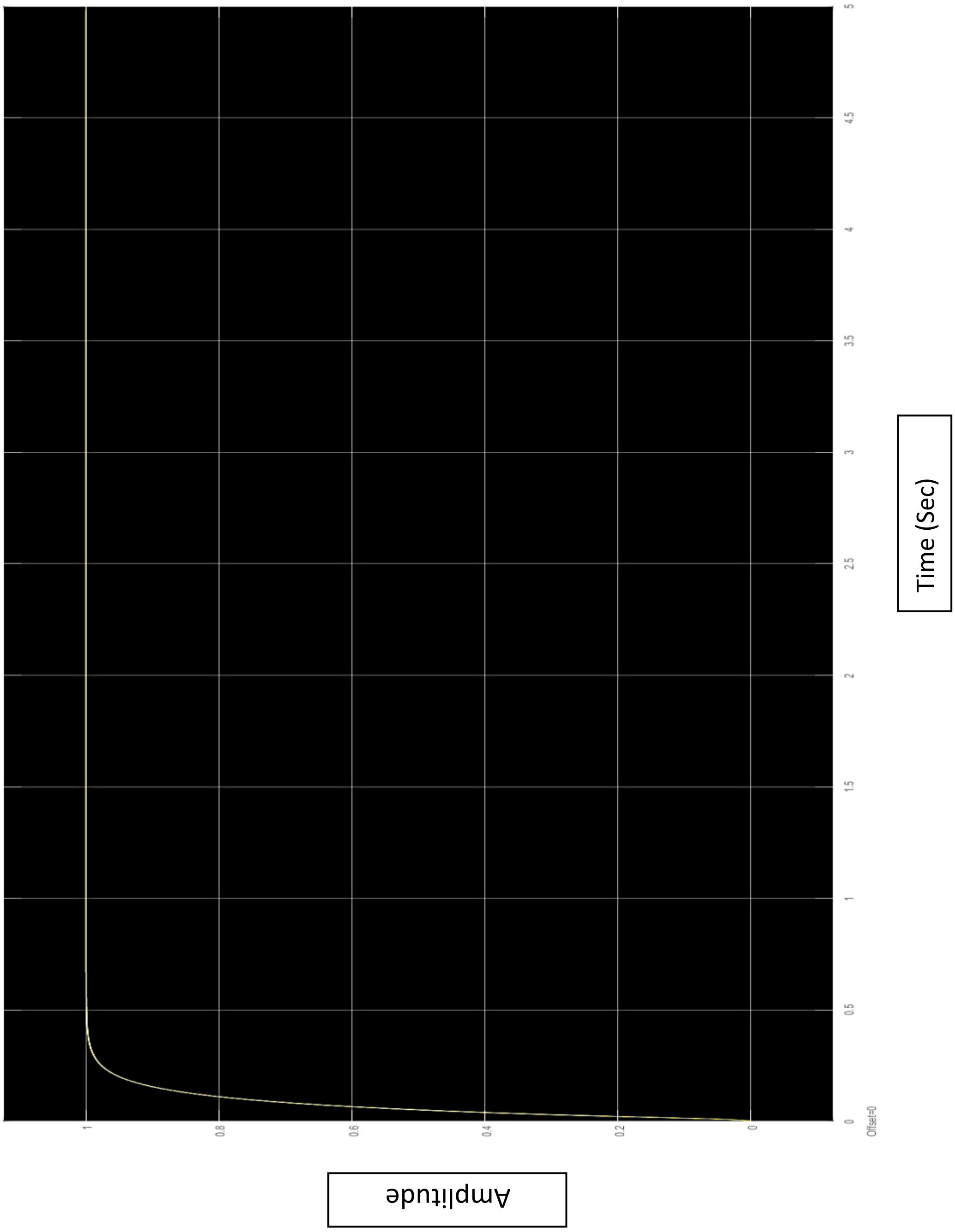

Figure (6.12) NPSAT-1 Response from Roll attitude control with PD-controller

The NPSAT-1 Roll control PD-compensated response shown in Figure (6.12). As per the design consideration settling time is ≤ 0.2. The derivative block is introduced for ‘D’ controller [176], [177]. Thus, the PD-compensated transient response is improved, the same as recorded from MATLAB simulations.

6.4.2. NPSAT-1 Pitch attitude control system

The closed loop response of pitch attitude dynamics is $\frac{\theta\,(s)}{T_y\,(s)}$.

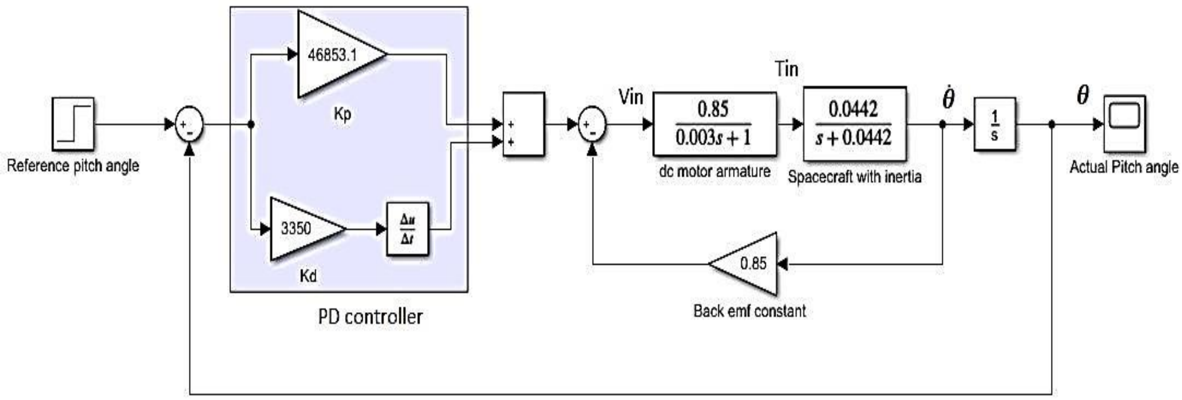

Figure (6.13) NPSAT-1 Pitch Attitude Control

The step response shown in figure (6.13) of pitch attitude transfer function without controller is given below. (Refers Appendix E)

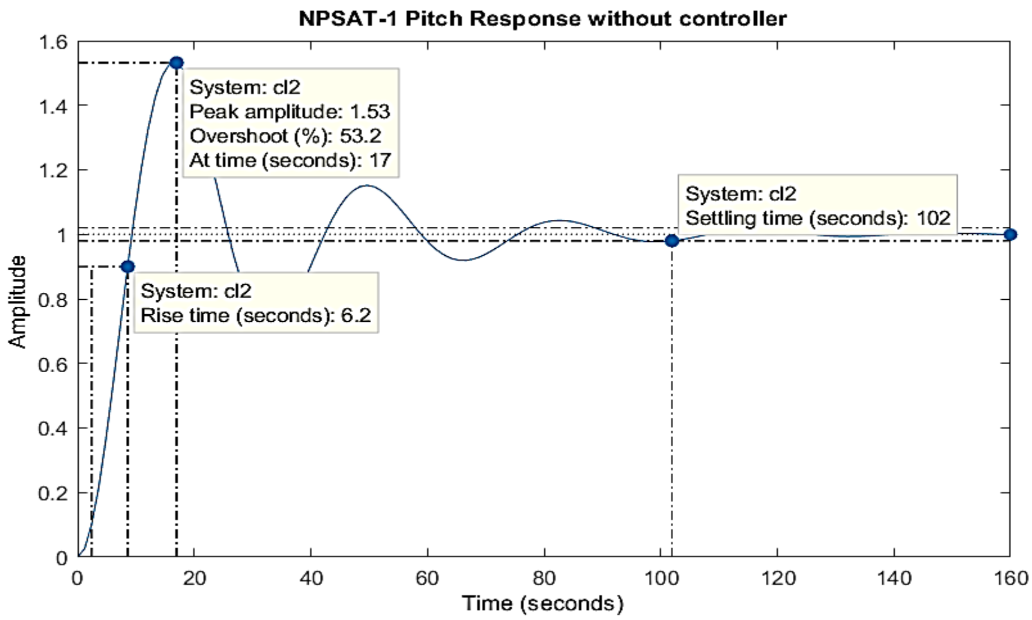

Figure (6.14) NPSAT-1 Pitch attitude response with step command (without controller)

From Figure 6.14, it is clear the damping of the roll attitude system has more overshoot is 53.2%. The oscillation gradually reduces with settling down at time 102 seconds (we need to reduce it to ≤ 0.2 seconds) [176]. And, the steady-state is settled exactly at 1 (zero steady-state error). Hence there is no need for integral control. The

NPSAT-1 roll attitude dynamics clearly indicates, there are three poles in the dynamics one on the origin of the s-plane another is -0.0761 and -333.2572 shown in Figure (6.15) finding the angles θ_1, θ_2 and θ_3 from closed dominant pole to other poles and zeros [166]. There are no zeros in the pole-zero plots. This method used to design the PD compensated controller by using root locus analysis

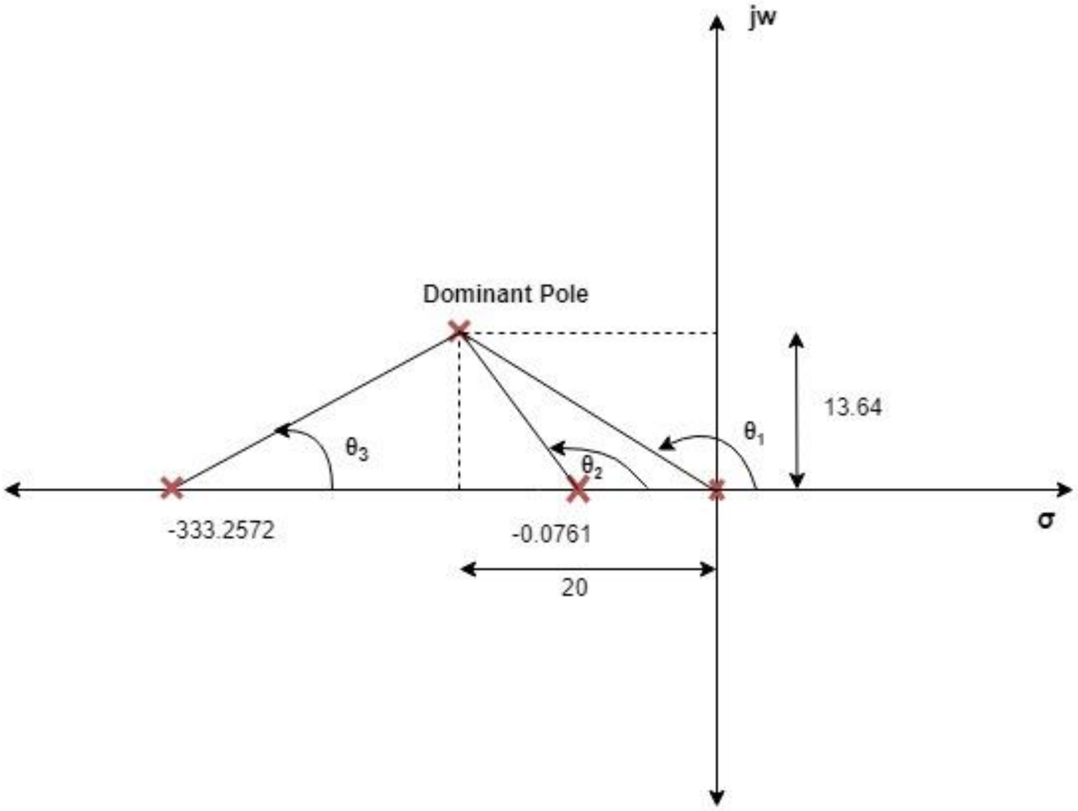

Figure (6.15) PD compensated design (Complex pole to others pole)

The angles from closed dominant pole to others pole are

$$\theta_1 = 180^0 - \left[tan^{-1}\ \left[\frac{13.64}{20}\right]\right] = 145.7°$$

$$\theta_2 = 180^0 - \left[tan^{-1}\ \left[\frac{13.64}{20-0.0761}\right]\right] = 145.6°$$

$$\theta_3 = \left[tan^{-1}\ \left[\frac{13.64}{-333.2572-20}\right]\right] = 2.493^0$$

This angle is used to find the zero location for finding the PD controller zero (z_c), The line connecting from complex pole to others pole at the origin and pole at -0.0761 and -333.2572. Let us assume complex pole considered as A.

The angles from complex pole A [153]

= 180^0 – (summation of angle measure from complex pole to other poles) + (summation of angle measure from complex pole to other zeros)

$$= 180 - (\theta_1 + \theta_2 + \theta_3) = 180 - (145.7 + 145.6 + 2.493) \approx \mathbf{-113.793°}$$

Now, find the PD compensated zero from Figure (6.16) from angle measured from complex pole A (**-113.793$^{\mathbf{0}}$**) [166]

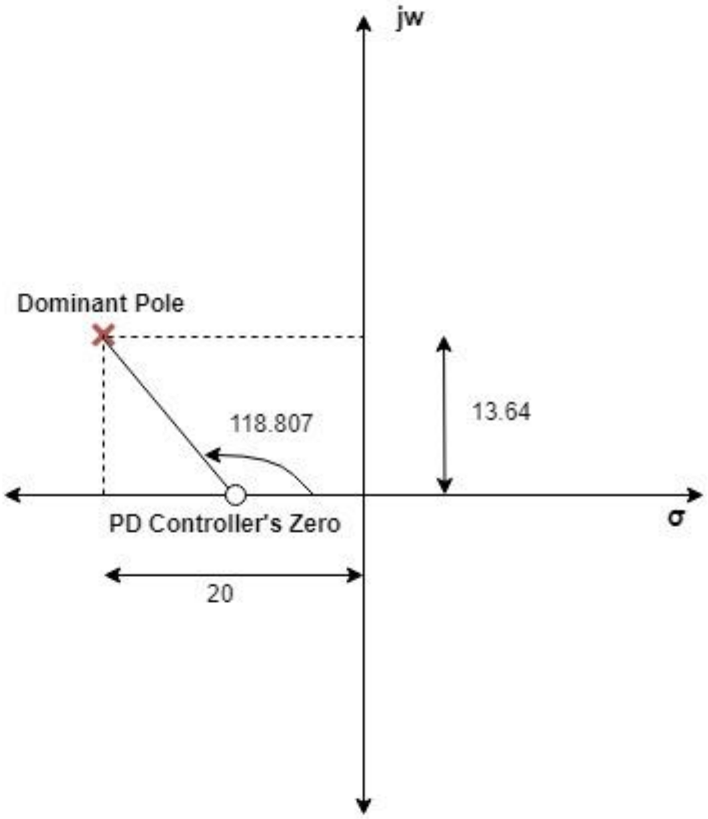

Figure (6.16) Finding the location of the attitude PD controller (z_c)

Using the geometry shown in Figure 6.16, tan (180^0 - 113.793^0) = $\frac{13.64}{20-z_c}$

To design the PD compensator zero (z_c,) from above geometry calculates the value **–13.986.** Now, the PD controller dynamics is ***K* (s + 13.986).** The K is the loop gain [167]. The loop gain found from the root locus at 1% maximum overshoot is 3350, damping ratio, ξ is 0.826, undamped natural frequency, $\boldsymbol{\omega_n}$ is 192 (rad/Sec) shown in figure (6.17)

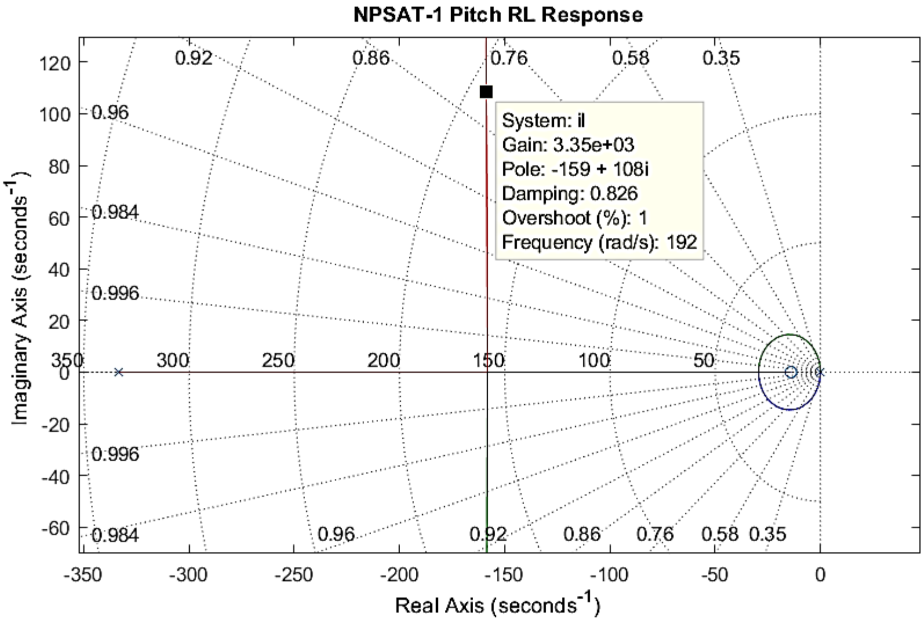

Figure (6.17) NPSAT-1 Pitch Attitude Root locus response

The MATLAB Simulation for closed loop system includes the DC motor dynamics, satellite inertia, and PD compensator in feed forward loop. (Refers Appendix E)

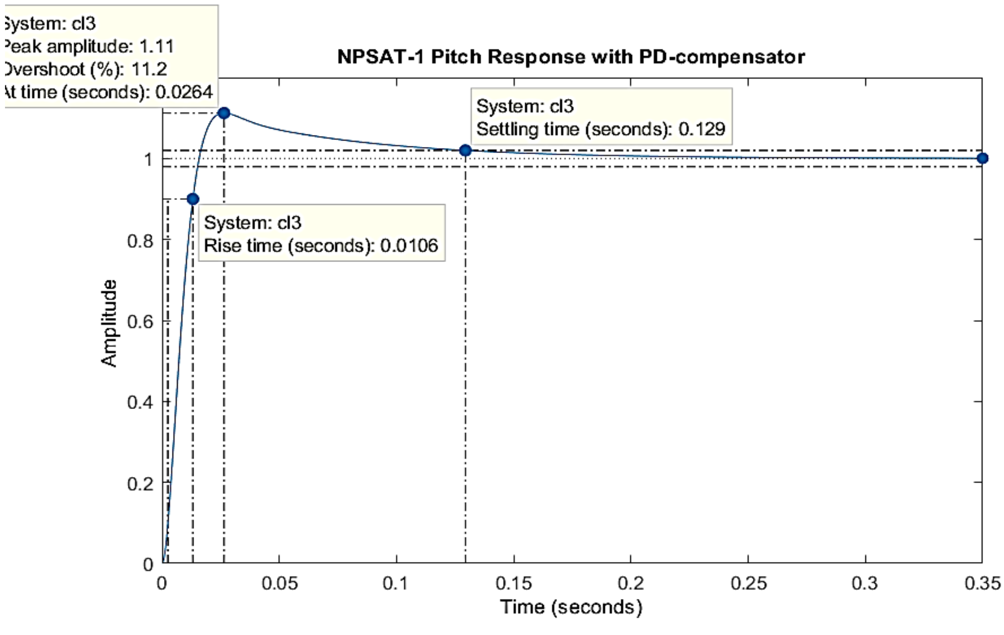

Figure (6.18) NPSAT-1 Pitch Attitude Response with PD controller

In Figure 6.18 shows the NPSAT-1 pitch response, as per design specifications Settling time 0.129 Sec, Rise time 0.0106 Sec, Overshoot (%Mp) 11.2 %, and peak time 0.025 Sec. at peak amplitude 1.11 were achieved.

6.4.3. NPSAT-1 Yaw attitude control system

The closed loop response of yaw attitude dynamics is $\frac{\psi\,(s)}{T_z\,(s)}$.

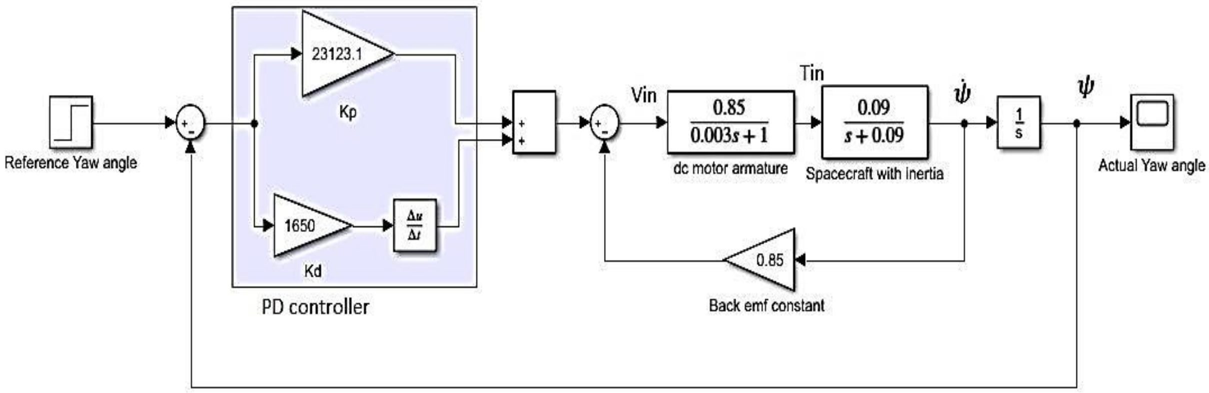

Figure (6.19) Dynamics of Yaw attitude control system

In Figure (6.19) shows the NPSAT-1 Yaw attitude step response of the transfer function without controller given below. (Refers Appendix E)

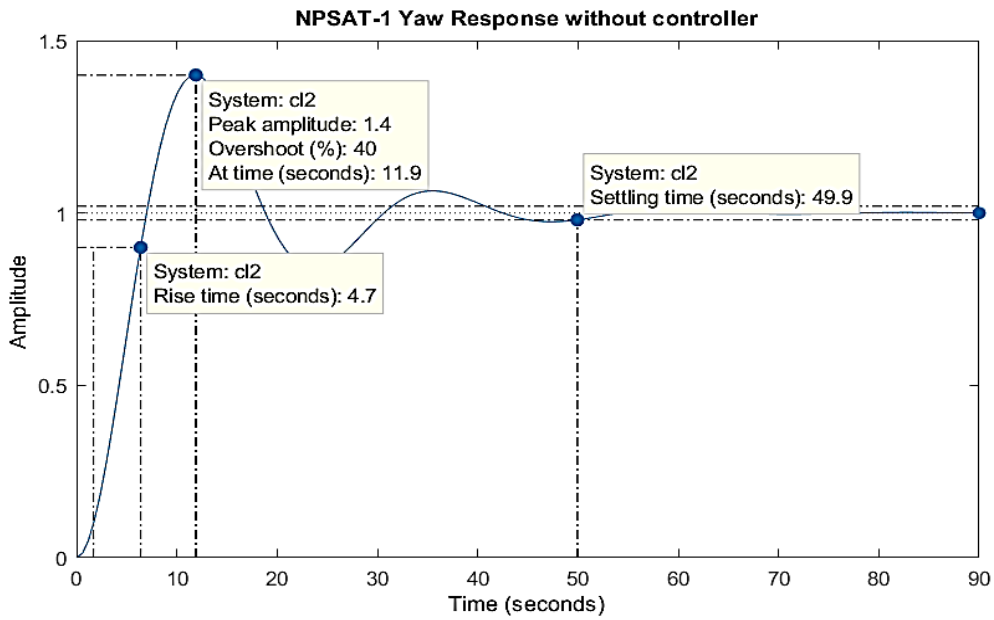

Figure (6.20) NPSAT-1 Yaw attitude dynamics response with step command (without controller)

From Figure 6.20, it is clear the damping of the yaw attitude system has more overshoot is 40%. The oscillation gradually reduces with settling down at time 49.9 seconds (we need to reduce it to ≤ 0.2 seconds) [176]. And, the steady-state is settled exactly at 1 (zero steady-state error). Hence there is no need for integral control. As per the design specification of NPSAT-1 is settling time is ≤ 0.2 seconds at closed dominant pole occurs at **20±13.64*j***.

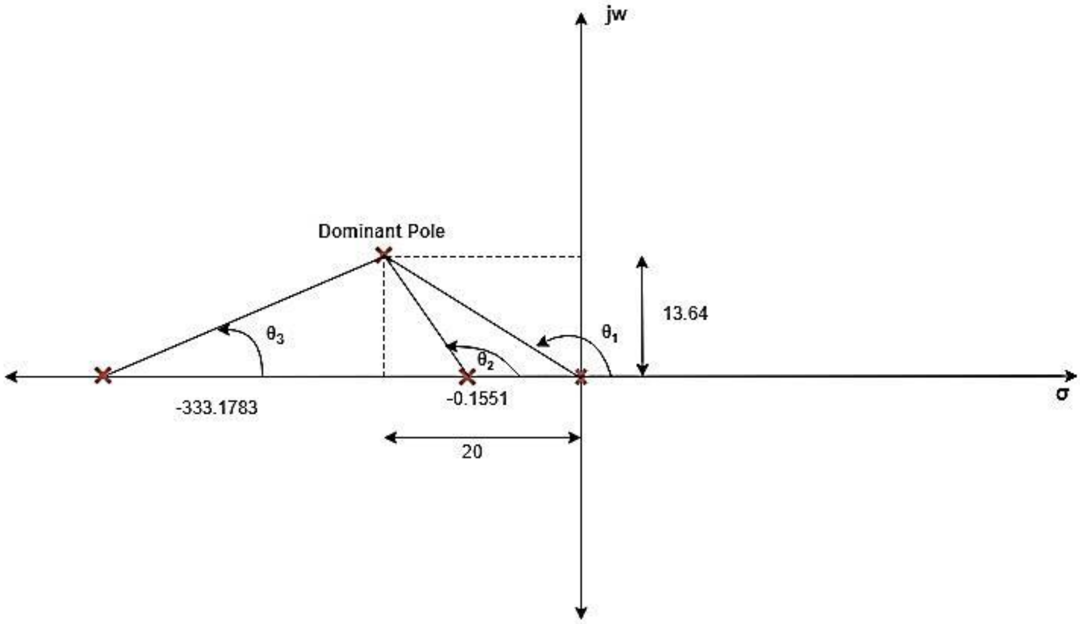

Figure (6.21) PD compensated design (Complex pole to others pole)

The NPSAT-1 Yaw attitude dynamics clearly indicates, there are three poles (See Figure 6.21) in the dynamics one on the origin of the s-plane another is -0.1551 and -333.1783. To finding the angles θ_1, θ_2 and θ_3 from closed dominant pole to other poles and zeros. There are no zeros in the pole-zero plots. This method used to design the PD compensated controller by using root locus analysis [166]

The angles from closed dominant pole to others pole are

$\theta_1 = 180^0 - \left[tan^{-1}\ \left[\frac{13.64}{20}\right]\right] = 145.7°$ $\theta_2 = 180^0 - \left[tan^{-1}\ \left[\frac{13.64}{20-0.1551}\right]\right] = 145.5°$

$\theta_3 = \left[tan^{-1}\ \left[\frac{13.64}{-333.1783-20}\right]\right] = 2.494^0$

This angle is used to find the zero location for finding the PD controller zero (z_c), The line connecting from complex pole to pole at the origin and pole at -0.1551 and -333.1783. Let us assume complex pole considered as **A** [167]. The angles from complex pole A = 180^0 – (summation of angle measure from complex pole to other poles) + (summation of angle measure from complex pole to other zeros) = 180 - $(\theta_1 + \theta_2 + \theta_3)$ = 180 – (145.7 + 145.5+2.494) ≈ **–113.694°**. Now, find the PD compensated zero from angle measured from complex pole A (**-113.694^0**)

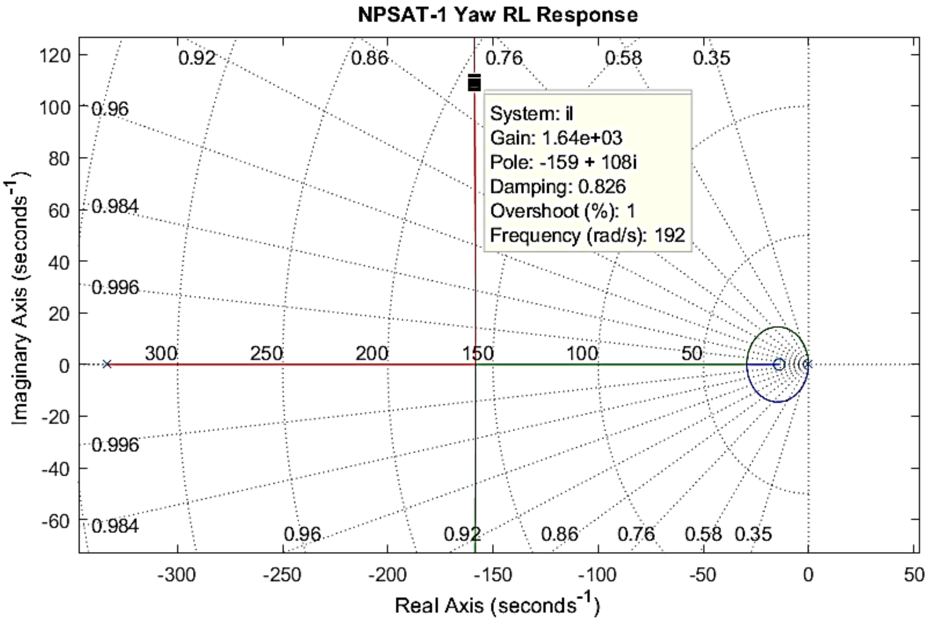

Figure (6.22) NPSAT-1 Yaw Attitude Root locus response

The MATLAB Simulation for closed loop system includes the DC motor dynamics, satellite inertia, and PD compensator in feed forward loop. From figure (6.22) shows the NPSAT-1 yaw attitude RL Responses. The loop gain is found as 1640.

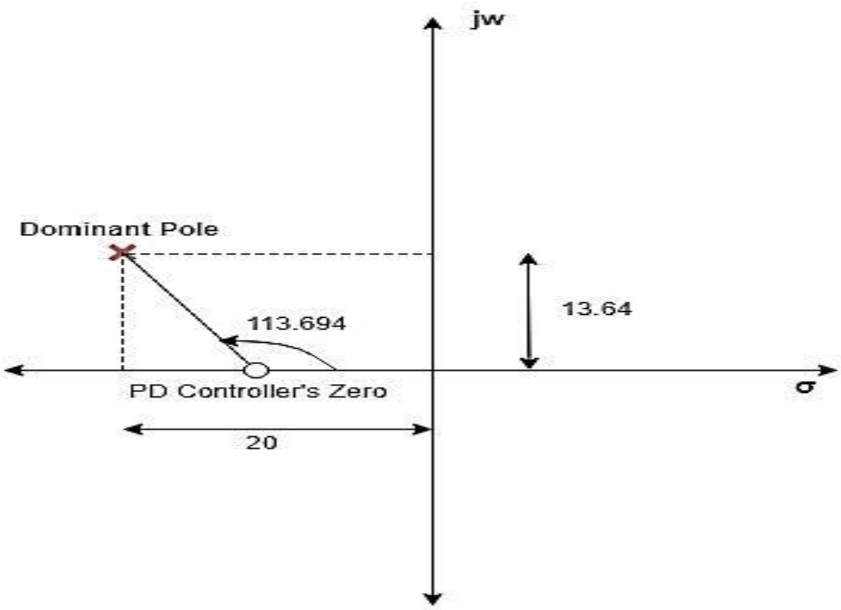

Figure (6.23) Finding the location of the attitude PD controller (z_c)

Using the geometry shown in Figure 6.23, tan (180^0 - 113.694^0) = $\frac{13.64}{20-z_c}$

To design the PD compensator zero (z_c,) from above geometry calculates the value – **14.014.** Now, the PD controller dynamics is ***K* (s + 14.014).** The K is the loop gain. The loop gain found from the root locus at 1% maximum overshoot is 1650 [166]. From figure 6.24 shows the NPSAT-1 yaw attitude MATLAB Simulation for closed loop system includes satellite yaw attitude dynamics and PD compensator.

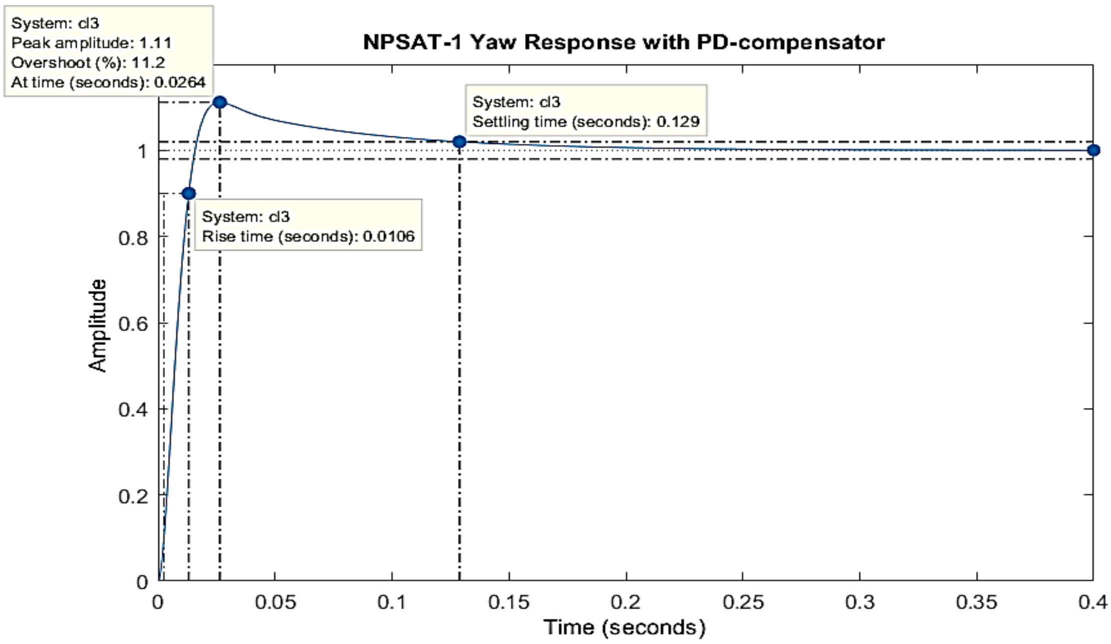

Figure (6.24) NPSAT-1 Yaw Attitude Response with PD controller

In Figure 6.24, The NPSAT-1 yaw attitude response with PD compensator. This includes the dynamics of satellites and orbital perturbation at the low earth orbiting satellite. Thus, PD controllers has been introduced ***K* (s + 14.014)** K is the loop gain calculating from root locus analysis 1650 at 1% overshoot. The oscillation of satellite due to the perturbation forces measured different time domain specification and variations in maximum overshoot expressed in (%). This indicates the damping of actual to the critical value [167]. As per the design specifications settling time is less than 0.2 Sec, after implemented the PD controller in the feed forward loop, the response's reaches settling time 0.129 Sec, Rise time 0.0106 Sec were achieved.

6.5 Attitude Control: SRM Satellite

The next spacecraft to be considered for attitude (pitch, yaw, and roll) control is SRM Satellite. The SRM satellite is a Nano satellite developed by students from the Sri Ramaswamy Memorial University in India [178]. These types of satellite are used for atmospheric measurement such as measures the Green House Gases. The launch was multi payload mission shared with Jugnu (IIT Kanpur satellite). The attitude control design of the Nano satellite at altitude of 867km in low earth circular orbit. The orbital angular velocity is 0.0010239 rad/s. The disturbances torque considered in the spacecraft is Magnetic Disturbance Torque (1.367 x 10^{-5}), Aerodynamic Torque (3.166 x 10^{-2}), and Solar Radiation Torque (6.647 x 10^{-6}). [178]

SRMSAT Principal Moments of inertia [178]

$$=\begin{bmatrix} 6.2911 & 0 & 0 \\ 0 & 5.9162 & 0 \\ 0 & 0 & 4.6085 \end{bmatrix} \text{kg-m}^2$$

6.5.1 SRM Satellite Roll Response:

The step response of the roll attitude transfer function without controller is shown in Figure 6.25, it is clear the SRM satellite roll transient responses, settling time 14.7 Sec, rise time 3.25 Sec, peak time 7.5 Sec, and damping of the roll attitude system overshoot is 14.3%.

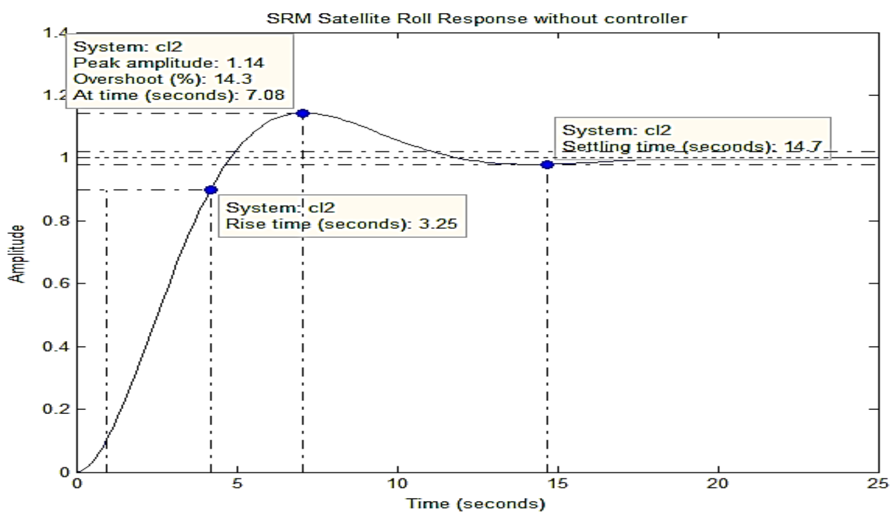

Figure (6.25) SRM Satellite Roll attitude dynamics response with step command

As per the design specifications (we need to reduce it to ≤ 0.2 seconds). And, the steady-state is settled exactly at 1 (zero steady-state error). Hence, here also there is no need for integral control [166]. The dynamics of the controller mentioned in the Appendix E. The angles from closed dominant pole to others pole are $\theta_1 = 145.7°$, $\theta_2 = 144.962°$, $\theta_3 = 2.494°$. The angles from complex pole A = 180^0 – (summation of angle measure from complex pole to other poles) + (summation of angle measure from complex pole to other zeros) = 180 - $(\theta_1 + \theta_2 + \theta_3)$ = 180 – (145.7 + 144.9620+ 2.494) ≈ -293.162. In figure 6.26 shows SRM satellite RL Responses used to finding loop gain 465 at damping ration 0.826 (one percent overshoot) [179]

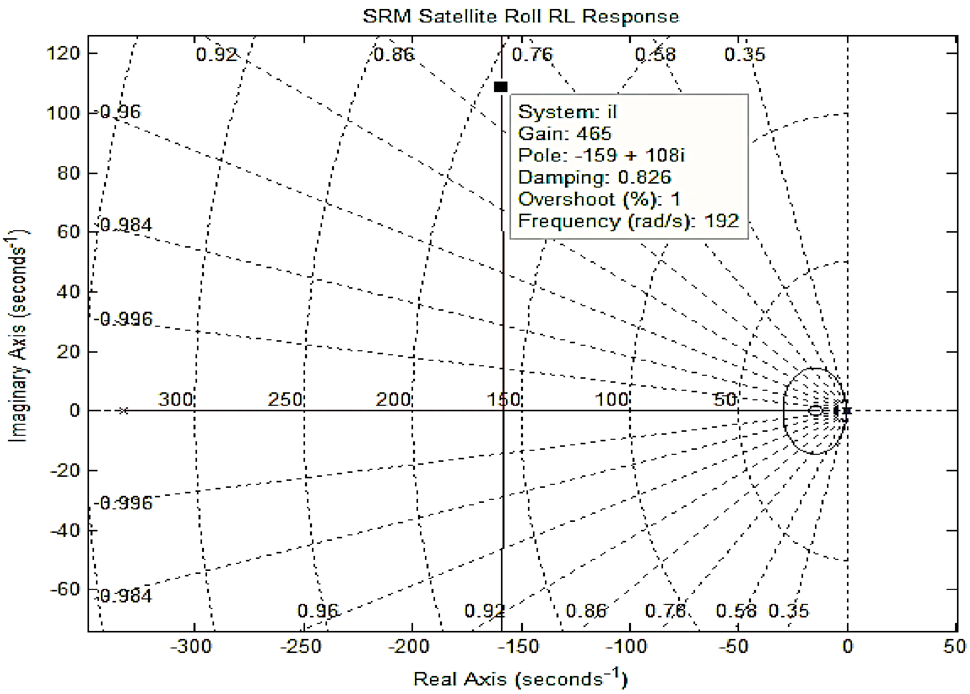

Figure (6.26) SRM Satellite roll attitude Root Locus Response

Using the geometry calculating the PD compensator, tan $(180^0\text{-}113.162^0) = \frac{13.64}{20-z_c}$, [154] Now, find the PD compensated zero from angle measured from complex pole A (**-113.162⁰**). To design the PD compensator zero (z_c,) from above geometry calculates the value **–14.16.** Now, the PD controller dynamics is ***K* (s + 14.16).** The K is the loop gain. The loop gain found from the root locus at 1% maximum overshoot is 465.

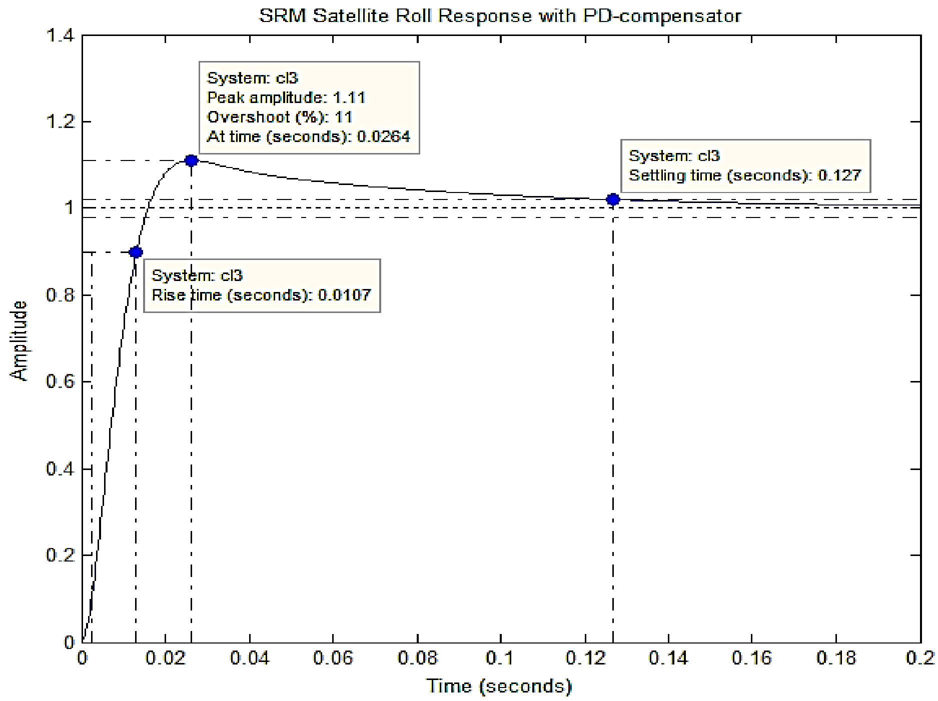

Figure (6.27) SRM satellite Roll Attitude Response with PD controller

Thus, PD controllers has been introduced ***K* (s + 14.16)** K is the loop gain calculating from root locus analysis 465 at 1% overshoot. The oscillation of satellite due to the perturbation forces measured different time domain specification and variations in maximum overshoot expressed in (%) [167]. This indicates the damping of actual to the critical value. As per the design specifications settling time is less than 0.2 Sec, after implemented the PD controller in the feed forward loop, the response's reaches settling time 0.127 Sec, Rise time 0.01067 Sec were achieved.

6.5.2. SRM Satellite Pitch Response:

The step response of the pitch attitude transfer function without controller is shown in Figure (6.28) it is clear the SRM satellite roll transient responses, settling time 22.2 Sec, rise time 3.79 Sec, peak time 9 Sec, and damping of the roll attitude system overshoot is 22.2% [178]. The oscillation gradually reduces with settling down at time 41.6600 seconds (we need to reduce it to ≤ 0.2 seconds). And, the steady-state is settled exactly at 1 (zero steady-state error). Hence, here also there is no need for integral control [166]. The dynamics of the controller mentioned in the Appendix E [167]. The angles from closed dominant pole to others pole are θ_1 = 145.7°, θ_2 = 145.313°, θ_3 = 2.4922°. The angles from complex pole A [156] = 180^0 – (summation of angle measure from complex pole to other poles) + (summation of angle measure from complex pole to other zeros) = 180 - $(\theta_1 + \theta_2 + \theta_3)$ = 180 – (145.7 + 145.313 + 2.4922)≈-293.5121

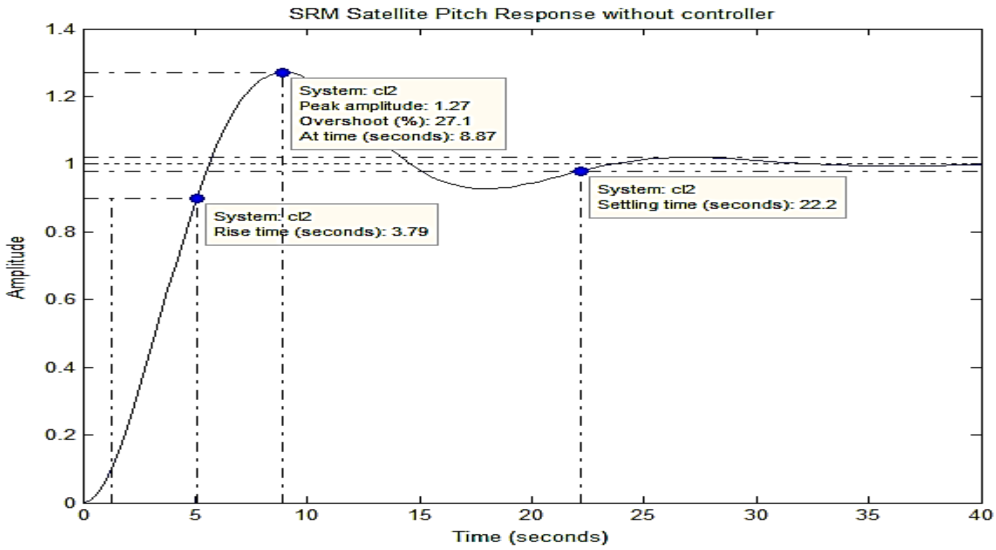

Figure (6.28) SRM Satellite Pitch response with step input

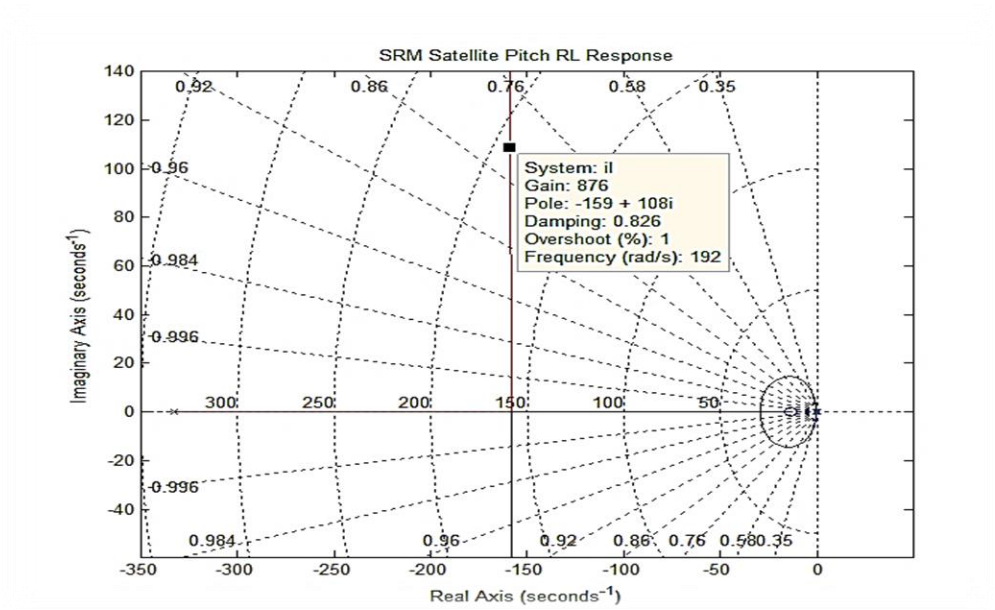

Figure (6.29) SRM satellite Pitch attitude Root locus response

Using the geometry calculating the PD compensator, tan (180^0-113.512^0) = $\frac{13.64}{20-z_c}$,

Now, find the PD compensated zero from angle measured from complex pole A (-**113.512^0**) [156]. To design the PD compensator zero (z_c,) from above geometry calculates the value **–14.06.** Now, the PD controller dynamics is ***K* (s + 14.06).** The K is the loop gain. The loop gain found from the root locus at 1% maximum overshoot is 876.

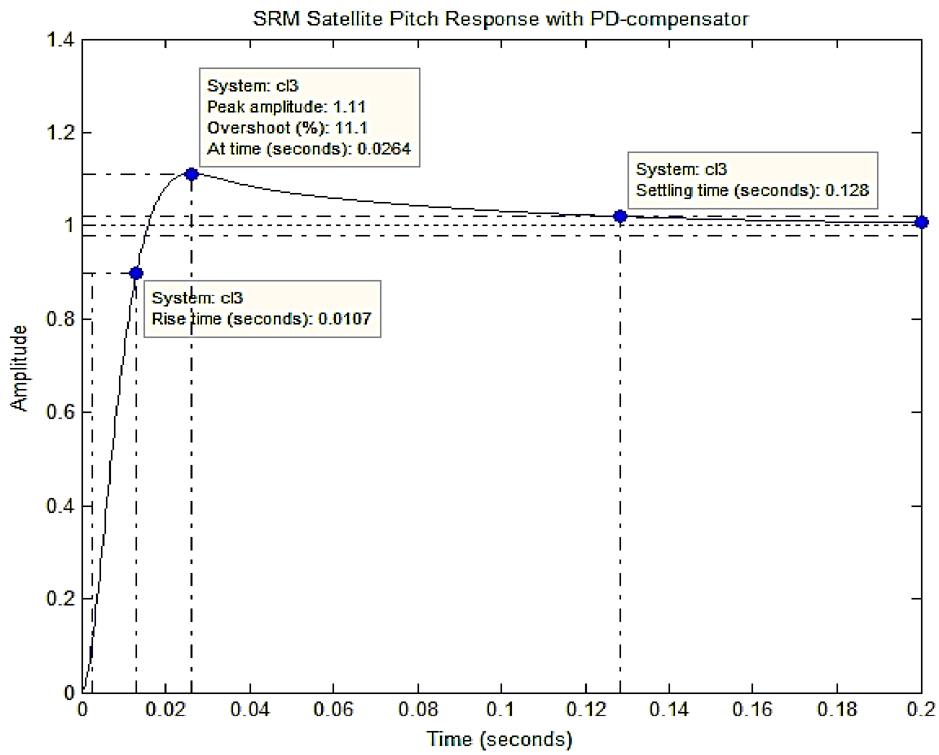

Figure (6.30) SRM Satellite Pitch Attitude Response with PD controller

Thus, PD controllers has been introduced ***K* (s + 14.106)** K is the loop gain calculating from root locus analysis 876 (See figure 6.29) at 1% overshoot. The oscillation of satellite due to the perturbation forces measured different time domain specification and variations in maximum overshoot expressed in (%). This indicates the damping of actual to the critical value [179], [180]. As per the design specifications settling time is less than 0.2 Sec, after implemented the PD controller in the feed forward loop. In figure (6.30) shows the response's reaches settling time 0.128 Sec, Rise time 0.0107 Sec, maximum overshoot 11.1 (%) at 1.11peak amplitude were achieved.

6.5.3. SRM Satellite Yaw Response:

The step response of the yaw attitude transfer function without controller is shown in Figure (6.31) it is clear the SRM satellite roll transient responses, settling time 19.5 Sec, rise time 3.54 Sec, peak time 8 Sec, and damping of the roll attitude system overshoot is 19.5% [178]. As per the design specifications (we need to reduce it to ≤ 0.2 seconds). And, the steady-state is settled exactly at 1 (zero steady-state error). Hence, here also there is no need for integral control.

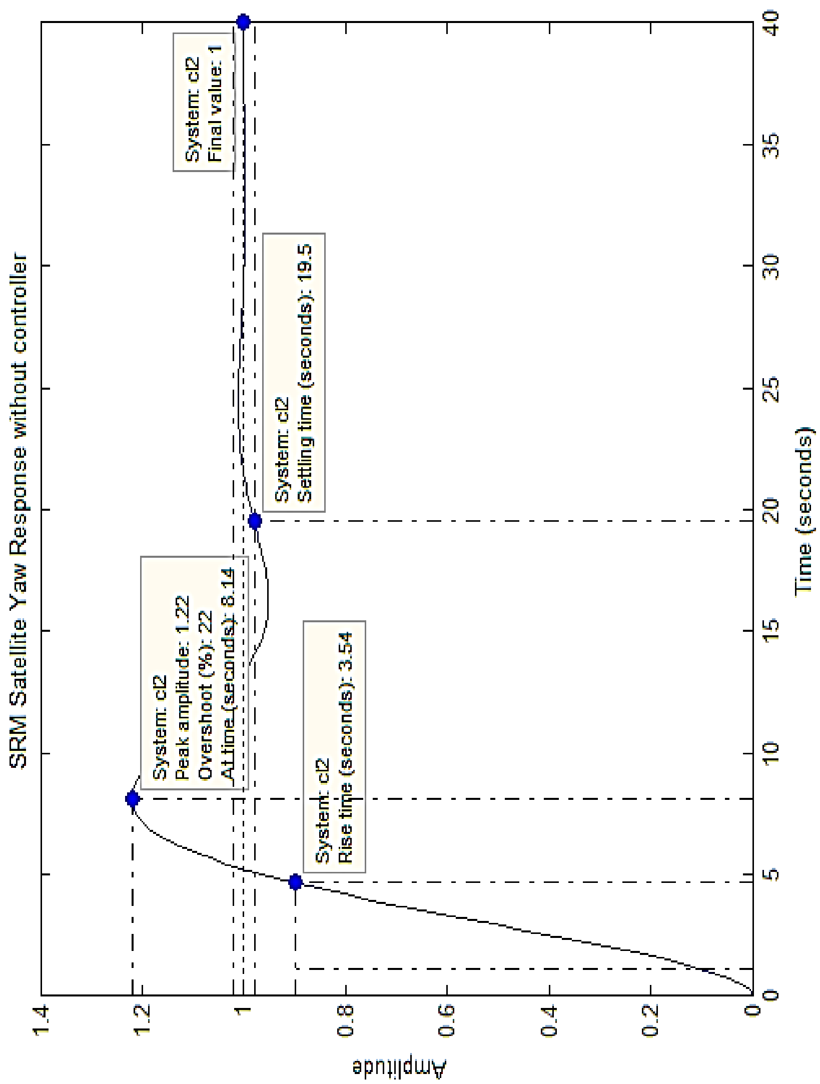

Figure (6.31) SRM Satellite Yaw attitude response with step command

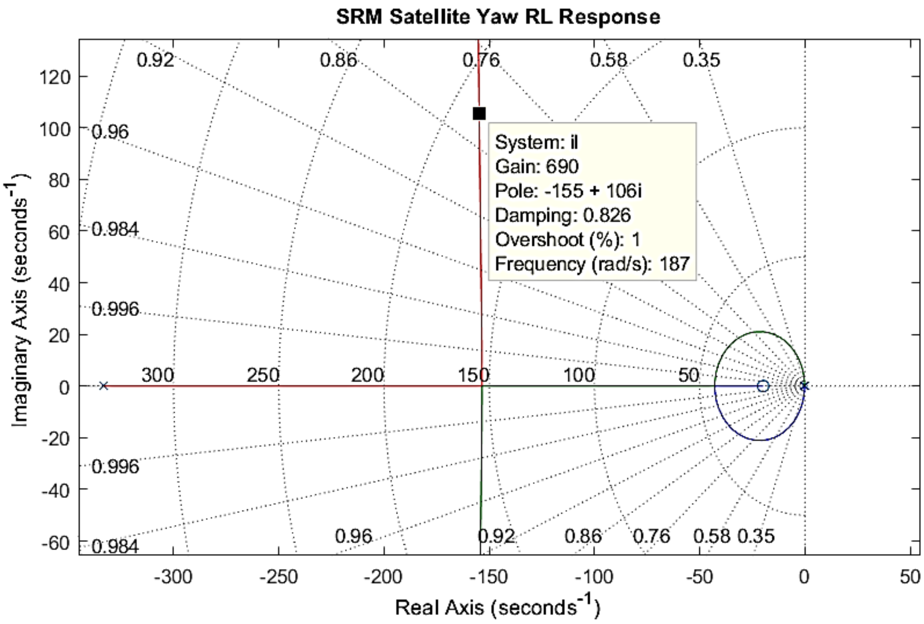

Figure (6.32) SRM satellite Yaw attitude Root locus response

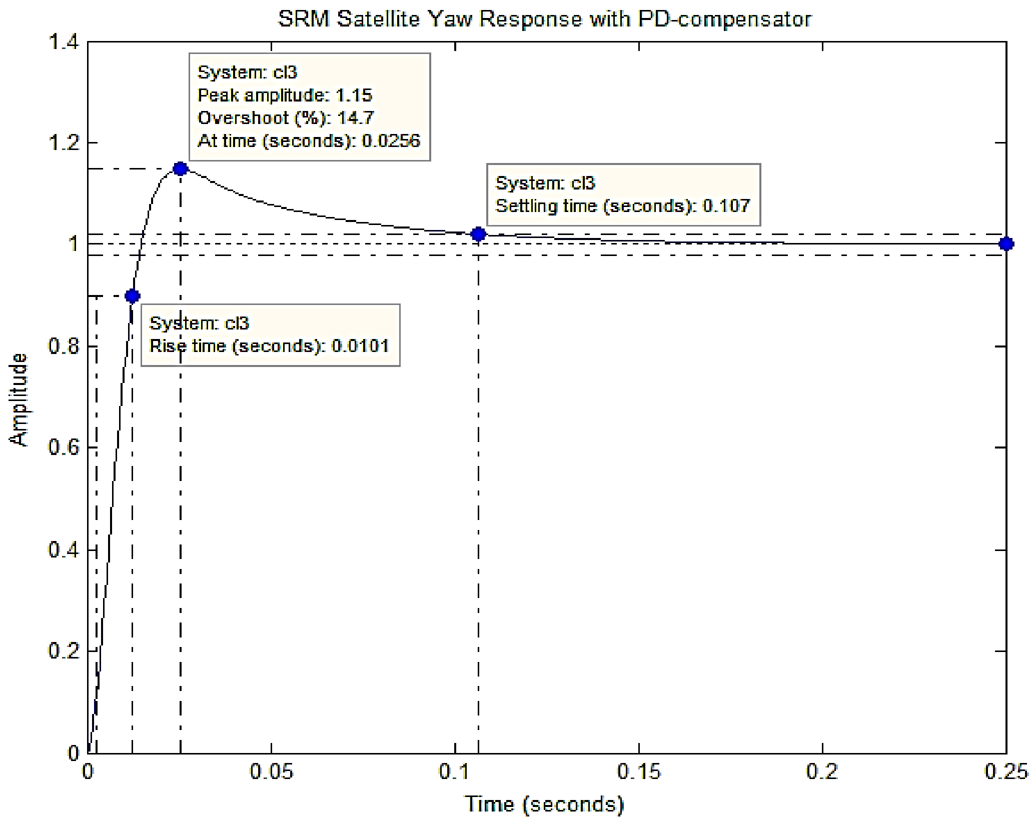

Figure (6.33) SRM Satellite Yaw Attitude Response with PD controller

Using the geometry calculating the PD compensator, tan (180^0-113.399^0) = $\frac{13.64}{20-z_c}$,

Now, find the PD compensated zero from angle measured from complex pole A (-**113.399^0**). To design the PD compensator zero (z_c,) from above geometry calculates the value **–19.84** [158]. Thus, PD controllers has been introduced ***K* (s + 19.84)** K is the loop gain calculating from root locus analysis 690 (See figure 6.32) at 1% overshoot [166]. The oscillation of satellite due to the perturbation forces measured different time domain specification and variations in maximum overshoot expressed in (%). This indicates the damping of actual to the critical value. As per the design specifications settling time is less than 0.2 Sec, after implemented the PD controller in the feed forward loop. In figure (6.33) shows the response's reaches settling time 0.107 Sec, Rise time 0.0101 Sec, maximum overshoot 14.7 (%) at 1.15peak amplitude were achieved.

6.6. Attitude Control: Pratham Satellite

The specifications of Pratham Satellite are 817 km altitude, Polar Sun Synchronous Orbit (PSSO), Mass, 10 kg, Size 26×26×26 cm, Orbital angular velocity = 0.0010346 rad/s [134]

Principal moments of inertia [134] of PRATHAM

$$= \begin{bmatrix} 0.116 & 0 & 0 \\ 0 & 0.109 & 0 \\ 0 & 0 & 0.114 \end{bmatrix} \text{kg-m}^2$$

6.6.1. Pratham Satellite Roll Response

The step response of the roll attitude transfer function without controller is shown in Figure (6.34) the settling time 7.72 seconds, rise time 4.3 Seconds. As per the design specifications, we need to reduce the settling time to ≤ 0.2 seconds. The dynamics of the controller mentioned in the Appendix E. The angles formed between the dominant pole and all other poles can be obtained θ_1 = 145.7°, θ_2 = 109.595°, θ_3 = *2.5451*. Now, the angle contribution required for the PD controller zero (z_c) to make the root locus to pass through the desired dominant pole can be obtained as [166]

Angle contribution = 180 - $(\theta_1 + \theta_2 + \theta_3)$

$$= 180 - (145.7 + 109.595 + 2.5451) \approx -257.846$$

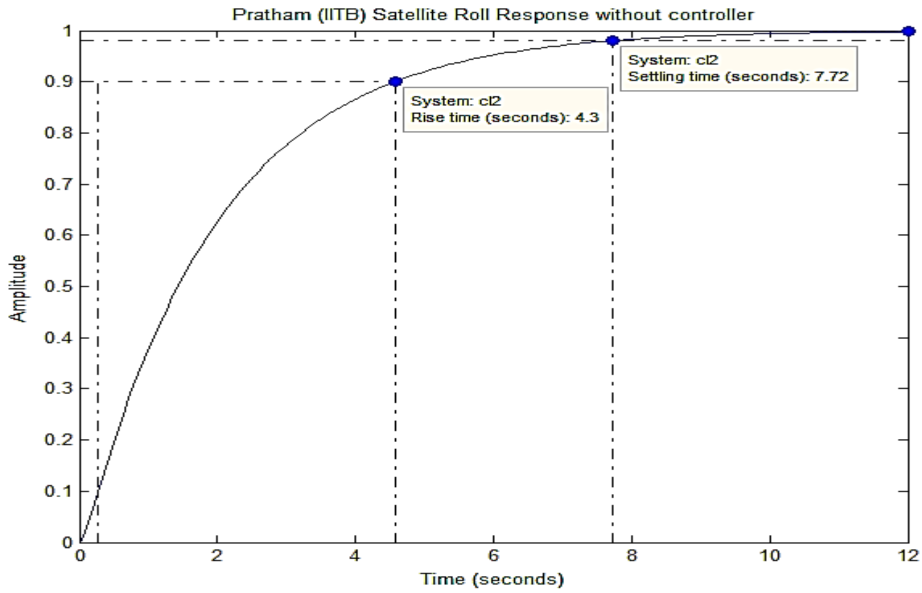

Figure (6.34) Pratham Satellite Roll attitude response with step command

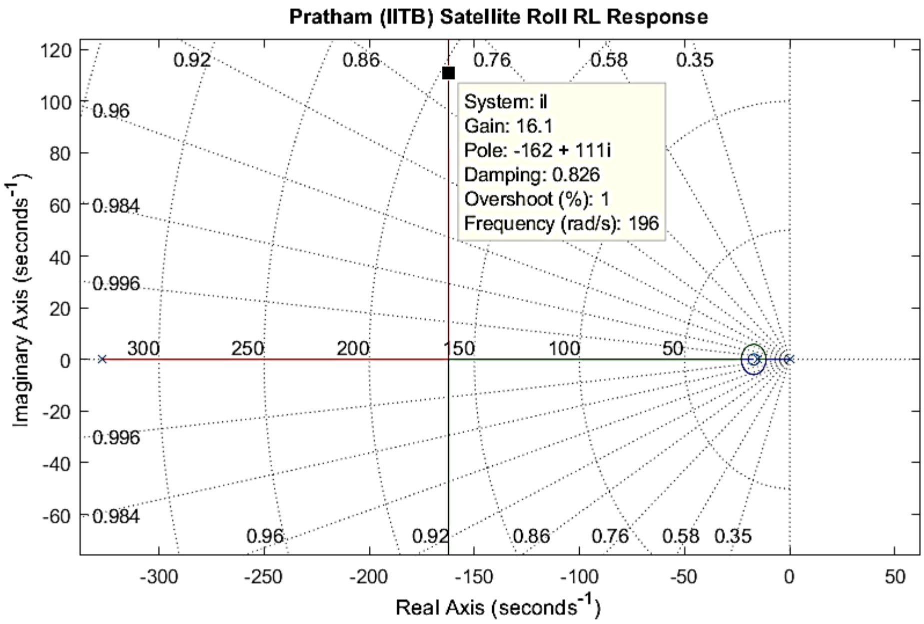

Figure (6.35) Pratham Satellite Roll attitude root locus response

Using the geometry calculating the PD compensator, tan (180^0-77.846^0) = $\frac{13.64}{20-z_c}$, from which the location of the PD compensator zero, z_c, is found to be –**17.0625** [166], [167]. Now, the loop gain K for the PD-compensated system is 16.1 from root locus analysis at 1% maximum overshoot.

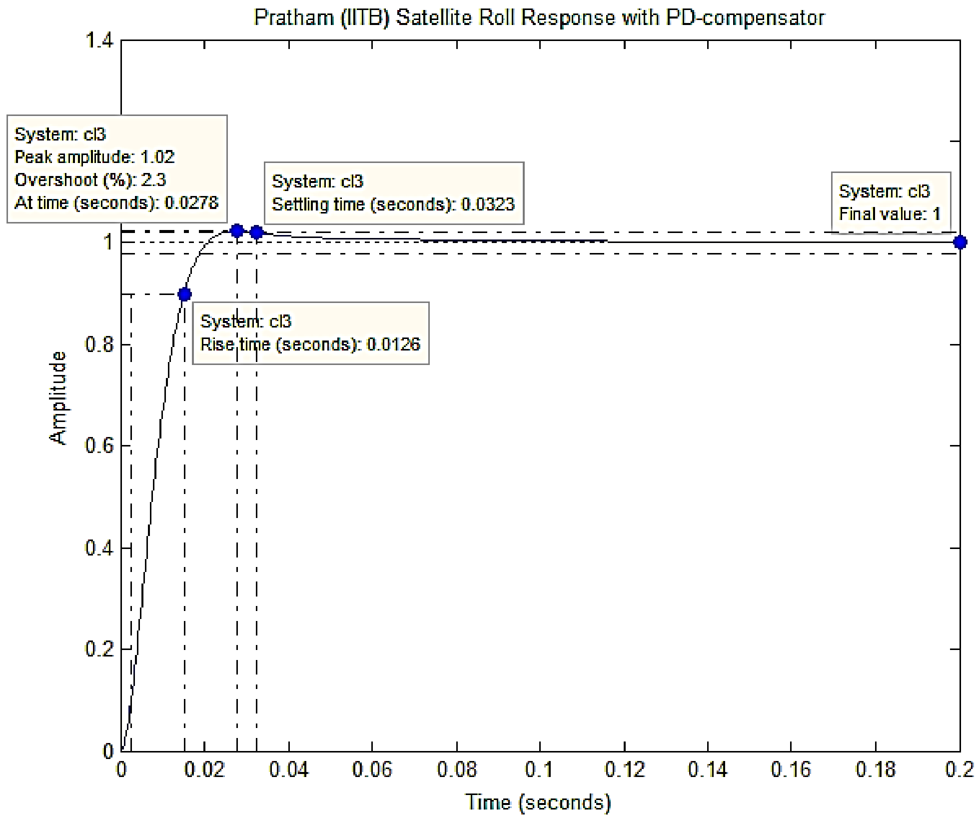

Figure (6.36) Pratham Satellite Roll Attitude Response with PD controller

Thus, PD controllers has been introduced ***K* (s + 17.0625)** K is the loop gain calculating from root locus analysis 16.1 (See figure 6.35) at 1% overshoot. The oscillation of satellite due to the perturbation forces measured different time domain specification and variations in maximum overshoot expressed in (%). This indicates the damping of actual to the critical value [181]. As per the design specifications settling time is less than 0.2 Sec, after implemented the PD controller in the feed forward loop. In figure (6.36) shows the response's reaches settling time 0.0323 Sec, Rise time 0.0126 Sec, maximum overshoot 2.3 (%) at 1.02 peak amplitude were achieved.

6.6.2. Pratham Satellite Pitch **response**

The step response of the pitch attitude transfer function without controller is shown in Figure (6.37). The settling time is 7.73 seconds and rise time 4.31 seconds (we need to reduce it to ≤ 0.2 seconds). The dynamics of the controller mentioned in the Appendix E. The angles formed between the dominant pole and all other poles can be obtained θ_1 = 145.7°, θ_2 = 105.845°, θ_2=2.547°. Now, the angle contribution required for the PD controller zero (z_c) in order to make the root locus to pass through the desired dominant pole can be obtained as [166], [167]. Angle contribution = 180 - $(\theta_1 + \theta_2 + \theta_3)$ = 180 – (145.7 + 105.845 + 2.547) ≈ -254.098

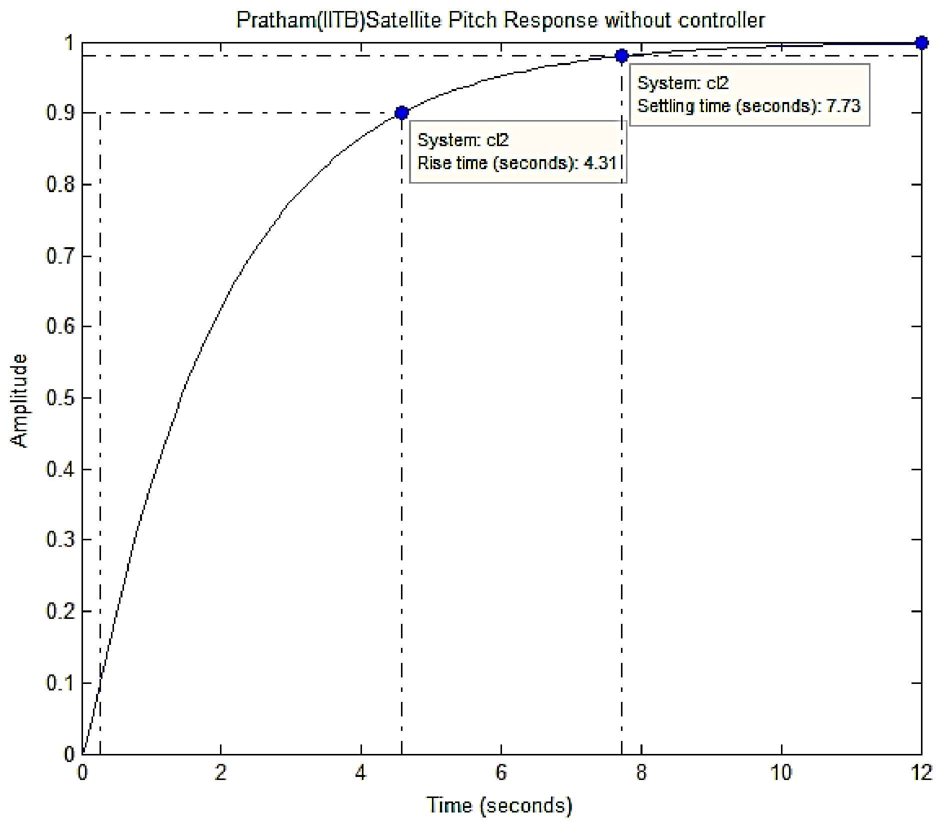

Figure (6.37) Pratham Satellite Pitch attitude response with step command (without controller)

Using the geometry calculating the PD compensator, tan (180^0-74.098^0) = $\frac{13.64}{20-z_c}$, from which the location of the PD compensator zero, z_c, is found to be **–16.114**. Now, the loop gain *K* for the PD-compensated system is 15 from root locus analysis at 1% maximum overshoot [166].

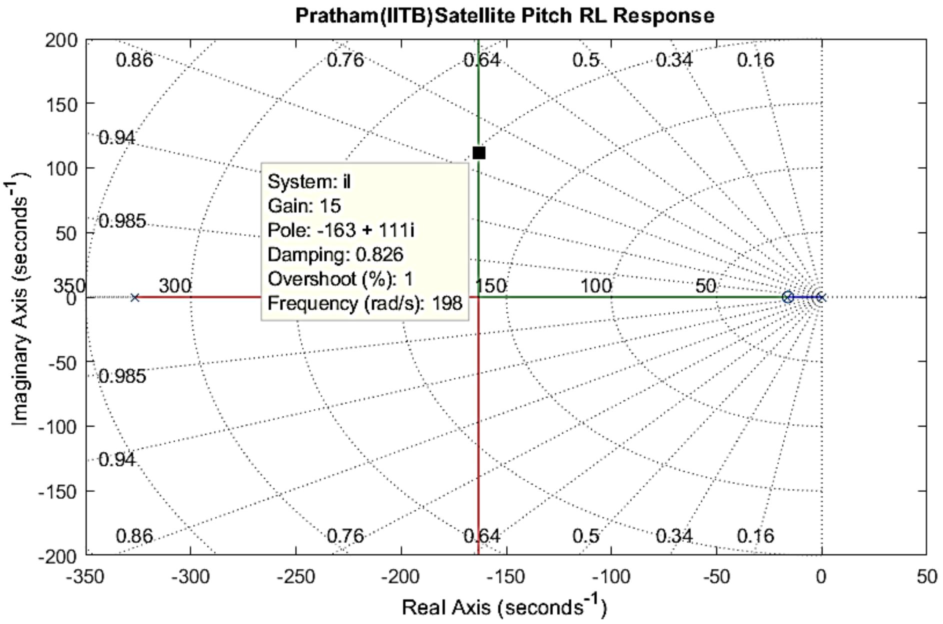

Figure (6.38) Pratham Satellite Pitch attitude Root locus response

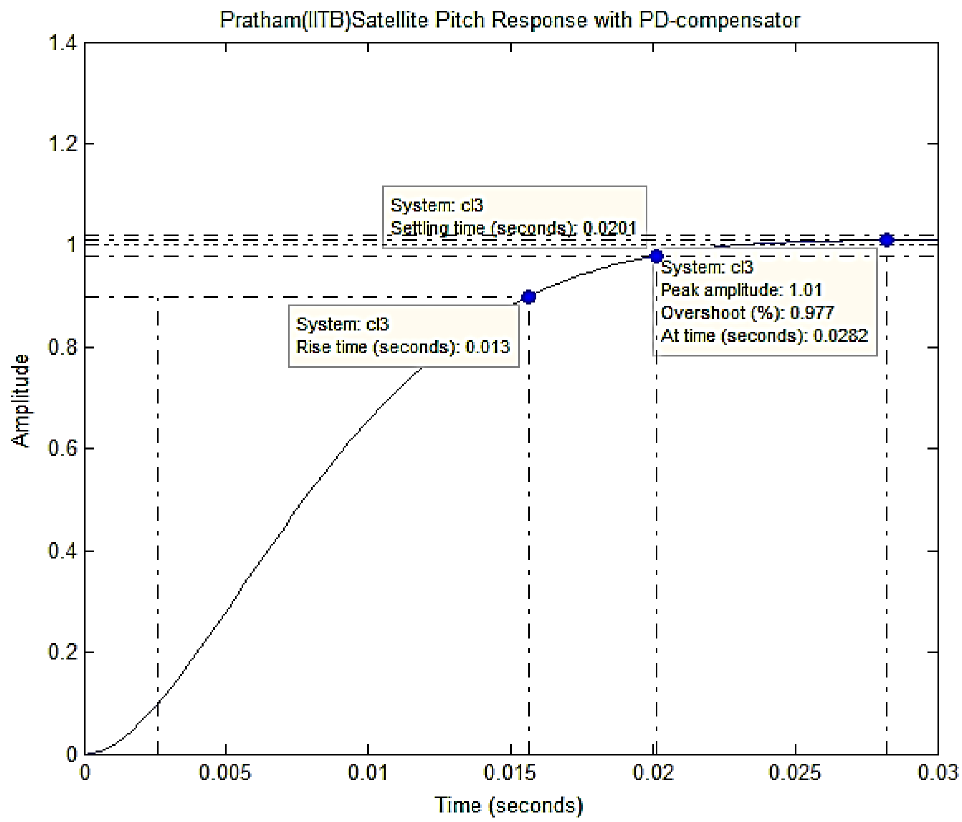

Figure (6.39) Pratham Satellite Pitch attitude response with PD controller

Thus, PD controllers has been introduced ***K* (s + 16.114)** K is the loop gain calculating from root locus analysis 15 (See figure 6.38) at 1% overshoot. The oscillation of satellite due to the perturbation forces measured different time domain specification and variations in maximum overshoot expressed in (%). This indicates the damping of actual to the critical value [181]. As per the design specifications settling time is less than 0.2 Sec, after implemented the PD controller in the feed forward loop. In figure (6.39) shows the response's reaches settling time 0.0201 Sec, Rise time 0.013 Sec, maximum overshoot 0.977 (%) at 1.01 peak amplitude were achieved.

6.6.3. Pratham Satellite Yaw **response*:***

The step response of the yaw attitude transfer function without controller is shown in Figure (6.40). The settling time is 7.72 seconds and rise time 4.3 seconds. As per the design specification, we need to reduce rise time to ≤ 0.2 seconds) [134]. The dynamics of the controller mentioned in the Appendix E. The angles formed between the dominant pole and all other poles can be obtained θ_1 = 145.7°, θ_2 = 108.551°, θ_3=2.5474^0. Now, the angle contribution required for the PD controller zero (z_c) to make the root locus to pass through the desired dominant pole can be obtained as angle contribution = 180 - $(\theta_1 + \theta_2 + \theta_3)$ = 180 – (145.7 + 105.551 + 2.5474) ≈ -256.8052^0

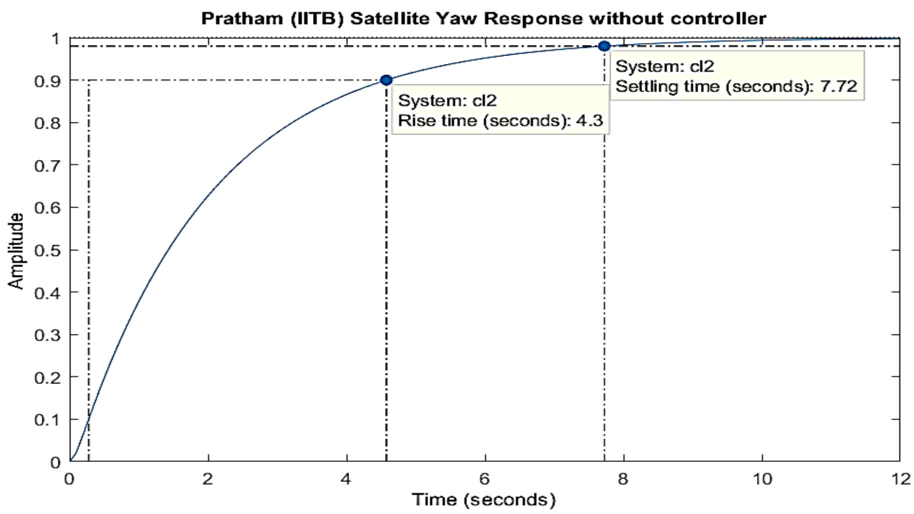

Figure (6.40) Pratham Satellite Yaw attitude response with step command

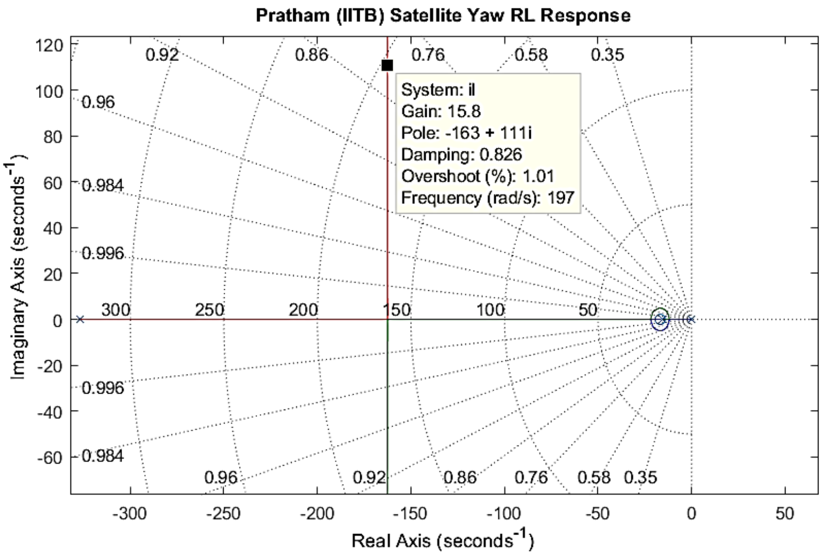

Figure (6.41) Pratham satellite Yaw attitude Root locus response

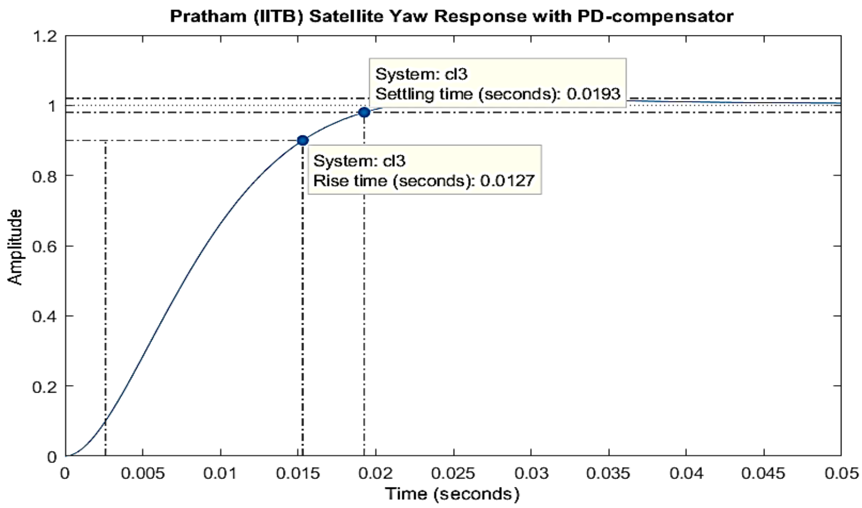

Figure (6.42) Pratham Satellite Yaw Attitude Response with PD controller

Using the geometry calculating the PD compensator, tan (180^0-76.805^0) = $\frac{13.64}{20-z_c}$, from which the location of the PD compensator zero, z_c, is found to be **–16.801**. Now, the loop gain *K* for the PD-compensated system is 15.8 (shown in Fig 6.41) calculates from root locus analysis at 1% maximum overshoot [166], [167]. Thus, PD controllers has been introduced ***K* (s + 16.801)** K is the loop gain calculating from root locus analysis 16.1 (See figure 6.41) at 1% overshoot. The oscillation of satellite due to the perturbation forces measured different time domain specification and variations in maximum overshoot expressed in (%). This indicates the damping of actual to the critical value. As per the design specifications settling time is less than 0.2 Sec, after implemented the PD controller in the feed forward loop [181]. The output response in figure (6.42) shows the response's reaches settling time 0.0193 Sec, Rise time 0.0127 Sec were achieved. In table 6.3 shows the Nano satellite attitudes (Roll, Pitch, Yaw) transient response of control system for NPSAT-1, SRM satellite, Pratham satellite (IITB) without controller and with PD compensated controller were compared.

Table 6.3: Nano Satellites Attitude Responses (a) NPSAT-1 (b) SRM satellite (c) Pratham satellite

Specifications	Roll Attitude Dynamics		Pitch Attitude Dynamics		Yaw Attitude Dynamics	
	Without controller	With controller	Without controller	With controller	Without controller	With controller
Rise time (Sec)	6.5	0.0106	6.2	0.0106	4.7	0.0106
Overshoot (%)	55.1	11.2	53.2	11.2	40	11.2
Settling time (Sec)	108	0.129	102	0.129	49.9	0.129
Peak time (Sec)	18	0.025	8	0.025	12	0.025

(a)

Specifications	Roll Attitude Dynamics		Pitch Attitude Dynamics		Yaw Attitude Dynamics	
	Without controller	With controller	Without controller	With controller	Without controller	With controller
Rise time (Sec)	3.25	0.0107	3.79	0.0107	3.54	0.010
Overshoot (%)	14.3	11	27.1	11.1	22	14.7
Settling time (Sec)	14.7	0.127	22.2	0.128	19.5	0.107
Peak time (Sec)	7	0.03	9	0.03	8	0.025

(b)

Specifications	Roll Attitude Dynamics		Pitch Attitude Dynamics		Yaw Attitude Dynamics	
	Without controller	With controller	Without controller	With controller	Without controller	With controller
Rise time (Sec)	4.3	0.0126	4.31	0.013	4.3	0.0127
Settling time (Sec)	7.72	0.0323	7.73	0.0201	7.71	0.0193

(c)

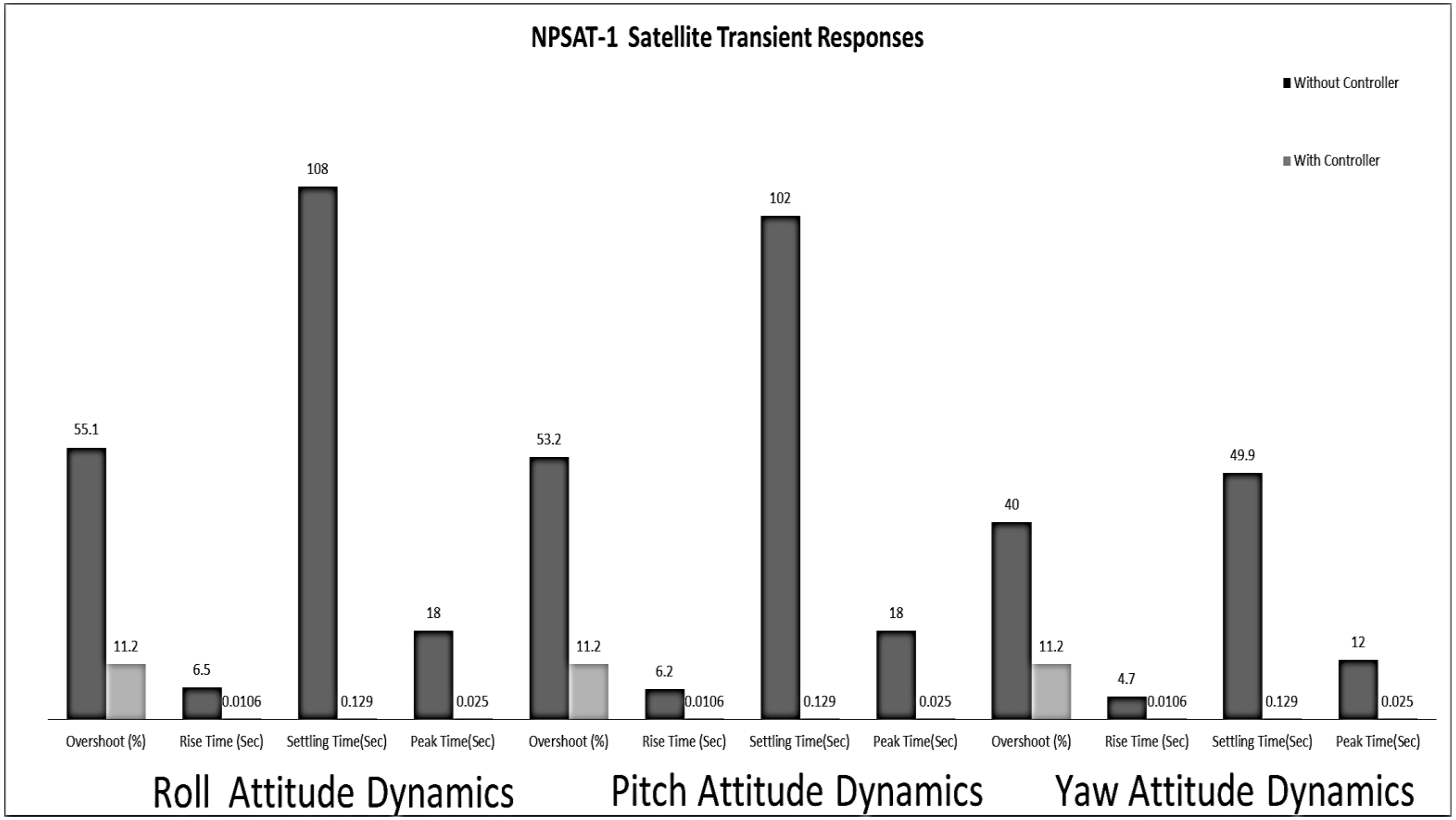

Figure (6.43) NPSAT-1 Satellite Transient Response (Comparative analysis)

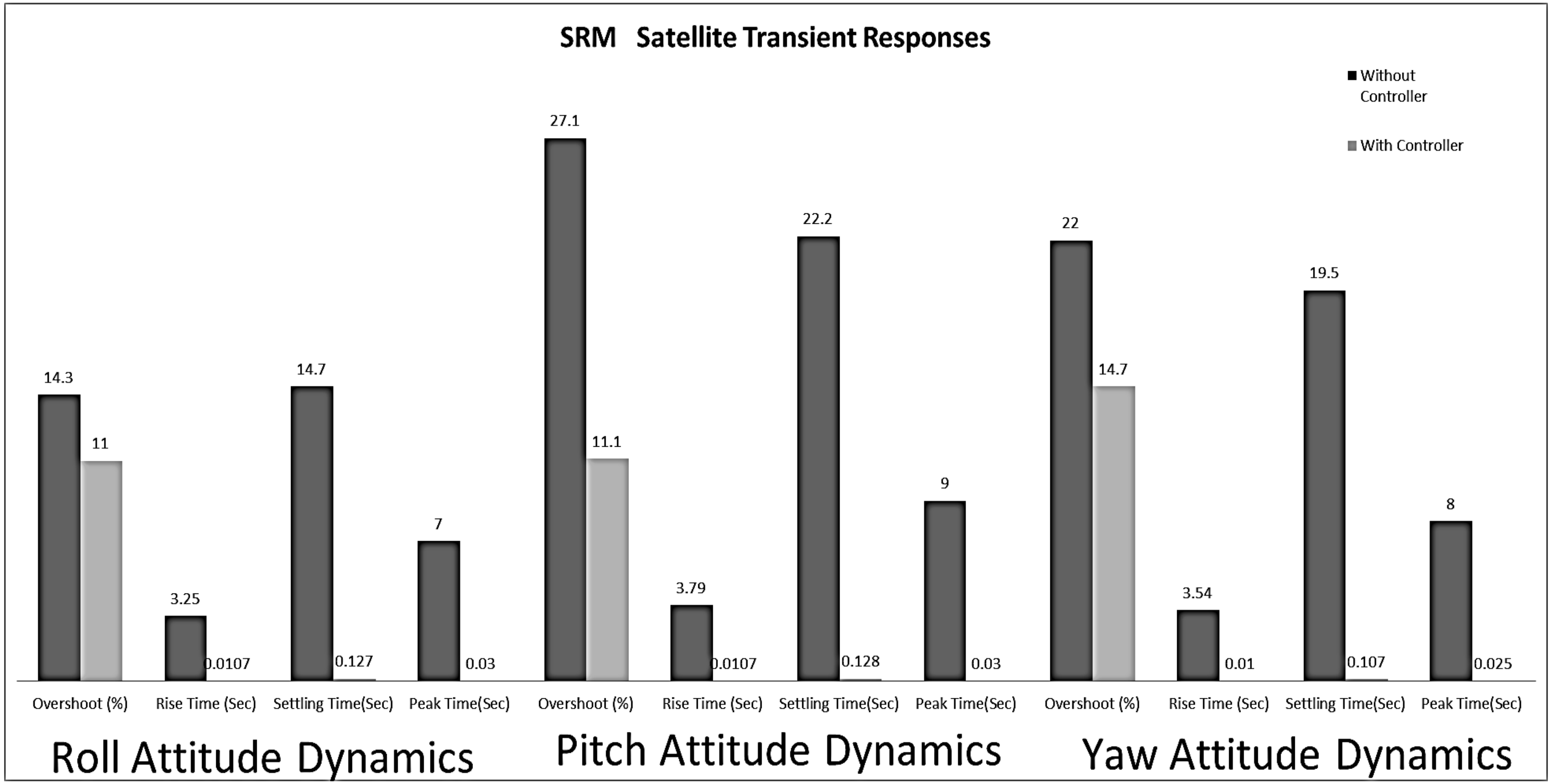

Figure (6.44) SRM Satellite Transient Response (Comparative analysis)

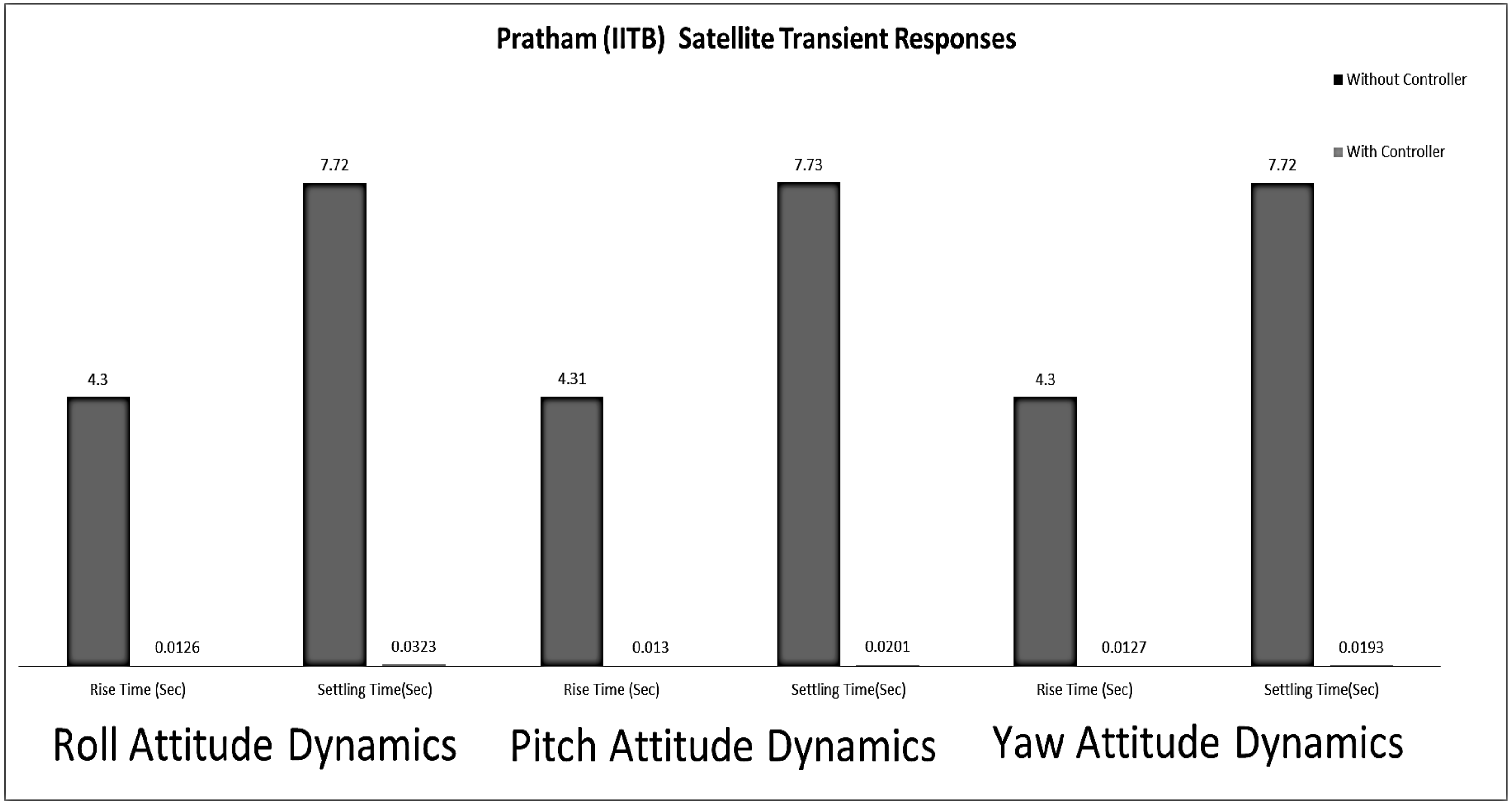

Figure (6.45) Pratham (IITB) Satellite Transient Response (Comparative analysis)

For, consider the NPSAT -1 design parameters is [I_{xx} = 24.67 I_{yy} = 22.63 I_{zz} = 11] kg-m^2, Ω = 0.0010239 rad/s (at 550 km Altitude,) Low Earth circular orbit (LEO), SRM satellite design parameters [I_{xx} = 6.2911 I_{yy} = 5.9162 I_{zz} = 4.6085] kg-m^2, Ω = 0.0010239 rad/s (at 867km Altitude), Pratham satellite design parameters [I_{xx} = I_{xx} = 0.116 I_{yy} = 0.109 I_{zz} = 0.114] kg-m^2, Ω = 0.0010346 rad/s (817km). After compared responses of all satellite with controller gain values varying from 3700 K for NPSAT-1 LEO satellite and lower value K for SRM satellite is 876, Pratham satellite is 15. Figures (6.43), (6.44), and (6.45) shows the outputs transient response of Nano satellites (NPSAT-1, SRM Satellite, and Pratham Satellite) analysis of without controllers and with PD compensated controller were compared. It is noticed that attitude responses of Nano satellite without controllers has large overshoot and settling time (NPSAT-1 is %Mp = 55.1%, & ts = 108 Seconds, SRM satellite is %Mp = 14.3% & ts = 14.7 Seconds, Pratham satellite is tr = 4.3 Seconds & ts = 7.72 Seconds). The PD controllers have been introduced in the forward loop of satellite dynamically. The spacecraft control system simulation of the PD-compensated system satisfies the design requirement. It is used to increase the transient response (Overshoot and Settling time) of the system. For, settling time is (desired value ≤ 0.2 seconds) wear achieved. The output responses of Nano satellite after implemented PD controllers of NPSAT-1 is %Mp = 11.2%, & ts = 0.129 Seconds, SRM satellite is %Mp = 11% & ts = 0.127 Seconds, Pratham satellite is tr = 0.0126 Seconds & ts = 0.0323 Seconds. The Nano satellites comparative analysis with PD compensated system is achieved as per the design specification settling time ≤ 0.2 seconds, All the Nano satellites output attitude transient response meet as per design requirements.

CHAPTER 7

CONCLUSION & RECOMMENDATION OF FUTURE WORK

In present work, the Nano satellite perturbation forces and attitude control were modeled. To study variation in attitude of satellite due to orbital perturbation in low earth orbit, Aerodynamic drag, the Gravitational attraction of the Earth, and solar pressure were considered. The perturbation analysis of Low earth orbits Nano Satellite included International Space Station, Pratham (IIT Bombay) Satellite, SRM Satellite in this report. The perturbation simulation is implemented using MATLAB Tools, Python, and GMAT. The Cowell's perturbation simulation Keplerian results are validated with General mission analysis tool. The design parameters of Nano satellites Moment of inertia, NORAD two-line element, Geometry parameters are considered. It is a very accurate tool comparing with Euler angle method. Singularity problems are omitted in quaternion attitude estimation techniques.

The armature control DC motor is introduced in the Nano satellite attitude control system. The GEO magnetic fields modeling is considered in the International Geomagnetic Reference Field (IGRF-12)**.** The attitude control for satellite using DC motor is performed. In obtained results the perturbing accelerations changes the satellite orbit in LEO. At LEO, International Space Station were investigated by the second order mathematical ODE equations by *Runge - Kutta* using Cowell's Method. To obtain the output of the numerical ODE integration, the initial position vectors and velocity vectors of the Nano satellite must be identified. The Kalman filter algorithm for determining the Nano-Satellite NPSAT-1 attitude (Roll, Pitch, Yaw) errors from on-board attitude sensor, like INS/GPS and Magnetometers are derived. The Kalman error estimation algorithm was developed using MATLAB package.

The detumble of spacecraft controlled by control torque generated from the actuator to plant dynamics. The attitude dynamics of pitch control, roll control, and yaw control of SRM Satellite, Pratham Satellite, and NPSAT-1 are considered. The oscillatory response is obtained from attitude dynamics of the Nano satellites. The design of low-cost filter with suitable feedback is incorporated for all the satellite attitudes in this work.

The comparative study illustrates the improved Nano satellites transient responses with PD compensated controller using Armature controlled DC motor. The simulation of attitude control is implemented in MATLAB/SIMULINK environment. This thesis concludes the design of low-cost attitude estimation using INS/GPS and Magnetometers with low volume, less weight, less power, more accurate at lower altitudes.

This work mainly considered two body problems like Earth- Satellite at low earth orbit satellite, the future work extends to discuss the various three body problems like SUN perturbation, MOON perturbation at High earth orbit (HEO) such as geosynchronous orbit. The GEO orbit attitude estimation mostly depends upon the star sensor, sun sensor, earth sensor and horizon sensor. The actuator dynamics of HEO mostly rely on the Control momentum Gyroscope (CMG) and Flywheels or Momentum wheels. At HEO attitude information from on-board sensor secular variations are very high. The perturbation in the orbital element is greater than the orbital period. So, the attitude estimation uses Monto- Carlo Simulations instead of Kalman filter.

REFERENCES

1. Ali Siahpush and Andrew Sexton, "A Study for Semi-Passive Gravity Gradient Stabilization of Small Satellites", Conference Proceedings, 1st Annual USU Conference on Small Satellites, October 1987.
2. H. E. Soken, C. Hajiyev, and S. Sakai, Robust Kalman Filtering for Small Satellite Attitude Estimation in the Presence of Measurement Faults, European. Journal. Control, vol. 20, 2014, pp. 64–72.
3. M. Eshagh and M. Najafi Alamdari, "Perturbations in orbital elements of a low earth orbiting satellite," Journal of the Earth & Space Physics, vol. 33, no. 1, pp. 1-12, 2007.
4. C. D. Hall, P. Tsiotras, H. Shen. Tracking rigid body motion using thrusters and momentum wheels. Journal of the Astronautical Sciences, Vol. 50, No. 3, 2002.
5. Krishnan, H., Reyhanoglu, M., and McClamroch, N. H., “Attitude Stabilization of a Rigid Spacecraft Using Two Control Torques: A Nonlinear Control Approach Based on the Spacecraft Attitude Dynamics,” Automatica, Elsevier Science Ltd. Vol. 30, No. 6, 1994, pp. 1023–1027.
6. Vadali, S.R., and Junkins, J. "Optimal Open-Loop and Stable Feedback Control of Rigid Spacecraft Attitude Maneuvers." Journal of the Astronautical Sciences, 1984: 105-122.
7. Psiaki, M. L., "Nanosatellite Attitude Stabilization Using Passive Aerodynamics and Active Magnetic Torque", Journal of Guidance, Control, and Dynamics, 2004, Issue 3, Vol. 27, pp. 347–355.
8. Schaub, H., Vadali, S., and Junkins, J., “Feedback Control Law for Variable Speed Control Moment Gyros,” Journal of the Astronautical Sciences, Vol. 46, No. 3, 1998, pp. 307–328.
9. ML Psiaki, F Martel and PK Pal, “Three-Axis Attitude determination via Kalman Filtering of Magnetometer Data”, Journal of Guidance, Control, and Dynamics, Vol.13, No.3, May-June 1989, pp.506- 514.
10. Schaub, H., and Junkins, J. L., “MATLAB Toolbox for Rigid Body Kinematics,” Proceedings of the AAS/AIAA Space Flight Mechanics Meeting,

Breckenridge, CO, American Astronautical Soc. Paper 99-139, Springfield, VA, 7–10 Feb. 1999, pp. 549–560.

11. Hale, M. J., Vergez, P., and Meerman, M. J., "Kalman Filtering and the Attitude Determination and Control Task," AIAA-2004-6018, U.S. Air Force Academy Department of Astronautics, Colorado Springs, Colorado, September 2004.
12. Tingguo Pei, Shilu Chen, Xinggang Li. Nonlinear Estimation Algorithm for Attitude Determination of Micro Satellite [J]. Journal of Projectiles, Rockets, Missiles and Guidance, 2006, 26(3):67-70.
13. Giebelmann J. Development of an active magnetic attitude determination and control system for picosatellites on highly inclined circular low earth orbits. MS Thesis, School of Aerospace, Mechanical and Manufacturing Engineering Science, Engineering and Technology, Portfolio RMIT University, MA, June 2006.
14. Murty S. Challa, (2016) "A Simple Attitude Unscented Kalman Filter: Theory and Evaluation in a Magnetometer-Only Spacecraft Scenario", IEEE Proceedings, 10.1109/Access.2016.2559445, Page(s): 1845 – 1858, 27 April 2016.
15. Karataş S, (2006) "LEO Satellites: Dynamic Modelling, Simulations and some Nonlinear Attitude Control Techniques" Master Thesis, Middle East Technical University, The Graduate School of Natural and Applied Sciences, Electrical and Electronics Engineering, April 2006.
16. Sami Kadhim Hasan Ar-Ramahi, "PID controller design for the Satellite Attitude Control System", Journal of Engineering, Volume 15 March 2009.
17. Mbaocha C. C, Eze C. U, Ezenugu I. A, Onwumere J. C, "Satellite Model for Yaw-Axis Determination and Control Using PID Compensator", International Journal of Scientific & Engineering Research, Volume 7, Issue 7, July-2016
18. Stephanie Joy Clark, "Design of orbital maneuvers with Aeroassisted Cube satellites", master thesis, university of arkansas, department of mechanical engineering, May 2012.

19. Perry, W.R. (1967). "Orbital Mechanics". In Theodore Baumeister. Marks' Standard Handbook for Mechanical Engineers (Seventh Ed.). New York City: McGraw Hill. pp. 11:151–52. ISBN 0-07-142867-4.
20. Mohammed Chessab Mahdi, “Orbit Design and Simulation for Kufasat Nanosatellite”, Journal of Artificial Satellites, vol. 50, no. 4 – 2015 Doi: 10.1515/arsa-2015-0013.
21. Steven P. Hughes, “General Mission Analysis Tool”, Navigation & Mission Design, NASA Goddard Space Flight Center, 14 Mar. 2016
22. Levesque, J., "Passive Magnetic Attitude Stabilization using Hysteresis Materials.", 17th AIAA/USU Conference on Small Satellites, 2003.
23. Van Dyke, M. C., Schwartz, J. L., and Hall, C. D., “Unscented Kalman Filtering for Spacecraft Attitude State and Parameter Estimation,” Proceedings of the AAS/AIAA Space Flight Mechanics Conference, AAS Paper 2004-115, Maui, Hawaii, 8–12 Feb. 2004.
24. H. D. Curtis, Orbital Mechanics for Engineering Students, Florida: Elsevier Butterworth-Heinemann publications, 2005.
25. Anderson, John D. (2004), Introduction to Flight (5th ed.), McGraw-Hill, ISBN 0-07-282569-3
26. Gerhard Hermann, “The Design and Simulation Analysis of an Attitude Determination and Control System for a Small Earth Observation Satellite”, Master Thesis, Department of Electrical and Electronic Engineering, March 2015
27. Richie, D. J., Lappas, V. J., and Prassinos, G., “A Practical Small Satellite Variable-Speed Control Moment Gyroscope for Combined Energy Storage and Attitude Control,” AAS/AIAA Astrodynamics Specialist Conference, Honolulu, HI, AIAA Paper 2008-7503,18–21 Aug. 2008.
28. H. E. Soken and C. Hajiyev, UKF for the Identification of the Pico Satellite Attitude Dynamics Parameters and the External Torques on IMU and Magnetometer Measurements, in 4th International Conference on Recent Advances in Space Technologies, 2009, pp. 547–552.

29. Natanson, G. (1992, September). A Deterministic Method for Estimating Attitude from Magnetometer Data only (Paper No. IAF-92-0036). Proceedings of the World Space Congress. Washington, DC.
30. Huijuan Zhang, Jiancheng Fang. Robust Backstepping Control for Agile Satellite Using Double-Gimbal Variable-Speed Control Moment Gyroscope. Journal of Guidance, Control, and Dynamics.
31. Fischel, R. E, (1963) “Passive Magnetic Attitude Control for Earth Satellites”, Advances in the Astronautical Sciences, Volume 11, Western Periodical Company Hollywood, Calif.
32. S. K. Shrivastava, "Effects of solar radiation pressure and aerodynamic forces on satellite attitude dynamics and their utilization for control: a survey”, Department of Aeronautical Engineering, Indian Institute of Science, " Bangalore-12 Received on May 31, 1976 and in revised form on July 26, 1976. No. 12, pp. 391-410, 1976.
33. S. K. Shrivastava and V. J. Modi, "Satellite Attitude Dynamics and Control in the Presence of Environmental Torques” - A Brief Survey," Journal of Guidance, Vol 6, No.6, December 1983
34. M. D. Shuster and S. D. Oh, (1981) “Attitude Determination from Vector Observations”, Journal of Guidance and Control, Volume 4: Page No.70-77
35. M. D. Shuster., “A Survey of Attitude Representations,” Journal of the Astronautical Sciences, Vol. 41, No. 4 October-December 1993, pp. 439-517
36. T. Fukushima, "Generalization of Encke’s method and its application to the orbital and rotational motions of celestial bodies," The Astronomical Journal, vol. 112, no. 3, pp. 1263-1277, 1996
37. WH Steyn, “Comparison of Low-Earth Orbiting Satellite Attitude Controllers Submitted to Controllability Constraints”, AIAA Journal of Guidance, Control, and Dynamics, Vol.17, No.4, July-Aug.1994, pp.795-804
38. WH Steyn and Y Hashida, “In-Orbit Attitude and Orbit Control Commissioning of UoSAT-12”, 4th ESA International Conference on Spacecraft Guidance, Navigation and Control Systems, ESTEC Noordwijk, The Netherlands, 18-21 Oct.1999.

39. Jonas Elfving, (2002), "Attitude and Orbit Control for Small Satellites", PhD Thesis, Linköping University, Department of Electrical Engineering, 28th October 2002
40. A.M. Mohammed, A. Boudjemai, S. Chouraqui, (2006) "Magnetorquer Control for Orbital Maneuver of Low Earth Orbit Microsatellite" Proceedings of the 5th WSEAS International Conference on Applied Computer Science, Hangzhou, China, April 16-18, 2006 (pp1024-1027)
41. Diaz, Orlando X, (2010) "Analysis and Comparison of Extended and Unscented Kalman Filtering Methods for Spacecraft Attitude Determination", Master Thesis, Naval Postgraduate School, Monterey, California, December 2010
42. Wang, P., Zheng, W., Zhang, H., and Wu, Z. "Attitude Control of Low-orbit Micro-satellite with Active Magnetic Torque and Aerodynamic Torque." International Symposium on Systems and Control in Aeronautics and Astronautics. Harbin, China, June 2010. 1460-1464.
43. Wang, P., Zheng, W., Zhang, H., and Wu, Z. "Attitude Control of Low-orbit Micro-satellite with Active Magnetic Torque and Aerodynamic Torque." International Symposium on Systems and Control in Aeronautics and Astronautics. Harbin, China, June 2010. 1460-1464.
44. Shuster, M. D and Gregory A. Natanson, Quaternion Computation from a Geometric Point of View. *Journal of the Astronautical Sciences*, 41(4), October-December 1993, pp. 545-556
45. K. Groyekatthofer and Z. Yoon, "Introduction into Quaternions for Spacecraft Attitude," Technical University of Berlin, Department of Astronautics and Aeronautics, Berlin, Germany, 2012.
46. D. Fragopoulos, M. Innocenti. Autonomous Spacecraft 6 DOF relative motion control using Quaternions and H-infinity methods. In Proceedings of AIAA, Guidance, Navigation and Control Conference, San Diego, USA, pp. 1-12, 1996.
47. J. Diebel, "Representing Attitude: Euler Angles, Unit Quaternions, and Rotation Vectors", Stanford University, Stanford, California 94301–9010, 2oth october 2006.

48. Chaturvedi, N. A., Global Dynamics and Stabilization of Rigid Body Attitude Systems, Ph.D. Dissertation, Univ. of Michigan, Ann Arbor, MI, 2007
49. M. Blanke and M. B. Larsen, "Satellite Dynamics and Control in a Quaternion Formulation (2nd edition)," Technical University of Denmark, Department of Electrical Engineering, 2010
50. Blanke, Mogens; Larsen, Martin Birkelund, Satellite Dynamics and Control in a Quaternion Formulation, Automation and Control Group DTU Electrical Engineering Department Technical University of Denmark. Version 2f - September 2010
51. K. Vinther, K. F. Jensen, J. A. Larsen, and R.Wisniewski, Inexpensive Cubesat Attitude Estimation Using Quaternions And Unscented Kalman Filtering, Automatic Control Aerospace., vol. 4, 2011.
52. Jack B. Kuipers. Quaternions and Rotation Sequences. Princeton University Pres, 2002.
53. C. Kaplan. LEO Satellite, Attitude Determination and Control Components, Linear Control Methods, MSc. Thesis, METU 2006
54. Wertz. Spacecraft Attitude Determination and Control, Springer, Netherlands, 1987.
55. P. C. Hughes. Spacecraft Attitude Dynamics. USA: John Wiley & Sons. Inc. 1986
56. Rasmus Holst, “Satellite Attitude Control using Magnetorquers with Magnetic Dipole Moment Cancellation”, Master Thesis, Aalborg University, 2014.
57. Kristin Johansson, “Orbital Mechanics and Feedback Control”, Master Thesis, Department of Engineering Cybernetics, Norwegian University of Science and Technology, Trondheim, June 15, 2005
58. Fortescue, P., and Stark, J. Spacecraft Systems Engineering. 2nd Edition. England: Wiley, 1995.
59. S. J. Julier and J. K. Uhlmann. “A Consistent, Debiased Method for Converting Between Polar and Cartesian Coordinate Systems. The Proceedings of Aero Sense: The 11th International Symposium on Aerospace/Defense Sensing, Simulation and Controls, Orlando, Florida. SPIE, 1997. Acquisition, Tracking and Pointing XI.

60. M. Sidi. Spacecraft Dynamics and Control: a practical engineering approach. Cambridge University Press, 1997
61. Schaub, H., and Junkins, J. L., “MATLAB Toolbox for Rigid Body Kinematics,” Proceedings of the AAS/AIAA Space Flight Mechanics Meeting, Breckenridge, CO, American Astronautical Soc. Paper 99-139, Springfield, VA, 7–10 Feb. 1999, pp. 549–560.
62. M. D. Shuster and Oh S. “Three-axis attitude determination from vector observations”, Journal of Guidance and Control 1981; 4: 70–77
63. M. D. Shuster, “The Quest for Better Attitudes”, the Journal of the Astronautical Sciences, Vol. 54, Nos. 3&4, July-December 54:657-683, 2006.
64. Mark.L. Psiaki, "Magnetic Torquer Attitude Control via Asymptotic Periodic Linear Quadratic Regulation.", Journal of Guidance, Control, and Dynamics, Vol. 24, No.2, 2001
65. Erlank, A.O, “Development of CubeStar, A CubeSat-Compatible Star Tracker”. Master Thesis, Stellenbosch University, 2013.
66. T. Bak. Spacecraft Attitude Determination- a Magnetometer Approach. Ph.D. Thesis. Aalborg University, Denmark, 2002
67. Kusuda, Y, Takahashi, M. "Design of Feedback Control System using Nominal Inputs for Satellite Attitude Maneuver using Control Moment Gyros." AIAA Conference of Guidance, Navigation, and Control. Chicago, Aug 2009
68. Singh, S. & Yim,W. (1995), Dynamic Feedback linearization and large pitch attitude control of satellite using solar radiation pressure, in ‘Proceedings of the 1995 American Control Conference’, Vol. 5, American Control Conference 1995, pp. 3131–3135.
69. J.R. Wertz, and W.J. Larson, (editors). “Space Mission Analysis and Design”, Kluwer Academic Publishers, 1999
70. H. J. Kushner. “Dynamical Equations for Optimum Non-linear Filtering”, Journal of Differential Equations, 3:179–190, 1967.
71. Choukroun D. "Methods for Attitude Determination using Vector Observation”, PhD Thesis, Israel Institute of Technology, 2003
72. Beer, Ferdinand P, Johnston, Russell, Jr. (1972), “Vector Mechanics for Engineers: Statics & Dynamics”, McGraw-Hill

73. M. Eshagh, M. Najafi Alamdari, "Perturbations in Orbital Elements of a Low Earth Orbiting Satellite," Journal of the Earth & Space Physics, Vol. 33, No. 1, PP. 1-12, 2007.
74. Tewari, “Atmospheric and Space Flight Dynamics”, New York: Birkhauser Boston, 2007.
75. Flanagan R C “Effect of Environmental Forces on the Attitude Dynamics of Gravity-Oriented Satellites”, Ph.D. Thesis, Univ. of British Columbia, 1969.
76. George A. Weisskopf, “Application and Analysis of Satellite Orbit Prediction Techniques”, Mission Planning and Analysis Division National Aeronautics and Space Administration, Johnson Space Center Houston, Texas, JSC Internal note no. 77-fm-19, April 12, 1977
77. Anders W. Sandvik, “Numerical Solutions of Classical Equations of Motion”, Department of Physics, Boston University, PY 502, Computational Physics, fall 2018
78. L.M. Gomes, G. Yuksel, A.S. Curiel, A. Bradford, M. Sweeting. BILSAT: Advancing Small-Sat Capabilities, SS C03-VI-4, 17th AIAA/USU Conference proc. on Small Satellites
79. S. Rawashdeh, D. Jones, D. Erb, A. Karam, and J. E. Lumpp, Jr., "Aerodynamic Attitude Stabilization for a Ram-Facing CubeSat", Breckenridge, Colorado: AAS 32nd Annual Guidance and Control Conference, 2009.
80. J. Lee, A. Ng and R. Jobanputra, "On Determining Dipole Moments of a Magnetic Torquer Rod Experiments and Discussions." Canadian Aeronautics and Space Journal, Vol 48, No. 1, 2002, pp. 61-67
81. Fellenz, D.W. (1967). "Atmospheric Entry". In Theodore Baumeister. Marks' Standard Handbook for Mechanical Engineers (Seventh ed.). New York City: McGraw Hill. pp. 11:155–58. ISBN 0-07-142867-4
82. Tidwell, N.W, “Modelling of Environmental Torques of a Spin Stabilized Space Near Earth Orbit”, Journal of Spacecraft and Rockets 1970, 7 1425-1433.
83. Wallace, F. B. “On the Effects of Aerodynamic and Gravitational Torques on the Attitude Stability of Satellites”, AIAA Journal. 1966, 4, 2196-2202

84. K. A. Muhammad shamsul and R. Radzuan, "A Study of Perturbation Effect on Satellite Orbit using Cowell's Method," School of Aerospace Engineering, Engineering Campus University Science Malaysia 14300 Nibong Tebal Penang, Malaysia
85. Belokonov, I.V., Timbai, I.A., Ustyugov, E.V., "Method of Aerodynamic Stabilization of CubeSat class Nanosatellite and a Device for its Implementation", Eurasian patent for the invention (21) 201 400 132 (13) A1, 2015.
86. S. P. Shuster, "A Survey and Performance Analysis of Orbit Propagators for LEO, GEO, and Highly Elliptical Orbits," All Graduate Theses and Dissertations, Utah, 2017
87. Pawel Zagorski, (2012) "Modeling disturbances influencing an Earth-orbiting satellite" Journal of Pomiary Automatyka Robotyka AGH University of Science and Technology, Vol. 16, No. 5/2012, 98-103, 2012
88. G. E. Cook, "Lunar-Solar Perturbations of the Orbit of an Earth Satellite," The Geophysical Journal of the Royal Astronomical Society, vol. Volume, no. 3, pp. 271-291, 1962.
89. Alvar Saenz-Otero. Design Principles for the Development of Space Technology Maturation Laboratories aboard the International Space Station. Ph.D. Thesis, Massachusetts Institute of Technology, Cambridge, MA, May 2005.
90. S. Grover, K. Bradford, M. Anderson, E. Stromberg, B. Sharp, and S. Burr, "Miniature wire Boom System for Nano Satellites," in Proceedings of AIAA/Utah State University Conference on Small Satellites, Aug. 2010.
91. Evans, W. J, "Aerodynamic and Radiation Disturbance Torques on Satellites having Complex Geometry", Astronautical Journal, 1962, 9, 93-99.
92. Poliakhova, E. N, "Solar Radiation Pressure and the Motion of an Earth Satellite", AIAA Journal, 1963, 1, 2893-2909.
93. Bryant, R. W, "The Effect of Solar Radiation Pressure on the Motion of an Artificial Satellite", Astronautical Journal, 1961, 66, 430.
94. Kumar K, "Effect of Solar Radiations on the Attitude Dynamics or Gravity-Oriented Satellites", Ph.D. Thesis, Univ. of British Columbia, 1972.

95. Hablani, H.B. "Momentum Accumulation due to Solar Radiation Torque, and Reaction Wheel Sizing, with Configuration Optimization." AIAA Journal of Guidance, Control, and Dynamics, 1994: 805-814.
96. J De Lafontaine and S C Garg, “A Review of Satellite Lifetime and Orbit Decay Prediction”, Proceeding. Indian Acad. Sci. (Engg. Sci.) Vol. 5, Pt. 3, September 1982 pp, I97-258.
97. Van D Ha, J. C., and Lappas, V. J., “Long-Term Attitude Drift of Spinning Spacecraft under Solar Radiation Torques,” Journal of Guidance, Control, and Dynamics.
98. Kim B, Velenis E, Kriengsiri P, et al. A Spacecraft Simulator for Research and Education. In: Proceedings of the AIAA/AAS Astrodynamics Specialists Conference, AIAA, Reston, VA, 30 July–2 August 2001, pp.897–914; also, AAS Paper 01-367, 2001.
99. Dennis S. Bernstein, N. Harris McClamroch, and Anthony Bloch. “Development of Air Spindle and Triaxial Air Bearing Testbeds for Spacecraft Dynamics and Control Experiments," Proceedings of the American Control Conference. Pages 3967-3972. American Automatic Control Council (AACC), June 2001.
100. A. Craig Stickler, K. T. Alfriend, "Elementary Magnetic Attitude Control System." Journal of Spacecraft and Rockets, Vol. 13, No.5, 1976, pp. 282
101. Sun, Z., Yang, X., and Yang, D. "Active Magnetic Control Methods for Small Satellite." Journal of Aerospace Engineering, 2003: 38-44.
102. S. Rawashdeh, J. Lumpp, “Nano-Satellite Passive Attitude Stabilization Systems”, Design by Orbital Environment Modeling and Simulation”, AIAA Infotech Aerospace 2010, Atlanta, GA.
103. Johannes S, “Attitude Determination and Control System of a Nanosatellite”, University of Stellenbosch, Department of Electrical Engineering, Matieland, South Africa, October 2007
104. R. R. Kumar, D. D. Mazanek, M. L. Heck., "Simulation and Shuttle Hitchhiker Validation of Passive Satellite Aero stabilization", Vol. 32, No. 5, 1995, pp. 806–811." Journal of Spacecraft and Rockets, 1995, Issue 5, Vol. 32, pp. 806-811.

105. L. Rossini, “Electromagnetic Modeling and Control aspects of a Reaction Sphere for Satellite Attitude Control,” Ph.D. Dissertation, Swiss Federal Institute of Technology of Lausanne (EPFL), 2014.
106. K. L. Makovec. A Nonlinear Magnetic Controller for Three axis Stability of Nanosatellites. Master Thesis, Virginia 2001.
107. J. R. Wisniewski. Satellite Attitude Control using only Electromagnetic Actuation. Ph.D. Thesis, Department of Control Engineering. Aalborg University. Denmark. 1996
108. R.Wisniewski, Satellite Attitude Control using Magnetic Actuation only [Ph.D. Thesis], Dissertation, Dept. of Control Engineering, Aalborg University, Denmark, 1996
109. K. Woodham, K. Blackman, P. Sanneman, Solar and Magnetic Attitude Determination for Small Spacecraft, A97-32198.
110. Das, S., Sinha, M., Kumar, K.D., and Misra, A. "Reconfigurable Magnetic Attitude Control of Earth-Pointing Satellite." Journal of Aerospace Engineering, 2010: 1309-1326.
111. Z. Q. Zhou, “Spacecraft Attitude Tracking and Maneuver using Combined Magnetic Actuators,” AIAA Guidance, Navigation, and Control Conference, Toronto, Ontario, Canada, August 2010.
112. J. R. Forbes and C. J. Damaren, “Geometric Approach to Spacecraft Attitude Control using Magnetic and Mechanical Actuation,” Journal of Guidance, Control, and Dynamics, vol. 33, no. 2, pp. 590–595, 2010
113. Deutschmann, J., and I. Bar-Itzhack, "Comprehensive Evaluation of Attitude and Orbit Estimation using Real Earth Magnetic Field Data", Proceedings of the 11th Annual AIAA/USU Conference on Small Satellites, Logan, UT, September 15-18, 1997.
114. Gerhardt, D. T., “Passive Magnetic Attitude Control for CubeSat Spacecraft,” Proceedings of the AIAA/USU Conference on Small Satellites, Logan, UT, August 2010.
115. H. Black. “A Passive System for Determining the Attitude of a Satellite”, AIAA Journal 2 (7): 1350-1351, 1963.

116. Battagliere, M.L., Fiorillo, F., Ferrara, E., and Santoni, F. "Permeable Rods Ground Testing System for Cubesat Angular Velocity and Residual Oscillations Damping." 61st International Astronautical Congress (IAC). Prague, Sept 2010. 2217-2225.
117. Park, G., Seagraves, S., and McClamroch, N. H., "A Dynamic Model of a Passive Magnetic Attitude Control System for the RAX Nanosatellite," Proceedings of the AIAA Guidance, Navigation, and Control Conference, Toronto, August 2010.
118. M. Abdekrahman and S. Y. Park, "Integrated Attitude Determination and Control System via Magnetic Measurements and Actuation," Acta Astronautica, vol. 69, no. 3-4, pp. 168–185, 2011
119. C.C. Finlay, "International Geomagnetic Reference Field: the eleventh generation", Geophysics. Journal of International., Vol. 183, Issue 3, 2010, pp. 1216 – 1230.
120. Finlay C. International Geomagnetic Reference Field, IAGA. (Available:http://www.ngdc.noaa.gov/IAGA/vmod/igrf.html)
121. Barba, P.M., and Aurbrun, J.N. "Satellite Attitude Acquisition by Momentum Transfer." AIAA Journal, 1976: 1382-1386.
122. Lappas, V.J., Steyn, W.H., Underwood, C.I., Control Moment Gyro Gimbal Angle Compensation using Magnetic Control During External Disturbances, AIAA Guidance, Navigation and Control Conference, Montreal, Quebec, Canada, 2001
123. G. Borque Gallego, "Angular Velocity Estimation of a Reaction Sphere Actuator for Attitude Satellite Control," Master Thesis, Swiss Federal Institute of Technology of Lausanne (EPFL), 2016.
124. G. Boersma and F. J. Sonnenschein, "Preparatory Study of Satellite Attitude Control with Momentum Wheels", National Aerospace Laboratory, NLR-TR-72148-U, Amsterdam, Netherlands, June 1972.
125. Kim, S., and Kim, Y., "Spin-Axis Stabilization of a Rigid Spacecraft using two Reaction Wheels," Journal of Guidance, Control, and Dynamics, Vol. 24, No. 5, 2001, pp. 1046–1049.doi:10.2514/2.4818.

126. Lian, B., and Bang, H., “Momentum Transfer Based Attitude Control of Spacecraft with Backstepping,” IEEE Transactions on Aerospace and Electronic Systems, Vol. 42, No. 2, 2006, pp. 453–462.doi:10.1109/TAES.2006.1642563.
127. Daan Stevenson, Hanspeter Schaub, “Nonlinear Control Analysis of a Double-Gimbal Variable-Speed Control Moment Gyroscope” Journal of Guidance, Control, and Dynamics Vol. 35, No. 3, May–June 2012.
128. D. E. Andersen, “Computing NORAD Mean Orbital Elements from a State Vector,” Master Thesis, Air University, 1994. [Online]. Available: http://www.dtic.mil/cgi-bin/GetTRDoc?AD=ADA28928
129. International Space Station (ISS) https://spaceflight.nasa.gov/realdata/sightings/SSapplications/Post/JavaSSOP/orbit/ISS/SVPOT.html
130. Wertz, J.R. "Spacecraft Control System." Kluwer, 1978.
131. Hoots, F. R. and Roehrich, R., \Models for Propagation of NORAD Element Sets. Space track Report no. 3." U.S. Air Force: Aerospace Defense Command. 1980.
Available: http://earthobservatory.nasa.gov/Features/OrbitsCatalog/
132. S. Alam and M. Yasir, "Satellite Attitude and Orbital Dynamics Simulator," Journal of Space Technology, Vol. 1, No. 1, PP. 40-44, 2011
133. Schwartz JL. The Distributed Spacecraft Attitude Control System Simulator: from design concept to decentralized control. PhD Thesis, Virginia Polytechnic Institute and State University, Blacksburg, VA, 7 July 2004
134. Pratham IIT Bombay Student Satellite – Critical Design Report – Attitude Determination and Control System (ADCS) for Pratham”, 2010
135. NORAD NOAA elements. (n.d.). CelesTrak. [Online].
Available: http://www.celestrak.com/NORAD/Elements/Noaa.txt.
Accessed 21 Aug 2014.
136. Akash Rateesh et al, “SRMSAT: A Feasibility Study on Small Satellite Mission to Moon”, 54th AIAA Aerospace Sciences Meeting, AIAA SciTech 2016, At San Diego, CA

137. D. E. Andersen, “Computing NORAD Mean Orbital Elements from a State Vector,”Master, Air University, 1994. [Online]. Available: http://www.dtic.mil/cgi-bin/GetTRDoc?AD=ADA28928
138. Grewal, M. S., & Andrews, A. P. (2008). Kalman Filtering: Theory and Practice using MATLAB (3rd Ed.). John Wiley and Sons.
139. H. W. Sorenson, Editor. Kalman Filtering: Theory and Application. IEEE Press, 1985.
140. WH Steyn, “Magnetic Attitude Determination and Control for Low Earth Orbiting Small Satellites”, Department of Electrical and Electronic Engineering, University of Stellenbosch, PO Box 1 Matieland 7602
141. Eun-Hwan Shin, Accuracy Improvement of Low Cost INS/GPS for Land Applications, M.Sc Thesis, Department of Geomatics Engineering, University of Calgary, December 2001
142. Markley, F. L., “Attitude Error Representation” Journal of Guidance, Control, and Dynamics, Vol. 26, No. 2, 2003, pp. 311–317.
143. Oshman, Y, and F.L. Markley, "Spacecraft Attitude/Rate Estimation using Vector- Aided GPS Observations", IEEE Transactions on Aerospace and Electronic Systems, Vol. 35, No. 3, July 1999.
144. Crassidis, J. L., Markley, F. L., Cheng, Y., “Survey of Nonlinear Attitude Estimation Methods,” Journal of Guidance, Control, and Dynamics, Volume 30, No. 1, January-February 2007.
145. Wu, Y., Hu, D., Wu, M., & Hu, X. (2005, June). Unscented Kalman Filtering for Additive Noise Case: Augmented vs. Non-augmented. American Control Conference.
146. Crassidis, J. L., Markley, F. L., “Unscented Filtering for Spacecraft Attitude Estimation,” Journal of Guidance, Control, and Dynamics, Vol. 26, No. 4, pp. 536-542, July-August 2003. Julier, S. J. and Uhlmann, J. K. [1997], ‘A New Extension of the Kalman Filter to Nonlinear Systems”, The Robotics Research Group, Department of Engineering Science, The University of Oxford, Oxford, OX1 3PJ, UK

147. J. W. Austin and C. T. Leondes. “Statistically Linearized Estimation of Reentry Trajectories”, IEEE Transactions on Aerospace and Electronic Systems, AES-17(1):54–61, January 1981.
148. C. B. Chang, R. H. Whiting and M. Athans. “On the State and Parameter Estimation for Maneuvering Reentry Vehicles”, IEEE Transactions on Automatic Control, AC-22:99–105, February 1977.
149. John Vitalich, “Design and Simulation of a Three-Axis Stabilized Satellite and Kalman Filter Rate Estimator”, Master Thesis, Electrical Engineering, Naval Postgraduate School, Monterey, California, June 2003
150. H. W. Sorenson and A. R. Stubberud. “Non-linear Filtering by Approximation of a Posteriori Density”, International Journal of Control, 8(1):33–51, 1968
151. S. J. Julier and J. K. Uhlmann, “Unscented filtering and nonlinear estimation,” Proc. IEEE, Vol. 92, No. 3, PP. 401–422, 2004.
152. Lefferts, E. J.; Markey, F. L.; M. D. Shuster., “Kalman Filtering for Spacecraft Attitude Estimation.” Journal of Guidance, Control and Dynamics, Vol. 5, No. 5, PP. 417-429, 1982
153. Jiang, X.-Y. [2005], ‘Unscented Kalman Filter for Spacecraft Attitude Estimation and Calibration using Magnetometer Measurements’ Proceedings of the Fourth International Conference on Machine Learning and Cybernetics.
154. S. J. Julier, J. K. Uhlmann and H. F. Durrant-Whyte. “A New Approach for Filtering Nonlinear Systems”, In the Proceedings of the American Control Conference, Seattle, Washington., Pages 1628–1632, 1995.
155. N. J. Gordon, D. J. Salmond and A. F. M. Smith. “Novel Approach to Nonlinear/Non-Gaussian Bayesian State Estimation”, IEEE Proceedings-F, 140(2):107–113, April 1993.
156. J. Bibby and H. Toutenburg, Prediction and Improved Estimation in Linear Models. New York: Wiley, 1977.
157. Grewal, Andrews, (2001), Kalman Filtering Theory Using MATLAB, Joun Wiley& Sons.
158. D. Sakoda and J. A. Horning, “Overview of the NPS Spacecraft Architecture and Technology Demonstration Satellite, NPSAT1,” Naval Postgraduate

School, Monterey, Tech. Rep., 2002. [Online]. Available http://www.digitalcommons.usu.edu/cgi/viewhttp: //digitalcommons.usu.edu/cgi/viewcontent.cgi?article=1896\&context=smallsat

159. H. E. Soken and C. Hajiyev, UKF for the Identification of the PICO Satellite Attitude Dynamics Parameters and the External Torques on IMU and Magnetometer Measurements, in 4th International Conference on Recent Advances in Space Technologies, 2009, pp. 547–552.
160. Mohinder S. Grewal, Lawrence R. Weill & Angus P. Andrews, Global Positioning Systems, Inertial Navigation, and Integration, John Wiley & Sons, 2001
161. Deutschmann, J., R. Harman, and I. Bar-Itzhack, "An Innovative Method for Low Cost, Autonomous Navigation for Low Earth Orbit Satellites", Proceedings of the AAS/AIAA Astrodynamics Specialists Conference, Boston, MA, August 10-12, 1998.
162. Ripka, P. and Acuna, M. H., Magnetic Sensors and Magnetometers, chap. 10: Applications of Magnetic Sensors, Artech House, 2001, pp. 369–402.
163. P. Landiech, Extensive Use of Magnetometers and Magnetotorquers for Small Satellites Attitude Estimation and Control, Advances in the Astronautical Sciences, Guidance and Control AAS 95-012 1995.
164. Navabi, N., and Nasiri, N. "Three-axis Stabilization of a Low Earth Orbit Spacecraft Utilizing Magnetorquers and Reaction Wheels Combinations, According to Energy Consumption." 61st International Astronautical Congress. Prague, Sept 2010. 4769-4777.
165. Kim, E., Bang, H., and Lee, S.H. "Attitude-Independent Magnetometer Calibration Considering Magnetic Torquer Coupling Effect." Journal of Spacecraft and Rockets, 2011: 691-694.
166. N. S. Nise, Control Systems Engineering. New Delhi: John Wiley and Sons, Ch. 9, PP. 439-449, International Student Version, 2010
167. I. Nagarath and M. Gopal, Control Systems Engineering. New Age International (P) Limited Publishers, Ch. 4, PP. 417-453, 2004.
168. Mbaocha C. C, Eze C. U, Ezenugu I, “Satellite Model for Yaw-Axis Determination and Control using PID Compensator”, International Journal of

Scientific & Engineering Research, Volume 7, Issue 7, July-2016, ISSN 2229-5518 IJSER

169. Sami Kadhim Hasan Ar-Ramahi, “PID Controller Design for the Satellite Attitude Control System”, Journal of Engineering, Volume 15, March 2009.

170. G. P. Candini, F. Piergentili, and F. Santoni, “Miniaturized Attitude Control System for Nanosatellites,” Acta Astronautica, vol. 81, pp. 325–334, 2005

171. Mortar Pedersen Topland, “Nonlinear Attitude Control of the Microsatellite ESEO”, M.Sc. Thesis in Department of Engineering Cybernetics, NTNU, July 2004.

172. D. Sakoda and J. A. Horning, “Overview of the NPS Spacecraft Architecture and Technology Demonstration Satellite, NPSAT1,” Naval Postgraduate School, Monterey, Tech. Rep., 2002. [Online]. Available http://www.digitalcommons.usu.edu/cgi/viewhttp: //digitalcommons.usu.edu/cgi/viewcontent.cgi?article=1896\&context=smallsat

173. F. Moeller, “Positioning, Navigation and Timing Solution for NPSAT-1,” Master Thesis, Naval Postgraduate School, Monterey, 2013.

174. Wen, J., and Kreutz-Delgado, K., “The Attitude Control Problem”, IEEE Transactions on Automatic Control, Vol. 36, No. 10, 1991, pp. 1148–1162. DOI:10.1109/9.90228.

175. Horri, N.M., and Palmer, P. "Practical Implementation of Attitude-Control Algorithms for Underactuated Satellite." Journal of Guidance, Control, and Dynamics, 2012: 40-50.

176. B. E. Tossman, F. F. Mobley, G. H. Fountain, K. J. Heffennan, J. C. Ray, and C. E. Williams, "Magsat Attitude Control System Design and Performance”, AIAA 80-1730, 1980.

177. Bolandi, H., Bayat, F., and Nasirian, M. "Attitude Control of Spinning Satellite Subject to Actuators Restriction using Eigen structure Assignment." 1st International Symposium on Systems and Control in Aerospace and Astronautics. Harbin, Jan 2006. 1413-1419.

178. Akash Rateesh et al, “SRMSAT: A Feasibility Study on Small Satellite Mission to Moon”, 54th AIAA Aerospace Sciences Meeting, AIAA SciTech 2016, At San Diego, CA
179. T. El.M. Brembo, (2005), Sensor Modeling, Attitude Determination and Control for Microsatellite, M. Sc. Thesis, Norwegian University of Science and Technology.
180. R. Kristiansen. Attitude Control of a Microsatellite. Master Thesis, Department of Engineering Cybernetics, NTNU, 2000
181. Gene F. Franklin, J. David Powell, and Abbas Emami-Naeini. Feedback Control of Dynamic Systems. Series in Electrical and Computer Engineering: Control Engineering. Addison Wesley, Massachusetts, 3rd edition, 1994

MODEL CODES

COWELL'S PERTURBATION'S SIMULATION CODES

```
rho = input(' Density rho [kg/m^3] = ');
Cd = input(' Coefficient of Drag Cd  = ');
A = input(' Area of the satellite A [m^2] = ');
u = input(' Velocity of the satellite u [m/s] = ');
v = input(' Velocity of the satellite v [m/s] = ');
w = input(' Velocity of the satellite w [m/s] = ');

E_ad = 0.5 * rho * Cd * A * u^2;
F_ad = 0.5 * rho * Cd * A * v^2;
G_ad = 0.5 * rho * Cd * A * w^2;

M = input(' Mass of the satellite M [kg] = ');
p_ad = E_ad / M;
q_ad = F_ad / M;
r_ad = G_ad / M;

mu = 3.986 * 10^14;                          % m^3/s^2
x = input(' Distance between the satellite and the Earth x [m] = ');
y = input(' Distance between the satellite and the Earth y [m] = ');
z = input(' Distance between the satellite and the Earth z [m] = ');

% step size
h = 7200;
t = 0:h:86400;  %in seconds
A = zeros(1,10);
B = zeros(1,10);
% initial condition
x(1) = x;
u(1) = u;
y(1) = y;
v(1) = v;
z(1) = z;
w(1) = w;

% Functions
Fx = @(x,t) u;
Fu = @(u,t) p_ad - ((mu)/(x^2));
Fy = @(y,t) v;
Fv = @(v,t) q_ad - ((mu)/(y^2));
Fz = @(z,t) w;
Fw = @(w,t) r_ad - ((mu)/(z^2));
```

```
for i=1:(length(t))                    % calculation loop
    k_1 = Fx(u(i));
    l_1 = Fu(x(i));
    k_2 = Fx(u(i)+0.5*k_1);
    l_2 = Fu(x(i)+0.5*h);
    k_3 = Fx(u(i)+0.5*k_2);
    l_3 = Fu(x(i)+0.5*h);
    k_4 = Fx(u(i)+k_3);
    l_4 = Fu(x(i)+h);

    x(i+1) = x(i) + (1/6)*(k_1+2*k_2+2*k_3+k_4);
    u(i+1) = u(i) + (1/6)*(l_1+2*l_2+2*l_3+l_4);

    m_1 =  Fy(v(i));
    n_1 =  Fv(y(i));
    m_2 =  Fy(v(i)+0.5*m_1);
    n_2 =  Fv(y(i)+0.5*h);
    m_3 =  Fy(v(i)+0.5*m_2);
    n_3 =  Fv(y(i)+0.5*h);
    m_4 =  Fy(v(i)+m_3);
    n_4 =  Fv(y(i)+h);

    y(i+1) = y(i) + (1/6)*(m_1+2*m_2+2*m_3+m_4);
    v(i+1) = v(i) + (1/6)*(n_1+2*n_2+2*n_3+n_4);

    r_1 = Fz(w(i));
    s_1 = Fw(z(i));
    r_2 = Fz(w(i)+0.5*r_1);
    s_2 = Fw(z(i)+0.5*h);
    r_3 = Fz(w(i)+0.5*r_2);
    s_3 = Fw(z(i)+0.5*h);
    r_4 = Fz(w(i)+r_3);
    s_4 = Fw(z(i)+h);

    z(i+1) = z(i) + (1/6)*(r_1+2*r_2+2*r_3+r_4);
    w(i+1) = w(i) + (1/6)*(s_1+2*s_2+2*s_3+s_4);

    R = [x(i+1) y(i+1) z(i+1)]
    V = [u(i+1) v(i+1) w(i+1)]
    A(:,i) = sqrt(sum(R.^2))
    B(:,i) = sqrt(sum(V.^2))

end
A = A/1000;
B = B/1000;
```

```
A(1,:);
B(1,:);

figure(1)
plot(t,B, 'Linewidth', 1.5, 'color', 'blue')
xlabel('Time(sec)')
ylabel('Velocity(km/s)')
legend('Velocity vs Time')
figure(2)
plot(t,A, 'Linewidth', 1.5, 'color', 'red')
xlabel('Time(sec)')
ylabel('Position(km)')
legend('Position vs Time')
```

KEPLERIAN CODES FOE INTERNATIONAL SPACE STATION (ISS) (ACTUAL/PREDICTED ORBITS)

```
mport matplotlib.pyplot as plt
x =  [0,0.01,0.02,0.03,0.04]
y_blue =[51.875,51.866,51.866,51.855,51.845]
y_orange = [51.875,51.872,51.867,51.855,51.845]
plt.xlabel('Time (Days) ')
plt.ylabel("Orbital Inclination(Deg)")
plt.plot(x,y_blue,label="Predicted",marker='o')
plt.plot(x,y_orange,label="Actual",marker='o')
b1=sum(y_orange)/5
b=sum(y_blue)/5
Pdiff = (b1-b)/b*100
print(b,b1,Pdiff)
plt.ylim(bottom=51.825,top=51.88)
plt.xlim(left=0,right=0.045)
plt.title("Orbital Inclination vs Time")
plt.text(0.0325,51.8270,"Percentage Difference=\n          0.002 %",fontsize=8)
plt.grid(color='black',linewidth=0.25,linestyle='--')
plt.legend()
plt.show()

import matplotlib.pyplot as plt
x =  [0.025,0.03,0.035,0.04,0.045,0.05,0.055,0.06]
y_blue =[55,80,100,110,120,121,129,145]
y_orange = [62,83,101,120,120,124,130,143]
plt.xlabel('Time (Days) ')
plt.ylabel("Argument Of Perigee")
```

```
plt.plot(x,y_blue,label="Predicted",marker='o')
plt.plot(x,y_orange,label="Actual",marker='o')
b1=sum(y_orange)/8
b=sum(y_blue)/8
Pdiff = (b1-b)/b*100
print(b,b1,Pdiff)
plt.ylim(bottom=0,top=180)
plt.xlim(left=0,right=0.07)
plt.title("Argument of Perigeee vs Time")
plt.text(0.05,10,"Percentage Difference=\n          2.67 %",fontsize=8)
plt.grid(color='black',linewidth=0.25,linestyle='--')
plt.legend()
plt.show()
import matplotlib.pyplot as plt
x =  [0,0.01,0.02,0.03,0.04]
y_blue =[110,150,222,280,306]
y_orange = [96,155,222,280,304]
plt.xlabel('Time (Days) ')
plt.ylabel("True Anomaly(Deg)")
plt.plot(x,y_blue,label="Predicted",marker='o')
plt.plot(x,y_orange,label="Actual",marker='o')
b1=sum(y_orange)/5
b=sum(y_blue)/5
Pdiff = (b1-b)/b*100
print(b,b1,Pdiff)
plt.ylim(bottom=0,top=350)
plt.xlim(left=0,right=0.045)
plt.title("True Anomaly vs Time")
plt.text(0.0325,20,"Percentage Difference=\n          1.02 %",fontsize=8)
plt.grid(color='black',linewidth=0.25,linestyle='--')
plt.legend()
plt.show()
import matplotlib.pyplot as plt
x =  [0,0.01,0.02,0.03,0.04]
y_blue =[6786,6785.2,6782.8,6780.3,6778.1]
y_orange = [6786.2,6785.9,6784,6780,6777.2]
plt.xlabel('Time (Days) ')
plt.ylabel("Semi Major Axis(Km)")
plt.plot(x,y_blue,label="Predicted",marker='o')
plt.plot(x,y_orange,label="Actual",marker='o')
b1=sum(y_orange)/5
b=sum(y_blue)/5
```

```
Pdiff = (b1-b)/b*100
print(b,b1,Pdiff)
plt.ylim(bottom=6776,top=6788)
plt.xlim(left=0,right=0.045)
plt.title("Semi Major Axis vs Time")
plt.text(0.0325,6785,"Percentage Difference=\n          0.002 %",fontsize=8)
plt.grid(color='black',linewidth=0.25,linestyle='--')
plt.legend()
plt.show()
import matplotlib.pyplot as plt
x =  [0,0.1,0.2,0.3,0.4,0.5,0.6,0.7,0.8,0.9,1]
y_blue =[36,35,34,33,32.8,32.5,32.1,31,30,30,29.8]
y_orange = [36,35,34,33,32.8,32.5,32.5,32,31,30.5,30]
plt.xlabel('Time (Days) ')
plt.ylabel("RAAN (Deg)")
plt.plot(x,y_blue,label="Predicted",marker='o')
plt.plot(x,y_orange,label="Actual",marker='o')
b1=sum(y_orange)/11
b=sum(y_blue)/11
Pdiff = (b1-b)/b*100
print(b,b1,Pdiff)
plt.ylim(bottom=0,top=40)
plt.xlim(left=0)
plt.title("RAAN vs Time")
plt.text(0.76,2,"Percentage Difference=\n          0.87 %",fontsize=8)
plt.grid(color='black',linewidth=0.25,linestyle='--')
plt.legend()
plt.show()
import matplotlib.pyplot as plt
x =  [0,0.01,0.02,0.03,0.04]
y_blue =[0.00039,0.00039,0.00039,0.000265,0.0002]
y_orange = [0.00036,0.00037,0.00038,0.00026,0.0002]
plt.xlabel('Time (Days) ')
plt.ylabel("Eccentricity")
plt.plot(x,y_blue,label="Predicted",marker='o')
plt.plot(x,y_orange,label="Actual",marker='o')
b1=sum(y_orange)/5
b=sum(y_blue)/5
Pdiff = (b1-b)/b*100
print(b,b1,Pdiff)
plt.ylim(bottom=0,top=0.00045)
plt.xlim(left=0,right=0.05)
```

```
plt.title("Eccentricity vs Time")
plt.text(0.0365,0.00035,"Percentage Difference=\n          3.97 %",fontsize=8)
plt.grid(color='black',linewidth=0.25,linestyle='--')
plt.legend()
plt.show()
```

KALMAN FILTER CODE FOR ATTITUDE ERRORS ESTIMATION

```
clc
clear all
close all

load magneto.txt;

Ix = 24.67;    % kg-m^2
Iy = 22.63;    % kg-m^2
Iz = 11;     % kg-m^2

mag = magneto';
[m n] = size(mag);

h = 10;  % angular momentum of momentum wheel (Nms)
w = 0.0011068;    % angular velocity (rad/s)
Td = 1.04 * 10^(-4);      % Disturbance torque (Nm)
dt = 0.1;   % time duration (s)
w_dot = w/dt;   % rate of change of angular velocity (rad/s per second)

% controller gain and matrix
pos_x = 2;
vel_x = 2;
pos_y = 2;
vel_y = 2;
pos_z = 2;
vel_z = 2;

F = [pos_x/Ix vel_x/Ix 0 0 0 0;
   0 0 pos_y/Iy vel_y/Iy 0 0;
   0 0 0 0 pos_x/Ix vel_x/Ix];

% Initial state matrix
x0 = [0;0;0;0;0;0];

% Initial error covariance matrix
P0 = [10^(-6) 0 0 0 0 0; 0 10^(-6) 0 0 0 0; 0 0 10^(-6) 0 0 0; 0 0 0 10^(-6) 0 0; 0
0 0 0 10^(-6) 0; 0 0 0 0 0 10^(-6)];
```

```
% process noise covariance matrix
Q = [1e-6 0 0 0 0 0; 0 1e-6 0 0 0 0; 0 0 1e-6 0 0 0; 0 0 0 1e-6 0 0; 0 0 0 0 1e-6
0; 0 0 0 0 0 1e-6];

% measurement noise covariance matrix
R = [1e-2 0 0; 0 1e-2 0; 0 0 1e-2];

% Disturbance torque input matrix
ud = [(Td + (w*h))/Ix ; (Td + (Iy*w_dot))/Iy ; (Td - (w*h))/Iz];

% B Matrix
B = [0 0 0;1 0 0;0 0 0;0 1 0;0 0 0;0 0 1];

% H Matrix
H = [1 0 0 0 0 0; 0 0 1 0 0 0; 0 0 0 0 1 0];

% A matrix
A = zeros(6,6);
A(1,1) = 0;
A(1,2) = 1;
A(1,3) = 0;
A(1,4) = 0;
A(1,5) = 0;
A(1,6) = 0;
A(2,1) = ((-4*(w^2)*(Iy-Iz)) + (w*h)) / Ix;
A(2,2) = 0;
A(2,3) = 0;
A(2,4) = -h/Ix;
A(2,5) = w_dot;
A(2,6) = ((-w*(Iy-Ix-Iz))+h) / Ix;
A(3,1) = 0;
A(3,2) = 0;
A(3,3) = 0;
A(3,4) = 1;
A(3,5) = 0;
A(3,6) = 0;
A(4,1) = (-w*h) / Iy;
A(4,2) = -h/Iy;
A(4,3) = (-3*(w^2)*(Ix-Iz)) / Iy;
A(4,4) = 0;
A(4,5) = (-w*h) / Iy;
A(4,6) = -h/Iy;
A(5,1) = 0;
A(5,2) = 0;
```

```
A(5,3) = 0;
A(5,4) = 0;
A(5,5) = 0;
A(5,6) = 1;
A(6,1) = -w_dot;
A(6,2) = ((-w*(Ix-Iy+Iz))-h) / Iz;
A(6,3) = 0;
A(6,4) = h/Iz;
A(6,5) = ((-(w^2)*(Iy-Ix)) + (w*h)) / Iz;
A(6,6) = 0;

for i = 1:n
   x_p = ((A - (B*F))*x0) + B * ud;
   P_p = (A * P0 * A') + Q;

   % Kalman gain
   Kk = P_p * H' * inv(H * P_p * H' + R);

   % Measurement
   zk = mag(:,n);

   % State update
   x_new = x_p + Kk * (zk - H * x_p);

   % state covariance update
   P_new = (eye(6) - Kk * H) * P_p;

   x0 = x_new;
   P0 = P_new;

   x_vector(:,i) = x_new;

   time(i,1) = i;
end

state = x_vector';

roll = magneto(:,1);
pitch = magneto(:,2);
yaw = magneto(:,3);

roll_error = state(:,1);
pitch_error = state(:,3);
yaw_error = state(:,5);
```

```
roll_est = roll + roll_error;
pitch_est = pitch + pitch_error;
yaw_est = yaw + yaw_error;

figure
plot(time,roll);
hold on
plot(time,roll_est,'r');
title('Estimated Roll angle - actual (black) vs estimated (red)')
xlabel('Time in seconds');
ylabel('Degrees');

figure
plot(time,pitch);
hold on
plot(time,pitch_est,'r');
title('Actual Pitch angle - actual (blue) vs estimated (red)')
xlabel('Time in seconds');
ylabel('Degrees');

figure
%plot(time,yaw);
%hold on
plot(time,yaw_est,'r');
title('Yaw angle - actual (blue) vs estimated (red)')
xlabel('Time in seconds');
ylabel('Degrees');
```

SIMULATION CODES FOR NANO SATELLITE (NPSAT-1) ATTITUDE CONTROL

```
%%% NPSAT-1 Roll attitude control
Dcmotor=tf(.85,[.003 1]);
Spacecraftwithinertia=tf(.04,[1 .04]);
integrator=tf(1,[1 0]);
a=Dcmotor*Spacecraftwithinertia;
cl=feedback([a],[0.85]);
openloop=cl*integrator;
withoutcontroller=feedback(openloop,1);
comp=tf([1 13.98],1);
il=openloop*comp;
figure(1)
rlocus(il)
title ('NPSAT-1 RL Response')
```

```
cl2=feedback(openloop,1);
figure(2);
step(cl2)
title('NPSAT-1 Roll Response without controller')
gain=3700;
wc=gain*comp*openloop;
cl3=feedback(wc,1);
figure(3)
step(cl3)
title('NPSAT-1 Roll Response with PD-compensator')



%%% Design NPSAT-1 Pitch Response with PD controller
Dcmotor=tf(.85,[.003 1]);
Spacecraftwithinertia=tf(.0442,[1 .0442]);
integrator=tf(1,[1 0]);
a=Dcmotor*Spacecraftwithinertia;
cl=feedback([a],[0.85]);
openloop=cl*integrator
withoutcontroller=feedback(openloop,1);
comp=tf([1 13.98],1);
il=openloop*comp;
figure(1)
rlocus(il)
title ('NPSAT-1 RL Response')
cl2=feedback(openloop,1);
figure(2);
step(cl2)
title('NPSAT-1 Pitch Response without controller')
gain=2500;
wc=gain*comp*openloop;
cl3=feedback(wc,1);
figure(3)
step(cl3)
title('NPSAT-1 Pitch Response with PD-compensator')



%%% NPSAT-1 yaw Attitude control system
Dcmotor=tf(.85,[.003 1]);
scSpacecraftwithinertia=tf(.09,[1 .09]);
integrator=tf(1,[1 0]);
a=dc*sc;
```

```
cl=feedback([a],[0.85]);
openloop=cl*int
withoutcontroller=feedback(openloop,1);
comp=tf([1 13.98],1);
il=openloop*comp;
figure(1)
rlocus(il)
title ('NPSAT-1 RL Response')
cl2=feedback(openloop,1);
figure(2);
step(cl2)
title('NPSAT-1 Yaw Response without controller')
gain=2500;
wc=gain*comp*openloop;
cl3=feedback(wc,1);
figure(3)
step(cl3)
title('NPSAT-1 Yaw Response with PD-compensator')
```

APPENDIX-A (Satellite NORAD Data)

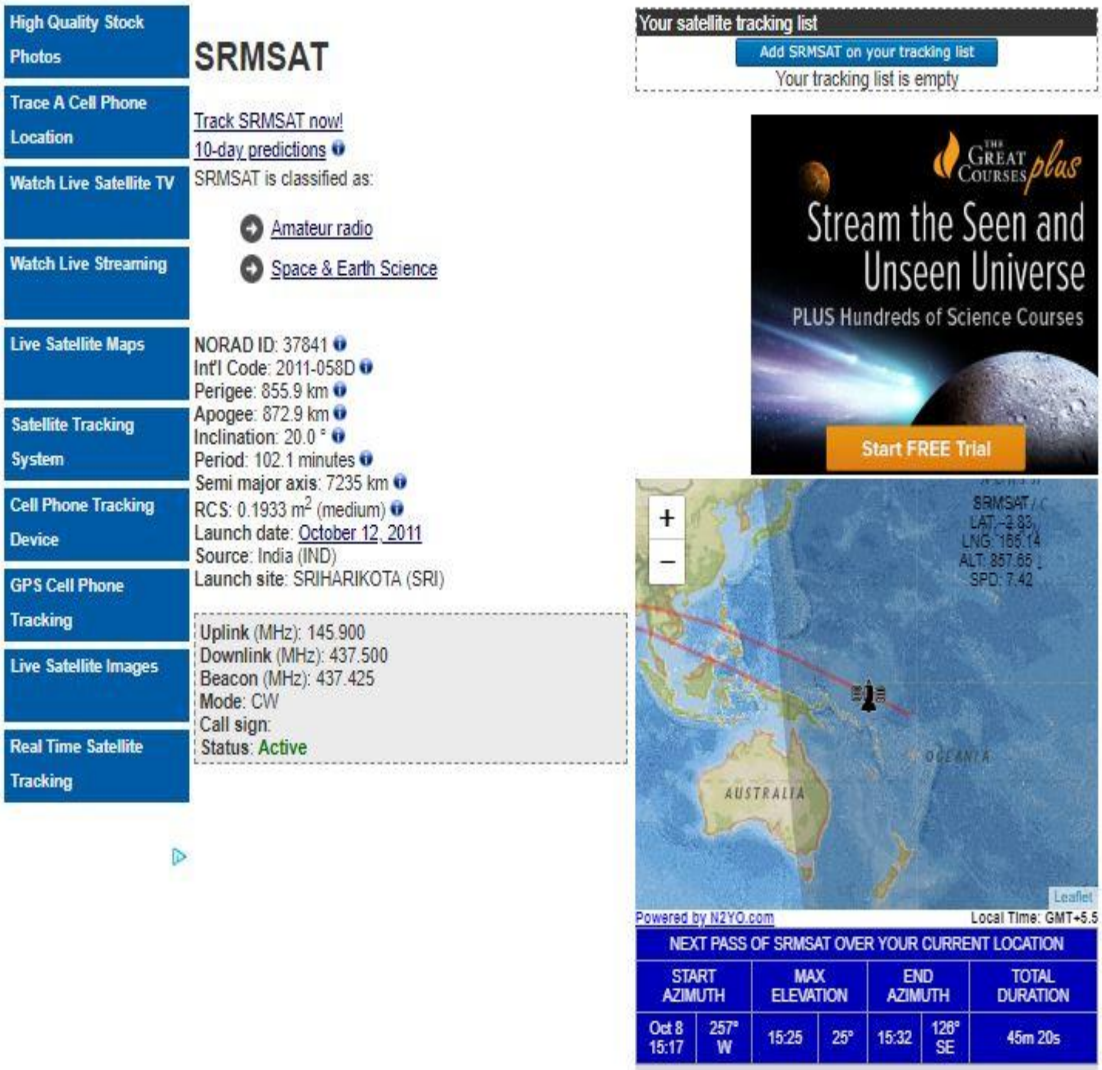

High Quality Stock Photos
Trace A Cell Phone Location
Watch Live Satellite TV
Watch Live Streaming
Live Satellite Maps
Satellite Tracking System
Cell Phone Tracking Device
GPS Cell Phone Tracking
Live Satellite Images
Real Time Satellite Tracking

SRMSAT

Track SRMSAT now!
10-day predictions
SRMSAT is classified as:

- Amateur radio
- Space & Earth Science

NORAD ID: 37841
Int'l Code: 2011-058D
Perigee: 855.9 km
Apogee: 872.9 km
Inclination: 20.0 °
Period: 102.1 minutes
Semi major axis: 7235 km
RCS: 0.1933 m^2 (medium)
Launch date: October 12, 2011
Source: India (IND)
Launch site: SRIHARIKOTA (SRI)

Uplink (MHz): 145.900
Downlink (MHz): 437.500
Beacon (MHz): 437.425
Mode: CW
Call sign:
Status: Active

Your satellite tracking list
Add SRMSAT on your tracking list
Your tracking list is empty

Powered by N2YO.com
Local Time: GMT+5.5

NEXT PASS OF SRMSAT OVER YOUR CURRENT LOCATION						
START AZIMUTH		MAX ELEVATION		END AZIMUTH		TOTAL DURATION
Oct 8 15:17	257° W	15:25	25°	15:32	126° SE	45m 20s

- High Quality Stock Photos
- Trace A Cell Phone Location
- Watch Live Satellite TV
- Watch Live Streaming
- Live Satellite Maps
- Satellite Tracking System
- Live Satellite Images
- GPS Cell Phone Tracking
- Real Time Satellite Tracking
- Cell Phone Tracking Device

PRATHAM

Track PRATHAM now!
10-day predictions

PRATHAM is classified as:

- Amateur radio
- Space & Earth Science
- CubeSats

NORAD ID: 41783
Int'l Code: 2016-059A
Perigee: 666.2 km
Apogee: 715.5 km
Inclination: 98.1 °
Period: 98.4 minutes
Semi major axis: 7061 km
RCS: Unknown
Launch date: September 26, 2016
Source: India (IND)
Launch site: SRIHARIKOTA (SRI)

Uplink (MHz):
Downlink (MHz): 437.455
Beacon (MHz): 145.980
Mode: 1200bps AFSK CW
Call sign: PRATHAM
Status: Inactive

PRATHAM is an Indian ionospheric research satellite which will be operated by the Indian Institute of Technology Bombay as part of the Student Satellite Initiative. Its primary mission is to count electrons in the Earth's ionosphere.

Your satellite tracking list

Add PRATHAM on your tracking list

Your tracking list is empty

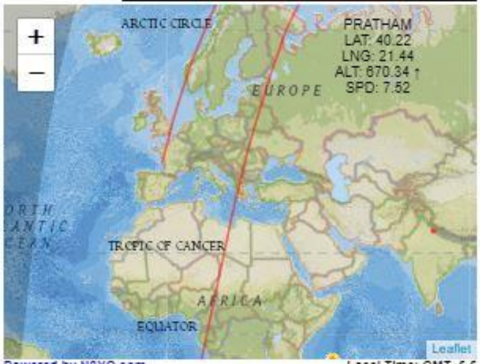

Powered by N2YO.com Local Time: GMT+5.5

NEXT PASS OF PRATHAM OVER YOUR CURRENT LOCATION

START AZIMUTH		MAX ELEVATION		END AZIMUTH		TOTAL DURATION
Oct 8 20:08	119° ESE	20:13	12°	20:18	17° NNE	40m 25s

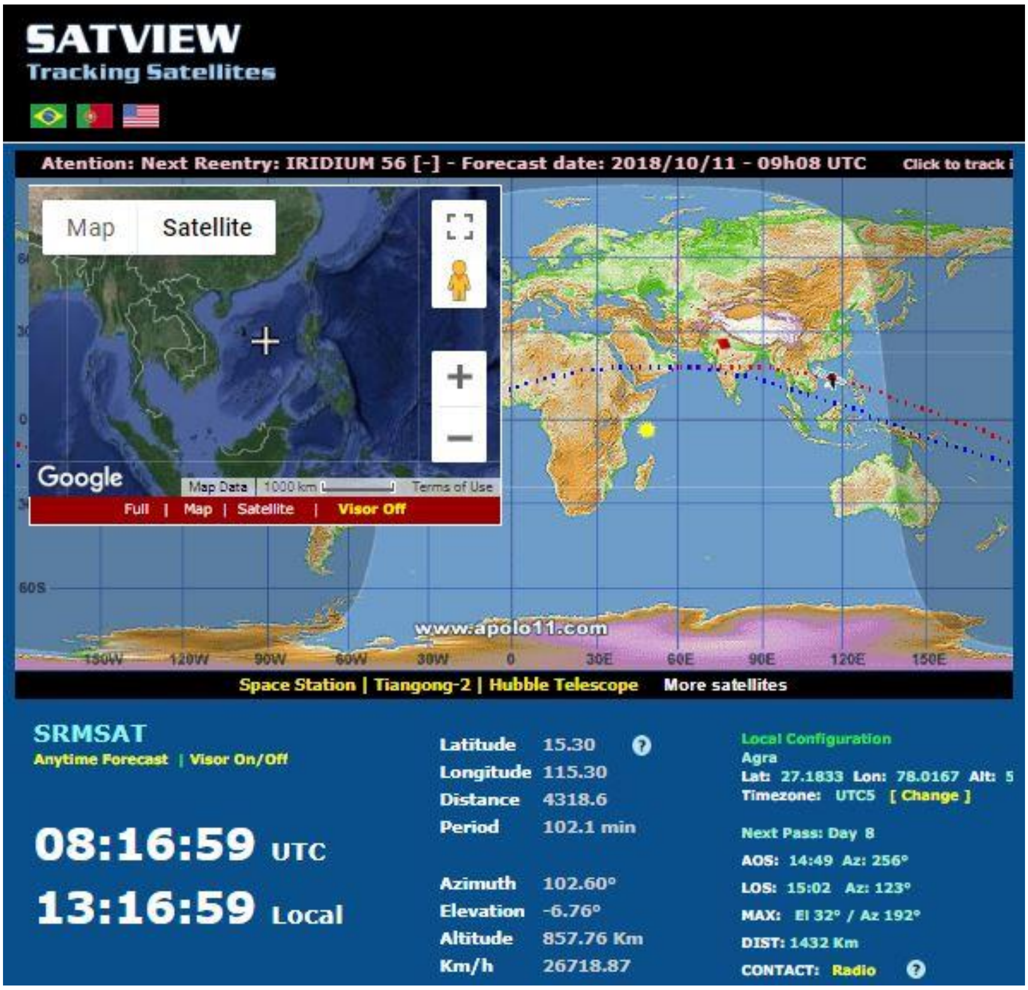

https://www.amsat.org/tle/current/nasa.all

https://www.n2yo.com/satellite/?s=41783#results

https://www.celestrak.com/NORAD/elements/supplemental/

https://www.heavens-above.com/satinfo.aspx?satid=41783&lat=0&lng=0&loc=Unspecified&alt=0&tz=UCT&cul=en

http://www.satview.org/

https://www.space-track.org/documentation#/tle

https://amsat-uk.org/tag/srmsat/

http://stuffin.space/

Appendix: (TLE: Two Line Elements)

SRM Satellite Two Line Element Set (TLE):

1 37841U 11058D   18280.99540663 .00000306 00000-0 22990-4 0 9994
2 37841 19.9713 124.7250 0011809 289.9476 221.8409 14.10615917360831

Pratham Satellite Two Line Element Set (TLE):
1 41783U 16059A   18280.71788194 +.00000066 +00000-0 +22131-4 0 9993
2 41783 098.1057 340.3887 0034923 102.0312 258.4808 14.62946942108414

International Space Station Two Line Element Set (TLE):

1 25544U 98067A   08264.51782528 -.00002182 00000-0 -11606-4 0 2927
2 25544 51.6416 247.4627 0006703 130.5360 325.0288 15.72125391563537

First Line:

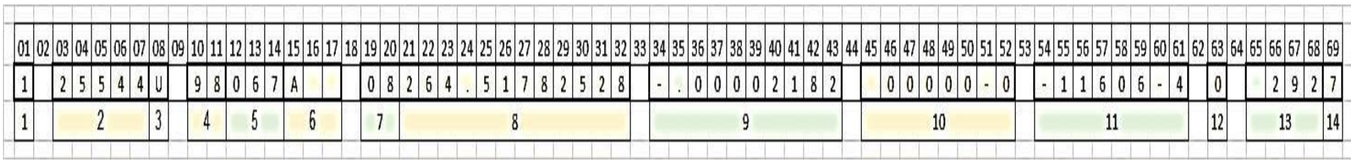

Field	Columns	Content	Example
1	01–01	Line number	1
2	03–07	Satellite number	25544
3	08–08	Classification (U=Unclassified)	U
4	10–11	International Designator (Last two digits of launch year)	98
5	12–14	International Designator (Launch number of the year)	067
6	15–17	International Designator (piece of the launch)	A
7	19–20	Epoch Year (last two digits of year)	08
8	21–32	Epoch (day of the year and fractional portion of the day)	264.51782528
9	34–43	First Time Derivative of the Mean Motion divided by two [11]	−.00002182
10	45–52	Second Time Derivative of Mean Motion divided by six (decimal point assumed)	00000-0
11	54–61	BSTAR drag term (decimal point assumed) [11]	-11606-4
12	63–63	The number 0 (originally this should have been "Ephemeris type")	0
13	65–68	Element set number. Incremented when a new TLE is generated for this object.[11]	292
14	69–69	Checksum (modulo 10)	7

Second Line:

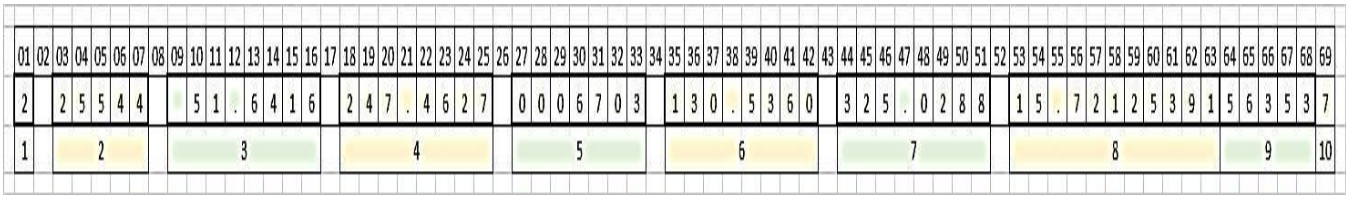

Field	Columns	Content	Example
1	01–01	Line number	2
2	03–07	Satellite number	25544
3	09–16	Inclination (degrees)	51.6416
4	18–25	Right ascension of the ascending node (degrees)	247.4627
5	27–33	Eccentricity (decimal point assumed)	0006703
6	35–42	Argument of perigee (degrees)	130.5360
7	44–51	Mean Anomaly (degrees)	325.0288
8	53–63	Mean Motion (revolutions per day)	15.72125391
9	64–68	Revolution number at epoch (revolutions)	56353
10	69–69	Checksum (modulo 10)	7

APPENDIX -B

ISS TRAJECTORY DATA

Lift off time (UTC) : N/A
Area (sq ft) : 21963.7592
Drag Coefficient (Cd) : 2.00
Monthly MSFC 50% solar flux (F10.7-jansky) : 74.2
Monthly MSFC 50% earth geomagnetic index (Kp) : 2.468
ET - UTC (sec) : 68.18
UT1 - UTC (sec) : 0.00

Maneuvers contained within the current ephemeris are as follows:

IMPULSIVE TIG (GMT) IMPULSIVE TIG (MET) DT	M50 DVx(FPS) M50 DVy(FPS) M50 DVz(FPS)	LVLH DVx(FPS) LVLH DVy(FPS) LVLH DVz(FPS)	DVmag(FPS) Invar Sph HA Invar Sph HP
132/22:41:26.692	-1.1	1.1	1.1
N/A	-0.1	-0.1	222.0
000/00:02:49.384	-0.0	-0.0	213.9
134/06:25:00.000	0.0	0.0	0.0
N/A	0.0	0.0	222.1
000/00:00:00.000	0.0	0.0	213.9

Coasting Arc #1 (Orbit 3140)

Vector Time (GMT): 2018/122/12:00:00.000
Vector Time (MET): N/A
Weight (LBS) : 928423.9

M50 Cartesian		M50 Keplerian	
X =	4422324.43-meter	A =	6777892.10
Y =	-214547.33-meter	E =	.0007413
Z =	5128165.55	I =	51.27620
XDOT =	2036.764769	Wp =	48.67787
YDOT =	7253.759472 meter/sec	RA =	245.45874 deg
ZDOT =	-1446.770461	TA =	55.34489
		MA =	55.27504
		Ha =	221.586 n.mi
		Hp =	213.875

M50 Cartesian		J2K Cartesian	
X =	14508938.43	X =	4399484.51
Y =	-703895.45-meter	Y =	-165221.72
Z =	16824690.12	Z =	5149592.57
XDOT =	6682.299112	XDOT =	1962.527649
YDOT =	23798.423466 feet/sec	YDOT =	7276.120938 meter/sec

ZDOT = -4746.622246	ZDOT = -1437.056468

TDR Cartesian	TDR Cartesian
X = 10665933.08	X = 3250976.40
Y = -9696226.22- meter	Y = -2955409.75
Z = 16920284.55	Z = 5157302.73
XDOT = 19605.714579	XDOT = 5975.821804
YDOT = 13322.224614 -meter/sec	YDOT = 4060.614062
ZDOT = -4704.230580	ZDOT = -1433.849481

The mean element set is posted at the UTC for which position is
Just north of the next ascending node relative to the above
Vector time

APPENDIX -C

Spacecraft Control Toolbar

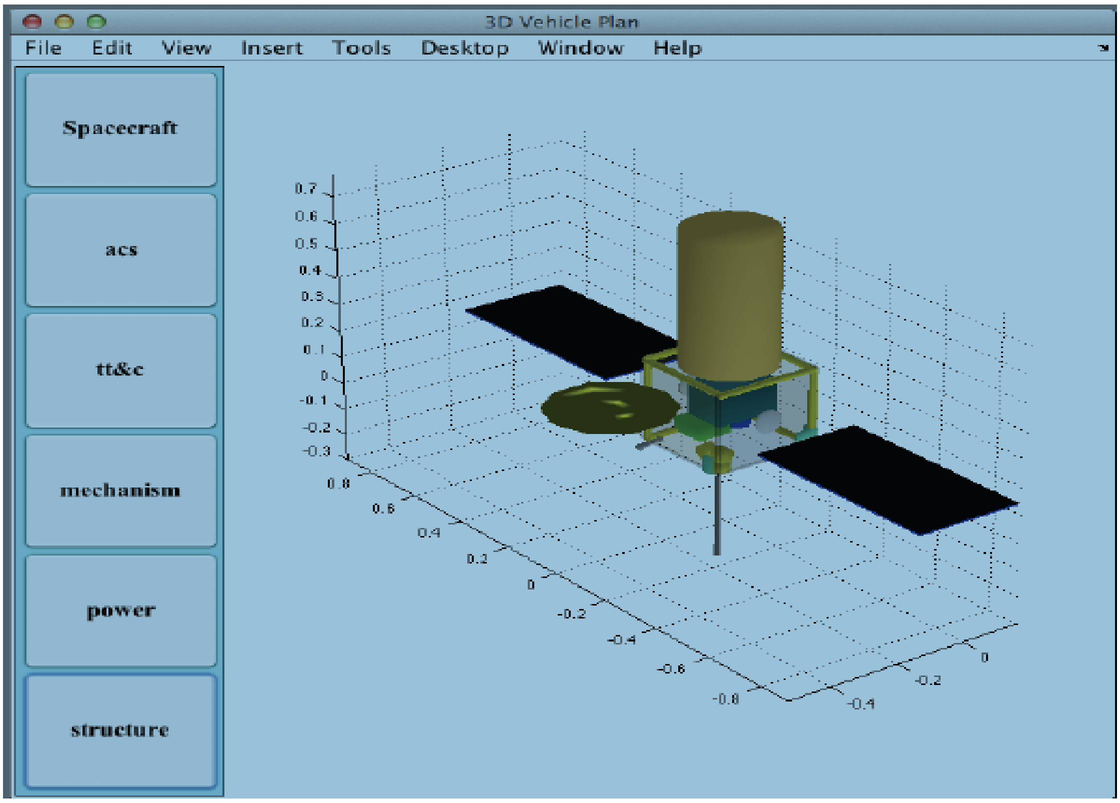

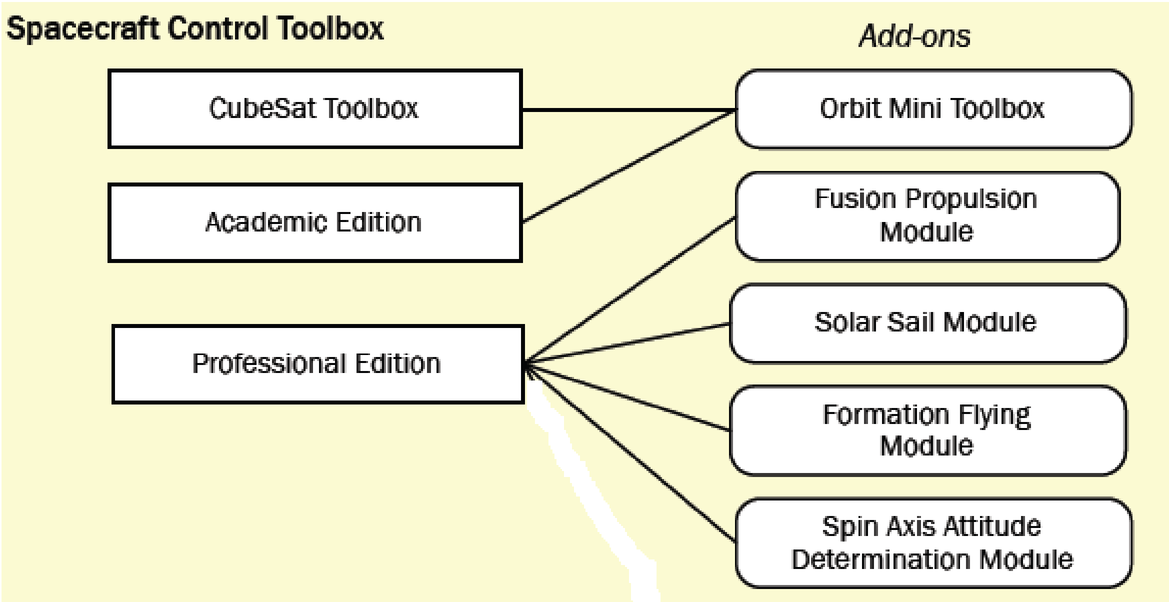

PlugInDemo at the end of the simulation

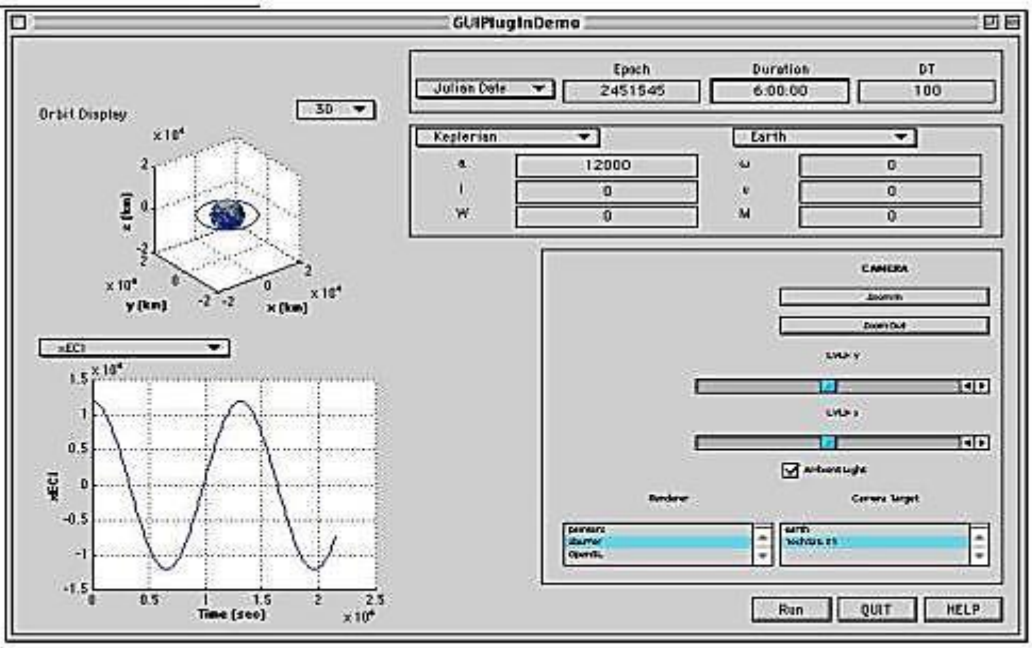

PlugInDemo on starting

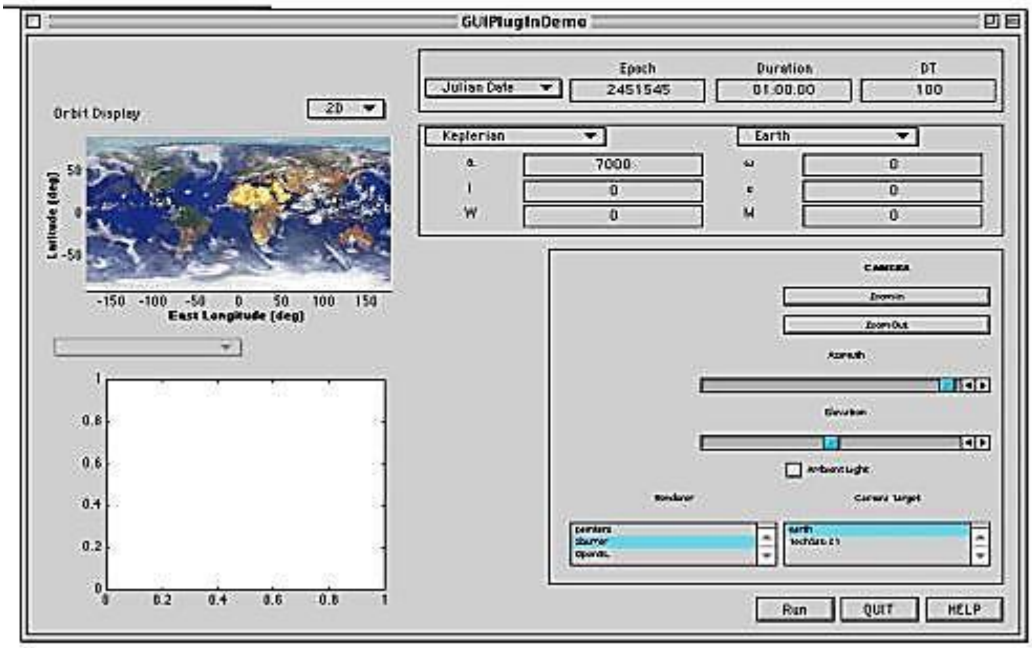

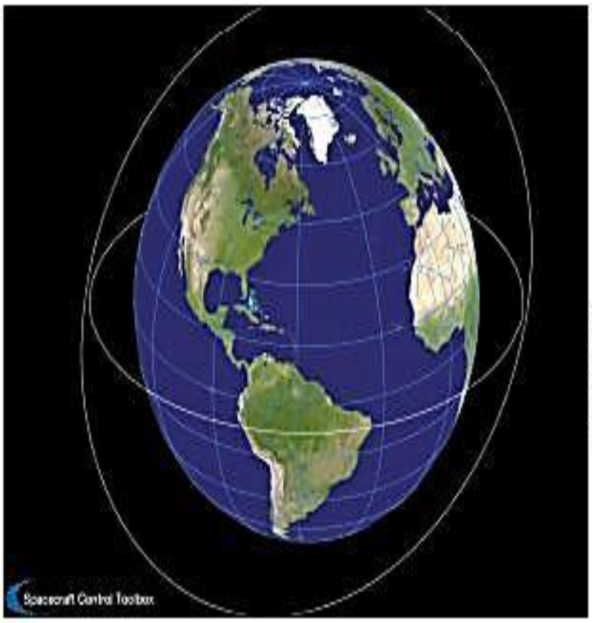
Spacecraft Control Toolbox

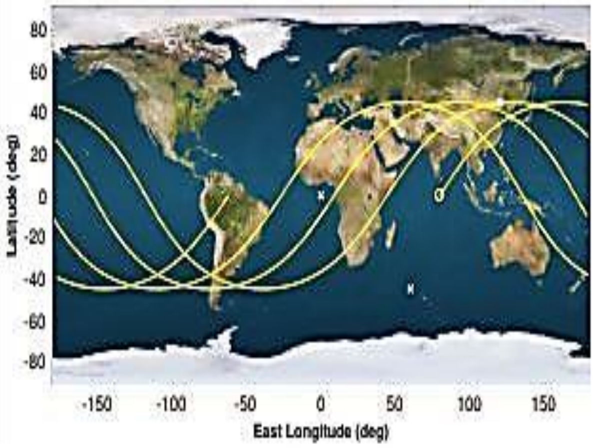
80
60
40
20
0
-20
-40
-60
-80
Latitude (deg)
-150
-100
-50
0
50
100
150
East Longitude (deg)

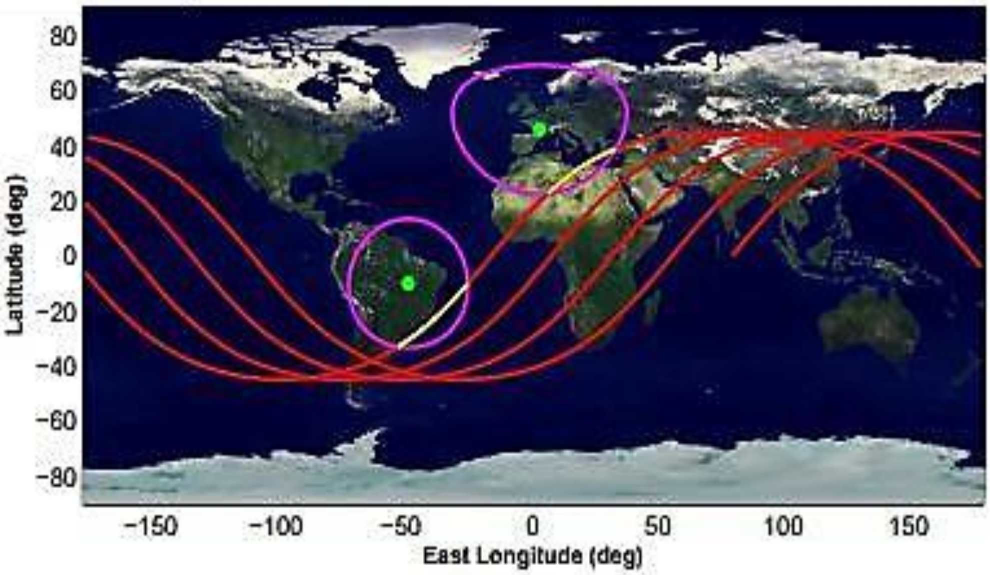
80
60
40
20
0
-20
-40
-60
-80
Latitude (deg)
−150
−100
−50
0
50
100
150
East Longitude (deg)

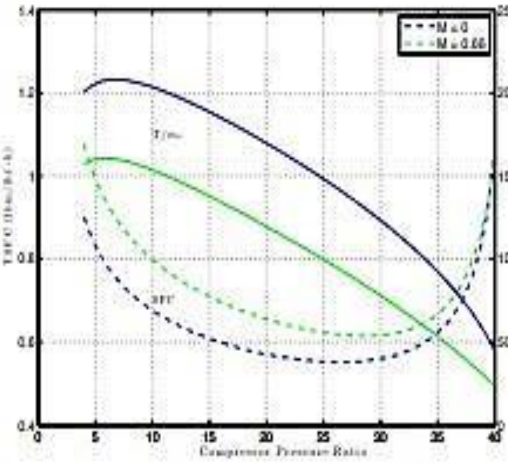

Jet engine modeling

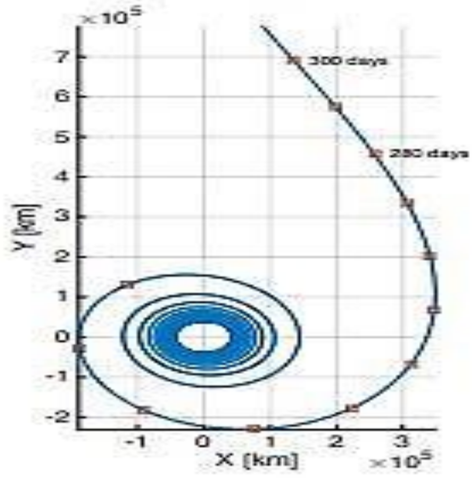

Simulation of Earth escape spiral

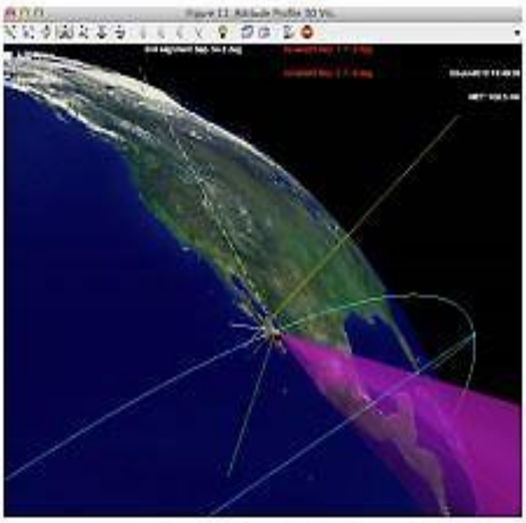

CubeSat Mission Planning

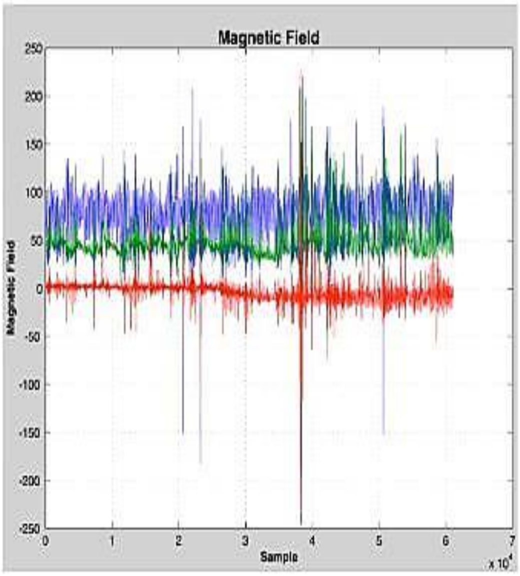

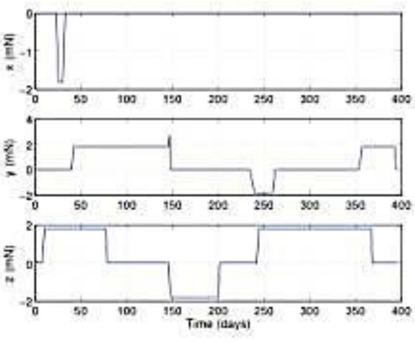

Thrust control vector in LVLH frame

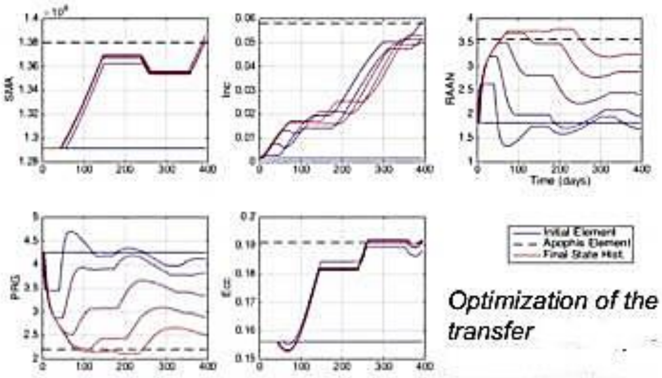

Optimization of the transfer

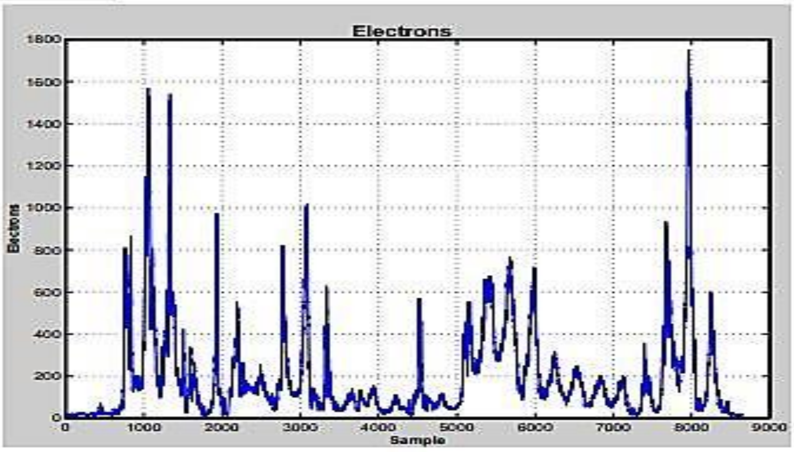

Electrons
Electrons
Sample

APPENDIX D

Satellite Attitude Data: https://www.raspberrypi.org/learning/

Kalman filter error covariance matrix: *Process and Measurements*

Q matrix: Process covariance

1.00E-06	0.00E+00	0.00E+00	0.00E+00	0.00E+00	0.00E+00
0.00E+00	1.00E-06	0.00E+00	0.00E+00	0.00E+00	0.00E+00
0.00E+00	0.00E+00	1.00E-06	0.00E+00	0.00E+00	0.00E+00
0.00E+00	0.00E+00	0.00E+00	1.00E-06	0.00E+00	0.00E+00
0.00E+00	0.00E+00	0.00E+00	0.00E+00	1.00E-06	0.00E+00
0.00E+00	0.00E+00	0.00E+00	0.00E+00	0.00E+00	1.00E-06

R matrix: Sensor Noise covariance

0.01	0	0
0	0.01	0
0	0	0.01

F is control matrix (Controllers PD Gain)

0.0810701256586948	0.0810701256586948	0	0	0	0
0	0	0.0883782589482987	0.0883782589482987	0	0
0	0	0	0	0.0810701256586948	0.0810701256586948

H matrix:

1	0	0	0	0	0
0	0	1	0	0	0
0	0	0	0	1	0

Z_k (Measurements)

52.8900000000000
1.71000000000000
186.200000000000

ATTITUDES DATA:

ROW_ID	pitch	roll	yaw	mag_x	mag_y	mag_z	gyro_x	gyro_y	gyro_z
1	1.49	52.25	185.21	-46.4228	-8.13291	-12.1293	0.000942	0.000492	-0.00075
2	1.03	53.73	186.72	-48.779	-8.30424	-12.9431	0.000218	-5.00E-06	-0.00024
3	1.24	53.57	186.21	-49.1619	-8.47083	-12.6428	0.000395	0.0006	-3.00E-06
4	1.57	53.63	186.03	-49.3419	-8.45738	-12.6155	0.000308	0.000577	-0.0001
5	0.85	53.66	186.46	-50.0567	-8.12261	-12.6783	0.000321	0.000691	0.000272
6	0.85	53.53	185.52	-50.2465	-8.34321	-11.9381	0.000273	0.000494	-5.90E-05
7	0.63	53.55	186.1	-50.4473	-7.93731	-12.1886	-0.00011	0.00032	0.000222
8	1.49	53.65	186.08	-50.6682	-7.7626	-12.2842	-4.40E-05	0.000436	0.000301
9	1.22	53.77	186.55	-50.7615	-7.26293	-11.9811	0.000358	0.000651	0.000187
10	1.63	53.46	185.94	-51.2438	-6.87527	-11.6725	0.000266	0.000676	0.000356
11	1.32	53.52	186.24	-51.6165	-6.81813	-11.8608	0.000268	0.001194	0.000106
12	1.51	53.47	186.17	-51.7817	-6.74435	-11.7484	0.000859	0.001221	0.000264
13	1.55	53.75	186.38	-51.9927	-6.52933	-11.5983	0.000589	0.001151	2.00E-06
14	1.07	53.63	186.6	-52.4092	-6.10015	-11.7199	0.000497	0.00061	-6.00E-05
15	0.81	53.4	186.32	-52.6485	-6.34696	-11.596	-5.30E-05	0.000593	-0.00014
16	1.51	53.34	186.42	-52.8507	-6.04319	-11.7441	-0.00024	0.000495	0.000156
17	1.82	53.49	186.39	-53.4491	-6.09123	-11.652	0.000571	0.00077	0.000331
18	0.46	53.69	186.72	-53.68	-5.80839	-11.7036	-0.00019	0.000159	0.000386
19	0.67	53.55	186.61	-54.159	-5.63871	-11.424	-0.0005	9.40E-05	8.40E-05
20	1.23	53.43	186.21	-54.4006	-5.29371	-11.099	-0.00034	1.30E-05	4.10E-05
21	1.44	53.58	186.4	-54.6094	-5.3559	-11.3701	-0.00027	0.000279	-9.00E-06
22	1.25	53.34	186.5	-54.7461	-5.15465	-11.5307	0.000139	0.000312	5.00E-05
23	1.18	53.49	186.69	-55.0914	-4.90302	-11.3636	-0.00049	8.60E-05	6.50E-05
24	1.34	53.32	186.84	-55.5163	-4.63189	-11.6334	0.000312	0.000175	0.000308
25	1.36	53.56	187.02	-55.561	-4.55227	-11.6051	-0.0001	-2.30E-05	0.000377
26	1.17	53.44	186.95	-56.0164	-4.51512	-11.427	0.000147	5.40E-05	0.000147
27	0.88	53.41	186.57	-56.3937	-4.35542	-11.005	-0.00013	-0.00019	0.000269
28	0.78	53.84	186.85	-56.5245	-4.30156	-11.2208	-0.00018	-0.00031	0.000361
29	0.88	53.41	186.62	-56.7916	-4.07602	-11.064	-0.00038	-0.00025	0.000132
30	0.86	53.29	186.71	-56.9155	-3.8673	-11.0856	3.10E-05	-0.00026	6.90E-05
31	0.64	53.57	187.09	-57.6625	-3.47845	-11.118	0.0002	0.000184	0.000275
32	1.02	53.41	186.79	-57.996	-3.39674	-10.8548	8.20E-05	-0.00022	-2.90E-05
33	0.87	53.54	187.12	-58.3175	-3.00518	-10.9324	0.000123	2.90E-05	-3.90E-05
34	0.35	53.55	187.03	-58.2887	-3.03725	-10.7718	0.000418	-5.30E-05	0.00016
35	1.47	53.48	187.33	-58.5083	-2.51236	-10.9999	0.000461	0.000641	0.000109
36	1.82	53.14	187.53	-58.7559	-2.48546	-11.2323	-0.00023	-3.00E-06	2.50E-05
37	1.37	53.3	187.49	-58.9523	-2.18282	-11.1746	0.000383	0.000363	0.000154
38	1.68	53.26	187.54	-58.8051	-2.15404	-11.1508	-8.10E-05	8.80E-05	-0.0003
39	0.83	53.58	187.79	-59.2215	-1.85493	-11.0891	0.000238	-0.00014	-7.50E-05
40	1.37	53.34	187.62	-59.5793	-1.66924	-10.7939	-0.00032	-0.00053	-6.00E-06

APPENDIX E (Satellite attitude dynamics)

Structure: Satellite response from with controller and without controller taken from MATLAB.

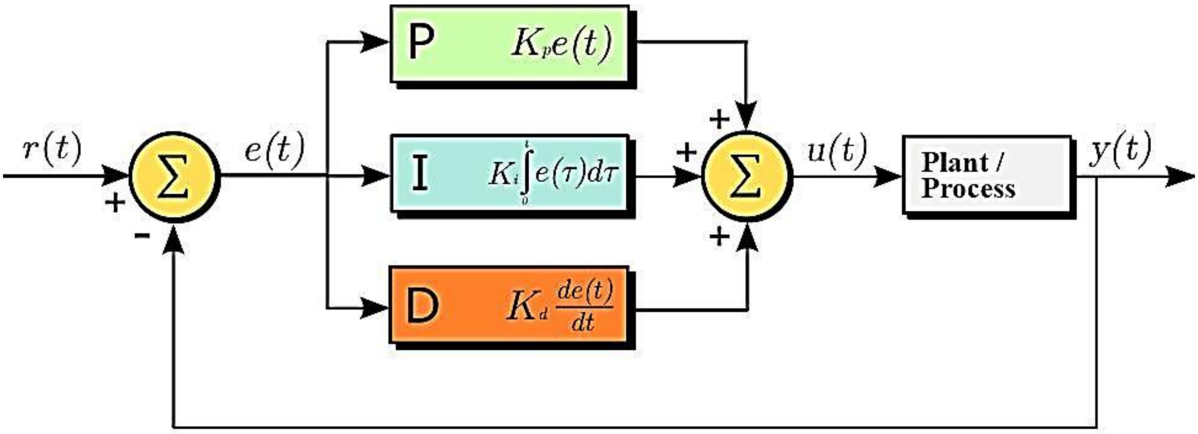

SRM Satellite Pitch Dynamics:

Pitch dynamics $\frac{\boldsymbol{\theta}\ (\boldsymbol{s})}{\boldsymbol{T_y}\ (\boldsymbol{s})} = \frac{\mathbf{0.1690}}{\boldsymbol{s}^2 + \mathbf{0.1690}\boldsymbol{s}}$

Closed loop Response=

0.169 s + 2.487

----

s2 + 0.338 s + 2.487

Continuous-time transfer function.

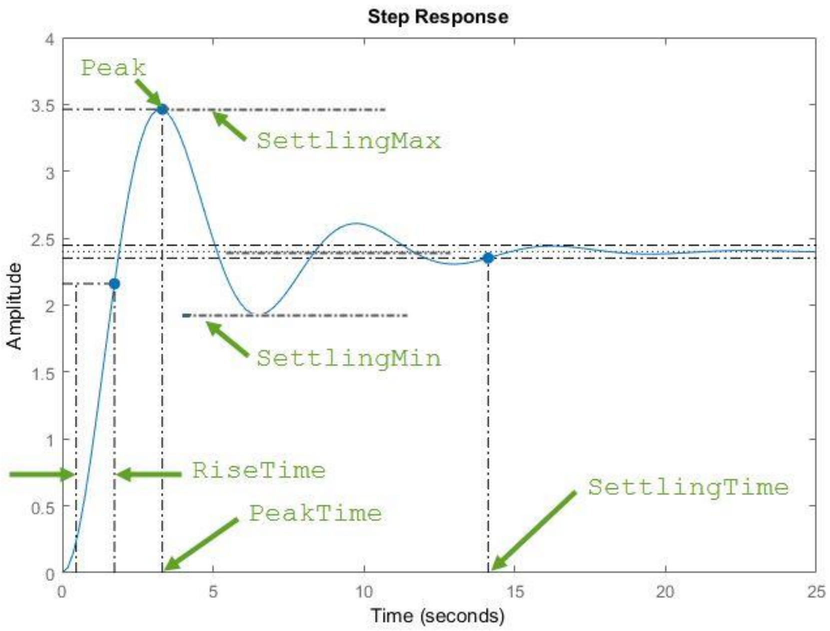

withoutcontroller =

RiseTime: 2.9526

SettlingTime: 41.6600

SettlingMin: 0.7336

SettlingMax: 1.5155

Overshoot: 51.5524

Undershoot: 0

Peak: 1.5155

PeakTime: 7.6299

withcontroller =

RiseTime: 0.0333

SettlingTime: 0.2111

SettlingMin: 0.9167

SettlingMax: 1.1716

Overshoot: 17.1642

Undershoot: 0

Peak: 1.1716

PeakTime: 0.0881

SRM Satellite Roll Dynamics:

Pitch dynamics $\frac{\boldsymbol{\phi}\,(\boldsymbol{s})}{\boldsymbol{T_x}\,(\boldsymbol{s})} = \frac{\mathbf{0.1589}}{\boldsymbol{s}^2 + \mathbf{0.1589}\boldsymbol{s}}$

withoutcontroller =

RiseTime: 3.0218

SettlingTime: 49.2573

SettlingMin: 0.7219

SettlingMax: 1.5276

Overshoot: 52.7614

Undershoot: 0

Peak: 1.5276

PeakTime: 8.1148

withcontroller =

RiseTime: 0.0332

SettlingTime: 0.2111

SettlingMin: 0.9168

SettlingMax: 1.1717

Overshoot: 17.1712

Undershoot: 0

Peak: 1.1717

PeakTime: 0.0881

SRM Satellite Yaw Dynamics:

Yaw dynamics $\frac{\boldsymbol{\psi}\,(\boldsymbol{s})}{\boldsymbol{T_z}\,(\boldsymbol{s})} = \frac{\mathbf{0.2169}}{\boldsymbol{s}^2 + \mathbf{0.2169}\boldsymbol{s}}$

Closed loop response =

$$\frac{0.2169\, s + 3.195}{s^2 + 0.4338\, s + 3.195}$$

Continuous-time transfer function.

withoutcontroller =

RiseTime: 2.6813

SettlingTime: 35.8677

SettlingMin: 0.7783

SettlingMax: 1.4703

Overshoot: 47.0268

Undershoot: 0

Peak: 1.4703

PeakTime: 6.7942

withcontroller =

RiseTime: 0.0333

SettlingTime: 0.2112

SettlingMin: 0.9159

SettlingMax: 1.1711

Overshoot: 17.1113

Peak: 1.1711

PeakTime: 0.0882

Pratham IITB Roll Dynamics:

Closed loop response =

$$\frac{8.62\, s + 160.9}{s^2 + 17.24\, s + 160.9}$$

Continuous-time transfer function.

withoutcontroller =

RiseTime: 1.9424

SettlingTime: 3.5335

SettlingMin: 0.9008

SettlingMax: 0.9985

Overshoot: 0

Undershoot: 0

Peak: 0.9985

PeakTime: 5.7863

withcontroller =

RiseTime: 0.0588

SettlingTime: 0.2449

SettlingMin: 0.9099

SettlingMax: 1.0898

Overshoot: 8.9797

Undershoot: 0

Peak: 1.0898

PeakTime: 0.1354

Pratham IITB Pitch Dynamics:

Closed loop Response=

$$\frac{9.17\, s + 174.2}{s^2 + 18.34\, s + 174.2}$$

Continuous-time transfer function.

withoutcontroller =

RiseTime: 1.9572

SettlingTime: 3.5591

SettlingMin: 0.9008

SettlingMax: 0.9998

Overshoot: 0

Undershoot: 0

Peak: 0.9998

PeakTime: 7.5608

withcontroller =

RiseTime: 0.0618

SettlingTime: 0.2494

SettlingMin: 0.9152

SettlingMax: 1.0841

Overshoot: 8.4097

Undershoot: 0

Peak: 1.0841

PeakTime: 0.1409

Pratham IITB Yaw Dynamics:

Closed loop response =

$$\frac{8.77\, s + 164.5}{s^2 + 17.54\, s + 164.5}$$

Continuous-time transfer function.

withoutcontroller =

RiseTime: 1.9466

SettlingTime: 3.5409

SettlingMin: 0.9010

SettlingMax: 0.9995

Overshoot: 0

Undershoot: 0

Peak: 0.9995

PeakTime: 6.7576

withcontroller =

RiseTime: 0.0598

SettlingTime: 0.2466

SettlingMin: 0.9060

SettlingMax: 1.0883

Overshoot: 8.8319

Undershoot: 0

Peak: 1.0883

PeakTime: 0.1365

International Space Station (ISS) Roll Dynamics:

Closed loop response=

$$\frac{1.39e\text{-}08\ s + 2.036e\text{-}07}{s^2 + 2.78e\text{-}08\ s + 2.036e\text{-}07}$$

Continuous-time transfer function.

withoutcontroller =

RiseTime: 1.5394e+04

SettlingTime: 5.6224e+08

SettlingMin: 0.0085

SettlingMax: 1.9955

Overshoot: 99.5531

Undershoot: 0

Peak: 1.9955

PeakTime: 1.3252e+05

withcontroller =

RiseTime: 0.0050

SettlingTime: 0.0474

SettlingMin: 0.9008

SettlingMax: 1.0303

Overshoot: 3.0310

Undershoot: 0

Peak: 1.0303

PeakTime: 0.0175

International Space Station (ISS) Pitch Dynamics:

closedloop =

$$\frac{1.72e\text{-}08\ s + 2.52e\text{-}07}{s^2 + 3.44e\text{-}08\ s + 2.52e\text{-}07}$$

Continuous-time transfer function.

withoutcontroller =

RiseTime: 1.1085e+04

SettlingTime: 4.5453e+08

SettlingMin: 0.0078

SettlingMax: 1.9961

Overshoot: 99.6091

Undershoot: 0

Peak: 1.9961

PeakTime: 4.5515e+05

withcontroller =

RiseTime: 0.0197

SettlingTime: 0.1633

SettlingMin: 0.9070

SettlingMax: 1.1096

Overshoot: 10.9628

Undershoot: 0

Peak: 1.1096

PeakTime: 0.0550

International Space Station (ISS) Yaw Dynamics:

Closed loop response =

$$\frac{8.04e\text{-}09\, s + 1.178e\text{-}07}{s^2 + 1.608e\text{-}08\, s + 1.178e\text{-}07}$$

Continuous-time transfer function.

withoutcontroller =

RiseTime: 6.4137e+04

SettlingTime: 9.7121e+08

SettlingMin: 0.0041

SettlingMax: 1.9880

Overshoot: 98.7951

Undershoot: 0

Peak: 1.9880

PeakTime: 2.9783e+06

withcontroller =

RiseTime: 0.0197

SettlingTime: 0.1631

SettlingMin: 0.9066

SettlingMax: 1.1095

Overshoot: 10.9529

Peak: 1.1095

PeakTime: 0.0549

PUBLISHED RESEARCH PAPERS

1. Raja M, Dr Ugur Guven, Dr OM Prakash, "***Design a Nano Satellite Attitude Control System Using Proportional-Derivative Controller***", International Journal of Research and Analytical Reviews (IJRAR), PP 451-459, Volume 5, Issue 4 (2018).
2. Raja M, Dr Ugur Guven, Dr OM Prakash, Aman Saluja "***Experimental Analysis of Low Earth Orbit Satellites due to Atmospheric Perturbations***", IAETSD Journal for Advanced Research in Applied Sciences, Volume 5, Issue 4, April/2018
3. Raja M, Dr Ugur Guven, Dr OM Prakash, "***Design and Analysis of Attitude Control Algorithm for Low Earth Orbiting Satellite with Magnetic Torquer Concepts using Non- Linear Unscented Kalman Filter***", International Journal of Engineering and Technology (UAE), ISSN 2227-524X, Vol 7 &. No 2.18 (2018).
4. Raja M, Dr Ugur Guven, Dr OM Prakash, "***Experimental and analysis of Attitude Control System for Low Earth Orbit Satellite Attitude Errors Estimation with unscented Kalman Filter***", International Journal of Emerging Technology and Advanced Engineering, PP 487-494, ISSN 2250-2459, ISO 9001:2008 Certified Journal, Volume 7, Issue 9, September 2017.
5. Raja M, Dr Ugur Guven, Dr OM Prakash, Saurabh Pandey "***Design of trajectory and perturbation analysis for satellite orbital parameters***", IAETSD Journal for Advanced Research in Applied Sciences, Volume 4, Issue 4, Sept /2017 ISSN (Online): 2394-8442